Modulation of Immune Checkpoints by Tumour Extracellular Vesicles

Thesis

Eriomina Shahaj

Degree in Biological Sciences

OU Personal Identifier: E749205X

Modulation of immune checkpoints by tumour extracellular vesicles

Thesis presented for the Degree of Doctor of Philosophy

The Open University, Milton Keynes, UK

Faculty of Science Technology Engineering and Mathematics (STEM)

School of Life, Health and Chemical Sciences

Date of submission: September 2019

Affiliated Research Centre:

Fondazione IRCCS Istituto Nazionale dei Tumori, Milan, Italy

Director of Studies: Dr. Monica Rodolfo

Internal Supervisor: Dr. Veronica Huber

External Supervisor: Prof. Federica Marelli-Berg

Table of contents

Abstract

Introduction. Melanoma extracellular vesicles (EVs) are endowed with pro-tumourigenic features and can condition the immune system favouring immune escape. Immune checkpoints (IC) are key molecules involved in the regulation of immune responses that can be expressed also by tumour cells. The expression of IC in melanoma cells can be conditioned by BRAF and MEK inhibitors, a standard treatment for patients affected by BRAF-mutated melanoma. Here, I investigated the IC expression in melanoma tumours, in melanoma cell lines and EVs, in association with the acquisition of drug resistance, a common event during treatment. The interaction of EVs with melanoma and with immune cells was investigated in the context of drug resistance, to uncover potentially targetable molecules for immunotherapeutic strategies. To this aim, the expression of IC was assessed in plasma EVs of melanoma patients during therapy with BRAF and MEK inhibitors.

Methodology. EVs released from melanoma cell lines were isolated by ultracentrifugation protocol and characterized for IC expression by qRT-PCR, western blot and latex beads flow cytometry. To study the IC modulation induced via EVs in target melanoma and immune cells, CD81GFP-tagged EVs derived from drug sensitive and resistant melanoma cell variants were used. In vivo IC relevance was assessed in plasma EVs and in tumour specimens of melanoma patients. EVs were characterized by Nanoparticle Tracking Analysis from the whole plasma. IC expression transcripts were evaluated by qRT-PCR isolating RNA from plasma EVs by three different methods: a) exoRNeasy kit; b) ExoQuick and c) ultracentrifugation protocol in combination with an RNA extraction kit from Mcherey-Nagel. IC expression proteins in plasma EV fractions isolated by differential ultracentrifugation were evaluated by western blot analysis.

Results. In melanoma lesions, IC transcripts CD155, HVEM and GAL9 displayed a modulation in association to resistance to treatment. In melanoma cell lines, PDL1, PDL2 and CD155 showed increased expression, and GAL9 and HVEM a decrease, upon the acquisition of resistance in a set of six drug sensitive and resistant cell line pairs. The expression of PDL1, PDL2 and GAL9 was modulated by treatment with IFNγ and regulated by CCL2 and specific miRNAs. Corresponding EVs reflected the IC expression pattern of originating cells carrying several IC. In vitro models showed that CD81GFP-EVs interacted with both melanoma and immune cells thereby transfer therapy resistance associated

features. The EV uptake in monocytes induced a myeloid-derived suppressor cell (MDSC) phenotype accompanied by modulation of IC expression, with PDL1 and HVEM increase. EVs isolated from plasma of melanoma patients during therapy displayed significant variations of numbers and size, and of studied IC levels, at protein and transcript level, which associated to treatment response.

Conclusions. Melanoma IC expression can be altered by BRAF and MEK inhibitors treatment. EVs reflect IC expression of originating cells and may represent a surrogate of melanoma resistance status. The effects of IC-carrying EVs on interacting cells suggest their involvement in immunomodulation and tumour immune escape, and their modulations in plasma may reflect patients' immune activation in response to therapy.

1. Introduction and aims of the thesis

1.1. Extracellular vesicles

1.1.1. Nature of EVs

Extracellular vesicles (EVs) are phospholipid bilayer membrane surrounded structures that are released by most types of cells. EVs are present in all body fluids such as plasma, serum, lymph, urine, saliva, tears and milk and they are important carriers of biological materials. The main function that has been recognized of EVs is to act as mediators of intercellular communication in physiological and pathological conditions [1]. Thanks to their rich composition, EVs can transfer molecular constituents, including proteins, nucleic acids and lipids from the cells of origin into recipient cells [2]. Their stability enables EVs to persist and protect their content even under harsh conditions, such as low pH, in different body fluids and, once their target has been reached, to act as potent signalling vectors. Due to their action and composition, EVs represent potential biomarkers and targets involved in pathological processes [3, 4].

The term “extracellular vesicles” was introduced by the International Society for Extracellular Vesicles (ISEV) to uniform the nomenclature of the heterogeneous types of vesicles isolated in different research groups. In 2018 a scientific consensus on calling the subtypes of vesicles EVs was obtained from the scientific community of researchers involved in the field [5]. This was a major step forward, as depending on the research group and the isolation method, the vesicles with overlapping characteristics received different names, mainly exosomes or microvesicles (MVs).

1.1.2. Discovery

The discovery of EVs dates back to 1940, when in plasma samples an “unknown” extracellular component which promotes clotting of blood [6] was discovered. More than 20 years later, these extracellular components were discovered to be small vesicles released from platelets and called “platelet dust” [7]. In 1987, EVs sized 40-100 nm released from multivesicular bodies (MVB) were isolated from reticulocyte medium and called exosomes. It was hypothesized that the role of the vesicles produced during reticulocyte maturation in erythrocytes consisted in externalisation of membrane proteins (Figure 1.1.2 [8]), and thus for the next decade exosomes were considered a mechanism for removing obsolete protein plasma membrane. Subsequently, in 1996 B cells and dendritic cells were found to release vesicles carrying essential molecules for the

triggering of adaptive immune response [9], firstly assigning to these structures a pivotal signalling function.

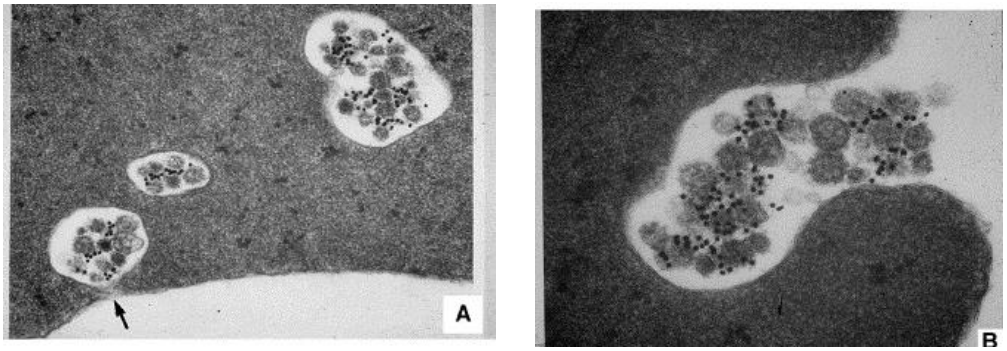

Figure 1.1.2. Exosomes in maturing sheep reticulocytes. Reticulocytes were labelled with monoclonal anti-transferrin receptor antibody and observed at A) 18 h and B) 36 h once attaching colloidal gold. The label was detectable in MVBs and at internal exosomes. MVB fuse with the cell membrane (arrow) and exosomes are released. Figure taken from [8].

1.1.3. EV subtypes and biogenesis

Different types of vesicles including exosomes, microvesicles (MVs), ectosomes, microparticles (MPs), oncosomes and apoptotic bodies are members of the big family of EVs (Figure 1.1.3.1 taken from [10]). These have been named and identified according to their origin, size, density, composition, functional properties or cell type derivation [11-14].

The dimensions that have been defined for each type of EV can be overlapping. In fact exosomes are defined as EVs with a size ranging from 50 to 150 nm while MVs measure between 100 and 1000 nm [15, 16]. Oncosomes derive, as their name specifies, from tumour cells and have first been described in 2008 as membrane-derived MVs that served to transfer functionally active EGFRvIII between glioma cells [17]. Oncosomes have a size ranging from 1 to 10 μm diameter and derive from bulky cellular protrusions. They could be identified in prostate cancer tissue specimens and patients' plasma [18, 19]. These type of EVs were studied primarily in glioma and prostate cancer and results showed that these vesicles contribute to reprogramming the microenvironment and promote disease progression [20, 21].

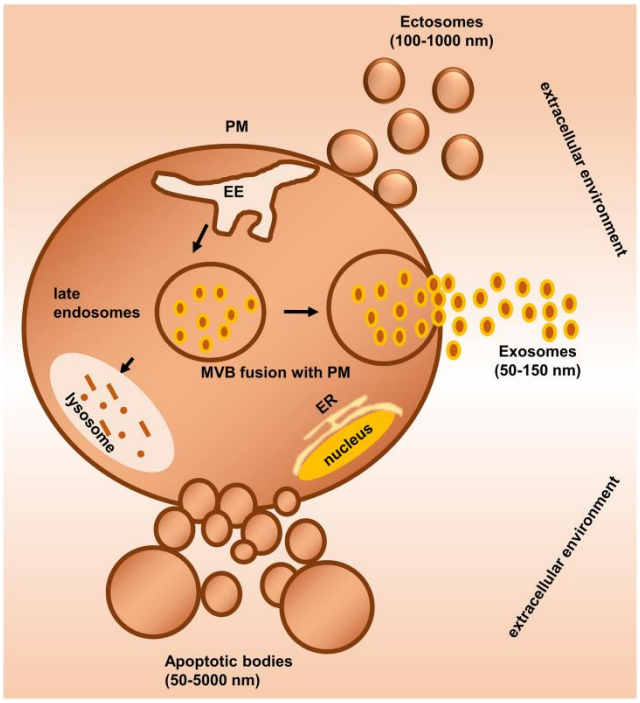

Figure 1.1.3.1. Subtypes of extracellular vesicles. During physiological or pathological conditions, cells release different type of vesicles of endocytic origin or membrane budding origin. EE: Early endosomes, ER: Endoplasmic reticulum, PM: Plasma membrane. Figure taken from [10].

MVs and MPs stem from the membrane like oncosomes. MVs deriving from platelets are generally called MPs and have been found to be relevant in homeostasis and vascular biology and diseases like thrombosis [22]. MPs or platelet-derived MVs play also major roles in cancer as they can mediate tumour immune escape and contribute to the metastatic processes [23]. Due to their membrane origin, MVs carry a selected surface repertoire of the secreting cell, among which Annexin A1 has been recognised as specific MV marker in a recent study [24]. This type of vesicle also comprises the ectosomes, which were first described as EVs released by neutrophils. Ectosomes were found to be produced by activated neutrophils at inflammation sites to focus antimicrobial activity onto opsonized surfaces [25].

Exosomes are the most studied EVs, they originate from MVBs of the releasing cells and uptaken by recipient cells [11]. Exosomes differ from the other EV types for their markers, which include CD9, CD63 and CD81 tetraspanins, HSC70 and HSC90 heat shock proteins, Alix and TSG101 endocytic membrane transport machinery proteins (ESCRT), GTPases membrane transporters, and lipid-bound proteins [26, 27]. MVBs contain intraluminal vesicles (ILVs) that form by inward budding of late endosomal membranes. The ILVs contain proteins and RNAs deriving from the cytosol. MVBs fuse with the plasma membrane and release ILVs into the extracellular compartment, these represent the exosomes. Alternatively, MVBs may also be subject to lysosomal degradation [10]. These

processes are controlled by RAB27A and RAB27B that contribute to the recruitment of MVBs to the plasma membrane [28].

Exosomes can derive from ILVs formed in an ESCRT-dependent or independent way. First, ESCRT complexes sort the molecular cargoes after ubiquination into the late endosomes. This is followed by the invagination of the endosomal membranes and the formation of ILVs inside the MVBs. In addition, proteins are engulfed from the cytosol. ESCRT members comprise typical exosomal proteins such as Alix and TSG101 (Anand et al., 2019). In contrast, ESCRT-independent sorting of exosomes, involves lipids, tetraspanins and RabGTPases. This alternative biogenesis pathway appears to rely on the formation of ILVs by conversion of sphyngomyelin to ceramide (Figure 1.1.3.2 [10]).

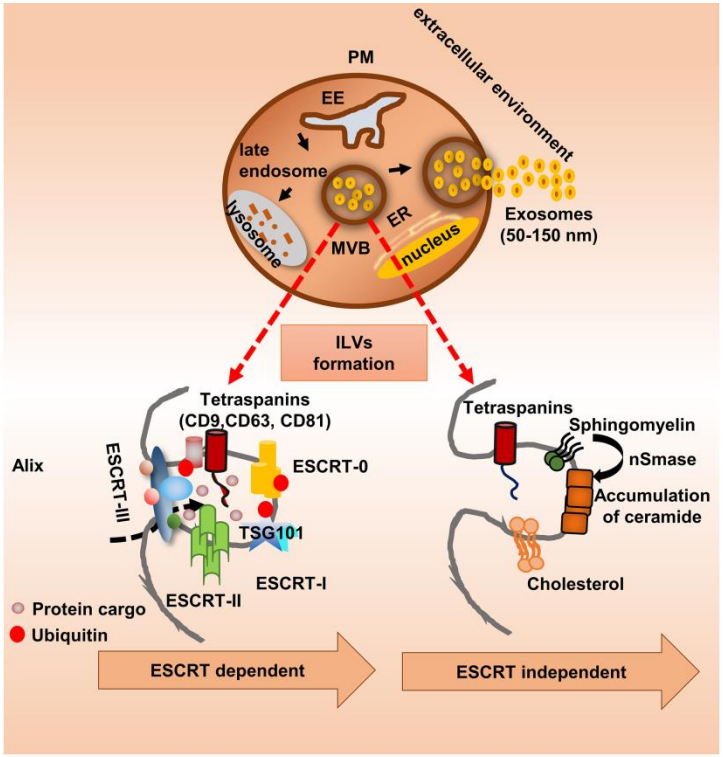

Figure 1.1.3.2. Schematic representation of biogenesis of exosomes. Biogenesis of exosomes involves ESCRT machinery and Alix that are recruited to the endosomal membrane and sort the ubiquitinated proteins into intraluminal vesicles (ILVs). In addition, there are ESCRT independent mechanisms that include lipids and tetraspanins. MVBs: Multivesicular bodies, ILVs: Intraluminal vesicles. Figure taken from [10].

A recent study has reclassified EVs based on a thorough characterization of the RNA, DNA, and protein constituents. The authors employed high-resolution density gradient fractionation and direct immunoaffinity capture to isolate and analyse the composition of EVs released by tumour cell lines and isolated from plasma, in order to precisely establish the different cargoes of EV subpopulations. They provide evidence

that, in contrast to other studies, exosomes are not carriers of dsDNA and DNA-binding histones [24].

Finally, apoptotic bodies and apoptotic vesicles are generated during apoptosis. These EVs display variable dimensions ranging from 100 nm to 5 µm and are characterised by PS exposure, thus becoming easily detectable by Annexin V [24]. It is evident that although overlapping sizes and characteristics are shared by different EV subpopulations, as reported for CD9, CD81 and CD63 expression as well as other markers, major concerted effort is being made to find discriminating features to help distinguishing between the EV types.

EVs can carry a cargo of proteins and nucleic acids, a discovery made by most groups investigating in the EV field, which is particularly attractive to understand their roles as mediators or biomarkers. The general consensus is that sorting into EVs is not occurring by chance but that instead the presence of selected molecules follows rules still largely unknown. The mechanisms controlling the sorting of selected proteins into EVs depend on the ESCRT machinery and post-translational modifications (PTMs). These latter are alterations of the proteins that enable their active or inactive state [29]. Among the different PTMs ubiquitination, sumoylation, phosphorylation and glycosylation appear as the most frequent during packaging of proteins into EVs [10]. The sorting of nucleic acids into EVs is described in Section “1.1.10. Tumour EVs as biomarker”.

1.1.4. Isolation and characterisation of EVs

The heterogeneity of EV populations and the heterogeneity of single EVs belonging to the same EV subtype, but showing differences in composition or surface marker expression complicates research in the field ever since the discovery of the EVs. The overlapping dimensions and marker expression additionally hampers the isolation of distinct and “pure” populations [5]. There are different methods to isolate EVs and each presents advantages as well as disadvantages in terms of contaminations, purity and yield. Like many other research groups also my hosting laboratory stumbled across same technical challenges in 2001. Due to the nanometer size of the vesicles the main isolation method was differential ultracentrifugation combined or not with density gradient separation for many years [30].

No definitive consensus has been found yet on the optimal isolation method, which often depends also on what kind of vesicle is the subject of the investigation or particular characteristics such as expression of particular proteins. The choice of a particular

purification method can also depend on what is the target material that will be investigated, e.g. proteins or nucleic acids. As shown in Figure 1.1.4 and reviewed by [31], the main methods applied to purify EVs are the following: differential ultracentrifgation, floatation-related methods, precipitation-based protocols, immunoaffinity isolation, flow cytometry, ultrafiltration, field flow fractionation and size-exclusion chromatography (SEC). Different studies have been performed to compare the different isolation methods on the same starting biological samples, however the choice of a protocol remains a challenging question that often influences the results of the investigations.

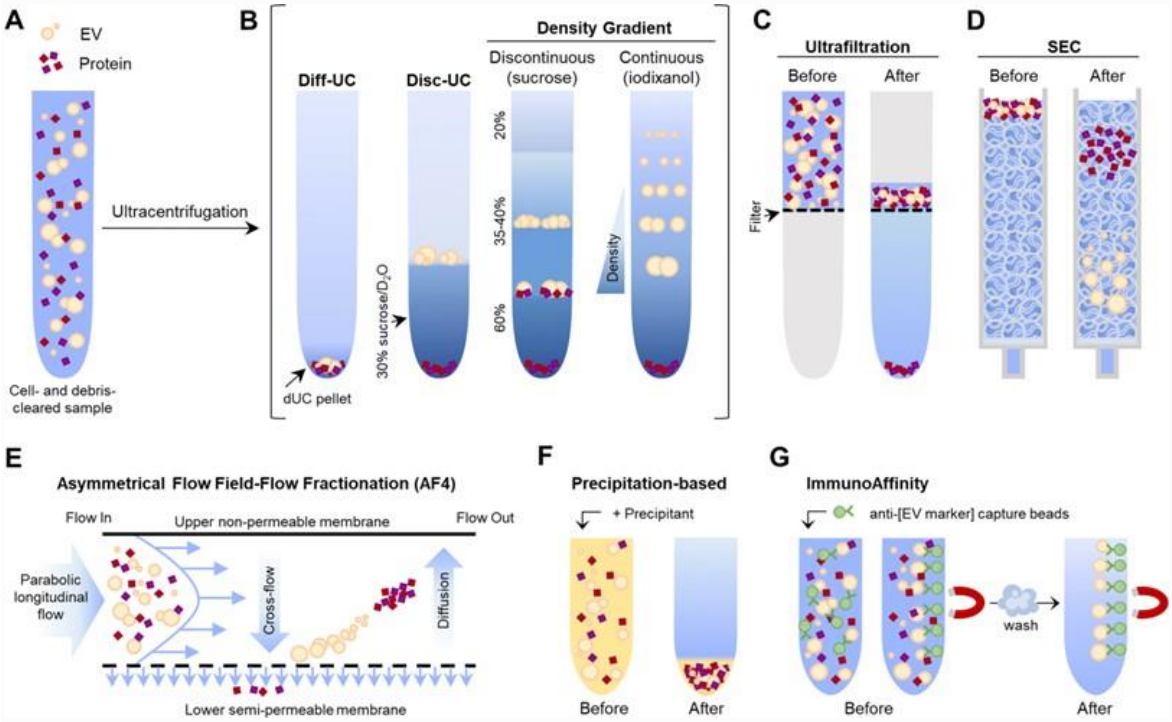

Figure 1.1.4. EV isolation methods. The different methods currently used to isolate EVs and their subpopulations. A) ultracentrifugation B) gradient-based isolation C) ultrafiltration D) size-exclusion chromatography E) asymmetrical field-flow fractionantion F) precipitation-based G) immunoaffinity-based separation. Figure taken from [31].

The most widely used ultracentrifugation method refers to indications from 2006: two centrifugations at 400×g (to eliminate cells) and 2,000×g (to eliminate debris); then the supernatant is subjected to centrifugation at 10,000×g to obtain apoptotic bodies and MVs in the pellet. After this, the supernatant is subjected to an ultracentrifugation at 100,000×g for 1–2 h to obtain an EV pellet that can be further suspended and washed in a by ultracentrifugation at 100,000×g for 1–2 h [30]. The combination of ultracentrifugation methods with floatation separates vesicles according to the density of EV subtypes, being exosome density 1.15-1.19 g/ml, endoplasmic reticulum vesicles density 1.18–1.25 g/ml, Golgi vesicles density 1.05–1.12 g/ml [30] and protein at 1.35–1.41 g/ml [32].

Ultrafiltration separates EVs based on molecular weight cut-offs or defined pore sizes of semipermeable membranes.

While the ultracentrifugation is a time-consuming method that can lead to aggregation and variable contaminations in the EV pellet, ultrafiltration is a faster method that interferes at minimal level with the EVs [33]. This can also be said for field-flow fractionation that separates the vesicles in a channel with parabolic longitudinal flow combined with an external gradient or "field". However, this method does not discriminate between EV populations or separates proteins [31].

A promising method seems to the size-exclusion chromatography that is based on the different elution profiles characterizing the differently-sized EVs, which run through a porous polymer that constitutes the stationary phase (gel filtration matrix or resin) and carried through the mobile phase of the SEC column. This technique separates EVs from proteins. Indeed, these are slowed down when they enter the polymer pores, thereby eluting later than EVs. Instead the bigger EVs travel faster along the column and so elute first, right after the column's void volume, because they are bigger than the polymers' pores [34].

Precipitation-based protocols, such as ExoQuick, rely on polyethylene glycol (PEG)-based volume exclusion precipitation. Here the yield is high, but the pellet contains all soluble particles including proteins and EVs. The EV preparations obtained with this method may be acceptable for RNA and microRNA studies especially in the translational setting where samples of biological fluids are often limited, but are not recommended for functional studies, due to contaminants that would influence obtained results.

Another major isolation method is the immunoaffinity separation that aims at recovering only specific EVs based on their surface protein expression. Here, EVs are captured through specific antibodies, which can be coupled to beads to be then separated magnetically or by centrifugation (Figure 1.1.4). This represents a good method to obtain only a certain population of EVs, e.g. EVs expressing the tetraspanins CD63, CD9 and CD81, but the lack of a pan-EV marker that still needs to be identified if existing, limits the utility of this isolation technique.

1.1.5. Intercellular crosstalk via extracellular vesicle

Once released in the extracellular compartment, EVs can interact with the recipient cells in several ways. As shown in the Figure 1.1.5, they can dock at the plasma membrane of a target cell or they can fuse directly with the plasma membrane; otherwise, they can be

endocytosed or uptaken by micropinocytosis and phagocytosis and release their content inside of the recipient cells [11, 35].

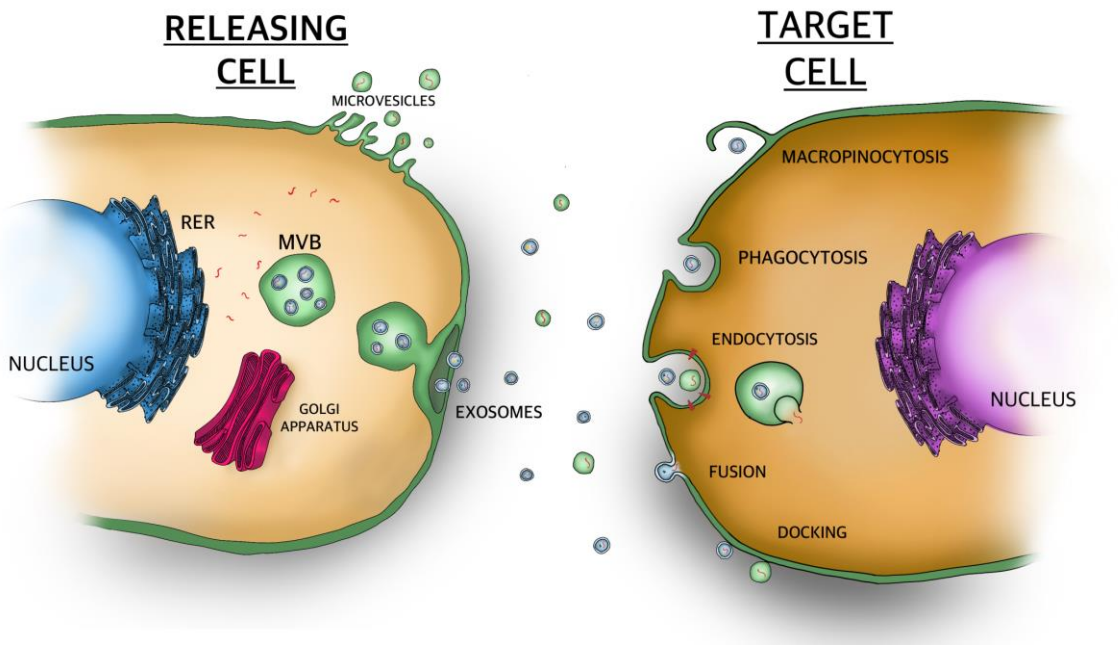

Figure 1.1.5. Different types of extracellular vesicle uptake. EV can interact with the target cells in different ways as illustrated and release its content inside the recipient cell. Figure is an original artwork by A. Shahaj.

The individual types of interaction of EVs is probably dependent on their surface composition that determines recognition by the target cells. As with the sorting of proteins or nucleic acids, the uptake of EVs by one cell rather than another seems to be a controlled and specific process. These aspects are subject to intense investigation and the first studies date back to 2000 years, when Denzer and coworkers reported that B lymphocyte-derived exosomes that contain major histocompatibility class II (MHC Class II) specifically bind to follicular dendritic cells, but not to other cell types [36].

EVs can interact with target cells also only via membrane-membrane interaction without delivering their content, as has been shown for MVs derived from activated platelets, which are coated with tissue factor and which can interact with P-selectin expressed by neutrophils, macrophages and other platelets [37]. Similarly, EVs expressing MHC Class II have been shown to stimulate T cell receptor (TCR) of cognate T cells [38]. Apart from the delivery of the content of an EV into the acceptor cell, several studies have demonstrated an involvement of EVs in exchange of proteins, RNA or toxic components, such as prions [17, 39, 40].

A definitive consensus on the mechanisms of targeting, interaction and uptake and their respective outcomes for the EV accepting cell is far from being reached by the

scientific community of the field. One fundamental aspect in need of elucidation is the targeting specificity of EVs. A generic uptake of EVs from different cellular origins has been shown for HeLa and other cell types cells, such as lung and colon cancer cell lines [41]. Even interspecies interaction could be observed between mouse and human. In fact, Valadi and colleagues could assess the presence of new mouse proteins in human mast cells, indicating that the genetic material present in mouse exosomes was functional and was translated after entering a cell [42].

1.1.6. Functions of EVs

Due to their heterogeneity and the limited understanding of their natural targeting and interaction mechanisms, the "real" functions of EVs remain to be unravelled. *In vitro* studies are usually performed using isolated EVs that are added to cell cultures to study the effects of EVs at different levels. This setting has a major disadvantage in that the EV-cell interaction is artificially created. Nonetheless, major advances in the understanding of EV functions have been achieved using this experimental setting.

Importantly, experiments performed in *in vivo* settings have greatly elucidated the natural targeting of EVs [43]. Since the release of vesicles is a conserved mechanism across species, a wide variety of biological functions have been described to EVs. The first function that has been identified is the elimination of unwanted material, a concept that has been recently revisited by Michel Vidal, who advanced the view that reticulocytes and other cells use EVs to dispose of components that may prevent their differentiation or any other development process [44].

Other widely investigated functions include the transfer of proteins and nucleic acids signalling to the acceptor cells after docking on their membrane via cell surface or to endosomal receptors. For example, EVs carrying microRNA miR-21 have been shown to function through binding to endosomal TLR8 in human immune cells, thereby triggering IL-6 and TNFα release that sustains tumour growth and metastatic potential [45].

Regarding their physiological functions the identification of the physiological targets of EVs will greatly enhance the current understanding of EV turnover and effects and will help to develop new experimental models and assays. Examples of physiological functions have been described in immune cell intercellular crosstalk. Early research showed that during immune response exosomes exposing MHC-peptide complexes secreted by B cells could stimulate T cells by activating the T cell receptor [9, 38]. Similarly, EVs from antigen presenting cells (APCs) were shown to activate CD4 and CD8

T cells due to their expression of MHC Class I and II. These discoveries stimulated great interest in the use of EVs as natural stimulators of the immune system in cancer. To this end, dendritic cell derived exosomes (DEX) were identified as suitably equipped devices for cancer immunotherapy [46]. This gave rise to clinical trials, which advanced cancer patients received DEX only or DEX derived from IFNγ-matured dendritic cells [47].

One major study has elegantly demonstrated the role of EVs and their microRNA content in the immunological synapse during intercellular communication of APCs and T cells. Mittelbrunn et al demonstrated the existence of an antigen-dependent unidirectional transfer of microRNAs by exosomes from the T cell to the APC, thus suggesting a targeted and controlled mechanism of intercellular crosstalk can be mediated by EVs [48]. Other physiological functions of EVs have been identified in angiogenesis and tissue regeneration. EVs can indeed deliver complex information to endothelial cells thereby inducing a pro- vs an anti-antigogenic signalling, leading to the control of blood vessel formation in tissues [49]. Similarly, EVs have been shown to play major roles in cardiac hypoxia and regeneration, as show in newborn mammalian and zebrafish hearts, which in contrast to adult mammalian hearts can regenerate completely after injury [50].

1.1.7. Tumour EVs

Tumour cells release EVs endowed with pro-tumorigenic features and can act at multiple levels [51]. Tumour EVs have been shown to boost angiogenesis, activate cancer associated fibroblasts, trigger tumour cell epithelial-mesenchymal transition and mould the immune environment to a condition of immune escape, thus promoting tumour progression and metastasis. These actions may operate between neighbouring tumour cells or at distance via EV circulation [52-54].

Functional studies with tumour EVs helped to define the molecular mechanisms involved in their pro-tumorigenic functions such as creating a premetastatic niche, as elegantly demonstrated by Peinado and co-workers in 2012 in mice, whose bone marrow progenitor cells were educated by administrated melanoma exosomes isolated from conditioned medium of highly metastatic melanoma cells. These exosomes increased the metastatic behaviour of primary tumours thereby supporting growth and metastasis [4]. EVs also contribute to the organotropic metastasis based on their integrin expression, namely exosomal integrins α6β4 and α6β1 were associated with lung metastasis, while exosomal integrin αvβ5 was linked to liver metastasis [55].

Through the release of EVs the tumour cells can influence and shape the whole tumour microenvironment. In fact, it has been shown that EVs can interact with fibroblasts, endothelial cells, mesenchymal stem cells, myofibroblasts and cells from the immune system to generate a favourable microenvironment that fosters tumour growth and disease progression. Additionally, tumour EVs contribute to drug resistance by sequestering drugs, as shown for immunotherapeutic antibodies like trastuzumab, anti-CD20 or even anti-PD-L1 avelumab [56]. Tumour EVs have also been shown to actively export cytotoxic drugs from the cells thereby preserving the cells from drug action [57].

Another mechanism exploited by tumour cells for self-protection is to use intercellular EVs transfer to propagate drug resistance by horizontal transfer of molecules that alter apoptotic programs and cell cycle control. The several examples include: drug efflux pumps thereby contributing to multidrug resistance; survivin, an anti-apoptotic protein that promotes cell survival; microRNAs that can be transferred or expulsed via EVs to maintain tumour cell homeostasis; transfer of pro-survival cargoes such as platelet-derived growth factor receptor-beta (PDGFR-β) that has been found as enriched during escape of melanoma cells subjected to BRAF inhibitor PLX4720 [56]. Figure 1.1.7 summarises the main detrimental effect of tumour EVs.

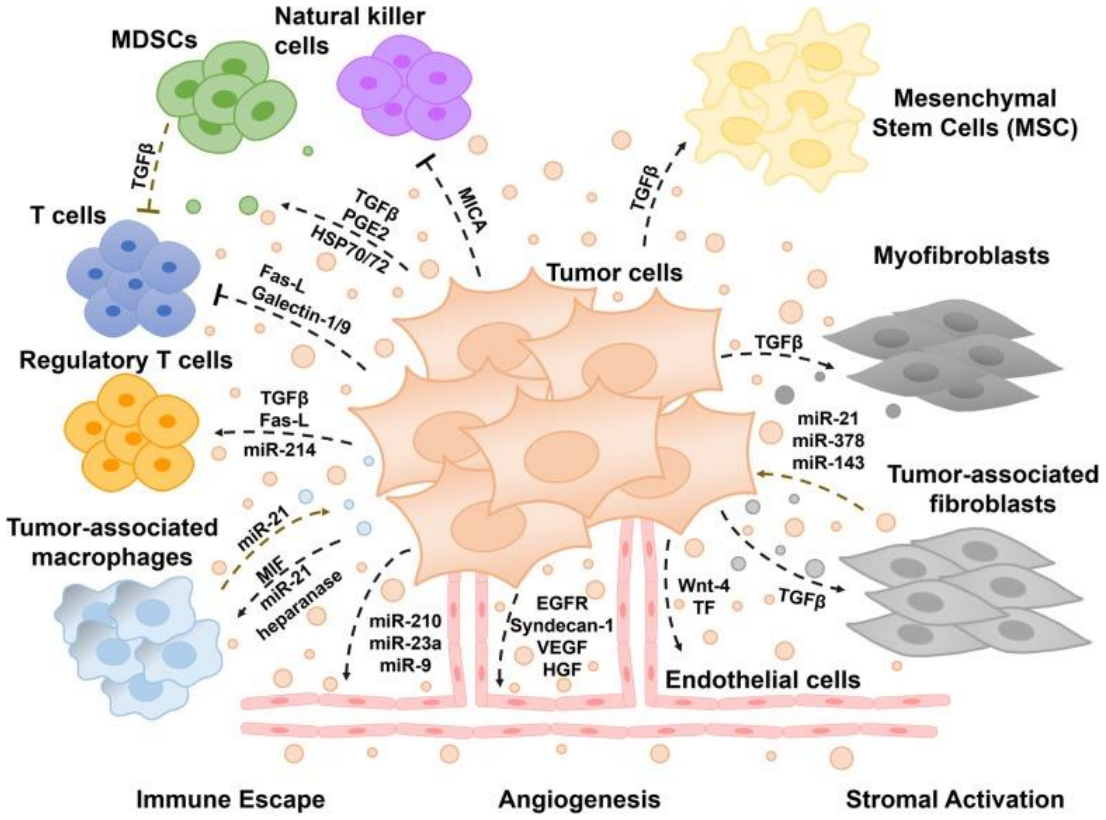

Figure 1.1.7. Effects of tumour EVs. General scheme of how EVs secreted by tumour cells can influence the cells composing the tumour microenvironment. Through their transport of bioactive molecules tumour EVs create a favourable environment in support of tumour growth and metastatisation. Figure taken from [56].

1.1.8. Immunomodulatory properties of tumour EVs

1.1.8.1. Tumour immune escape

Cancer development creates or originates from a chronic inflammation condition due to reactive oxygen and nitrogen species that typically generate mutations. In addition, various mechanisms contribute to suppress the immune system thereby creating a microenvironment that fosters tumour growth. These pro-tumorigenic pathways shape both innate immune cells, such as monocytes, macrophages, neutrophils, dendritic (DC) and natural killer cells (NK) and adaptive immunity T and B lymphocytes.

To avoid immune responses, tumours can impair the capacity of the immune system to eliminate them or, by losing target antigen expression, determine a state of non-recognition by immune cells. Main tumour immune evasion mechanisms can be summarized as follows: down regulation of MHC Class I expression, lack of co-stimulatory signals necessary for antigen presentation, secretion of immunosuppressive factors by cancer to inhibit immune responses, modulation of antigen expression, limiting the ability of the immune system to recognise the tumour cell as 'non-self', lack of release of

inflammatory warning signals by cancer cells. In my project I focused mainly on the mechanisms exploited by melanoma EVs in conditioning immune cells in the context of IC expression and targeted therapy resistance development. My hosting laboratory contributed to the identification of pathways exploited by melanoma to skew monocytes into myeloid-derived suppressor cells (MDSCs), which they first discovered in 2007 [58].

1.1.8.2. Innate immunity and MDSCs

The innate immunity is crucial in the maintenance of homeostasis and represents the first defence mechanism of the organism against pathogens. In the context of tumours, members of the innate immunity can detect mutated cells as altered self in response to damage-associated molecular pattern (DAMPs), such as tumour-derived DNA, and eliminate them (via NK i.e. granzyme B release) or alert and prime the adaptive immune system via antigen presenting cells (DC and macrophages producing IFNγ). Nonetheless, tumours have developed strategies to skew innate immune cells such as monocytes and neutrophils into potent tumour allies called MDSCs. These are pro-tumorigenic cells with immunosuppressive properties often recruited to tumour site by chemoattractant cytokines.

MDSCs exert their function in the tumour microenvironment (TME) by inhibiting T and NK cells through various mechanisms. Among others, MDSCs can express IC such as, PDL2, GAL9, CD155 and the binding to their receptors PD1, TIM3, CD226, TIGIT, CD96 localised in the T and NK cell surface, leads to inhibitory signalling and immune suppression [59, 60]. Thus, MDSCs are associated with increased tumour burden in several cancer types [61]. Gabrilovich et al wrote several reviews to explain the MDSC heterogeneity. It is known that MDSCs originate from different myeloid progenitors whose maturation is interrupted. In physiological conditions these cells would develop into granulocytes, dendritic cells or macrophages but in the tumoral condition, bone marrow myelopoiesis deviates into MDSC generation.

Several factors such as tumour cells or microenvironment may be involved in MDSC expansion and activation involving IL-6 or TGFB and IFNγ production. This myeloid cell dysfunction can also be induced by tumour EVs [62, 63]. The MDSC immunosuppressive function depends on their phenotype, as described in 2009 by Gabrilovich & Nagaraj. These authors explained that cytokines generally secreted by tumour cells can induce MDSCs to produce arginase-1 enzyme, which increases production of reactive oxygen and

nitrogen species by L-arginine depletion. These events inhibit T cell proliferation or reduce T cell survival [64-66].

Concerning the MDSC phenotype, their heterogeneity is a challenging issue. They do not express cell-surface markers that are specific for monocytes, macrophages or DCs, instead they display a granulocytic and monocytic mixture morphology. Indeed, there are two populations of MDSCs in humans: granulocytic or PMN-MDSCs ($CD15^{+}CD11b^{+}$ PMNs), and monocytic M-MDSCs ($CD14^{+}HLA\text{-}DR^{neg}$) detectable in whole blood and purified plasma and peripheral blood mononuclear cell (PBMCs) [67]. Both types of MDSCs inhibit T cell responses including T-cell proliferation and function with different mechanisms [68]. IC molecules are directly involved in these mechanisms and for this reason are part of this study. In fact, recent evidence showed that PDL1 is expressed by tumour-induced MDSC in an autocrine manner via type I IFN. Thus, MDSCs can continue to suppress T cell activity maintaining PDL1 expression even in absence of IFNγ [69]. Moreover, EVs from drug-resistant cell variants can enhance TGFβ secretion and anti PDL1 expression in drug sensitive breast carcinoma cells, thus enhancing resistance to the anti-tumour immune response [70].

1.1.8.3. Adaptive immunity and IC expression

T cell activation requires two different stimuli: one occurs through the MHC antigen presentation by APC to the antigen-specific T cell receptor TCR, while the other is represented by co-stimulatory or co-inhibitory signals, which tightly regulate T cell activity. These signals are conveyed by one of the more than twenty discovered IC molecules that belong to immunoglobulin gene superfamily (CD28, CD226, TIM, BTLA, CD160, CD155, TIGIT, CD96, LAG3), or part of the tumour necrosis factor (LIGHT) or tumour necrosis factor receptor (HVEM) genes [71].

The negative IC effects compete with co-stimulatory signals to control T cell activity, by suppressing activation and impairing T cell survival. Controlling the co-inhibition reduces the risk of tumour development from chronic inflammation but, in the case of tumour development, T cell inhibition on the contrary, may have a pro-tumorigenic effect. Thus, investigating these IC may be important to discover potential drug targets for cancer therapy. On the other hand, the identification of a non-invasive way to monitor the activation of the immune system in patients undergoing therapy may help to predict their response.

Given that IC have different effects on T cells depending on the counterpart molecule they bind (co-inhibitory or co-stimulatory) it seems important to investigate the entire panel of molecules, ligands and receptors, to get a complete overview of the immune response scenario. Among T cell subpopulations, regulatory T cells abundantly express negative IC. This type of T cells is in fact devoted to the maintenance of tolerance to self-antigens thereby preventing autoimmune disease. In cancer Treg are major contributors to immunosuppression together with MDSC. Treg are $CD4^+$ T cells displaying a CD25 and Foxp3 expression that secrete TGFβ and IL-10. Treg prevented co-stimulation of T cells through the expression of CTLA-4, an IC targeted by ipilimumab, an immune checkpoint inhibitor widely used in cancer therapy [72]. IC expression by T cell subsets is detailed in 1.2 Section.

1.1.8.4. Tumour EVs target immune cells

Tumour cells release a considerable amount of EVs into the TME, which can interfere with the immune system through several mechanisms acting on different cell types and mainly contributing to create a pro-tumorigenic and immunosuppressive environment [73, 74]. Among the different EV subfamilies several studies identified especially tumour exosomes as active contributors to tumour escape mechanisms by interfering with the components of the innate and adaptive immune response via ligand-receptor interaction or modulating gene expression via microRNA [75, 76]. Major effects on the different immune cell populations are summarized in Table 1.1.8.4 [54].

Monocytes

In some tumours like glioblastoma, tumour EVs have a predilection for monocytes inducing a M2 phenotype and PDL1 upregulation via STAT3 pathway [77]. Moreover, tumour EVs are involved in the resistance to chemotherapy via microRNA by targeting human monocytes in neuroblastoma through miR-21/TLR8-NF-κB and miR-155/TERF1 pathways [78].

Macrophages

Tumour EVs deriving from breast cancer cells can alter macrophage polarization into M2 phenotype via gp130/STAT3 causing a decrease of IFNγ gene expression and the increase of IL-1β, IL-6, IL-10, CCL2, CXCR4 [79]. In addition, it has been shown that macrophage activity is modulated by breast cancer-derived exosomes also via TLR2 and NF-kB pathway

[80]. A crucial role in immunomodulation is played by the exosomal microRNA cargo; in fact, miR-222 and miR-301a were reported in ovarian and pancreatic cancer, respectively, to induce an M2 phenotype in macrophages involving SOCS3/STAT3 pathway or in a HIF-1a or HIF-2a-dependent manner [81, 82]. Moreover, there is evidence showing that PD1 immune checkpoint is upregulated in macrophages of patients with advanced-stage gastric cancer and that treatment of macrophages with tumour exosomes *in vitro* could be responsible for this phenomenon [82]. Indeed, the expression of negative immune checkpoints on immune cells has an immunosuppressive effect on the immune system.

Dendritic cells

Recent data from *in vivo* experiments shows that the treatment of dendritic cells with tumour exosomes from hepatocellular carcinoma significantly increases the number of $PD1^{+}CD8^{+}$T cells and also the response to targeted therapy (sorafenib) when combined with both exosome treatment and anti-PD1 antibody [83]. This information may be used in the clinics to improve the treatment outcome and enhance the relevance of combined therapies. Other evidence showed that tumour-derived exosomes interact with dendritic cells via microRNA miR-203, which contributes to the dysfunction of dendritic cells by controlling TLR4 expression and production of cytokines, such as TNF-α and IL-12 [84]. In addition, tumour exosomes promote IL-6 secretion by dendritic cells via TLR2 and TLR4 signalling through a membrane associated mechanism that relies on HSP72 expressed by the exosomes [85].

MDSCs

Tumour EVs possess immunomodulatory properties that can deviate monocyte differentiation into MDSCs [53, 62]. EVs from breast, lung and ovarian cancer express HSP70 on their membrane and are able to interact and activate MDSCs via TLR2. In addition, the number of HSP70 expressing EVs is higher in cancer patients compared with healthy donors. Gobbo et al. also showed that their number increased after *in vivo* and *in vitro* treatment of tumour-bearing mice or melanoma cells with chemotherapeutic agents [86]. Furthermore, in renal cell carcinoma, exosomal HSP70 can determine the suppressive activity of MDSCs via phosphorylation of STAT3 in a TLR2-MyD88-dependent manner, justifying exosomal HSP70 as a significant target in this context [87]. Finally, tumour exosomes can mediate an increased proliferation of MDSC in the bone marrow of multiple myeloma via STAT3 [88] and a decrease of normal hematopoiesis in AML [89].

T cells

The detrimental effects of tumour EVs affect also T cells in an indirect fashion, i.e. acting through innate immunity cells, or in a direct fashion. In fact, cancer EVs may directly affect T cells by controlling their recruitment via CCL20 [90] and by increasing the activity of regulatory T cells through surface signalling and TGFβ [91, 92]. In addition, exosomes were shown to inhibit T cell proliferation and to increase the suppressor phenotype of T CD8+, in head and neck cancer and in breast cancer [93, 94].

Natural Killer cells

Exosomes isolated from plasma of AML patients before therapy displayed a high level of proteins involved in immune suppression, such as TGFβ1/LAP, CD39/CD73 ectoenzymes, PD1/PDL1 or Fas/FasL. In addition, the incubation of these exosomes with NK-92 cells reduced the expression of NKG2D, a molecule that positively correlates with NK cell-mediated cytotoxicity [95]. Moreover, *in vitro* breast cancer-derived exosomes from mice reduced NK cytotoxic activity against tumour cells.

Table 1.1.8.4 Tumour EV target immune cells and suppress the immune system

Target cell	Tumour	Effects/ Mechanisms
Dendritic cell	Melanoma	[c]↑ immunosuppressive activity via IL-6 and TGFβ
	Pancreatic cancer	[d]↓TLR4 expression and cytokines via miR-203
	Melanoma	↑IL6 via HSP72/ HSP105 in a TLR2/4 manner
[a]MDSC	Breast/Lung/Ovarian	↑ activation via HSP70/TLR association
	Renal cell carcinoma	↑immunosuppressive activity via p-STAT3
	Multiple myeloma	↑proliferation activation via STAT3
Macrophage	Breast	↑M2 phenotype via STAT3 transfering gp130
	Breast	↑pro-inflammatory activity via TLR2/NF-kB
	Ovarian	↑M2 phenotype via miR-222
	Pancreatic cancer	↑M2 phenotype via miR-301a
	Gastric cancer	↑PD-1 and M2 phenotype
Monocyte	Glioblastoma	↑M2 phenotype and PD-L1
	Neuroblastoma	↑chemotherapy resistance by miR-21,miR-155
	Melanoma	↑MDSC phenotype
Treg	Nasopharyngeal	↑cell recruitment via CCL20
	Head and neck	↑TGFβ, IL-10, COX-2, CD39, CD73
	Colorectal cancer	↑T reg induction via TGFβ
T CD8+	Head and neck	↑suppressor phenotype by loss of CD27/CD28
	Breast	↓proliferation
[b]NK	Acute myeloid leukemia	↓NKG2D expression and cytolytic activity
	Breast	↓cytotoxic activity
	Lung carcinoma	↓activity via TGFβ, miR23a

Notes: [a] increase; [b] decrease. Table adapted from [54]

1.1.9. EVs as therapeutic devices

Due to their small dimensions, their presence in body fluids attesting their ability to long distance travel and their natural origin, EVs have been envisaged as attractive tools for the delivery of therapeutic agents in various diseases. Although still in its infancy, growing preclinical and clinical evidence highlights the importance of EVs as therapeutic devices, especially in regenerative medicine. These aspects have been recently reviewed by Wiklander and other ISEV members (2019) who summarised the current understanding of the role of EVs as therapeutic devices thereby accentuating the increasing importance of such approaches. Indeed, mesenchymal stem cell (MSC)-derived EVs derived from diverse sources including human umbilical cord, bone marrow and adipose tissue were effective in tissue regeneration under pathological conditions such as respiratory hypertension, renal inflammatory and acute injury, hepatic injury and fibrosis, bone fractures and arthritis, myocardial infarction and neurological injuries [96].

A similar scenario can be depicted for the employment of EVs in clinical trials, which experienced a tremendous development in the last decade. In most clinical trials the source of EVs is either dendritic cells or mesenchymal stem cells. EVs are administered either unmodified or modified, e.g. loaded with chemotherapeutics, microRNAs or peptides, as in the case of DC-derived EVs administered to cancer patients. Interestingly, also plant EVs deriving from grapefruits or loaded with curcumin are being tested in cancer patients (Figure 1.1.9 [96]).

My hosting laboratory contributed to research in this setting with TRAIL-bioengineered EVs aimed at killing TRAIL-sensitive tumours [97]. Furthermore, great efforts are being made to engineer exosomes for systemic siRNA delivery to offer a less toxic and more potent alternative to synthetic nanoparticles in systemic delivery applications [98].

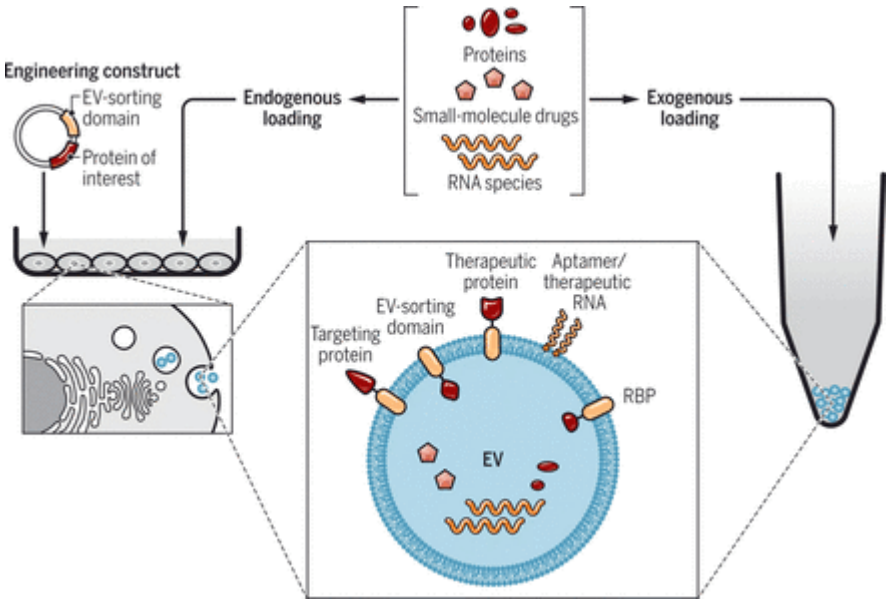

Figure 1.1.9. Strategies of EV loading and engineering. Loading of EVs with RNA, proteins, small molecule drugs after isolation or during EV biogenesis. Manipulation of the EV-secreting cell to obtain EVs expressing therapeutic and targeting proteins, EV-sorting domains, RNA-binding proteins and aptamers [96].

1.1.10. Tumour EVs as biomarker

EVs deriving from cancer cells are considered as a valuable target to identify novel biomarkers that could potentially be used in the clinics to predict patient outcomes or treatment responses. The main reason for the interest of cancer EVs as non-invasive biomarkers is that EVs reflect the biological molecule expression abnormalities of the originating cells maintaining the molecules' stability thanks to their protection by their lipid bilayer membrane [99, 100]. Additionally, EVs are part of the liquid biopsy and can be detected in almost all body fluids, comprising blood (plasma/serum), urine, saliva, tears, cerebrospinal fluid, milk, ascites and others and have been assessed in physiological as well as pathological conditions such as cancer.

The research in this field is rapidly growing, especially in view of exploitation as biomarkers, and EVs display a large array of functionally active molecules, including tumour antigens, RNAs and microRNAs that could help distinguishing cancer-derived from non-cancer-derived EVs. For example, tumour-related large EVs termed oncosomes that carry DNA have been detected in blood of prostate cancer patients, and due to their dimensions of 1-10 µm they can be detected by immunohistochemistry [19].

For EVs of melanoma patients, a subset originates from tumour cells, as suggested by the expression of melanoma antigens such as gp100, Melan-A/Mart-1 and TYRP2, together with VLA-4, HSP70 and HSP90 [4, 53]. Apart from tumour-derived EVs, also EVs originating from tumour-altered immune cells abundantly represented in plasma are particularly

appealing as source of biomarkers for monitoring early and advanced melanoma patients. These aspects, especially in view of the wide application of immunotherapeutic antibodies, which target molecules such as PDL1 and other IC also expressed by EVs, are discussed in detail in the IC Section 1.2.

Tumour EVs appear also particularly interesting due to their content of RNA and microRNA. MicroRNAs (miRNAs or miRs) are a family small non-coding regulatory RNAs. miRs regulate gene expression by acting at the post-transcription level by binding to messenger RNAs (mRNAs), promoting their repression or leading to the mRNA complete degradation (Figure 1.1.10). A single miR can target hundreds of mRNAs by interacting with the 3'untranslated region (UTR) or with the 5'UTR or with the promoter of the gene. This interaction depends on several factors, including the sequence affinity between the two RNAs, their concentration and cellular location [101]. miRs are implicated in almost all biological processes and are have a role in intercellular cross-talk [102].

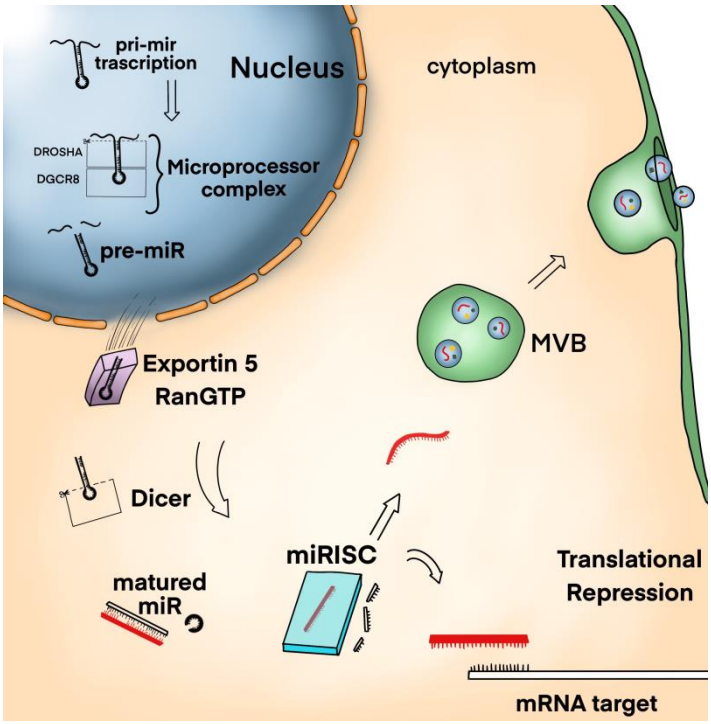

Figure 1.1.10. Overview of microRNA biogeneis. Once miRNA are transcribed in the nucleus, they undergo a maturation process through several cleavages. Mature miRs can directly inhibit mRNA translation or leave the cell of origin via EVs. Original artwork by A. Shahaj.

At the present time, 1917 miRs have been characterized in the human system (miRbase, release October 2018). miR genes are dispersed in the genome, generally located in introns and rarely in exons, and are usually co-transcribed with the gene in which they reside. Some miRs are instead intergenic and have their own promoter regulating

transcription. The functional role of miR is connected with the target gene transcripts and their biological function. Thus, miR are involved in a variety of cellular processes in physiological and disease conditions.

In tumours, miR expression is dysregulated and miR studies are relevant in different cancer research areas, from the discovery of biomarkers, by the definition of their expression patterns in tumours and in blood as a liquid biopsy, to the identification of potential therapeutic targets therapy. miRs can be shuttled from one cell to another via EVs, and several studies showed the transfer of miR loaded in exosomes through packaging in MVB [103]. A recent study showed the transfer of miRs via plasma membrane-derived EVs, a mechanism regulated by the ARF6-Exportin-5 axis and studies on cell-cell communication via EV have defined the transfer of miRs as key actors in the context of pro-tumorigenic mechanisms [104, 105].

In view of the complexity of analysing body fluids such as blood that contains not only EVs but also non-EV particles like lipoproteins and soluble proteins and cells, the ISEV community is working towards a consensus to improve standardisation and reproducibility of EV research in view of obtaining more clinical relevance of the studies [106]. Of particular interest for biomarker research are serum, plasma and urine. In the latter exosome microRNA profiling identified different profiles for progression in prostate cancer patients, as compared to healthy volunteers [107]. Commercially available EV-based diagnostic kits first appeared on the US market in 2016: ExoDx Prostate (IntelliScore) that detects prostate cancer markers in urine, and ExoDx Lung (ALK) that detects lung cancer markers in blood. Both tests were developed by Exosome Diagnostics, Inc. (USA) [108].

In the era of immune and targeted therapies major effort is dedicated to identify EV-based biomarkers to predict response to therapy. In this context, my hosting laboratory and I recently identified a set of microRNAs expressed by plasma EVs we called MDSC-microRNAs which associate to resistance to immunotherapy of advanced melanoma patients [62].

1.2. Inhibitory immune checkpoints

Immune checkpoints (IC) are cell receptors and ligands devoted to the control of immune responses, switching on or off the immune system during pathogenic infections. Several of the ligands bind to multiple receptors, some delivering costimulatory signals and others inhibitory signals, generally displaying distinct expression kinetics. The immune

checkpoints involved in switching off the immune system are also called inhibitory IC. These negative regulators are involved in modulating the duration and amplitude of the response, the maintenance of immune homeostasis and of tolerance to self-antigens, protecting the organism from autoimmune diseases [109].

IC belong to different families of membrane-bound receptors, including B7 family, the immunoglobulin superfamily and TNF family members showing distinct functional profiles and signalling pathways (Figure 1.2.1 [110]).

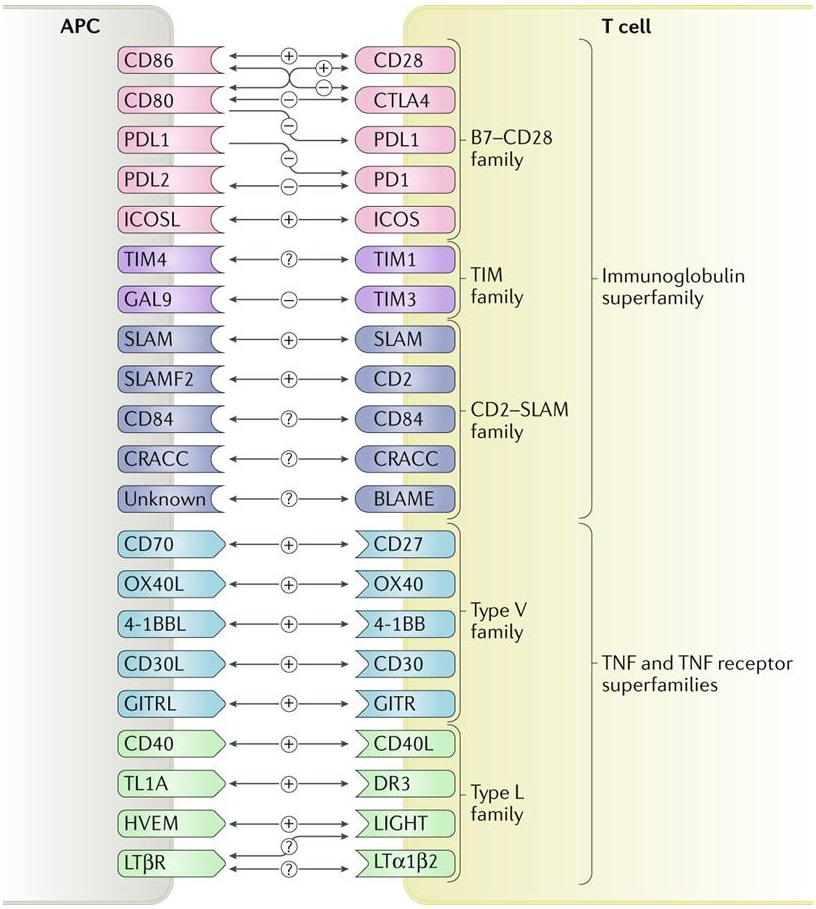

Figure 1.2.1. Immune checkpoints. IC molecules are involved in the complex array of ligand–receptor interactions between T cells and antigen-presenting cells (APCs) that regulate the T cell response to antigen via co-stimulation (+) and co-inhibition (–) signals. The different checkpoint superfamilies are shown. Figure taken from [110]

In cancer patients, negative IC may be expressed not only by immune cells but also by tumour cells, determining the suppression of the immune response at the tumour site and the promotion of tumour immune escape [111-114]. In addition, tumour cells release EVs which may carry inhibitory IC in the circulation thus playing a systemic effect [115, 116]. However, it is pharmacologically possible to unleash anti-tumour immune responses and re-establish immune-mediated tumour control by blocking the negative immune checkpoint regulators with specific antibodies [109, 117]. This discovery is based on the

pioneering work of James Allison who demonstrated that the T-cell protein CTLA-4 functions as a brake for T cells and that antagonist antibodies unlock antitumor T cell activity and cure tumours in mice [117]. Tasuku Honjo, who shared with Allison the Nobel prize for medicine in 2018, discovered another T cell brake, PD1, showing promising results as a therapeutic target [118].

After the initial studies showing the clinical effects of CTLA-4 and PD1 blockade, the success and expansion of immunotherapy targeting IC has been dramatic. At the moment, six IC inhibitors have been approved for the treatment of different tumour types by FDA in the US and by EMA in Europe: Pembrolizumab, Nivolumab and Cemiplimab anti-PD1 antibodies, and Durvalumab, Atezolizumab and Avelumab, which are anti-PDL1 antibodies [119]. Other IC are currently being studied as potential target molecules for tumour immunotherapy. In addition, the study of IC expressed in tumours and the thorough characterization of IC expression in EVs will possibly identify predictive or prognostic biomarkers [120, 121].

IC expressed by APC or tumour cells bind to different ligands that can be either inhibitor or activator molecules expressed by T cells implying a big challenge for their studies (Figure 1.2.2 AdipoGen Life Sciences).

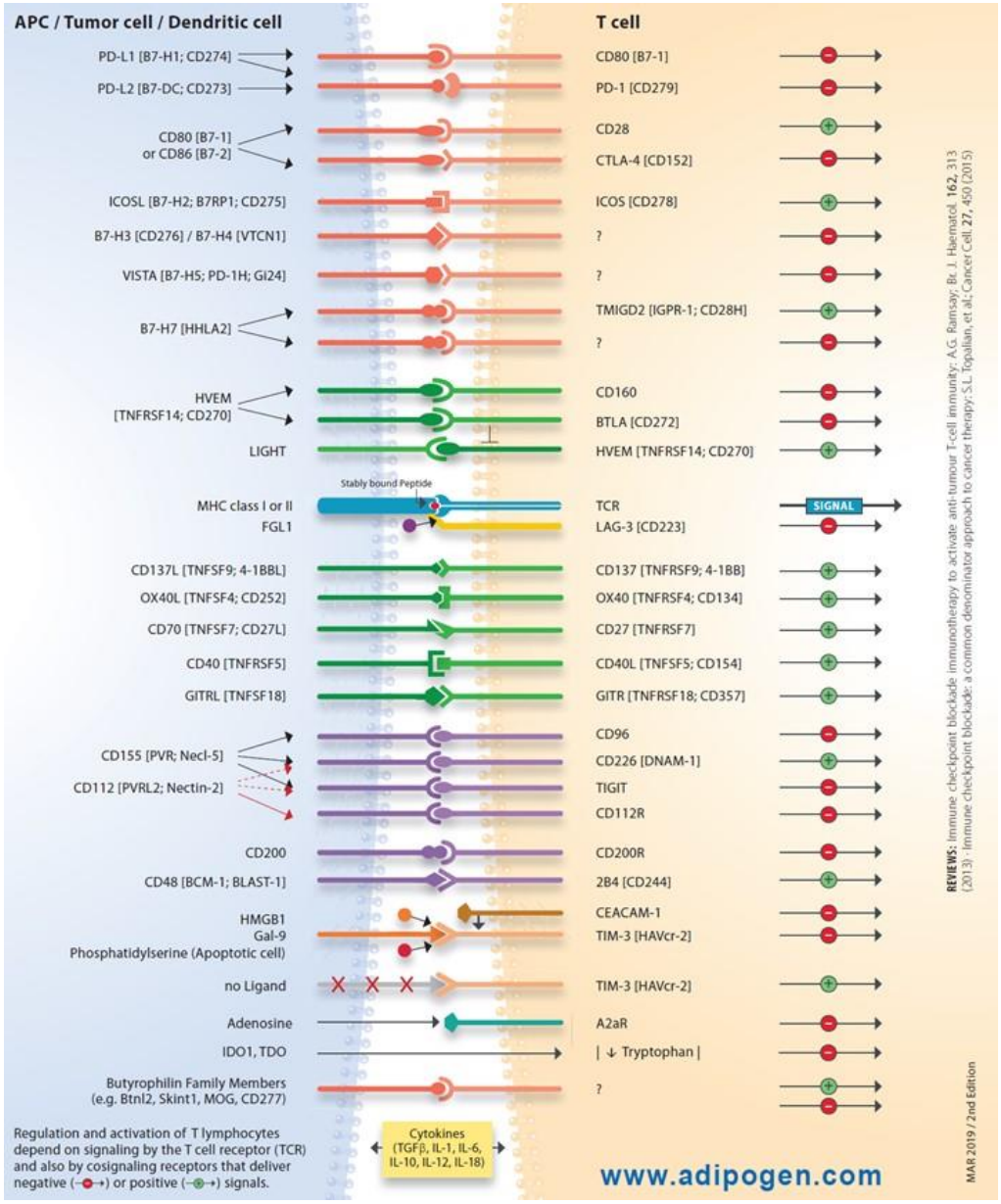

Figure 1.2.2. Immune checkpoint molecules as receptors and ligands. IC expressed by APC, tumour and T cells and the result of their interaction as a positive (green plus arrows) or inhibitor stimulus (red minus arrows) is shown. Figure taken from AdipoGen Life Sciences.

For this project, I investigated a set of IC molecules described in the literature as expressed by tumour cells including PDL1, PDL2, HVEM, GAL9, VISTA, CD155 to investigate their expression in EV released by melanoma cells (Figure 1.2.3). In addition, I analysed IC expressed by APC or by T cells, including PD1, BTLA, LIGHT, CD160, TIM3, VISTA, CD226, TIGIT, and CD96. *In vivo* relevance of the studied IC in the context of response to targeted therapy was assessed in plasma EVs and in tumour specimens of melanoma patients.

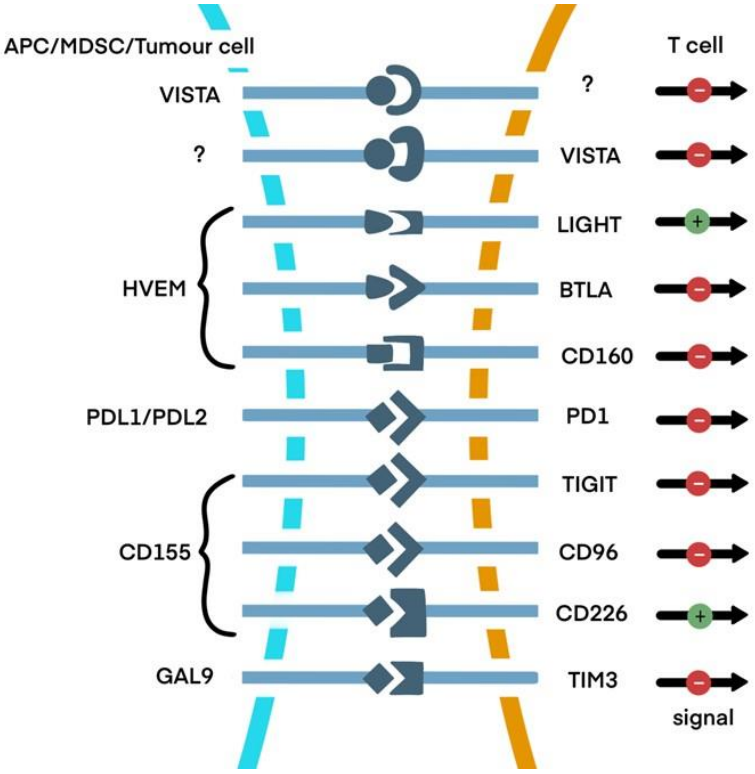

Figure 1.2.3. Selected IC studied in this project. IC molecules investigated for their inhibitory properties (red minus narrows) on T cells. Original artwork by A. Shahaj.

1.2.1. PDL1/PDL2 – PD1 axis

Programmed death-ligand 1 (PDL1) and its receptor programmed cell death protein (PD1) are the most studied IC because of the therapeutic effects when the axis is targeted in malignancies. The physiologic function of this axis is of crucial importance in normal tissues during inflammation to prevent autoimmunity and maintain homeostasis by inhibiting T cell activation and cytokine production [122].

PD1 binds both PDL1 and PDL2 (programme cell death 1 ligand 2). While PD1 is principally expressed by activated T cells, its two ligands are expressed by a large number of hematopoietic cells and other cell types, including neoplastic cells and stroma in tumours.

PDL1 and PDL2 belong to the B7 ligand Ig gene superfamily, which includes ten members regulating immune cells interaction. PDL1, alias B7-H1, is a 209 amino acids protein encoded by the CD274 gene, while PDL2, also named B7-DC or CD273, is a 273 amino acids protein encoded by the PDCD1LG2 gene. Both human CD274 and PDCD1LG2 genes have 7 exons, are located in chromosome 9, and have splice variants, one and three respectively [122].

PD1 is a 288 amino acids protein encoded by the PDCD1 Ig superfamily gene located in chromosome 2; PDCD1 has 5 exons encoding four splice variants. It is a transmembrane

protein displaying extracellular, transmembrane and cytoplasmic domains; the cytoplasmic domain presents two tyrosin-based activation sites that are absent in the PDL1 protein. After the interaction between PDL1 and PD1 takes place, the tyrosine motives of PD1 are phosphorylated by Scr kinases, and the two tyrosine phosphatase proteins SHP1 and SHP2 are recruited, determining T cell attenuation by targeting T cell receptor or CD28 co-stimulatory receptors (Figure 1.2.1.1 Bio-Rad Laboratories). The activity of T cell effectors can be impaired in different ways due to PD1-PDL1 interaction, i.e. by blocking cell proliferation or cytokine production, and by inducing T cell apoptosis [123].

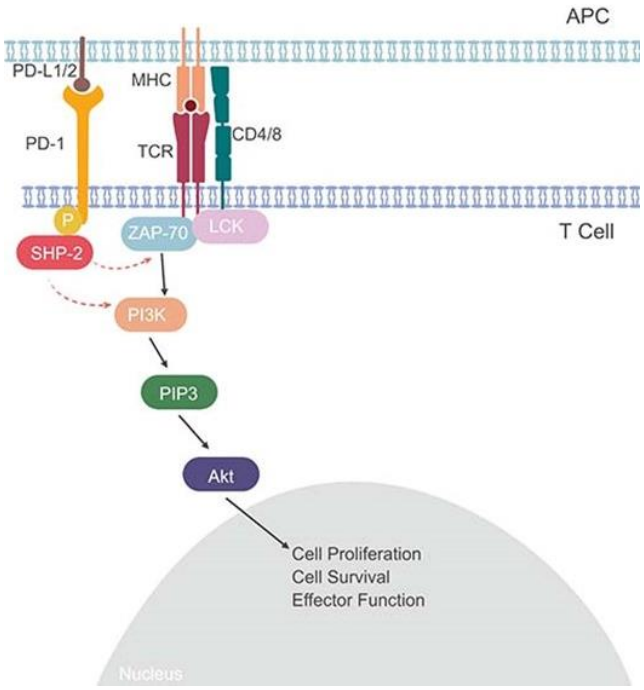

Figure 1.2.1.1. The PD1 Pathway. Binding of PD-L1 or of PDL-2 to the PD1 receptor leads to phosphorylation of SHP-2 and inhibition of signalling through ZAP-70/LCK, determining a reduction of T cell activation and effector functions. Red dotted arrows show inhibition, black arrows show activation. Figure taken from Bio-Rad Laboratories.

Although it has been shown that both PDL1 and PDL2 function in T cells overlap, PDL1 and PDL2 appear to have also individual downstream pathways which are still under investigation [124]. PDL2 binds to PD1 with higher affinity than PDL1 [125]. PDL2 is expressed by dendritic and macrophages, as well as mast cells, and its expression is induced by Th2 secreted cytokines [123].

PDL1 is constitutively expressed in several immune cells, and its expression is up-regulated in pro-inflammatory conditions [126]. Indeed, once IFNγ is produced by T cells, it activates JAK (Janus kinase) that activates STAT (the signal transducer and activator transcription) pathways, inducing IRF1 (transcription of interferon regulatory factor 1)

activation, which by binding to the promoter of PDL1 activates its transcription (Figure 1.2.1.2 [109]).

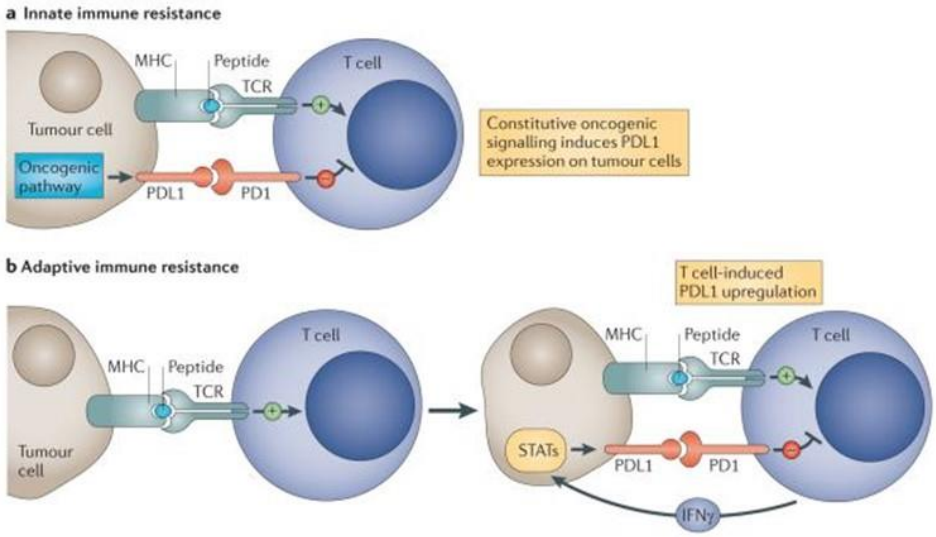

Figure 1.2.1.2. Mechanisms of PDL1 regulation. a) In innate immune resistance PDL1 is constitutively expressed by tumour cells independently of inflammatory signals in the tumour microenvironment. **b)** Adaptive immune resistance occurs when PDL1 is induced in response to inflammatory signals that are produced by an active antitumour immune response. Activation of the AKT and STAT3 pathways has been reported to drive PDL1 expression. IFNγ, interferon-γ; MHC, major histocompatibility complex; TCR, T cell receptor. Figure taken from [109].

The pathways regulating PDL1 expression are various depending on the type of cells (Figure 1.2.1.3 [122]). Especially in tumour cells, its expression can be induced by deregulated oncogenic pathways, or by epigenetic mechanisms including miRNAs (Table 1.2.1.1 [122]). All these mechanisms increase PDL1 expression in tumour cells and enhance immune escape by augmenting the inhibition of local T cell function [122], protecting tumours from immune system attack, and making tumour cells more resistant to apoptosis.

Table 1.2.1.1. Regulators of PD-L1

Type	Regulators of PD-L1	Tissue type
Inflammatory signalling	IFNγ, IFNα, IFNβ	↑ different tumours, endothelial cells, monocytes, dendritic cells, macrophages, neutrophils
	TLR4, TLR3	↑ different tumours, endothelial cells, monocytes, dendritic cells, macrophages
	IL-1β,IL-4, IL-6, IL-10, IL-12, IL-17, IL-24, IL-27	↑ different tumours, dendritic cells, monocytes
	TNF-α	↑ different tumours, monocytes, dendritic cells
	TGFβ	↑ dendritic cells, T cells ↓ monocytes
Oncogenic signalling	MYC, JUN	↑ different tumours
	HIF1α, HIF2α	↑ different tumours
	RELA,STAT3,MUC1-C	↑ different tumours
	PTEN loss, CDK5, PI3K-AKT-Mtor	↑ different tumours
	RAS, EGFR, ALK, MEK-ERK, MAPK14	↑ different tumours
microRNA	miR-513, miR-155, miR-34a, miR-142-5p,miR-138-5p	↓ different tumour types
	miR-93, miR-106b, miR-217,miR-200, miR-152, , miR-17-5p	↓ different tumour types
	miR-15a, miR-193a, miR-16, miR-570, miR-197	↓ different tumour types
	miR-20, miR-21, miR-130b	↑ CRC
Genetic alteration	amplifications, translocations, disruption of 3' UTR region	↑ different tumours
Post-translational regulation	CMTM6, CMTM4	↑ different tumours, dendritic cells
	CDK4, GSK3B	↓ cervical cancer, breast cancer
	B3GNT3, CSN5	↑ breast cancer

Adapted from [122]

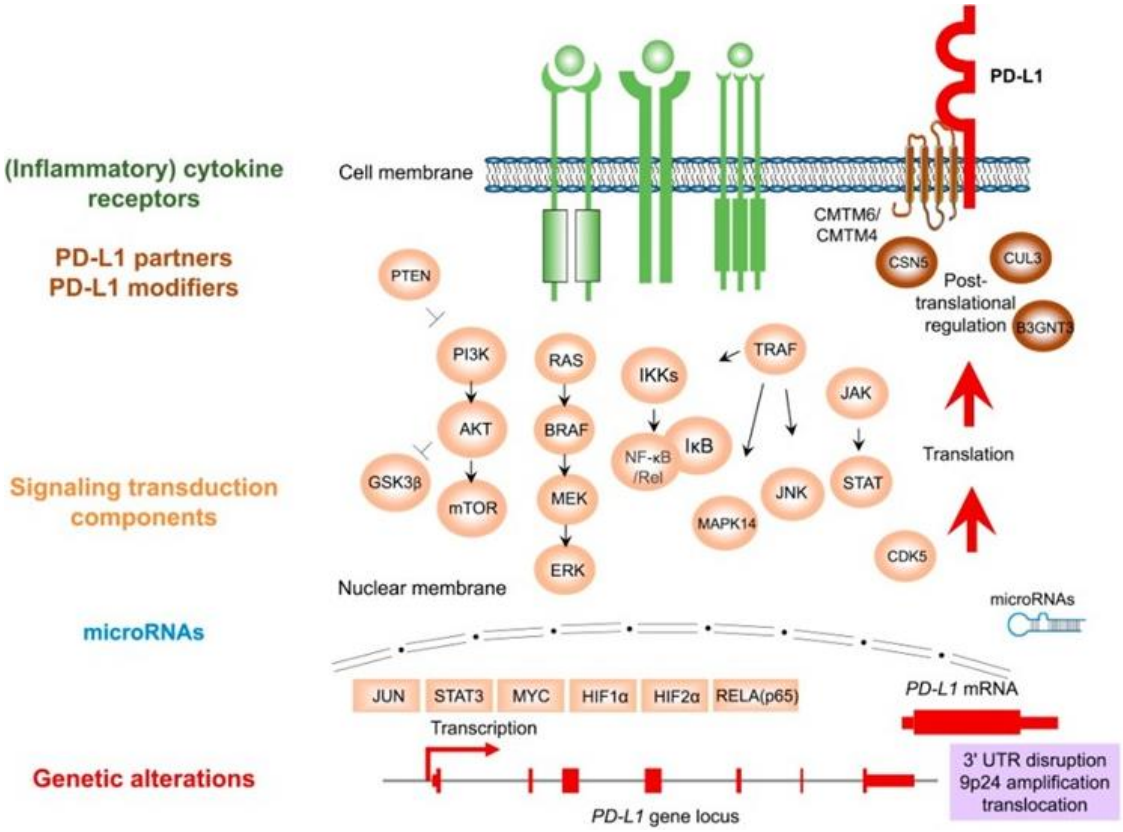

Figure 1.2.1.3. **Overview of the regulatory mechanisms of PD-L1 expression.** Regulators are color coded by class. Green, inflammatory cytokine receptors; orange, signal transduction components; blue, microRNAs; red, genetic alterations; brown, PD-L1 protein partners and modifiers. Directionality (‘‘up’’ or ‘‘down’’) and references are provided in Table 1.2.1.1. Figure taken from [122]

PDL1 expression may be a prognostic marker for some tumour types. Indeed it has been reported that tumours with high level of PDL1 expression are associated with poor prognosis, and tumours that were PDL1 negative had a good prognosis [126].

There are studies reporting PDL1 expression as a predictive biomarker of response to immunotherapy in melanoma, NSCLC and bladder cancer [121]. The relationship between PDL1 expression in the tumour and the response to immunotherapy was investigated in several clinical trials: some studies showed a correlation between PDL1 expression and the response rate but in other studies the response was not associated. These controversial results may be caused by differences in the analysis in the clinical trials, such as a different antibody used for IHC, a different cut-off used for positivity or even staining misinterpretation due to its dynamic alteration and tumour heterogeneity [127].

Since tumour cells may also express PDL2, a recent study investigated the relevance to immunotherapy of PDL2 expression in 400 tumour samples of seven different types [128].

Interestingly, results showed a high expression level of PDL2 in breast and gastric carcinomas, which was highly correlated with PDL1 expression, while in contrast, only half of the HNSCC expressed PDL2, and a low expression level was observed in melanoma and RCC. In addition, the study showed that clinical response to treatment with Pembrolizumab, an anti-PD1 antibody, correlated with PDL2 expression in HNSCC tumours, and that patients positive for both PDL1 and PDL2 at the tumour site responded better than patients that expressed only PDL1. These results indicated that PDL2 not only may predict clinical response to anti-PD1 immunotherapy, but also that targeting both PDL1 and PDL2 might enhance the clinical response.

Even though a PD1-independent mechanism promoting tumour immunity via PDL1 and PDL2 was described [129], the most studied mechanism considers both ligands having PD1 as a unique receptor, and the binding leads to anergy in PD1-positive T cells. Indeed, knockout mice for PD1 develop lupus-like autoimmune disease, and show altered T cell maturation in thymus. In cancer, T cells lose their function becoming exhausted, and the high expression level of PD1 maintains this inhibited condition. It is clear that PD1 is expressed by all active T cells, although other immune cells including B cells and macrophages may express PD1 [122, 123]. Sonja Kleffel et al showed that PD1 is expressed in melanoma cells and can promote tumour growth after activation via mTOR signalling pathway [130]. Recently, Ogando J et al identified a new downstream element of PD1 connecting mitochondrial dysfunction with T cell inhibition, enlightening novel possible targeting strategies to restore T cell activity blocked by PD1 axis [131].

During the last years immunotherapy has been concentrated on PDL1-PD1 axis, and several drugs based on blocking antibodies including nivolumab, pembrolizumab, atezonizumab, durvalumab and avelumab are approved for treatment of different types of tumours, such as melanoma, NSCLC, RCC, HNSCC, urothelial carcinoma, Merkel cell carcinoma, Hodgkin's lymphoma, MSI-H and dMMR CRC, MSI-H and dMMR solid tumours, HCC and gastric cancer [122].

Although immunotherapy repeatedly showed survival benefit in these tumour types, the clinical responses are generally observed in a minority of treated patients and predictive markers are still missing. Besides the rate of positivity of PDL1/PDL2 at the tumour level, it has been shown that the patient's tumour burden, the amount of genetic tumour mutations, the level of systemic inflammation reflected in lymphocyte-to-monocyte ratio

from full blood count, LDH values and ECOG performance status are all factors associated to response to immunotherapy [132].

In the recent years the potential of liquid biopsy has been widely investigated for biomarker detection. In parallel with PDL1 evaluation by immunohistochemistry on tumour tissue sections, several studies considered plasma PDL1 levels in relation to clinical outcome [132]. Moreover, since PDL1 is carried by EVs, its expression level has been evaluated in EVs isolated from plasma, also because studies showed EV-PDL1 can bind to PD1 on T cells and suppress its activity, thus representing a potential systemic mechanism impairing immunotherapy. In line with this, EVs from tumour cells genetically engineered to lack PDL1 expression in released vesicles showed the induction of systemic anti-tumour immunity and memory responses in a mouse model of prostate cancer [133]. In melanoma patients, high levels of PDL1 in plasma EVs were found associated with poor prognosis in [115]. In HNSCC patients, PDL1 but not PD1 expression by plasma EVs correlated with disease stages [134]. The presence of PDL1 transcript in plasma EVs was associated with good response in melanoma and NSCLC patients treated with anti-PD1 antibody [135]. In plasma EVs from glioblastoma patients and in EVs from glioblastoma cells, PDL1 expression was shown to correlate with tumour volume and T cell suppression, respectively [136]. Data regarding IC studies in EVs are reassumed in Table 1.2.1.2. Furthers studies are needed to enlighten the complexities of IC modulations occurring during anti-PD1 immunotherapy, as tumours may acquire resistance to immunotherapy by up-regulating other inhibitory IC. For example during anti-PD1 treatment, tumour cells increase expression of TIM3 as shown by mouse studies and lung cancer patients [137].

Table 1.2.1.2. Immune checkpoint expression by cells and EVs.

IC	Ligand	Immune cells	Tumour cells	EVs	Biofluid EVs	Ref
PDL1	PD1	T cells, B cells, DC, Mϕ, MDSC, Mast Cells	Melanoma, breast cancer, GC, NSCLC, GMB, CRC, PA, PCA	Melanoma, PC, GBM	Plasma melanoma, NSCLC, HNSCC, GBM	[115, 133-136]
PDL2	PD1	DC, Mϕ, Mast cells	Melanoma, breast cancer, EC, LC, HNSCC RCC, NSCLC, GC, BC	NA	Plasma HNSCC	[134]
PD1	PDL1/PDL2	T cells, B cells, NK cells, NKT	Melanoma, CRC, RCC, CLL	NA	Plasma and synovial fluid RA	[138]
HVEM	CD160/BTLA/ LIGHT	T cells, B cells, NK, DC, Mo	Melanoma, HCC, lung, CRC, GC	NA	NA	
CD160	HVEM	T cells, NK	CLL	NA	NA	
BTLA	HVEM	T cells, B cells, NK, DC, Mϕ	GC, CLL, DLBCL	NA	NA	
LIGHT	HVEM	T cells, B cells, NK, DC	Melanoma	NA	NA	
CD155	TIGIT/CD96/ CD226	DC, Mϕ, neutrophils	Melanoma, NB, glioma, CCA, OC, LAD, ML, CRC, PCA, OSA, HNSCC, MIBC	Melanoma, OC, PC	NA	[139-141]
TIGIT	CD155	Memory T cells, Tregs, NK	CRC	NA	NA	
CD96	CD155	T cells, NK	AML, T-ALL	NA	NA	
CD226	CD155	T cells, B cell, NK, Mo	Lymphoma	Platelets	Urine PC	[142, 143]
GAL9	TIM3	T cells, DC, Mϕ, Mo	Melanoma, GC, CRC, HCC, BC, ccRCC, LC, PA, ampullary cancer, breast cancer	NPC	Serum ACR Plasma NSCLC	[90, 116, 144]
TIM3	GAL9	T cells, Tregs, NK, NKT, DC, Mo	Melanoma, ccRCC, NSCLC	NA	Plasma NSCLC	[144]
VISTA	-	T cells, NK, DC, Mϕ, Mo, neutrophils	Melanoma, OC, endometrial cancer, GC	NA	NA	

Abbreviations: ACR-acute cellular rejection; AML-acute myeloid leukaemia; BC-bladder cancer; CCA-cholangiocarcinoma; ccRCC-clear cell renal cell carcinoma; CLL-chronic lymphocytic leukaemia; CRC-colorectal carcinoma; DC-dendritic cells; DLBCL-diffuse large B-Cell lymphoma; EC-esophageal carcinoma; GBM-glioblastoma; GC-gastric cancer; HCC-hepatocellular carcinoma; HNSCC-head and neck squamous cell carcinoma; LAD-lung adenocarcinoma; LC-lung cancer; MDSC-Myeloid-derived suppressor cells; MIBC-muscle invasive bladder cancer; ML-myeloid leukaemia; Mϕ-macrophage; Mo-monocyte; NB-neuroblastoma; NK-natural killer cells; NKT-natural killer T cells; NPC-nasopharyngeal carcinoma; NSCLC-non small cell lung cancer; OC-ovarian cancer; OSA-osteosarcoma; PC-prostate cancer; PCA-pancreatic cancer; RA-rheumatoid arthritis; RCC-renal cell carcinoma; T-ALL - T cell acute lymphoblastic leukaemia; NA- Not Assayed

1.2.2. GAL9 – TIM3 axis

TIM3 (T-cell immunoglobulin- and mucin-domain-containing molecule 3) receptor is encoded by HAVCR2 (hepatitis A virus cellular receptor) gene, and it exerts immunosuppressive effects by inducing apoptosis in Th1 cells when it binds to its ligand GAL9 [145]. TIM3 has been shown to bind also other ligands, including Ceacam-1 (carcinoembryonic antigen cell adhesion molecule 1), PS (phosphatidylserine), HMGB1 (high-mobility group protein B1), which are less characterized in tumour immunity (Figure 1.2.2.1 [146]).

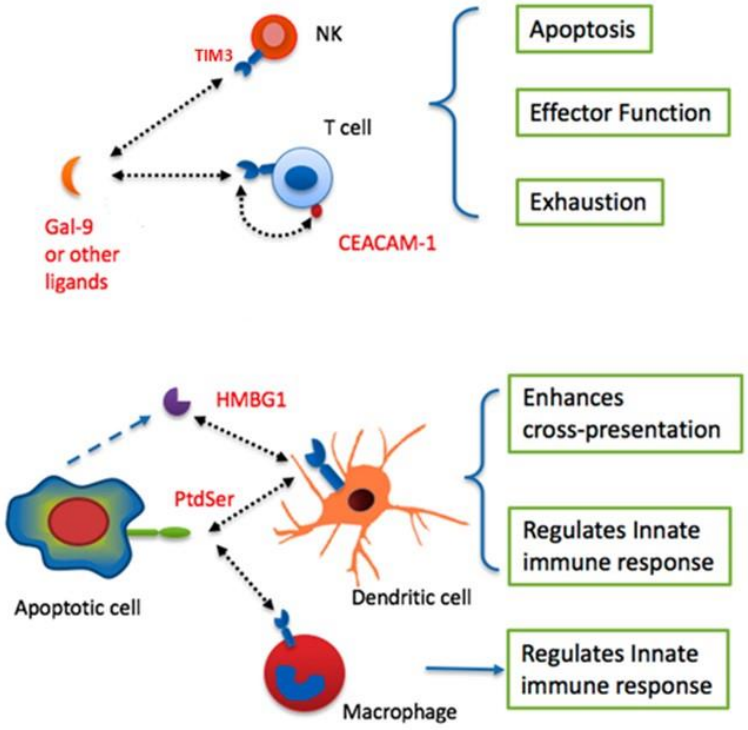

Figure 1.2.2.1. TIM3 ligands and biological functions. TIM3 signalling in T cells and NK cells may lead to the development of effector functions, apoptosis, or exhaustion. Likely dependent on the cellular context, TIM-3 signalling can enhance cross-presentation of dendritic cells (DC) or inhibit innate immune responses of DC and macrophages. Figure adapted from [146].

HAVCR2 gene is located in chromosome 5q33.2 in the human genome, has seven exons and encodes for 302 amino acid TIM3 receptor, with an N-terminal extracellular domain followed by a mucin domain, a transmembrane domain and a cytoplasmatic tail carrying tyrosine and SH2-biding residues important for the downstream signalling to the TCR [147].

TIM3 expression is regulated by the transcription factor T-bet and is present in a large number of immune cells of the adaptive response [148]: *in vitro* and *in vivo* experiments showed that constitutive or transiently increased TIM3 expression marks differentiated IFNγ producing CD4 Th1 cells, cytotoxic effector CD8 T cells, and highly active CD4FoxP3

Treg cells [147]. Nonetheless, TIM3 is expressed also by cells of the innate immunity such as dendritic cells, monocytes, macrophages and NK cells (Table 1.2.1.2 [149]).

As a checkpoint TIM3 plays an important role in immune homeostasis maintenance preventing autoimmune disease. Its role in the maintenance of self-tolerance was demonstrated in a mouse model of experimental allergic encephalomyelitis (EAE), showing that mice treated with anti-TIM3 antibodies showed an atypical hyperacute EAE and increased mortality [150]. Moreover, TIM3 knockout mice showed significantly reduced CD8 T cell responses, and impaired IFNγ production [151]. In addition, Treg cells highly positive for TIM3 were shown to restrain allograft rejection [152] and to promote T cell dysfunction in tumour models [153].

TIM3 expression has been reported also in several human tumours, not only expressed by the T cell infiltrate, but also by cancer cells, such as melanoma, ccRCC, lung, cervical cancer, and osteosarcoma [148, 154-157]. Its expression level in T cells in patients with B cell non Hocking lymphomas, or in tumour-infiltrating Tregs in patients with NSCLC correlated with a poor prognosis [158, 159]. TIM3 protein and mRNA levels in tumour tissues of renal, prostate, colon, cervical, bladder, urothelial and gastric cancer were reported to associate with a poor prognosis [147].

TIM3 has been studied as a new target for immunotherapy in preclinical tumour models, including melanoma, AML, RCC, HCC, prostate, colon, lung and gastric cancer, with promising results [147]. In the clinical setting, the most recent data of treatment with the anti-TIM3-antibody LY332 were presented at the Symposium of the Society for Immunotherapy of Cancer Clinical Immuno-Oncology during the last ASCO congress (May 2019) by James J. Harding, medical oncologist at Memorial Sloan Kettering Cancer Center and Weill Cornell Medical College. He reported that expansion cohorts had been opened for monotherapy in patients with lung cancer, and that preclinical studies clearly indicated that blocking TIM3 reinvigorates T cell function and increases the efficacy PDL1 therapy. In addition, another anti-TIM3 antibody, TSR-022, is currently tested in clinical trials for the treatment of solid tumours and lymphomas (NCT03489343) and of liver cancer (NCT03680508). Other trials combining anti-TIM3 and anti-PD1 immunotherapy in metastatic solid tumours are ongoing (NCT02817633; NCT03099109).

Among the ligands of TIM3 receptors, Galectin-9 (GAL9) is the best characterized and appears of major importance in tumours. GAL9 is a 355 amino acid β-galactoside-binding lectin protein, encoded by *LGALS9* gene, located in *17q11.2* in the human genome and

counting 11 exons. Besides TIM3, GAL9 binds other receptors, i.e. CLEC7A, CD137, and CD40 [160-162]. GAL9 is characterized by two conserved carbohydrate recognition domains for galactose binding, one in the N-terminal involved in dendritic cell activation, and the other in the C-terminal region, responsible for T cell death and TIM3 recognition [163].

GAL9 is widely expressed in various tissues and immune cells, and, probably due to its broad distribution, it has numerous and even opposite functions, from promoting inflammation through cytokine production in monocytes, to anti-inflammatory activities such as inducing T cell apoptosis and supporting Foxp3 positive Treg differentiation [164]. In concanavalin A-induced hepatitis mouse model, GAL9 was up-regulated to promote liver T cell homeostasis via Foxp3 Tregs [165]. Moreover, GAL9 appears to regulate NK cells as GAL9 knockout mice display increased IFNγ production by NK cells and enhance their degranulation [166]. In addition, GAL9 is involved in modulating cell-cell and cell-matrix interactions in cell aggregation and adhesion processes [163].

There are studies focusing on the characterization of TIM3 functions testing GAL9 as an agonist ligand for TIM3. In mice chronically infected with *Herpes Simplex* virus, administration of GAL9 reduced TIM3 CD4 T cell number and increased the number of Tregs and MDSCs [167]. On the other hand, tumour-bearing mice treated with recombinant GAL9 increased the number CD8 T cells positive for TIM3, as well as that of dendritic cells [168]. These studies show the positive and negative effect of GAL9 on different cells and in different inflammatory contexts.

The role of GAL9 in tumours remains unclear. GAL9 expression in the cell membrane of hepatocellular carcinoma, prostate, cervical, and skin cancer resulted decreased when compared with the normal adjacent tissues, in contrast, in oral cancer, pancreatic cancer, and hematologic malignancies GAL9 expression was augmented; in gastric cancer, both a GAL9 protein increase and a GAL9 transcript decrease were reported [169]. In breast cancer, GAL9 expression in primary tumours was observed to be inversely correlated with distant metastasis since a low or absent GAL9 expression was detected in metastatic patients [170].

A meta-analysis that included publications from 2002 to 2017 regarding GAL9 expression in tumour tissues showed that a high expression of GAL9 was associated with a good prognosis, in particular for cancers of the digestive trait [163]. On the other hand, another meta-analysis published in 2017 reported an association between high levels of TIM3

expression and poor prognosis in patients with solid tumours [171]. These observations showing decrease of GAL9 and increase of TIM3 associated with poor prognosis suggest that the anti-tumour effect of GAL9 may be TIM3 independent [172].

Given its immunosuppressive role promoting tumour immune escape via TIM3 pathway, the study of GAL9 targeting can unveil information for cancer immunotherapy. However, anti-GAL9 antibodies would possibly lack specificity, and *in vivo* exposure might be problematic because of toxicity. Studies investigating the anti-tumour properties of human recombinant GAL9 showed the induction of apoptotic response in haematological, gastrointestinal and melanoma cells [169]. Moreover, recombinant GAL9 administration in mice suppressed lung metastasis in melanoma [173]. Thus, GAL9 can be an anti-cancer agent, although this effect needs to be confirmed and receptors involved identified. It appears that the carbohydrate recognition domains are involved in the anti-tumour function of GAL9 [169].

Despite the anti-tumour function of GAL9, other studies support the immunosuppressive role of GAL9-TIM3 axis in both adaptive and innate immunity. When GAL9 was evaluated in tumour and plasma of melanoma patients, most of the tumours coexpressed GAL9 and PDL1, and plasma levels were higher in patients compared with healthy donors. In addition, the study showed a correlation between GAL9 levels, Th2 polarisation and poor survival. When the immunomodulatory function of GAL9 was tested *in vitro* treating PBMCs from healthy donors, a reduced proliferation, Th1 promoted apoptosis and monocyte differentiation to M2 macrophage phenotype was shown, thus proposing GAL9 as a valuable therapeutic target for metastatic melanoma patients [174]. Moreover, Wang et al showed GAL9 up-regulation in CD4 CD25 Foxp3 positive Tregs, and that the blockade of this axis neutralised the suppressive activity of these cells *in vitro* and *in vivo*[175]. Therefore, it appears that GAL9 may promote or inhibit tumour progression based on its ligand interaction in immune or tumour cells. Further studies are essential to establish GAL9 or anti-GAL9 therapeutic usage.

TIM3 and GAL9 proteins have been reported as carried by EV released by tumour cells and in plasma EVs (Table 1.2.1.2). Firstly, Keryer-Bibes et al reported that nasopharyngeal epithelial carcinomas (NPC) cells produced exosomes carrying GAL9 showing intrinsic T cell inhibitory activity as a mechanism of immune escape [176]. These findings encouraged investigations of NPC exosomes in the blood of tumour patients for the assessment of their properties on various types of target cells, and other studies followed

showing that GAL9 expression in NPC exosomes supports tumour immune evasion [90, 116]. A recent study in NSCLC patients showed GAL9 up-regulation in plasma EV and the amount of TIM3 and GAL9 correlation with malignant parameters [144].

1.2.3. HVEM and its receptors BTLA, CD160 and LIGHT

HVEM (Tumour necrosis factor receptor herpesvirus entry mediator) is encoded by TNFRSF14 gene and acts as inhibitor when it binds to its two receptors in T cells, BTLA (immunoglobulin B and T lymphocyte attenuator) and CD160 (glycosylphosphatidylinositol-anchored ligand). On the other hand, it can also act as an activator when binding to the ligand LIGHT, that is encoded by *TNFSF14* gene in various immune cells. In addition, HVEM is also the receptor to LTα (lymphotoxin α), another member of TNF superfamily, and to HSV-1 gD (herpes simplex virus glycoprotein D).

HVEM and CD160 genes are located in chromosome 1p36.32 and 1q21.1, while BTLA and LIGHT in 3q13.2 and 19p13.3, respectively. HVEM is a type 1 transmembrane glycoprotein containing in the extracellular part four cystein-rich domain (CRD) with two distinct binding regions: a CRD1 region, binding BTLA and CD160 molecules, and CRD2 and CRD3 sites binding LIGHT, thus giving to HVEM the propriety to switch between both signalling (Figure 1.2.3.1 [177]). The short cytoplasmatic domain contains the binding site for TNF receptor associated factor (TRAF) family of ubiquitin E3 ligases that initiates activation of NF-κB responsible for downstream signalling of HVEM.

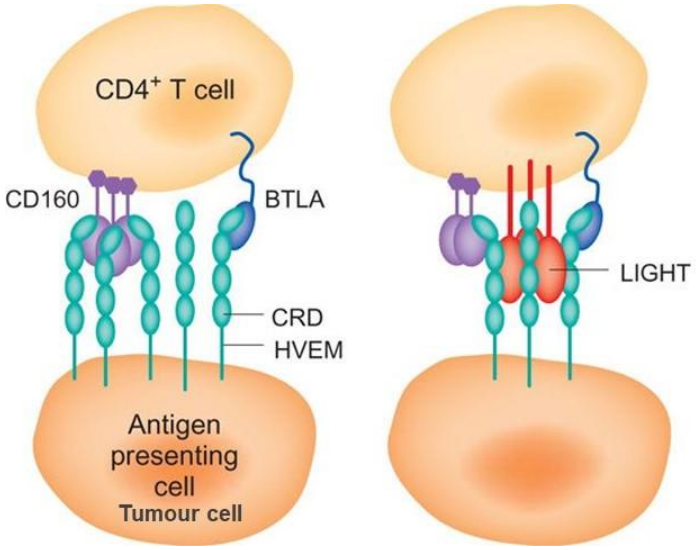

Figure 1.2.3.1. HVEM: a coinhibitory ligand binding to CD160 and BTLA and a costimulatory ligand binding to LIGHT. Both BTLA and CD160 bind the CDR1 domain of HVEM (left) and inhibit $CD4^+$ T cell activation. Binding of LIGHT to CRD2-CDR3 of HVEM does not inhibit the binding of BTLA or CD160 (right). For a T cell that expresses CD160, BTLA and LIGHT, the inhibitory signals mediated by CD160 and BTLA seem dominant. Figure adapted from [177].

The ability of HVEM to act through different signalling pathways determines a role for this axis in both immune stimulation and suppression. HVEM binds the different molecules in two distinct sites and plays important roles in inhibition or costimulation of T cells, in maintenance of dendritic cell homeostasis, and regulation of autoimmune response [178]. The interaction between HVEM and its co-inhibitory receptors BTLA and CD160 is more frequent than the interaction with LIGHT possibly depending on ligand-receptor affinity, or type of cells expressing these molecules or their differentiation stage. HVEM is also expressed by tumour cells, such as melanoma, HCC, lung, CRC and gastric cancer [179-184].

The roles of HVEM axis were investigated in human disease and disease models to discover novel therapeutic targets for cancer treatment. However, targeting this axis is challenging because of its dual function due to the multiple ligands binding HVEM.

BTLA is an immune suppressive molecule expressed by B and T cells and by other immune cells such as monocytes, dendritic and NK cells. It interacts with HVEM at a 1:1 ratio, and forms multimeric structures in the cell membrane that cluster HVEM to start the downstream signalling. BTLA has a long cytoplasmic tail of 111 amino acids that contains three tyrosine-based inhibition domains. Once BTLA binds with HVEM it recruits protein tyrosine phosphatases to limit the stimulatory pathways in the immune cells [178].

In BTLA-deficient B and T cells an increase of IgM antibodies production and hyperproliferation of T cells upon activated with anti-CD3 antibody were observed. In addition, BTLA knockout mice increased CD4 T cells in periphery and displayed higher autoimmune susceptibility disorders. Moreover, BTLA antagonists suppress alloreactive T cell responses in heart allografts [185]. The role of BTLA in tumour immunity is not clear yet. BTLA is expressed in exhausted activated anti-tumour CD8 T cells, however TILs expressing BTLA were shown to proliferate more and live longer, supporting a positive role for them in the tumour microenvironment [185].

CD160 is another ligand of HVEM, expressed only by two types of immune cells, NK and T cells. It competes with BTLA and LIGHT for binding HVEM, blocking LIGHT-HVEM interaction and the induced cytokine production [178]. The exact mechanism of this inhibition is unclear because CD160 does not have a transmembrane domain, but only a glycosylphosphatidylinositol anchors it to the membrane.

LIGHT is mainly involved in the maturation of dendritic cells and the expansion of T cells, but its expression can be induced also in B and NK cells. LIGHT is a typical membrane

ligand with cytoplasmic N-terminal and type II transmembrane domains, and an ectodomain that can be selectively cleaved by proteases and become a soluble form (sLIGHT). The binding with HVEM leads to NF-kB pathway activation and stimulates T cell proliferation, dendritic maturation, B and NK cell activation [178].

The cellular context of HVEM, BTLA and CD160 expression determines the response of this axis. If HVEM and BTLA/CD160 are expressed in the same cell (in cis), BTLA inhibits HVEM and turns off NF-kB dependent genes responsible for the survival. This inhibitory function of HVEM-BTLA interaction in cis is perhaps a self-tolerance mechanism of naive T cells competing with HVEM activation trans complex that is created when the two molecules are expressed in two different cells, and their interaction activates pathways that enhance cell proliferation [186]. All the studies investigating HVEM expression in tumours agree that HVEM expression correlates with a poor prognosis [179-184].

1.2.4. CD155 and its receptors TIGIT, CD96 and CD226

CD155 is a Nectin-like molecule also called Necl-5 that belongs to immunoglobuline superfamily and is involved in cell-to-cell adhesion, motility and proliferation. It can serve also as Polio Virus receptor, and for this reason it was originally called PVR. The CD155 gene has 8 exons and is located in chromosome 19q13.31. CD155 is expressed by immune cells and is overexpressed by tumour cells, and it was recently studied as a potential target for cancer immunotherapy [187]. CD155 has and IgV domain, a C1-like domain and a C2 domain in the extracellular region, and shows three conserved motifs with nectins in the IgV domain. CD155 has two transmembrane isoforms, and also two soluble isoforms secreted in body fluids (sCD155) [188].

CD155 binds to different inhibitory or activator receptors called PVR-like receptors expressed by NK and T cells modulating immune response in cancers (Figure 1.2.4.1 from [187]): a) TIGIT (T cell immunoglobulin and immunoreceptor tyrosine-based inhibitory motif domain), b) TACTILE (T cell activation increased late expression) also called CD96, and c) DNAM-1 (DNAX accessory molecule 1) or CD226 [187]. While TIGIT and CD96 interact with CD155 to inhibit immune cell activation, CD226 is a co-stimulatory receptor expressed on most immune cells [188].

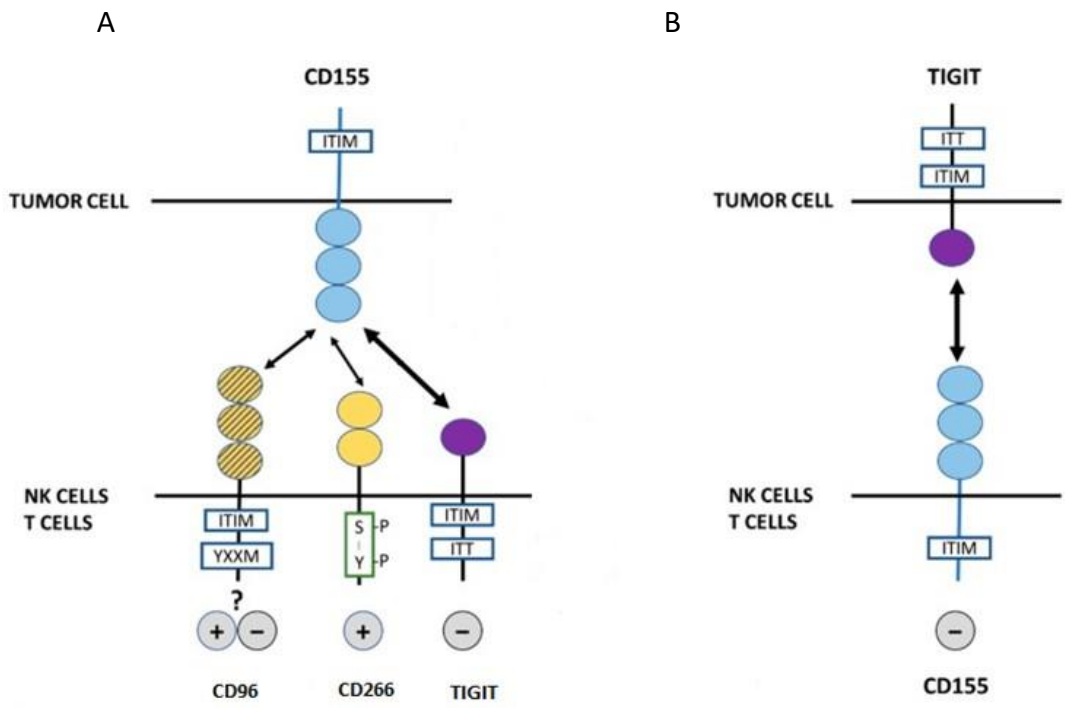

Figure 1.2.4.1. CD155 network and its receptors CD226, TIGIT and CD96. A) CD266, CD96 and TIGIT on NK and T cells interact with CD155 ligand on tumour cells and mediate activating and inhibitory signalling on cytotoxic cells. B) TIGIT expressed on tumour cells may inhibit NK and T cells by interaction with CD155. Figure adapted from [187].

CD155 was shown expressed in different tumour types, such as melanoma, neuroblastoma, glioma, cholangiocarcinoma, lung adenocarcinoma, myeloid leukaemia, colorectal, ovarian and pancreatic cancer, osteosarcoma, neck squamous cell carcinoma (HNSCC), muscle-invasive bladder cancer (MIBC), and its expression was generally correlated with a poor prognosis [188-191].

The expression of CD155 is regulated in cells by various stress conditions and stimuli, by oxygen and nitrogen reactive species (ROS and RNS), and by the activation of MEK/ERK, sonic Hedgehog (SHH) and NF-kB pathways (Figure 1.2.4.2 taken from [192]). Although CD155 is a molecule induced when cells are under stress, and consequently it should alert the immune system of potential malignancies, its overexpression in human neoplasms promotes tumour growth, invasion, and immune escape. Thus, targeting CD155 function may enhance antitumor immune responses [188]. In fact, *CD155 knockout* mice displayed reduced tumour growth and enhanced $CD8^+$ T and NK response. In addition, CD155 null tumour cells showed a slower tumour growth [193].

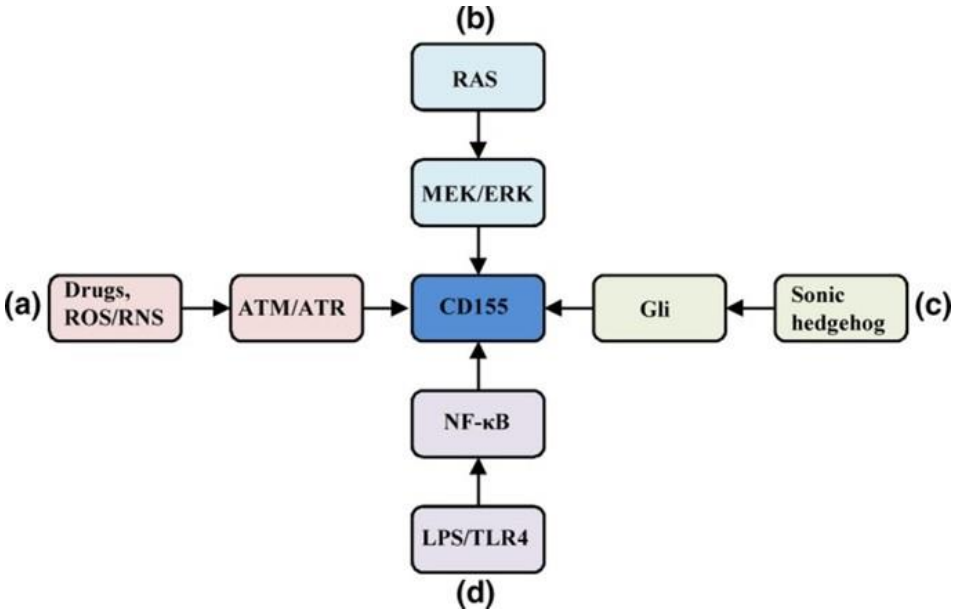

Figure 1.2.4.2. Regulation of CD155 expression. **a)** Chemotherapeutic agents and reactive oxygen species (ROS)/reactive nitrogen species (RNS) activate ATM and ATR kinases which upregulate CD155 expression. **b)** RAS via MEK/ERK signalling induces CD155 expression. **c)** Aberrant activation of sonic hedgehog induces CD155 expression. **d)** Combination of LPS with TLR4 activates NF-κB via adaptor protein MYD88 and TRIF, which stimulates CD155 expression. Figure taken from [192].

No data about CD155 expression in plasma EVs are available at present. Data have been reported showing that the levels of sCD155 are higher in the sera of patients with different tumour types compared to healthy donors, and decrease after surgery [194]. Moreover, in breast cancer, sCD155 serum levels correlated with high risk prognostic factors [195]. Tumour EV characterisation studies by proteomic analysis detected CD155 expression in EVs from melanoma, ovarian and prostate cancer cells [139-141].

The TIGIT cytoplasmic tail contains two domains called Ig tail tyrosine-like motif (ITT) and immunoreceptor tyrosine-based inhibitory motif (ITIM). Besides CD155, TIGIT also binds to CD112 and CD113, two other members of the nectin family [187]. Several studies have demonstrated that TIGIT can directly inhibit cytokine secretion and cytotoxicity in NK cells, and T cell proliferation by targeting TCR signalling by its ITIM domain present in the cytoplasmatic tail, or by direct inhibition of CD226. In addition, TIGIT can indirectly inhibit immune cells by induction of cytokine production in dendritic cells via CD155-TIGIT interaction [187, 188].

Recently TIGIT expression was reported in murine and human colorectal tumour cells, thus enlightening another mechanism of immune system inhibition mediated by the TIGIT-CD155 axis (Figure 1.2.4.1B [187, 196]). Several anti-TIGIT antibodies are now being tested in cancer immunotherapy clinical trials, and Phase 1 and 2 clinical trials are ongoing testing the combined of block of TIGIT and of PD1/PDL1 axis [187].

CD96 is also a member of Ig superfamily with two cytoplasmic domains, one is the ITIM-like inhibiting domain, and the other one YxxM activating motif which is present only in humans. Thus, its role in human NK and T cells is only partially characterised and still unclear. In mouse models CD96 exerts an inhibitory effect on NK cells, and its blockade supports anti-tumour responses [187]. In addition, in mouse tumour models, blocking of CD96 suppresses primary tumour growth in a $CD8^+$ T cell-dependent manner, and the combination of anti-CD96 with anti-PD1 and anti-TIGIT resulted in superior antitumor responses. This study showed that CD96 is an immune checkpoint expressed on $CD8^+$ T cells and by blocking it, T cell activity is enhanced and tumour suppressed [197].

CD226 molecule has an extracellular part composed by two Ig-like domains and a cytoplasmic domain containing three tyrosine residues. It is expressed in T cells, NK cells and monocytes and besides CD155 it can bind also CD112. CD226 down-regulation in NK cells was reported in healthy aged donors and in different diseases including cancer. Its role in potentiating NK cytotoxicity was shown in several mouse models [187].

EVs isolated from urine from prostate cancer patients showed high CD226 expression in proteomic analysis [143]. Another study showed that CD226 protein is expressed by platelet EVs [142].

1.2.5. VISTA immune checkpoint molecule

VISTA (V-domain Ig suppressor of T cell activation) is another negative IC receptor expressed by T cells. VISTA, also called PD1 homolog (PD1H), is a member of B7 family with large homology with PDL1 and PDL2 encoded by C10orf54 or VISIR gene. VISTA is a type I transmembrane protein encompassing 311 amino acids that presents a single extracellular domain, and a 96 amino acid long cytoplasmic tail [198] containing binding sites for protein kinase C and docking sites containing proline residues. This conformation makes VISTA to act both as a ligand or as a receptor [185]. In fact, little is known about ligands or receptors of VISTA. A recent study identified a novel ligand for VISTA called VSIG-3 (V-Set and Immunoglobulin domain containing 3), firstly discovered as IGSF11 member of immunoglobulin superfamily, highly expressed in colorectal cancer, intestinal-type gastric cancer and hepatocellular carcinoma. As a ligand of VISTA, it inhibits T cell proliferation and significantly reduces T cell cytokine and chemokine production, thus representing a possible new target for cancer immunotherapy [199] (Figure 1.2.5 [200]).

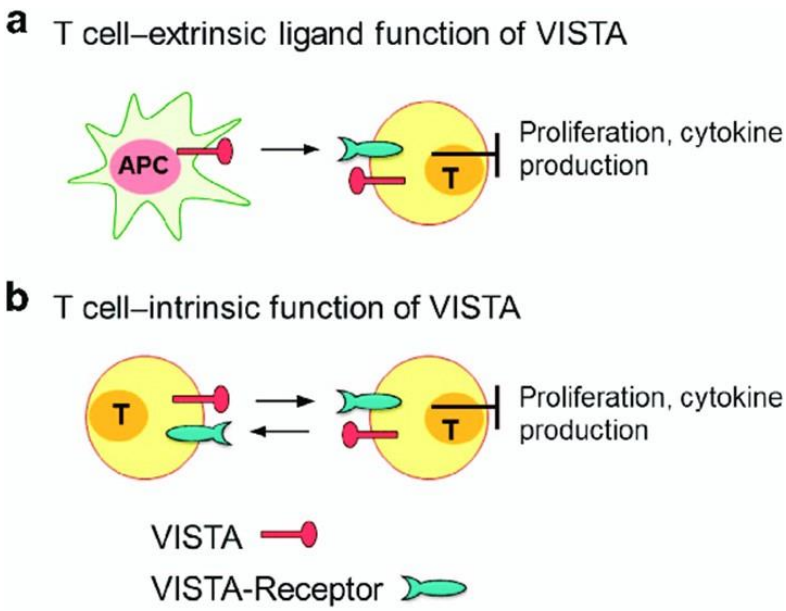

Figure 1.2.5. The ligand-or-receptor paradigm of VISTA in regulating T cell activation. VISTA is expressed on both APCs and T cells. VISTA suppresses T cell activation via both T cell-extrinsic and intrinsic mechanisms. **a)** VISTA acts as a ligand when expressed on APCs, and engages a putative inhibitory receptor on T cells that suppresses T cell proliferation and cytokine production. **b)** VISTA expressed on T cells may engage a putative inhibitory receptor on T cells via T cell-T cell interaction or may act as a self-signalling receptor. Both mechanisms will contribute to T cell suppression. The identity of the counter-receptor and detailed signalling downstream of VISTA remain to be elucidated. Figure taken from [200].

Although VISTA is expressed mainly by myeloid cells, low expression levels were detected in T and NK cells, but not in B cells [198, 201]. Moreover, VISTA is over expressed in tumour infiltrating immune cells such as MDSC and Tregs, confirming its role in immune suppression. Furthermore, VISTA deficient mice showed an enhanced anti-tumour immune response, although not sufficient to impair tumour growth. *In vitro* studies showed that soluble VISTA-Ig protein inhibits T cell proliferation, while VISTA blockade increases proliferation of T cells, although suppression of T cell proliferation was shown to last over time even in the absence of VISTA [185]. In addition, no T cell apoptosis was observed after VISTA blockade, as T cells just stopped proliferating or started to upregulate Foxp3 expression, and no effect were observed on B cells [198]. Furthermore, when overexpressed in sarcoma cells, VISTA has a protective antitumor immunity effect [202].

VISTA was reported to be expressed at mRNA and protein levels in ovarian cancer cells and endometrial cancer cell lines. Its presence in tumour cells was associated with T cell infiltration and with a poor prognosis [203]. VISTA expression was also shown in about 10% gastric cancers and liver metastases [204]. In addition, VISTA was reported expressed by human lung carcinomas [205] and by melanoma cells lines [206]. Thus, VISTA could

represent another new target for immunotherapy, and its increase during treatment with ipilimumab in patients with prostate cancer may support its targeting [207]. Indeed, CA-170, a small molecule drug targeting VISTA, PDL1 and PDL2 is currently tested in a phase I trial in advanced solid tumours and lymphomas (NCT02812875) [208].

1.3. Melanoma

Melanoma is a highly aggressive malignancy arising in the skin, eye or gut mucosa due to genetic mutations in melanocytes. Cutaneous melanoma is the most common form of melanoma: it occurs in about 1/7,000 in Italy [209] and is the most aggressive type of skin cancer. Melanoma is highly curable in its early stages but still life threatening in the advanced metastatic stages.

1.3.1. From melanocytes to melanoma

Melanocytes are a key cellular component in the skin and in the eye, but they are also located in the inner ear, brain and heart, adipose tissue, lung and gut mucosa. Melanocytes have different functions depending on their position: in skin and eye they are involved in pigmentation protecting from UV, while in the other tissues they are involved in detoxification and anti-inflammatory functions [210]. Melanocytes derive from precursor cells called melanoblasts originating from the neural crest during embryo development.

The primary function of melanocytes is the production of melanin, light-absorbing pigments derived from the oxidation and polymerization of tyrosine. Human melanocytes produce two main types of melanin, brownish-black eumelanin, synthesized from l-dopachrome, and reddish-yellow pheomelanin, whose synthesis is dependent on the availability of sulfhydryl compounds. The type and amount of melanin produced by melanocytes is determined genetically and is influenced by a variety of extrinsic and intrinsic factors, including exposure to UV light, hormonal changes, inflammation, and age [211]. Biosynthesis of melanin takes place in membrane-bound organelles termed melanosomes. In the basal layer of skin epidermis melanocytes are surrounded by keratinocytes, in a ratio one melanocyte to about 40 keratinocytes, to which they transfer the melanosomes [212]. Genetic, biochemical and pharmacological evidence has established that signalling from Melanocortin 1 receptor (MC1R) is the main factor dictating melanogenesis. Melanogenesis is then regulated by other signalling systems and different transcription factors including the tyrosine kinase receptor KIT, its ligand SCF,

and microphthalmia-associated transcription factor (MITF). Melanogenic enzymes, a number of highly similar metalloproteins, include tyrosinase (TYR), tyrosinase-related protein 1 (TYRP1) and tyrosinase-related protein-2 (TYRP2). Melanocytes can be identified by the expression of these and other melanocyte-specific markers, the most used being MITF, Pmel17/gp100 (premelanosome protein 17), melan-A/MART-1 (melanoma antigen recognized by T cells 1), (Figure 1.3.1.1 [213]), (Figure 1.3.1.2 [211]).

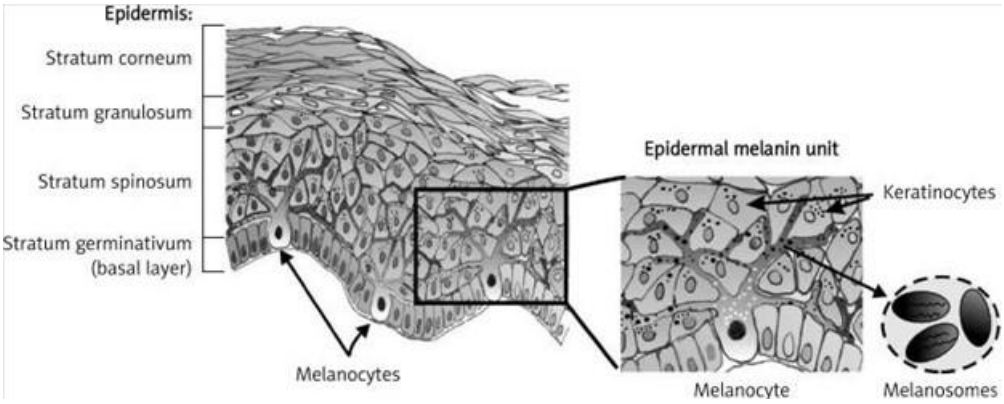

Figure 1.3.1.1. The epidermis structure. Melanocytes reside in the basal layer cells and form the epidermal melanin unit interacting with keratinocytes by dendritic processes. Melanin synthesized in melanocyte is transported by melanosomes to keratinocytes to protect them from UV radiation. Figure taken from [213].

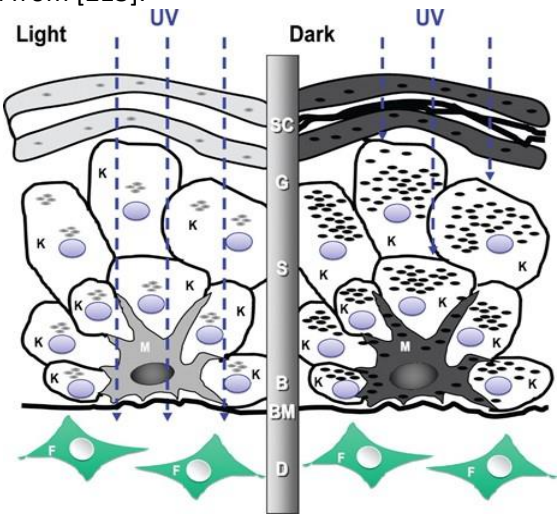

Figure 1.3.1.2. Schematic of human skin architecture from light and dark pigmented skin types. From *top* to *bottom*: *SC*, stratum corneum; *G*, stratum granulosum; *S*, stratum spinosum; *B*, stratum basale; *BM*, basement membrane; *D*, dermis. Cell types: *K*, keratinocyte; *M*, melanocyte; *F*, fibroblast; *shaded oval*, melanin granule. Figure taken from [211].

Benign proliferation of skin melanocytes results in melanocytic nevi (MN). The most common MN are generally referred to as acquired melanocytic nevi, although there are different subgroups of MN (congenital nevi, dysplastic or atypical nevi, Spitz nevi, Blue nevi). The development of these common benign tumours is a multifactorial process under genetic and environmental influences. MN are differentiated from melanoma and diagnosed on the basis of their clinical aspects and of histopathology, although the

diagnosis may prove quite challenging in intermediate cases, and especially in paediatric melanoma. The use of dermoscopy discriminating subsurface skin structures may aid the clinical diagnosis [214]. In addition, molecular diagnostic tests have been designed to differentiate melanoma from benign nevi by genetic profiling [215], though a consensus about the discriminating markers has not been reached yet. Although melanoma generally occurs independently from existing MN, high MN counts and atypical nevi are risk factors for cutaneous melanoma [216].

Cutaneous melanoma results from both intrinsic and extrinsic risk factors, the first including the individual genetic background conditioning nevi characteristics and familial susceptibility, and the second including sun exposure and environmental conditions, (Figure 1.3.1.3 [217]). In fact, the incidence of cutaneous melanoma is different in the different countries and populations, the highest registered in New Zealand and Australia fair skin inhabitants, Northern Europe and North America, while the incidence in the Mediterranean area is lower [217, 218]. Furthermore, cutaneous melanoma incidence is on the rise in the majority of these countries.

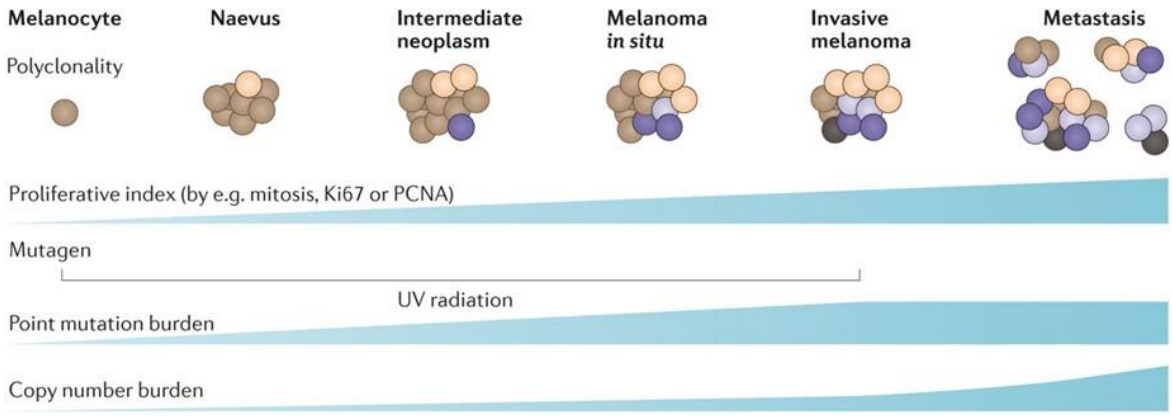

Figure 1.3.1.3. Melanocytic neoplasms become more proliferative and polyclonal as they evolve. Gene mutations caused by UV radiation accumulate during the transition to invasive melanoma. Once melanomas become invasive, copy number alterations become more prevalent. PCNA-proliferating cell nuclear antigen. Figure taken from [217].

1.3.2. Melanoma classification and clinical stages

Different types of cutaneous melanoma exist, based on histopathologic definition and body localization: superficial spreading melanoma and nodular melanoma are the most common and may develop at all body sites, especially in limbs and trunk, while acral

melanoma occurs in glabrous skin sites. Lentigo maligna are melanomas occurring in the elderly in the face and head [219].

Melanoma clinical staging is based on the extent of the primary tumour growth and on the occurrence of metastatic spread to regional or distant sites through lymphatic or hematogenous routes. Diagnostic histopathological examination of the primary tumour considers the vertical thickness (Breslow index) and the presence of microscopic ulceration for primary melanoma staging. The current AJCC clinical staging system takes into consideration the primary tumour classification and the presence of metastasis in the tumour-draining regional lymph nodes and/or at distance, to distinguish four disease stages: stages I-II considering the features of primary melanoma growth in the absence of metastatic dissemination, and stages III-IV when regional or distant metastases are present [220].

1.3.3. Molecular characterization of melanoma

The Cancer Genome Atlas (TCGA) Project of the US National Cancer Institute recently characterized a large number of cutaneous melanoma subtypes by a multiplatform molecular analysis of DNA, RNA, and protein, and defined four main genomic subtypes: mutant BRAF, mutant RAS, mutant NF1, and triple-wild-type [221]. Mutations in the BRAF gene are the most common mutations, detectable in about 50% of all cutaneous melanoma. The majority of BRAF mutations are point mutations resulting in T1799. A transversion and the substitution of valine to glutamic acid (V600E) gives place to a constantly active state of the BRAF serine/threonine kinase [222]. Although the BRAF mutation is also common in benign MN [223], it represents a major therapeutic target in melanoma. Other common mutations include RAS genes mutations, occurring in about 20% melanoma and benign MN, generally mutually exclusive with BRAF mutation, and NF1 mutations (Figure 1.3.3.1 [224]). Common mutations in tumour suppression genes CDKN2A, TP53 and PTEN are also observed [225] (Table 1.3.3 [217]). Genetic and transcriptomic data implicate activation of MAPK signalling at initiation and subsequent amplification of signalling during melanoma progression (Figure 1.3.3.2 [226]).

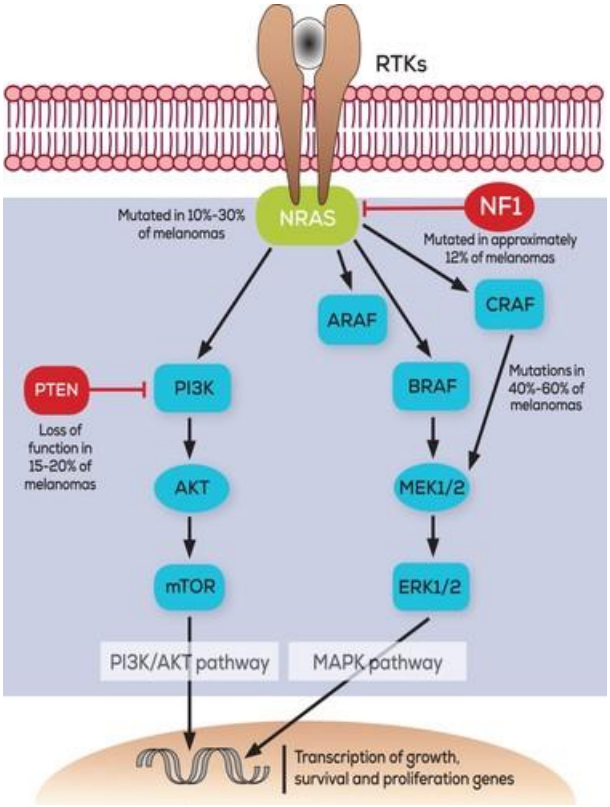

Figure 1.3.3.1. Recurrent mutations in melanoma affecting the MAPK and PI3K/AKT signalling pathways. The binding of a ligand to RTKs induces RAS activation and stimulation of the MAPK and PI3K/AKT pathways, leading to the transcription of genes involved in cell growth, survival, and proliferation. NRAS, BRAF, NF1, and PTEN mutation frequencies are indicated. Figure taken from [224].

Table 1.3.3. Common mutations and their role during melanoma progression

Pathway	Gene	Mutation	Subtype*	Progression phase‡	Role
MAPK	*BRAF*	V600E	Non-CSD	Naevi	Initiation
	BRAF	V600K, K601E and G469A, among other clustered nonV600E alterations	CSD	Intermediate and MIS lesions	Initiation
	NRAS	Q61R and Q61K, among other less common alterations affecting codon 61 or 12	CSD	Intermediate and MIS lesions	Initiation
	NF1	Disabling mutations occurring throughout the gene and deletions	CSD	MIS	Initiation
Telomerase	*TERT*	Promoter mutations affecting hg19 coordinates 1,295,228 or 1,295,250, among less common, nearby mutations	CSD and non-CSD	Intermediate and MIS lesions	Progression
RB	*CDKN2A*	Deletions and disabling mutations occurring throughout the coding region	CSD and non-CSD	Invasive melanoma	Progression
Chromatin remodelling	*ARID1A*, *ARID1B* and/or *ARID2*	Disabling mutations occurring throughout the protein	CSD and non-CSD	Invasive melanoma	Progression
PI3K	*PTEN*	Disabling mutations occurring throughout the protein and deletions	Non-CSD	Thicker invasive melanomas	Advanced progression
p53	*TP53*	Disabling mutations occurring throughout the protein	CSD	Thicker invasive melanomas	Advanced progression

ARID, AT-rich interaction domain; *CDKN2A*,cyclin-dependent kinase inhibitor 2A; CSD, chronically sun damaged; MIS, melanoma *in situ*; *NF1*, neurofibromin 1; *TERT*, telomerase reverse transcriptase. *Subtype refers to the melanoma subtype(s) predominantly associated with the mutation. ‡Progression phase refers to the earliest progression phase at which the mutation typically occurs.

Table taken from [217].

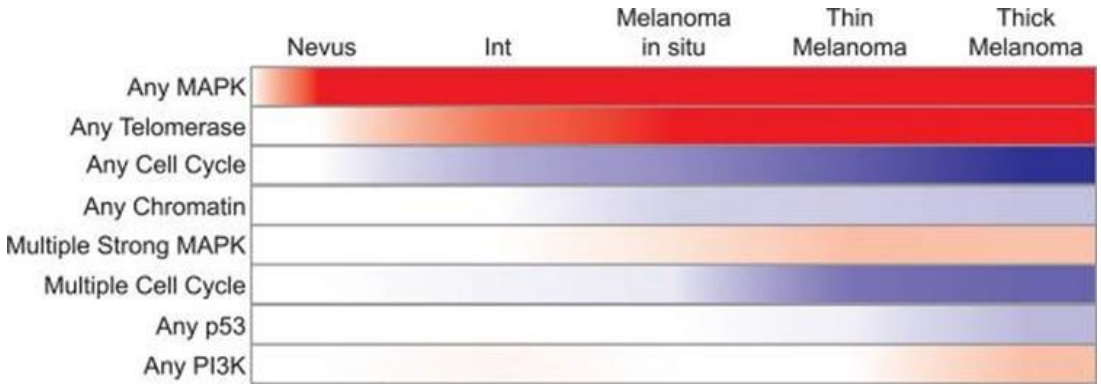

Figure 1.3.3.2. Somatic alterations in key signalling pathways that drive melanoma appear at specific points in the melanoma progression cascade. Each heatmap reflects the frequency that a given pathway is activated (red) or inactivated (blue) at a specific point in the melanoma progression cascade. Figure taken from [226].

Genome sequencing studies determined that melanoma is the human cancer showing the highest number of genetic alterations, resulting from UV light mutagenesis and other mutational processes [227]. These high number of mutations have been suggestively linked to melanoma immune-responsive state. In fact, melanoma has shown historically a high degree of response to immune therapy and to the recently developed immune checkpoint inhibitors (ICI). Mutation burden has been associated to response to ICI in multiple tumour types: the assumption is that passenger mutations in coding sequences generate neoantigens that may be recognized by the adaptive immune system. In addition, when the immune infiltrate of melanoma was thoroughly analysed in the TCGA dataset, the expression signatures of immune composition showed a clear enrichment in most samples [228].

Molecular characterization of melanoma by transcriptomic profiling has shown that melanoma includes heterogeneous subpopulations of cancer cells with different biological features. A *proliferative* and an *invasive* state have been identified in melanoma cell lines and specimens, the latter including also the category *immune,* characterized by a signature attributable to the presence of tumour-infiltrating lymphocytes [229, 230]. The different states can reversibly switch between the corresponding transcriptional programs, and this switch is governed *in vivo* by interactions occurring in the tumour microenvironment [231], (Figure 1.3.3.3 [231]). The MITF-rheostat model, whereby cells adopt an *invasive* phenotype at lower MITF levels and a *proliferative* phenotype when MITF expression is higher, has been proposed to encompass the transcriptional regulation underlying the different states [232], (Figure 1.3.3.4 [233]). Different other regulators have been associated to the regulation of the *invasive* cells, which adopt a slow cycling

stem cell-like, nonpigmented state, and the *proliferative* cells, appearing to be more melanocytic and highly pigmented [234]. The cell phenotype switching model is a prevalent model not only in tumour progression but also in drug resistance, as MITF-low invasive melanoma cells are more resistant than the others to BRAF inhibitors [235].

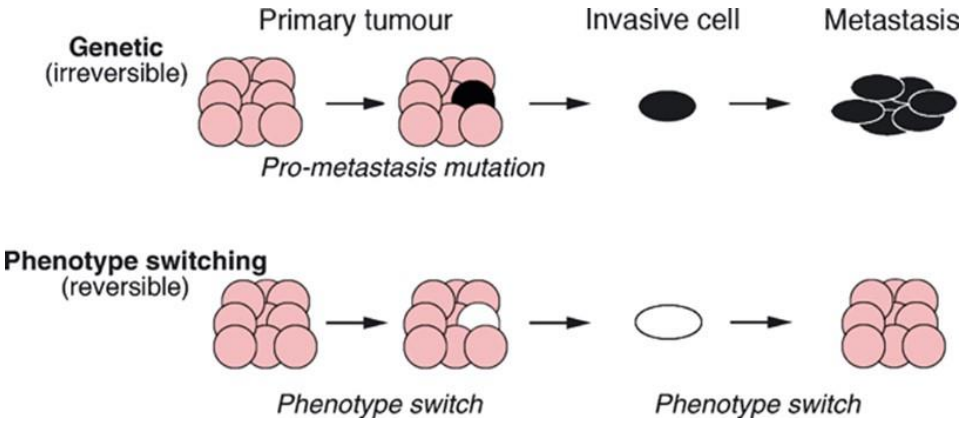

Figure 1.3.3.3. Pathways towards metastasis. In the genetic model, the acquisition of novel mutations promotes the generation of metastasis. By contrast, in the phenotype-switching model metastasis arise because of microenvironment-driven changes to the cell's phenotype. Figure taken from [231].

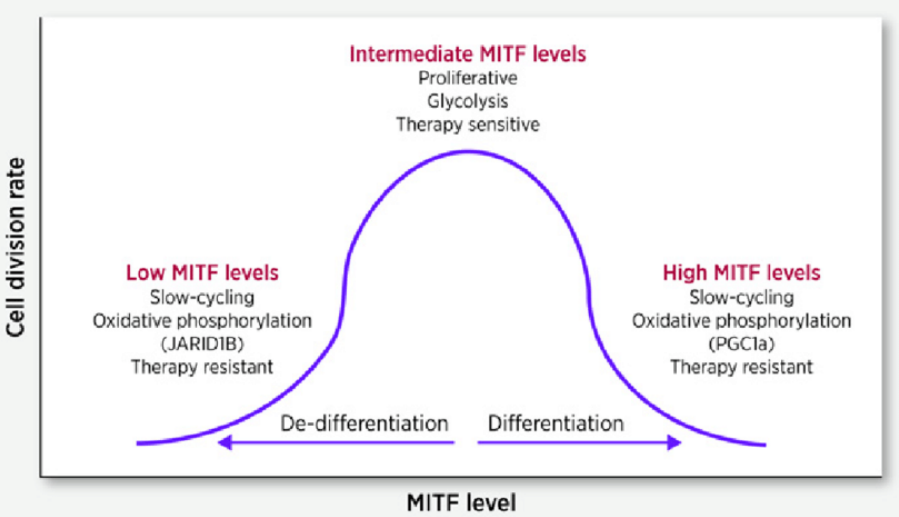

Figure 1.3.3.4. Low or high levels of MITF contribute to melanoma phenotype. The melanoma rheostat model proposes that different levels of MITF regulate distinct phenotypic states: low MITF is associated with dedifferentiation, intermediate MITF controls proliferation, and high MITF is associated with cell differentiation. The proliferative and slow-cycling phenotype are dependent on glycolysis and oxidative phosphorylation, respectively. The dedifferentiated state reduces the melanoma cell's dependency on the MAPK pathway, and consequently leads to resistance to MAPK pathway inhibition. Figure taken from [233].

Moreover, miRNAs negatively regulate gene expression post-transcriptionally and have important role in the epigenetic regulation of melanoma progression. Deregulated miRNA expression has been linked to tumour progression in melanoma as well as in a variety of other cancer types [236]. miRNA dysregulation has been observed during different stages of melanoma, and their role in the multiplicity of processes involved in melanoma

progression at the primary tumour site and at distant tissues have been highlighted in several studies [237].

1.3.4. Melanoma treatment: targeted drugs and immunotherapy

In the last years, the treatment of metastatic melanoma has been revolutionized by the advent of two types of therapy, targeted drugs and immunotherapy. Recently, randomized trials have confirmed the efficacy of both therapeutic approaches in both the adjuvant and neoadjuvant settings [238] (Figure 1.3.4.1 [235]).

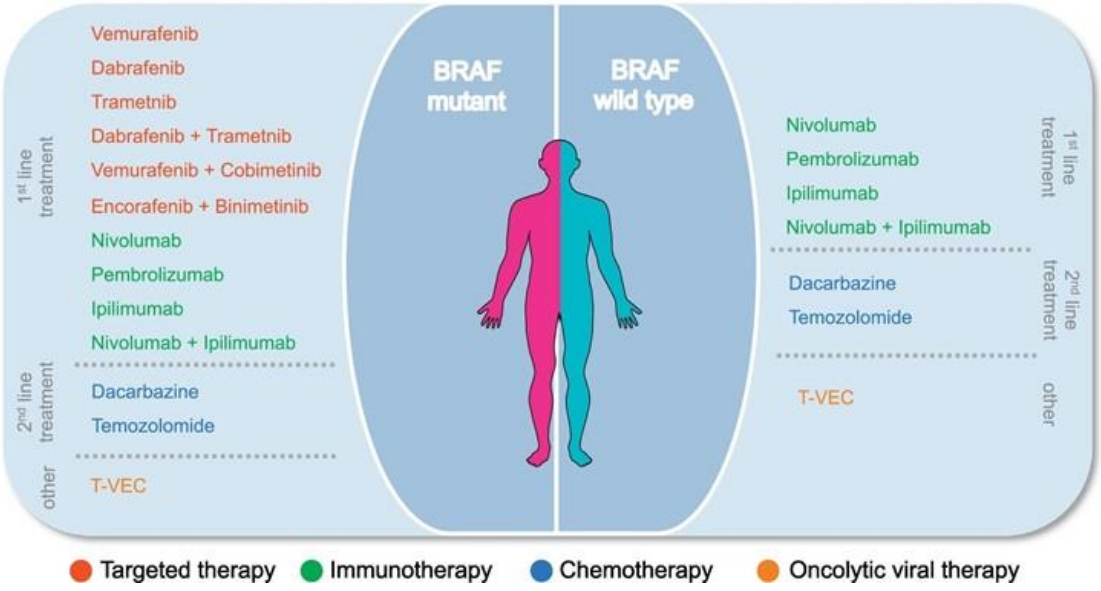

Figure 1.3.4.1. Treatment options for patients with unresectable metastatic melanoma. BRAF-mutant melanoma patients can receive targeted therapies or immunotherapies as first-line treatment. Patients with BRAF wild type tumours usually receive immunotherapies as first-line treatment. Patients that do not respond to BRAFi as first-line treatment generally receive immunotherapy as second line treatment. Additionally, other local treatment are used (T-VEC). Figure taken from [235].

Targeted drugs are kinase inhibitors that target BRAF (BRAFi) and MEK (MEKi) oncoproteins, currently used in combination to treat BRAF-mutated melanoma. Both proteins are involved in the RAF-MEK-MAPK pathway, which is activated by extracellular signals bound to their membrane receptor, usually a receptor tyrosine kinase (RTK). Targeted therapy with BRAF/MEKi has significantly improved overall survival of patients with metastatic melanoma. Although the majority of patients respond to this treatment regimen, clinical responses are often followed by the rapid occurrence of disease relapse due to emerging tumour drug resistance [239], (Figure 1.3.4.2 [240]).

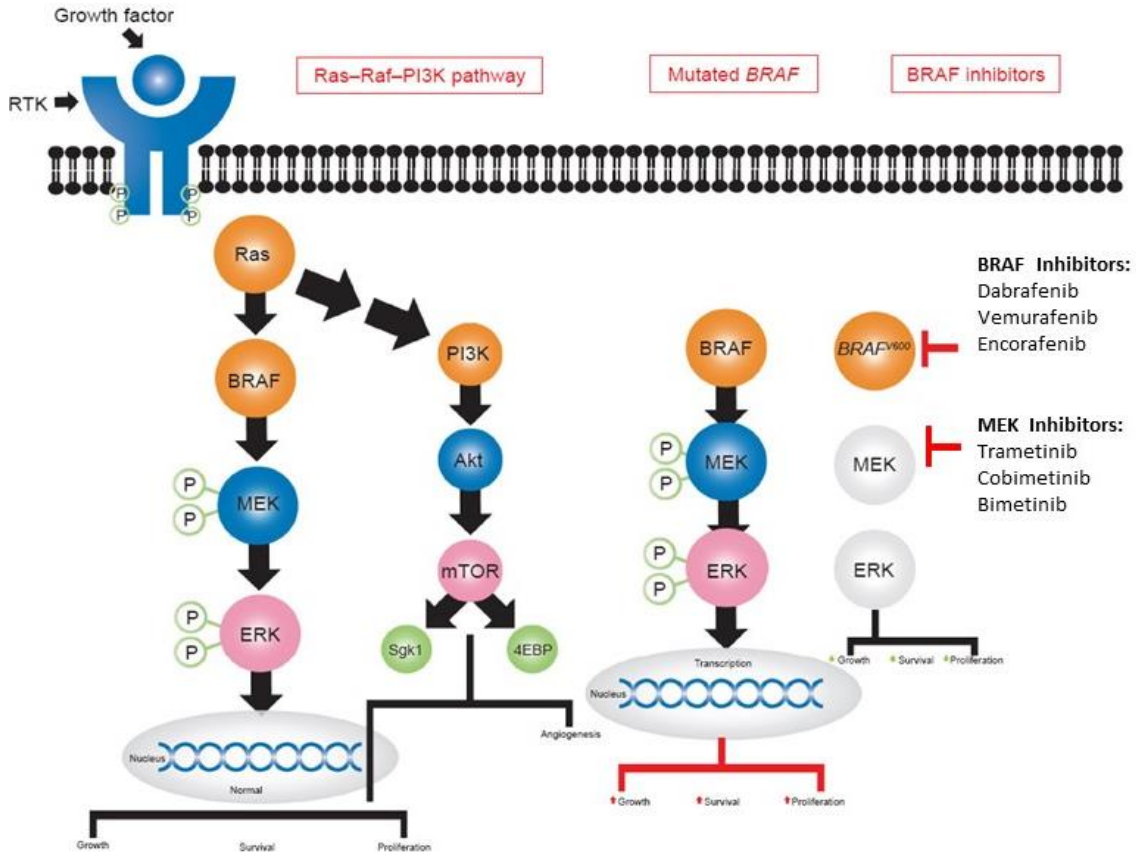

Figure 1.3.4.2. MAPK–PI3K–Akt pathway and *BRAF*^{V600} mutation in melanoma. *BRAF*^{V600} mutations in melanoma lead to constitutive activation of the MAPK pathway, which leads to uncontrolled cell survival, growth, and proliferation that might be blocked by treatment with BRAF inhibitors or MEK inhibitors. Figure adapted from [240].

Immunotherapy determines the reinforcement of patient immune system response against the tumour by blocking key immune inhibitory molecules. Immunotherapy regimens consist in the systemic infusion of specific engineered antibodies that bind and block negative checkpoint regulators of adaptive immune response [241]. Since immunotherapy does not target any tumour mutated protein it represents a mutation independent therapy that regulates T cell function via immunological synapses. The first immunotherapy drug was Ipilimumab, a molecule inhibiting CTLA4 in cytotoxic T lymphocytes developed by James Allison [242]. Few years later other antibodies targeting PDL-1 and PD1 have reached clinical practice and are currently used in the therapy of different tumour types.

1.3.5. Mechanisms of melanoma resistance to targeted therapy

BRAF/MEKi targeted therapy is currently the first line treatment for metastatic melanoma patients carrying BRAF-mutated tumours [240]. BRAF/MEKi treatment shows long-term benefit in approximately one third of the patients [243], but the emergence of drug resistance in the majority of patients strongly limits its clinical efficacy.

Several studies have assessed the genomic correlates of resistance to BRAF inhibitors, both induced by tumour changes under the drug selective pressure, i.e. *acquired*, and the pre-existing or *intrinsic* resistance, observed more rarely in cell lines and in patients with very short therapy responses. In general, drug resistance can result from a myriad of genetic and epigenetic events and shows a wide intra-patient and intra-tumoral heterogeneity of underlying mechanisms.

A variety of molecular mechanisms have been identified that act by sustaining MAPK signalling or parallel signalling networks despite BRAF inhibition, including mutations in RAS, MEK, NF1, RAC, RAF genes, or in genes of the PI3K/AKT pathway (AKT, PIK3, PTEN), and amplification or alternative splicing of BRAF gene. Other genetic mutations identified by next-generation sequencing approaches involved cell cycle control genes such as CDKN2A, and TP53 [244].

However, reactivation of the MAPK signalling derive more frequently from epigenetic mechanisms regulating the expression of receptor tyrosine kinase (RTK) genes involved in melanoma cell growth. Different signalling pathways downstream RTK have been associated with BRAFi resistance that involve other signalling axis besides the MAPK and the PI3K/AKT pathways, such as the SRC/STAT and Notch1 pathways, and RTKs such as AXL, EGFR, IGF1R, PDGFR, MET, ERBB3, to give some examples [245], (Figure 1.3.5.1 [246]).

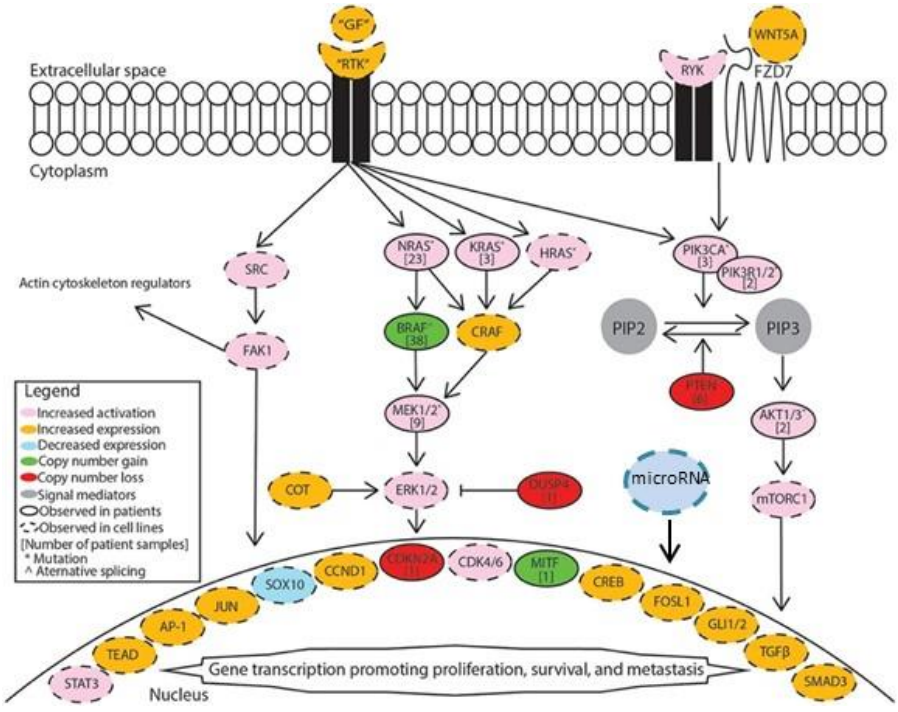

Figure 1.3.5.1. Mechanisms supporting BRAF inhibitor resistance in melanoma. Genetic and epigenetic processes regulating receptor tyrosine kinase (RTK) downstream pathways involved in melanoma cell growth. Figure adapted from [246].

The acquisition of a resistant state is characterised by a generalised de-differentiation leading to activation of several different new signalling pathways able to confer survival advantages in the presence of the drugs. Melanoma phenotype switching capacity to de-differentiated and slowly proliferating invasive cells expressing low MITF and high AXL levels has been identified as a mechanism of resistance to targeted therapy in a subset of melanoma patients as well as in cell culture systems. Moreover, a metabolic switch associates to drug resistance [235].

Transcriptomic studies revealed that other mechanisms favouring tumour cell proliferation may bestow BRAFi resistance. One example is the increased abundance of extracellular matrix (ECM) proteins conferring stiff and more rigid properties to the ECM, regulated by fibroblast secreted TGFβ via the HIPPO pathway and TEAD transcriptional partner, connected to the de-differentiated and invasive phenotype [230]. Another example stems from the observation that tumour cells can adapt to drug-induced stress by upregulating autophagy. The mechanisms leading to a BRAFi-mediated induction of tumour autophagy include ER stress pathways activation [247].

miRNA-mediated resistance mechanisms have been intensively studied, also in consideration of their potential manipulation for therapeutic strategies. Several miRNA were reported as upregulated in resistant melanoma by regulating nodes in the MAPK, PI3K/AKT, STAT3 and MITF pathways [248]. In my hosting lab a set of miRs including miR-34a, miR-100 and miR-125b were demonstrated to be upregulated in the BRAFi resistant variants of melanoma cells in parallel with increased production of CCL2; their inhibition restored the *in vitro* drug sensitivity. These results indicated that these miRs and CCL2 are potent prognostic factors and good targets for overcoming drug resistance in metastatic [249].

Currently, ongoing clinical studies are investigating combinations of targeted therapy with IC inhibitors [224]. Several studies reported that BRAF/MEKi-induced alterations strongly condition the TME thus influencing anti-tumour immunity [250]. Treatment was shown to generate an immune stimulating TME, characterized by increased tumour infiltration of immune cells, including cytotoxicity markers but also markers of T cell exhaustion, such as TIM3, PD1, and PDL1 [251, 252].

In vitro studies showed that upon BRAFi/MEKi treatment melanoma cell lines increase expression of melanoma antigens MART, TYRP1, TYRP2 and Gp100, and that at therapeutic concentrations BRAFi have no effects on lymphocytes viability and functions.

While BRAFi displayed a boosting effect on T cells by paradoxical activation of the MAPK signalling, in contrast MEKi showed suppressive effects on T cell functions, which were not confirmed by *in vivo* studies. Clinical studies confirmed that treatment does not affect blood cell counts, leukocyte subset frequencies or serum cytokine levels [253]. It has been hypothesized that the combination of targeted therapy and immunotherapy could enhance anti-tumour responses augmenting therapeutic outcome (Figure 1.3.5.2 [254]). However progressing tumours show increased expression of inhibitory molecules and immunosuppressive cell infiltration, concomitant to decreased T cell numbers.

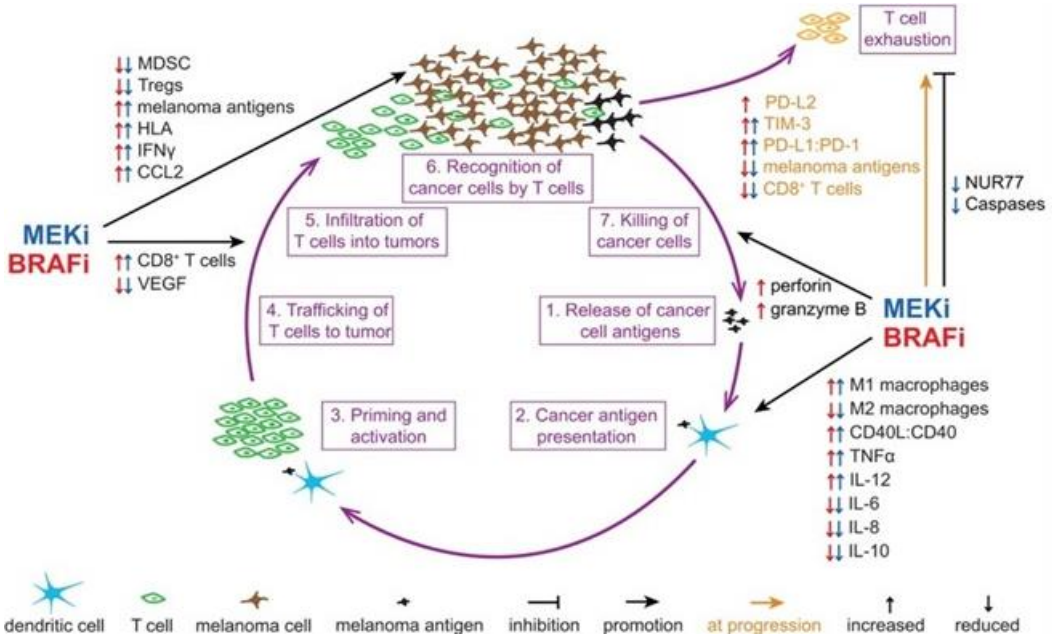

Figure 1.3.5.2. **Immunomodulatory effects of BRAF and MEK inhibitors.** Their beneficial influence on the antitumor immunity and the tumour microenvironment is mediated by different illustrated mechanisms. Figure taken from [254]

Resistant tumours were characterized by a transcriptional signature determining an immunosuppressive TME due to an increase in genes regulating epithelial-mesenchymal transition, cell adhesion, extracellular matrix remodelling, angiogenesis and wound-healing, predictive of resistance to immunotherapy, termed IPRES, for innate anti-PD1 resistance [255].

1.4. Aims of the thesis

Tumour EVs can shuttle a vast array of functionally active proteins and genetic material to other cells at distance or within the tumour microenvironment contributing thereby to tumour immune escape. Immune checkpoints control the immune response, and their expression level is a key factor for disease outcome of cancer patients. In melanoma, negative immune checkpoint molecules (IC), known from the literature to be involved in immune system inhibition can be modulated by targeted therapies, such as BRAF/MEK inhibitors (BRAF/MEKi). To study the potential role of EVs carrying IC in conditioning antitumour response, I investigated the immunomodulating effects of melanoma EVs deriving from BRAF/MEKi sensitive or resistant melanoma on tumour and immune target cells. To collect evidence about the clinical relevance of EVs carrying IC, I evaluated plasma EVs from melanoma patients undergoing targeted therapy for IC protein and transcript expression. Given the importance of immunotherapy in melanoma treatment, elucidating the role of EVs carrying IC could contribute to improve combined therapy planning and to the discovery of new potential immunotherapy targets to improve treatment responses as well as to uncover new predictive biomarkers. In particular I investigated:

1) the expression of a set of IC like PDL1, PDL2, HVEM, GAL9, VISTA and CD155, in BRAF-mutated melanoma cell lines and their released EVs before and after the acquisition of resistance to BRAF/MEKi

2) the effect induced by melanoma EVs on the expression of negative IC in melanoma and immune cells, taking advantage of an *in vitro* model of monocyte skewing MDSC set up by the hosting laboratory

3) the modulation of the expression levels of negative and positive IC in plasma EVs and in melanoma specimens, to assess the translational relevance of the obtained results

2. Materials and methods

2.1. Melanoma Patients Samples

Peripheral blood and surgical specimens were obtained by study protocols approved by the Institutional Review Board of Fondazione IRCCS Istituto Nazionale dei Tumori and the Independent Ethics Committee (code INT39/11 and INT40/11). All participants, including melanoma patients and healthy controls, gave their written informed consent. Healthy controls were blood donors of the Immunohematology and Transfusion Medicine Unit of the hospital used for in vitro PBMC co-culture experiments in this project. These donors were healthy subject selected with no previous and no current tumour disease or any other kind of disease. Plasma from stage IIIC-IV melanoma patients at the beginning and during targeted therapy with BRAF and MEK inhibitors were studied for circulating EVs. Table 2.1.1 represents data regarding melanoma patients involved in plasma EV studies.

Table 2.1.1. Melanoma patients treated with targeted therapy studied for plasma EVs

Patient ID	Treatment	TTP	OS	sex	age
CAP14-28	D + T	>19	>19	F	34
CP 14-15	D + T	>23	>23	F	42
BR14-22	V + C	>19	>19	M	60
RG 14-07	D + T	>25	>25	M	63
TN14-78	D +T	>20	>20	F	67
BD14-57	D +T	2,7	5,3	M	65
CA14-34	D + T	7,4	11,2	F	70
GT 14-20	D + T	5,9	5,9	F	65
MF14-29	D + T	0,8	4	F	37
RC14-35	V + C	7,8	10,6	F	49
SF14-50	D + T	4	8,1	F	48

D-Dabrafenib (BRAFi), T-Trametinib (MEKi), C-Cobimetinib (MEKi), V-Vemurafenib, TTP-time to progression in months, OS overall survival in months. The upper part of the table lists patients displaying TTP > 12 months, defined Long responders in these studies. The other patients displaying TTP <12 months were defined short responders. F-female, M-male.

Metastatic tumour specimens obtained from stage IIIC-IV melanoma patients were snap frozen and processed for RNA extraction and analyses. Table 2.1.2 shows characteristics of patients and melanoma tumour metastases.

Table 2.1.2. Characteristics of melanoma specimens and patients

Metastases location				Mutation		Stage		Age		Sex	
C	LN	V	PT	BRAF WT	BRAF mut	III	IV	<50	>50	F	M
28	23	6	1	27	31	28	30	17	41	29	29

C-cutaneous; LN-Lymph node; V-visceral; PT-primary tumour; WT-wild type; BRAF mut- V600E and V600K BRAF mutations; F-female; M- male

2.2. Cell lines and culture conditions

Human melanoma cell lines were previously obtained in the hosting laboratory from metastatic melanoma surgical specimens [256]. The vemurafenib-resistant cell line variants (R) were generated from the parental sensitive ones (S) by repeated exposure to the commercially available drug Vemurafenib (PLX4032, Active Biochem) [249, 257]. All cell lines were cultured in RPMI-1640 medium supplemented with 10% heat-inactivated foetal calf serum (FCS), 20 mM HEPES buffer, 2 mM glutamine, 100 IU/ml penicillin and 100 µg/ml streptomycin (Lonza). Standard culturing conditions included 21% O_2 at 37°C and 5% CO_2 in 95% humidity. For downstream analyses cells were grown at 80-90% monolayer confluence, washed once with 1X PBS and detached using Trypsin EDTA (Lonza). Cells were periodically checked by laboratory service for their identity by short tandem repeat loci characterization by GenePrint 10 System (Promega), and for the absence of mycoplasma contamination (N-GARDE Mycoplasma PCR Euroclone).

To generate a melanoma cell variant resistant to BRAF/MEKi from sensitive cell line LM16S, I treated cells in 150 cm^2 flasks with the combination of the BRAF inhibitor Dabrafenib (GSK2118436), and the MEK inhibitor Trametinib (GSK1120212), at 10nM. Both drugs are commercially available (Selleck). After 7 days of cells incubation in medium with the drugs, fresh medium without drugs was added on the few survived cells that than were grown to confluence. IC expression by flow cytometry analysis was monitored before repeating the section treatment. IC50 values to the drug combination were tested after each cycle.

2.3 Cell transfections

To set up cell transfection conditions, four different lipid transfection reagents were tested at different concentrations. Metafectene (Biontex) and Lipofectamine2000 (Invitrogen) were tested at 0.5-2 µl, TransIT-X2 (Mirus Bio) at 1.5-6 µl and HiPerFect (Qiagen) at 2-6 µl: all were mixed with DNA in 50 µl of final volume of medium FCS free. To select the best transfection reagent, the Red Fluorescent Control oligo DNA (BLOCK-iT Alexa Fluor, Invitrogen) was used as readout of transfection efficacy by evaluating the number of fluorescent cells at 48-72 h. Metafectene resulted the most efficient lipid for melanoma cells transfections.

Plasmid vectors pCMV6-AC-GFP coding for PDL1-GFP and CD81-GFP fusion proteins were purchased (OriGene) and replicated by Plasmid DNA Laboratory Facility. Plasmid DNA (2 µg) and Metafectene (1-2 µl) were used for stable transfection. To determine the

concentration required for the selection of transfectants acquiring resistance to Geneticin antibiotic (G418 Sulfate, Gibco), a dose-response test was performed. Initially I tested the same G418 concentrations (1000, 500, 125, 62.6 µg/µl), and after 21 days of treatment, LM16S cells death was clear at doses ≥ 250-500 µg/µl, while for LM16R it was ≥ 125-250 µg/µl. Based on these results, I set a second dose-response curve test, and identified 450 µg/ml as the dose for transfectants of LM16S cells, and 150 µg/ml that of LM16R.

Cell transfection were set by plating $35x10^4$ cells in 6 well plates; after 24 h the medium was removed and 2 µg of plasmid DNA mixed with metafectene were added in 800 µl of RPMI FCS free medium. After 4 h, complete medium containing G418 was added (1200 µl). In order to enrich for LM16S-GFP positive cells, the florescence-activated cell sorting technique (FACS) by BD FACSAria Fusion flow cytometer was applied in collaboration with the Flow Cytometry and Cell Sorting Facility. While FACS was an effective selection method for LM16S transfectants, it resulted unsuccessful in the purification of the LM16R-CD81-GFP transfectant, because of cell aggregation during sorting. Even though two different methods of FACS sorting were used ("Purify" and "Single Cell Sorting"), in both cases an heterogeneous population was obtained. To obtain enriched LM16R-CD81-GFP transfectant cells I cloned the sorted cells by limiting dilution in 96 plates and selected cell clones by GFP expression.

2.4. Isolation of EVs from melanoma cell lines

For EV isolation from the supernatant of melanoma cell lines, I used a standard ultracentrifugation (UC) protocol to enrich small vesicles, such as exosomes [30]. For these cultures, I used FCS that was depleted from calf EVs by over-night UC at 113,000 g followed by 0.22 µm filtration. Cultures were set in standard conditions seeding 5-10 x 10^6 cells in 150 cm^2 flasks; after 72 h, conditioned medium was collected, centrifuged at 300 g for 10 minutes to pellet the cell debris, filtered at 0.22 µm, followed by 4 h UC at 113,000 g at 4°C by SureSpin 630 Swinging Bucket Rotor to pellet EVs. The pellet was washed in 1,5 ml filtered 0.1 µm PBS (Microtube HighG, Thermo Fisher Scientific) for 1 h UC at 118,000 g at 4°C. EV pellets were resuspended in PBS and quantified by Bradford protein assay (Bio-Rad) or assessed by Nanoparticle Tracking Analysis (NTA) before storage in aliquots at -80°C. The proteins yields ranged between 4-7 µg /10^6 cells.

2.5. RNA extraction

RNA was extracted from cell pellets, melanoma EVs and CD14 cells after homogenizing the samples with 1 ml of TRIzol reagent (Ambion) and separating the two phases by adding chloroform: the upper clear aqueous layer containing RNA was collected, and RNA precipitated with 0.5 ml of 100% isopropanol. For melanoma cells, the time of incubation was 10 minutes at room temperature, while EV samples and CD14 cells were lysed overnight at 4°C. RNA was precipitated by centrifugation at 12,000 g for 10 minutes at 4°C; then the pellets were washed with 1 ml of 75% ethanol and dried out before adding H_2O. RNA was incubated at 55°C for 10 minutes and stored at -80°C. The RNA yield and purity were assessed by analysing OD_{260}/OD_{280} ratio by spectrophotometer (Picodrop Pico 100). For the RNA extraction from melanoma EVs, 100-500 µg protein were used, and the OD_{260}/OD_{280} ratio resulted often lower than 1.8-2.0.

For plasma EVs while comparing different protocols, RNA was extracted from samples isolated by ExoQuick precipitation (System Biosciences) resuspended in 100 µl of PBS without protein quantification by RNA NucleoSpin miRNA (Macherey-Nagel) kit. To eliminate any potential residual of non-exosomal RNA, freshly isolated EVs were treated with RNaseA (1:1000, Sigma) for 1 h at 37°C prior to RNA extraction. For IC studies on plasma EV from patients at different time points of the treatment, to assess IC modulation, another commercial kit including EV isolation and total RNA purification was used (ExoRNeasy Serum/Plasma kit, Qiagen). The EV isolation consisted in a membrane-based affinity binding step followed by phenol/guanidine-based lysis (QIAzol Qiagen): the aqueous and organic phases were then separated by adding chloroform and by centrifugation, the upper aqueous phase was transferred in a silicia-membrane spin column and RNA bound to the membrane was eluted in a small volume of water. RNA obtained from plasma EVs was reverse transcribed for qPCR without quantification because of its low quantity.

2.6. Quantitative Real Time PCR analysis

For cDNA synthesis, the High-Capacity cDNA Reverse Transcription kit (Thermo Fisher Scientific) was used with 0,1 to 1 µg RNA from melanoma cell lines and EVs. No RNA quantification was performed for plasma EV samples due to the low amount recovered from these samples. The reaction was carried out in the GeneAmp PCR System 9700 instrument (Thermo Fisher Scientific) incubating the samples and the RT mix at 25°C for 10 minutes and 60°C for 120 minutes. The cDNA was assayed by quantitative real-time PCR (qRT-PCR), performed in triplicates on an ABI PRISM 7900 Real-Time instrument using

a standard setting (50°C for 2 minutes, 95°C for 10 minutes and 40 cycles at 95°C for 15 seconds and at 60°C for 1 minute). TaqMan gene expression assays (Thermo Fisher Scientific) listed in Table 2.6.1 were used at a final concentration 0.2X. The transcript expression levels were calculated by normalising data to the expression of *ACTB* and *GAPDH* genes used as endogenous controls. Relative expression was determined using 2-ΔCt and expression fold change by 2-ΔΔCt method. Data were analysed with SDS 2.2.2 software and a cut-off of 35 Ct was used.

For EVs and cultured monocytes, a pre-amplification step was performed: one third of the cDNA was pre-amplified by using a pool of TaqMan assays at 0.2X final concentration prepared in 1X TE, mixed with TaqMan Preamp Master Mix (Thermo Fisher Scientific) and amplified in the thermocycler (95°C for 10 minutes, 10 cycles of 95°C for 15 seconds, followed by 60°C for 4 minutes). After 10 cycles, samples were placed on ice, the preamplification products were diluted 1:5 with 1X TE buffer and used for downstream analysis by PCR or stored at -20°C. The Ct value 40 was considered as cut-off. Water was used as negative control for cross-reaction and unspecific amplifications. To evaluate miR expression levels (listed in Table 2.6.2), qPCR analysis was performed according to manufacturer's instructions (Exiqon reagents). Endogenous controls used were U6 snRNA and SNORD48 to normalize miRs expression levels.

Table 2.6.1. Panel of TaqMan gene expression assay

Gene symbol	Description	Protein	Assay ID
CD274	Programmed Cell Death 1 Ligand 1	PDL1	Hs01125301_m1
PDCDLG2	Programmed Cell Death 1 Ligand 2	PDL2	Hs01057777_m1
PDCD1	Programmed Cell Death 1	PD1	Hs01550088_m1
PVR	Poliovirus Receptor	CD155	Hs00197846_m1
TNFRSF14	TNF Receptor Superfamily Member 14	HVEM	Hs00187058_m1
HAVCR2	Hepatitis A Virus Cellular Receptor 2	TIM3	Hs00958618_m1
LGALS9	Galectin-9	GAL9	Hs00371321_m1
C10orf54	V-Domain Ig suppressor of T cell activation	VISTA	Hs00735289_m1
CD226	DNAM-1	CD226	Hs00170832_m1
CD160	Natural Killer Cell Receptor, Ig Superfamily Member	CD160	Hs01073987_m1
TNFSF14	TNF Superfamily Member 14	LIGHT	Hs00542477_m1
CD96	T-Cell Surface Protein Tactile	CD96	Hs00976975_m1
CD3D	CD3-Delta	CD3	Hs00174158_m1
CD14	Monocyte Differentiation Antigen CD14	CD14	Hs02621496_s1
BTLA	B And T Lymphocyte Associated	BTLA	Hs00699198 m1
TIGIT	T Cell Immunoreceptor Ig and ITIM domains	TIGIT	Hs00545087 m1
GAPDH	Glyceraldehyde-3-Phosphate Dehydrogenase	GAPDH	Hs99999905_m1
ACTB	Actin Beta	Actin	Hs99999903_m1
CD163	Macrophage-Associated Antigen	CD163	Hs00174705_m1
CD68	Macrophage Antigen CD68	CD68	Hs02836816_g1
CD33	Myeloid Cell Surface Antigen CD33	CD33	Hs01076281_m1
CD4	T-Cell Surface Glycoprotein CD4	CD4	Hs01058407_m1
CD8A	T-Cell Surface Glycoprotein CD8 Alpha Chain	CD8	Hs00233520_m1
ITGAM	Integrin Alpha-M	ITGAM	Hs00355885_m1
FOXP3	Forkhead Box P3	FOXP3	Hs01085834_m1
HLA-DRA	MHC Class II Antigen DRA	HLA-DRA	Hs00219575_m1
HLA-A	MHC Class I Antigen A	HLA-A	Hs01058806_g1
PMEL	Premelanosome Protein	GP100	Hs00173854_m1

TYR	Tyrosinase	TYR	Hs00165976_m1
IL-6	Interleukin-6	IL6	Hs00985639_m1
TGFB1	Transforming Growth Factor Beta 1	TGFβ1	Hs00998133_m1
CCL2	C-C Motif Chemokine Ligand 2	CCL2	Hs00234140_m1

All gene assays were from Thermo Fisher Scientific company.

Table 2.6.2. miRCURY LNA Universal RT microRNA PCR Panel

microRNA Name	Target sequence	LNA™ PCR primer set, Product No
hsa-miR-100-5p	AACCCGUAGAUCCGAACUUGUG	205689
hsa-miR-34a-5p	UGGCAGUGUCUUAGCUGGUUGU	204486
hsa-miR-125b-5p	UCCCUGAGACCCUAACUUGUGA	205713
hsa-miR-100-5p	AACCCGUAGAUCCGAACUUGUG	205689
SNORD48	GATGACCCCAGGTAACTCTGAGTGTGTCGCTG ATGCCATCACCGCAGCGCTCTGACC	203903
U6 snRNA	GTGCTCGCTTCGGCAGCACATATACTAAAATTGGA ACGATACAGAGAAGATTAGCATGGCCCCTGCGCAA GGATGACACGCAAATTCGTGAAGCGTTCCATATTTT	203907

All miRNA assays were from Exiqon company

2.7. Co-culture experiments of melanoma cells

Sensitive and resistant melanoma cells were seeded in the chambers of 24 well transwell plates with 0.4 μm pore size (Corning Costar) at a density 2 x 10^5/well. After 72 h of incubation the insert was removed and cells of the bottom chambers were used for downstream analyses. These included western blot and flow cytometry analyses, as well as qRT-PCR for evaluation of IC modulation after co-culture incubation.

2.8. Cell viability assay

The MTT colorimetric assay was used to determine melanoma cell viability after treatment with BRAFi, MEKi, IFNγ, or melanoma EVs. Cells were seeded in 96-cell well/plates at a density of 1.5 x 10^4/well in triplicates left overnight to adhere prior to treatment with the drugs. After 72 h, MTT (50 μl of 5 mg/ml, Sigma) was added to each well and incubated for 2 h at 37°C; then, the MTT was removed, 100 μl of SDS/DMF were added and absorbance at 570 nm was detected by microplate spectrophotometer (Tecan).

2.9. Flow cytometry analysis of melanoma cell lines

To analyse IC expression on melanoma cells by direct flow cytometry, 2x10^5 cells were suspended in 50 μL of PBS and incubated with specific APC/PE/AlexaFlour647/PerCP-Cy5.5-conjugated antibodies or respective isotype controls, at 1:25 dilution, in single analysis or in combination, for 30 minutes at room temperature in the dark; an unstained control sample was included to set sample acquisition. After incubation, the cells were washed with 1 ml of PBS, centrifuged at 300 g for 10 minutes, and fixed in 200 μl of 1% formalin PBS in cytometry tubes. Tubes were gently vortexed before acquisition with BD

FACSCalibur flow cytometer (BD Biosciences). Data were analysed with FlowJo v8.8.6 (Becton Dickinson) software, presented as delta geometric mean (ΔgMFI), calculated as the experimental gMFI minus the background gMFI of antibody fluorescence) or percentage of positivity after setting the marker according to the negative isotype control. The used antibodies are listed in Table 2.9.

Table 2.9. Anti-human antibody used for flow cytometry staining

Antibody	Dye	Clone	Host/Isotype	Company	Catalogue no.
anti-CD274	PE	MIH1	Mouse IgG1, κ	BD Pharmingen	557924
anti-CD273	APC	MIH18	Mouse IgG1, κ	eBiosience	17-5888
anti-HVEM	Alexa Fluor647	94801	Mouse IgG1, κ	BD Pharmingen	564411
anti-Galectin-9	PE	9M1-3	Mouse IgG1, κ	BD Pharmingen	565892
anti-VISTA	PE	730804	Mouse IgG2b, κ	R&D System	FAB71261P
anti-CD155	PerCP/Cy5.5	SKII.4	Mouse IgG1, κ	BioLegend	337612
anti-CD3	PerCP	SK7	Mouse IgG1, κ	BD Pharmingen	345766
anti-CD25	APC	M-A251	Mouse IgG1, κ	BD Pharmingen	555434
anti-CCL2	APC	5D3-F7	Mouse IgG1, κ	eBiosience	17-7099
anti-CD8	PerCP	SK1	Mouse IgG1, κ	BD Pharmingen	345774
anti-CD4	PE	RPA-T4	Mouse IgG1, κ	BD Pharmingen	555347
anti-HLA-DR	PE CY	L243	Mouse IgG2a, κ	BD Pharmingen	655874
anti-CD14	FITC	M5E2	Mouse IgG2a, κ	BD Pharmingen	555397
anti-CD14	APC	MφP9	Mouse IgG2b, κ	BD Pharmingen	560180
anti-CD81	PE	5A6	Mouse IgG1, κ	BioLegend	349506
anti-CD9	PE	HI9a	Mouse IgG1, κ	BioLegend	312106
anti-CD63	PE	H5C6	Mouse IgG1, κ	BD Pharmingen	556020
IgG	PE	MOPC-21	Mouse IgG2b, κ	BD Pharmingen	556437
IgG	APC	MOPC-21	Mouse IgG1, κ	BD Pharmingen	550854
IgG	PerCP/Cy5.5	MOPC-21	Mouse IgG1, κ	BioLegend	400149
IgG	Alexa Fluor647	MOPC-21	Mouse IgG1, κ	BD Pharmingen	557714
IgG	PE	MOPC-21	Mouse IgG1, κ	BD Pharmingen	555749

2.10. Flow cytometry analysis of melanoma EVs

Melanoma EVs were analysed by flow cytometry after coupling them to 5 µm diameter latex-beads (Invitrogen) to detect them according the standard protocol of Thery et al., 2006. To this aim, 10 µl of latex-beads were mixed with 10 µg of EVs for 15 minutes at room temperature, and then incubated overnight in a final volume of 1 ml PBS at 4°C on a test tube rotator. Then, 110 µl of 1 M glycine were added, the mix was incubated for 30 minutes at room temperature, washed 3 times in PBS 0.5% BSA by centrifugation at 4,000 rpm in a benchtop microcentrifuge for 5 minutes. Finally, the EV-covered beads were divided in different test tubes in 50 µl PBS plus 0.5% BSA for antibody labelling. 5 µl of each antibody, including IgG isotype, was added separately to each tube and incubated for 30 min at 4 °C. After the incubation the mix was washed twice with PBS 0.5% BSA as previously described. Finally the ab-EV-beads were resuspended in 250 µl of PBS 0.5% BSA and acquisition in flow cytometry was performed.

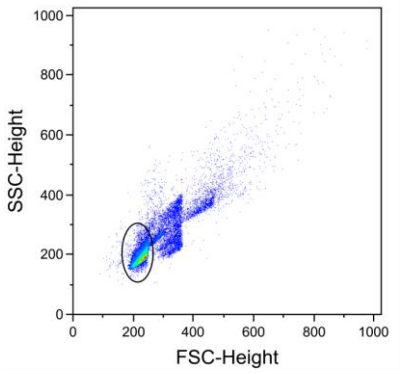

Figure 2.10. Extracellular vesicles on beads analysed by flow cytometry analysis. The circled area contains the single bead-EV events. The events non included in the area are considered beads aggregates, and thus they were not considered for analyses.

2.11. Western blot analysis

Cell protein lysates were obtained in RIPA buffer (Invitrogen) completed with 1X PhosphoSTOP phosphatase inhibitors and 1X complete EDTA-free Protease Inhibitor Cocktail (Roche), quantified by Bradford Protein Assay (Bio-Rad), and boiled for 5 minutes at 95°C in 1X NuPAGE LDS Sample Buffer (Thermo Fisher Scientific) in the presence of 1,4-dithiothreitol (DTT), a reagent that maintains SH groups in reduced state. In contrast, EV samples were mixed with 1X LDS and 1X DTT and boiled at 95°C for 5 minutes without a previous lysing step.

Samples were loaded on precasted NuPAGE Novex 4-12% Bis-Tris gels in 1X MOPS running buffer (Invitrogen), electrophoretically separated and transferred onto nitrocellulose filters using a Dry Blotting System (Invitrogen). After 1 h of blocking in 5% of BSA, filters were incubated with primary antibodies overnight at 4°C, washed three times with 1X TBST (Cell Signaling) and incubated for 1 h with horseradish peroxidase conjugated secondary antibody. The used antibodies are listed in Table 2.11. The immuno-reactive bands were visualised by chemiluminescence after 5 minutes incubation in the dark at room temperature with HRP substrate (ECL Western Blotting Detection Reagent, Amersham), substrate removal and filter exposure on the UVITEC chemiluminescence imaging system (Uvitec Alliance Q9 Advanced). Image acquisition was carried out with standard or manual programs in case of weak chemiluminescence signal. The Intensity Volume of the signals was analysed by NineAlliance software, and the ratio between the intensity volume of the protein of interest and of the control was calculated.

Table 2.11. Anti-human antibody used for western blot analysis

Antibody	Clone	Isotype	Dilution	Company	Catalogue no.
anti-PDL1	405.9A11	Mouse IgG1	1:1000	Cell Signaling	29122
anti-CD155	D3G7H	Rabbit IgG	1:1000	Cell Signaling	13544
anti-CD9	TS9	Rabbit IgG	1:500	Invitrogen	10626D
anti-β-Actin	AC-15	Mouse IgG1	1:1000	Sigma	A5441
anti-Alix	3A9	Mouse IgG1,k	1:1000	Biolegend	634502
anti-tGFP	2H8	Mouse IgG2b	1:2000	Origen	TA150041
anti-GM130	35/GM130	Mouse IgG1,k	1:250	BD	G65120
anti-BIP/GRP78	40/BiP	Mouse IgG2a	1:250	BD	G73320
anti-Rab5b	15/Rab5	Mouse IgG1,k	1:500	BD	610725
anti-STAT3	K-15	Rabbit IgG	1:500	Santa Cruz	sc483
anti-Stat1α p91	C111	Mouse IgG1	1:500	Santa Cruz	sc-417
anti-IRF1	D5E4	Rabbit IgG	1:1000	CellSignaling	8478
anti-gp100	HMB45	Mouse IgG	1:500	abcam	ab787

2.12. Confocal microscopy analysis

Confocal microscopy analysis of melanoma cells co-cultured with EVs was performed by incubating $3x10^4$ cells/well with 30 µg of EVs in open wells µ-Slide (Ibidi). After overnight culture, medium was removed, cells were washed with 1X PBS to remove the non-internalized EVs, fixed in 120 µl of 4% paraformaldehyde for 10 minutes, washed twice and stained with 5 µg/ml of wheat germ agglutinin (WAG) conjugates (Invitrogen), which selectively bind to N-acetylneuraminic acid (sialic acid) residues labelling in red the cell membrane. After washing twice with PBS, cells were incubated for 5 minutes with 300 nM blue-fluorescent DAPI nucleic acid (Invitrogen) diluted in PBS, followed by three washes with PBS. Finally, 150 µl of Ibidi Mounting Medium were added to optimize the fluorescence signal, and cells were analysed by confocal microscopy. The used Leica SP8 AFC AOBS WLL HyD microscope has detector sets for super-sensitive imaging with high quantum efficiency, low noise and large dynamic range, acting in synergy with the filter-free spectral detection system and the acousto-optical beam splitter in the gapless light detection with maximum photon efficiency, making it suited for imaging of green fluorescent nanovesicles. The analysis set was performed by ImageJ software in collaboration with Cell Imaging Facility at our institute, and merged images were generated from acquisition in green, blue and red channels.

2.13. Transmission electron microscopy

TEM was performed in collaboration with Dr A Villa from M.I.A Consortium. To this aim I prepared two pellet of isolated EVs (from 200 to 300 µg of protein) from two melanoma cell lines LM16S and LM16R by ultracentrifugation protocol. The fresh vesicles were fixed in 100 µl of paraformaldehyde 4 % for 20 minutes at room temperature. After the incubation, 1.5 ml of PBS were added to wash the EVs following 1h of high speed

ultracentrifugation at 53,000 rpm with Beckman TLA100.3 Fixed Angle Centrifuge Rotor. Finally the washed pellets were resuspended in 10 µl of phosphate buffer 0.12 M. The pellet was sent to our collaborators for immunohistochemistry analyses for the detection of CD63 marker.

2.14. Plasma and peripheral blood mononuclear cell (PBMC) collection

Blood processing was performed within two hours of venipuncture. PBMCs and plasma were isolated from whole blood collected in EDTA tubes. To obtain the plasma free of platelets, whole blood was centrifuged for 15 minutes at 1,700 g, and plasma was collected for a second centrifugation at 1,700 g of 10 minutes before storage at -80°C. The blood cell pellet was resuspended in PBS to isolate white blood cells by Ficoll-Paque gradient (GE Healthcare Life Sciences). After centrifugation at 800 g for 15 minutes at room temperature with brake off, the upper layer containing PBMCs were collected and washed once with PBS. Ammonium-Chloride-Potassium Lysing Buffer (ACK) treatment was used to lyse red blood cells by adding 5 ml of ACK and incubation at 4°C for 5 minutes. After washing in PBS cells were counted with Trypan Blue solution prior to further experiments or storage at -80°C in freezing solution (RPMI 40% FBS and 10% DMSO) in a cool cell (Biocison). For $CD14^+$ cell isolation, CD14 MicroBeads for human monocytes were applied to PBMCs according to the manufacturer's instructions (MACS Miltenyi Biotec). Both the $CD14^+$ monocyte and the $CD14^-$ cells fraction were collected for further experiments. The purity of obtained fractions was assessed by flow cytometry (Figure 2.14).

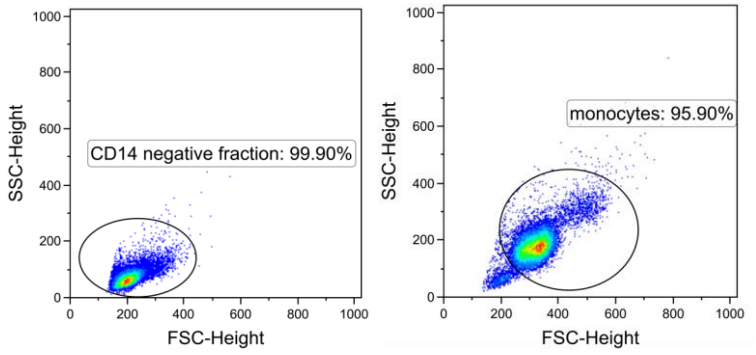

Figure 2.14. Negative and positive CD14 cells isolated by microbeads from PBMCs of an healthy donor.

2.15. Labelling of EVs for immune cell interaction

To evaluate the interaction of melanoma EVs with immune cells, EV (20 µg) were labelled with the membrane lipophilic dye green fluorescent carbocyanine SP-$DIOC_{18}$(3) (Thermo

Fisher Scientific). The SP-DiOC$_{18}$(3), or 3,3'-Dioctadecyl-5,5'-Di(4-Sulfophenyl) Oxacarbocyanine Sodium Salt, is a DiO analogue soluble in water because of a sulfonate group that when incorporated into membranes is highly fluorescent. SP-DiOC was diluted 1:100 in PBS and vortexed for few seconds. EVs were brought to a final volume of 198 µl with PBS, 2 µl of the diluted SP-DiOC were added mixing well and incubated for 15 minutes at room temperature in the dark. The EVs were washed twice in 1 ml of exosome-free FBS and thereafter once with 1 ml of PBS for 30 minutes of ultracentrifugation at 100,000 g using Beckman Coulter TLA 100.3 ultracentrifuge rotor. The stained EVs were suspended in RPMI for co-culture experiments.

2.16. Interaction of labelled EVs with immune cells

Sp-DioC-labelled, CD81-GFP$^+$ or PDL1-GFP$^+$ EVs 20 µg were added to 2 x 10^5 PBMCs to assess the uptake by monocytes and T cells. After an overnight incubation PBMCs were harvested and labelled with fluorochrome-conjugated antibodies against CD14, CD3 and PDL1 to identify monocytes, T cells, EV uptake level and potential modulation of IC such as PDL1. After an incubation with the antibodies of 30 minutes at room temperature, samples were washed and acquired with a FACSCalibur flow cytometer and analysed with FlowJo software (Becton Dickinson).

2.17. Monocyte-melanoma EV co-cultures

For monocyte-EV co-cultures CD14$^+$ cells were purified from buffy coats of healthy donors by sorting with anti-CD14$^+$ beads (MACS, Miltenyi Biotech) according to manufacturer's instructions. Their purity (>95%) was assessed by flow cytometry using a FACSCalibur flow cytometer (Becton Dickinson) after labelling samples with APC-conjugated anti-CD14 monoclonal antibody (Becton Dickinson). Isolated CD14$^+$ cells (1 x 10^6 in 1ml) were co-cultured with purified melanoma EVs (100 µg) in complete medium additioned with 10% EV-depleted FCS for 24 h. Then, monocytes were harvested to assess their phenotype by flow cytometry. To this aim, cells were labelled with antibodies against CD14 and HLA-DR to detect the presence of M-MDSCs in concomitance with IC expression of PDL1, PDL2, CD155, GAL9. EV conditioned CD14$^+$ cells were also analysed by qRT-PCR (chapter 2.5. and 2.6.). Harvested EV-conditioned CD14$^+$ cells were next co-cultured with autologous CD14$^-$ fraction containing T cells to measure their immune suppressive potential.

2.18. Proliferation experiments

EV-conditioned monocytes were tested for their suppressive potential on T cell proliferation. To test the T cell proliferation by flow cytometry, the $CD14^-$ fraction were labelled with Carboxyfluorescein succinimidyl ester (CFSE, Thermo Fisher Scientific) before co-culturing them with monocytes pre-treated with EVs.

For CFSE labelling 5 x 10^6 cells were mixed with 100 µl of a diluted solution of CFSE (1:100 in complete medium). After mixing cells with the solution, additional 800 µl of medium were added to the mix and incubated for 15 minutes at 37 °C. Following the incubation, cells were washed twice with 1.5 ml of EV-depleted FCS. To this aim, cells were centrifuged at 1600 rpm for 10 minutes, and after counting the labelled cells they were resuspended in medium in sterile tubes for co-culture incubation (PBMC 3x10^5 cells in 300 µl). For the CD14 negative fraction, 10^5 cells were seeded into 96 well plates in 100 µl. In addition, 1 µl of Dynabeads T-Activator CD3/CD28 were added on cells in a final volume of 200ul. After 120 h of incubation, cells were collected and stained for flow cytometry analysis with the following antibodies: CD4, CD8, CD25 (Figure 2.18).

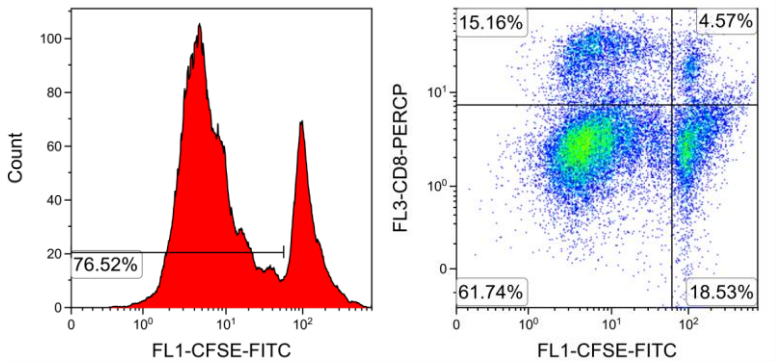

Figure 2.18. T cell proliferation by flow cytometry analysis. The histogram on the left is gated on CD3 positive cells and shows the proliferation of total T cells. The dot plot (on the right) shows the proliferation (CFSE negative cells) in two different subpopulations of CD3, the CD8 positive and negative cells.

2.19. Nanoparticle Tracking Analysis (NTA) of EVs

NTA was performed with NS300 Nanosight instrument (Malvern Panalytical). For whole plasma analysis, samples were thawed at room temperature, vortexed for 20 seconds and 2 µl of plasma were diluted 1:450 in PBS filtered 0.1 µm and vortexed for further 20 seconds. Nanosight parameters were set as follows: threshold from 4 to 7, camera level value 15 or 16, and screen gain=1. Samples were acquired for 60 seconds for three times. Prior to start the automatic analysis by NTA software, I checked the particles per frame (P/F) parameter, which should range between 20 to 120 particles per field; new dilutions and measurements were performed in case of a higher P/F value.

NTA analysis of purified EVs from melanoma cell lines was performed using 2 µl of ultracentrifugation isolated EVs diluted in 500µl of filtered PBS and vortexed for 20 seconds. Both, plasma and isolated EV from cell supernatant are represented in Figure 2.19.

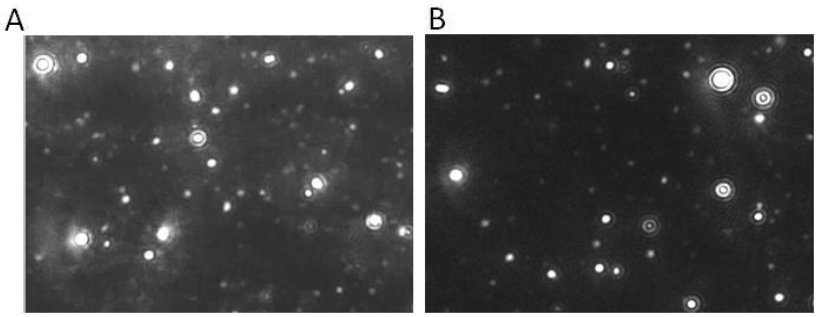

Figure 2.19. Representative snapshots of EVs by NTA. A) plasma EV of melanoma patients and B) EVs isolated from conditioned medium of melanoma cell lines.

2.20. Isolation of plasma EVs by ultracentrifugation

500 µl of plasma were diluted 1:8 in PBS previously filtered 0.1 µm and centrifuged at 16,500 g for 10 minutes to collect the first pellet (fraction 1, F1); supernatant was recovered and ultracentrifuged at 118,000 g for 90 minutes to obtain the second fraction (F2). A Beckman TLA100.3 Fixed Angle Centrifuge Rotor was used for UC. F1 and F2 pellets were resuspended in 100 µl of filtered PBS for downstream analysis and protein was quantified by spectrophotometer analysis and by Bradford staining. Both methods distinguished the protein yields of the two fractions, as the F1 fraction displayed a low protein content ranging between 50 to 300 µg, and the F2 fraction showed a higher protein content, in the range of 300 to 1,500 µg. The obtained fractions were subsequently used for western blot analysis or functional analysis in co-culture with autologus $CD14^+$ monocytes.

2.21. Isolation of plasma EVs by ExoQuick

Thawed plasma was centrifuged 3,000 g for 15 minutes to remove cell debris, mixed with ExoQuick polymer (System Bioscience), 65 µl for 250 µl of plasma, and incubated at 4°C for 30 minutes. Then, the mixture was centrifuged at 1,500 g at room temperature for 30 minutes, the supernatant removed and the pellet was resuspended in 100 µl of PBS for downstream analysis such as qRT-PCR.

2.22. Statistical analysis

Data were analysed using GraphPad Prism 5 Software (GraphPad Software Inc.). Results are analysed using unpaired or paired Student's *t*-test, Mann-Whitney test, Pearson and Spearman correlation, as specified. Data were considered significant if $p < 0.05$.

3. Modulation of IC expression in melanoma

At the beginning of my studies, I selected a set of IC molecules of potential interest based on the available literature data reporting expression in melanoma or in other tumour types. The list included PDL1, PDL2, PD1, HVEM, GAL9, CD155 and VISTA.

3.1. Expression of IC in melanoma tissues and melanoma cell lines

I first analysed the expression levels of these molecules by qRT-PCR in a series of cutaneous, lymph node and visceral metastatic melanoma specimens from stage III and stage IV melanoma patients for which other data displayed in Table 2.1.2 were available in the hosting laboratory [62]. Results showed that all IC transcripts were expressed, with HVEM resulting as the most expressed IC, followed by GAL9 and VISTA. An array of immune cell markers including CD14, CD163, CD68, CD33, CD3, CD4, CD8 displayed high expression levels in these samples, indicating the occurrence of an immune tumour infiltrate, although at lower levels than melanoma markers PMEL, MLANA and TYR (Figure 3.1.1).

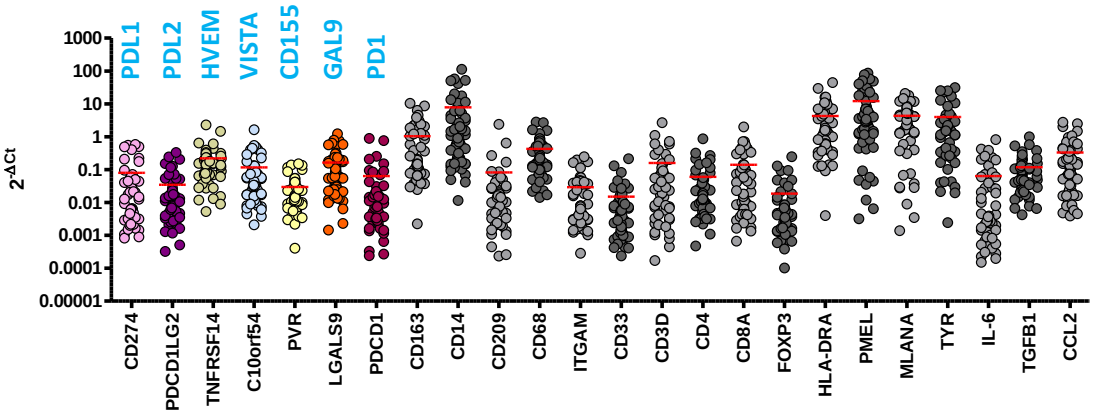

Figure 3.1.1. Gene expression in tumour specimens. Expression levels of IC and other genes related to melanoma and immune infiltrate in metastatic melanoma specimens (n=58). GAPDH was used as endogenous control for the relative quantification. IC protein names are written in blue. Each gene was tested in triplicate.

Next, I analysed the correlation between the expression of IC and of immune infiltrate-related genes. IC resulted highly correlated between each other and also correlated with the immune cell markers, but were unrelated to the melanoma markers. The representation in a correlation matrix of the r values of significant correlations showed that the IC also correlated with the expression of cytokines, especially TGFβ and CCL2 (Figure 3.1.2).

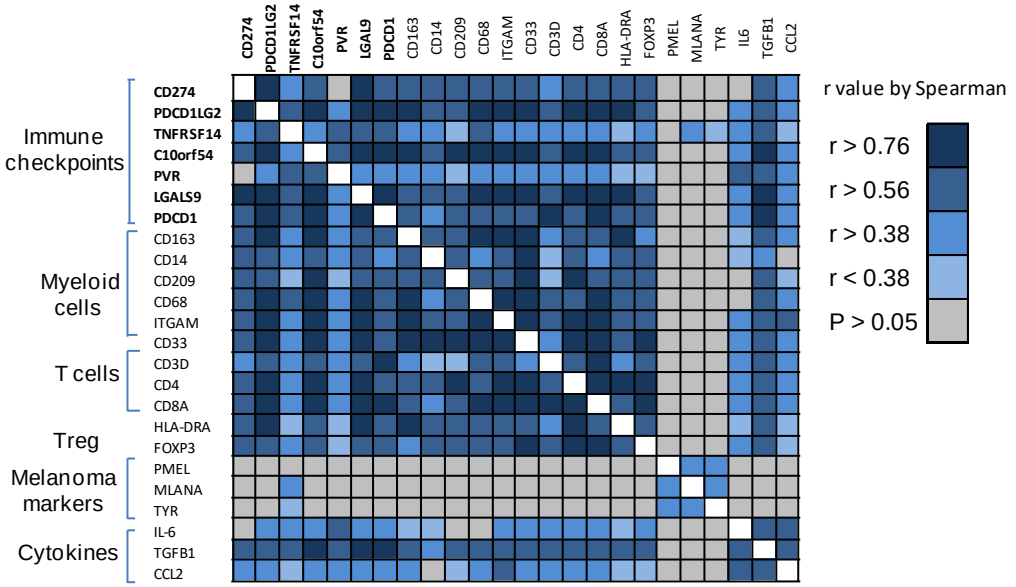

Figure 3.1.2. Correlation matrix of the expression levels of IC, myeloid and T cell markers, melanoma markers and cytokines genes in melanoma specimens. The indicated r values result from univariate Spearman analysis. Each gene was tested in triplicate.

To study if the IC were similarly expressed also in melanoma cell lines, I performed by qRT-PCR an initial screening in 31 melanoma cell lines obtained in the hosting laboratory from melanoma metastatic specimens [256] (Figure 3.1.3). PDL1, PDL2, HVEM and GAL9 were expressed at similar levels in melanoma cell lines and specimens, while PD1 and TIM3 were not detected in a first set of 14 studied cell lines, thus I decided to not further investigate their expression in the 17 remaining cell lines. These data indicate that several IC are expressed in melanoma cells and in tumour tissues, where the expression levels are highly correlated to markers of immune infiltrate.

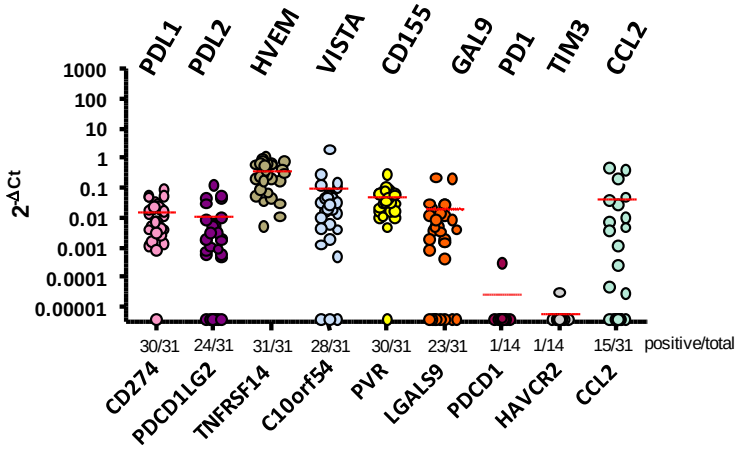

Figure 3.1.3. Expression of IC genes in 31 melanoma cell lines. Positive/total tested lines are indicated. On top are written the protein names of the ICs. Each gene was tested in triplicate.

3.1.1. IC expression by melanoma during acquisition of resistance to BRAF/MEKi

Few studies investigated the potential modulation of IC expression during the acquisition of resistance to BRAF and MEK inhibitors [258-260]. To explore this issue and study the molecular mechanisms involved in IC modulation, a BRAF-mutated melanoma cell line sensitive to BRAF/MEKi was repeatedly exposed to the drugs and IC expression was monitored after each cycle of selection.

After treatment with the combination of Dabrafenib and Trametinib, cells were cultured without the drugs to let them re-grow, and IC expression and drug sensitivity were assessed after each treatment cycle. The selection cycles resulted in a reduction of the drug effect on cell proliferation, as shown by the results of MTT assays depicted in Figure 3.1.1.1A. A change in morphology was also observed, with increased cell size and a switch from an epithelial-like polygonal shape to a fibroblast-like shape (Figure 3.1.1.1B). IC expression assessed by flow cytometry showed that PDL1, PDL2, and CD155 were upregulated after the second cycle of treatment, while HVEM and GAL9 displayed a small decrease in the percentage of positive cells (Figure 3.1.1.1C). Overall, these data indicate that epigenetic modulations occurring upon chronic exposure to BRAF/MEKi include pathways regulating the expression of different IC molecules, defining an association between increased IC expression and the acquisition of drug resistance in melanoma cells as shown by the high level of IC50 value (Figure 3.1.1.1A).

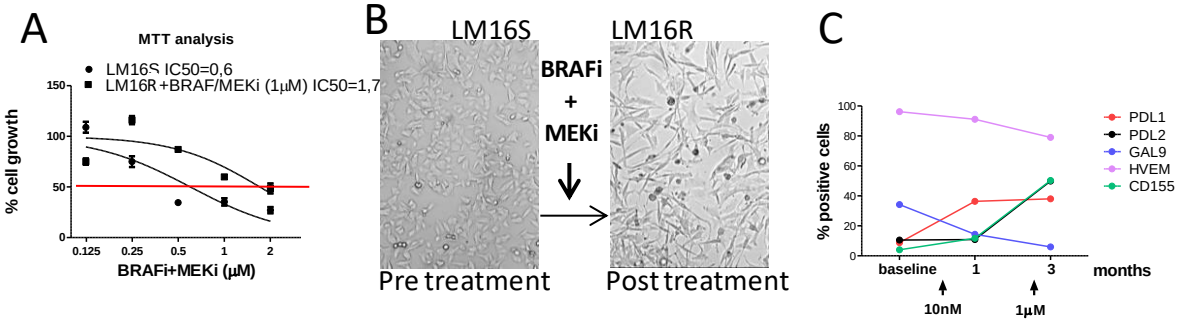

Figure 3.1.1.1. Melanoma cell selection with the combination of BRAF/MEKi until the acquisition of resistance. A) MTT analysis of cells after chronic exposure to BRAF/MEKi at 1 μM depicted an IC50=1,7 of LM16R compared to an IC50=0,6 of the parental LM16S cells. B) Changes in cell morphology after drug selection and resistance acquisition. C) Flow cytometry analysis of IC expression in LM16S (pre) and LM16R (after drug selection) at 1 and 3 months of treatment. The percentage of positivity is calculated as the difference between the positivity of each IC and its isotype control. The study started with two different cell lines (LM16S and LM47S) but for technical problems it was concluded with only one cell line (LM16).

3.1.2. Expression of IC in melanoma cell lines resistant to BRAF/MEKi

To obtain an adequate model system to investigate the IC cargo of EVs released by melanoma cells and their role in protumoral cell interactions, I characterized a set of

resistant BRAF-mutated melanoma cell lines. Taking advantage of a set of six resistant cell lines previously obtained in my hosting laboratory I determined their IC expression and their potential association with BRAFi resistance. These resistant variants were obtained by repeated selection cycles with the BRAF-inhibitor Vemurafenib (PLX4032) until the onset of stable resistance [257]. These cell lines displayed cross-resistance to BRAF inhibitor Dabrafenib (GSK2118436) and to MEK inhibitor Trametinib (GSK1120212) and did not show additional gene mutations compared to their parental cell lines in a set of studied genes.

Before IC studies, I standardized cell culture conditions to obtain samples at similar monolayer confluence. The analysis of IC genes in matched resistant (R) and parental sensitive (S) cell line pairs depicted in Figure 3.1.2.1 showed different expression patterns. PDL1, CD155 HVEM and VISTA transcripts were detectable in all cell lines at different levels, while PDL2 and GAL9 showed some negative samples. PDL1 was expressed at higher levels in R compared to S in four cell line pairs (LM16, LM11, LM43, LM47), and PDL2 transcript was higher in LM16R and LM47R compared to the sensitive counterparts. CD155, GAL9 and HVEM transcripts showed higher expression in three resistant cell lines compared to the sensitive counterparts, i.e. in LM16, LM43, LM47 for CD155, and in LM11, LM17, LM43 for GAL9 and HVEM. VISTA transcripts showed lower expression levels in five R cell lines compared to S cells.

In summary, the expression of PDL1 and PDL2 transcripts were increased in resistant compared to sensitive cells, VISTA decreased in resistant cells, while HVEM and GAL9 were similarly expressed in S and R lines. On the other hand, CD155 increased in 3 to 6 resistant cell lines, and decreased in the other three.

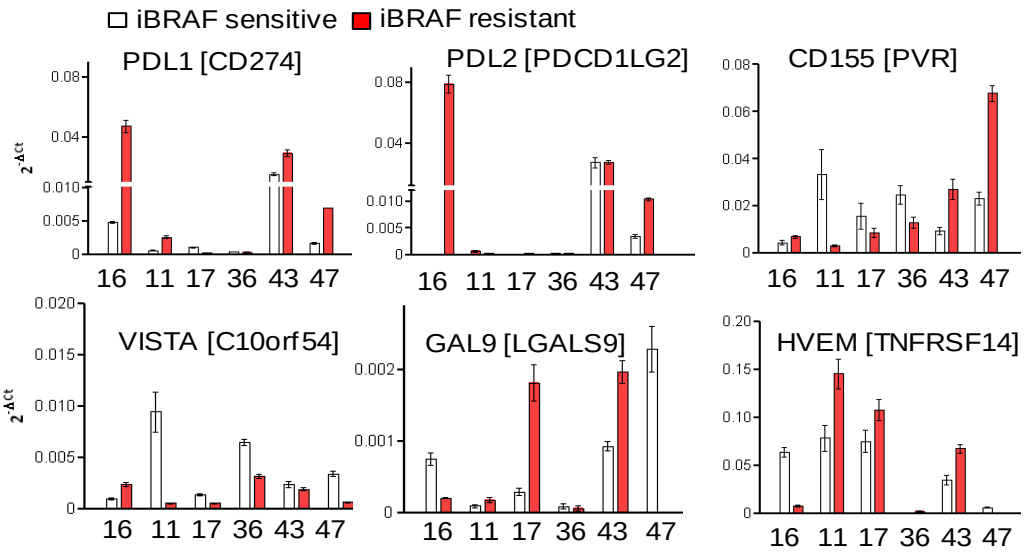

Figure 3.1.2.1. IC gene expression levels in resistant and sensitive melanoma cell line pairs. Expression levels of IC genes in R resistant (red bars), S sensitive cell lines (white bars) are reported. This experiment was repeated at least twice. Each gene was tested in triplicate and the error bars represent the standard deviation of the triplicates.

Western blot analysis confirmed a higher PDL1 expression in R with respect to S cell lines in three cell line pairs (LM16, LM43, LM47), while PDL1 was negative in the others. In addition, CD155 signal appeared as a double band in most of the samples (Figure 3.1.2.2).

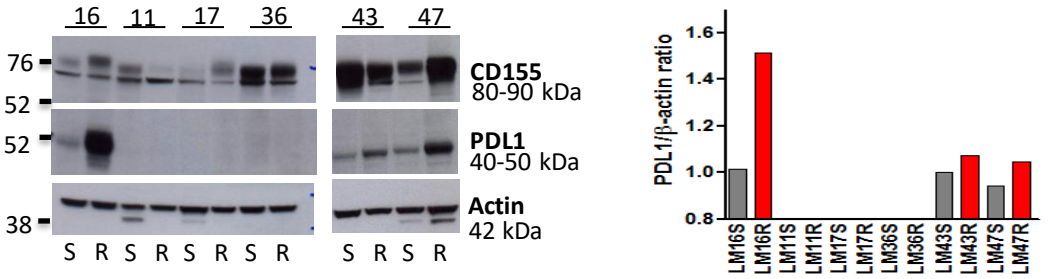

Figure 3.1.2.2. Protein expression level of PDL1 and CD155 in melanoma cells by western blot analysis. The bar plot on the right represents relative quantification of PDL1 expression after normalising the signal with B-actin. Grey bars- S cell lines; Red bars- R cell lines. This experiment was performed at least twice. Results in the figure show representative data.

Based on these results, three S and R cell line pairs, namely LM16, LM43 and LM47, were selected for further studies. Flow cytometry analysis of IC expression showed that resistant cell lines LM16R and LM47R co-expressed PDL1 and PDL2, and high levels of CD155, while their sensitive counterparts were negative or weakly positive. Furthermore, HVEM and GAL9 expression was higher in LM16S and LM47S than in the resistant variants. In contrast, LM43 S and R cells showed a similar IC expression pattern, both lacked PDL1 and PDL2, while expressing HVEM and CD155. VISTA protein was not detectable in any cell lines, despite I could detect its gene transcript. This difference may

result from a potential post-transcriptional regulation of the protein expression or from the expression of a different VISTA splicing variant transcript (Figure 3.1.2.3).

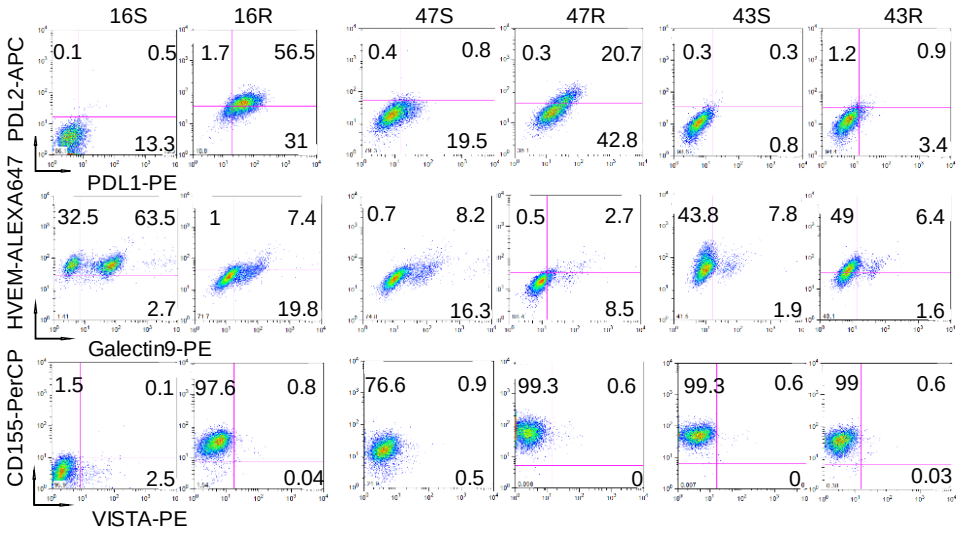

	LM16S		LM16R		LM47S		LM47R		LM43S		LM43R	
IC	[ΔgMFI]	% pos	[ΔgMFI]	% pos	ΔgMFI	% pos	ΔgMFI	% pos	ΔgMFI	% pos	ΔgMFI	% pos
PDL1	0-2	13.8	28-47	87.5	4.1	20.3	13.3	63.5	0.1	1.1	1.3	4.3
PDL2	0	0.6	22-50	58.2	1.6	1.2	11.9	21.0	0	0.6	0.1	2.1
Gal-9	2-20	66.2	4-18	27.2	8.3	24.5	4.1	11.2	3.8	9.7	2.6	8.0
HVEM	30-70	96.0	7-13	8.4	10.6	8.9	4.3	3.2	31.5	51.6	24.5	55.4
VISTA	0	2.6	0	0.8	0	1.4	0	0.6	0	0.6	0	0.6
CD155	0-6	1.6	13-24	98.4	12.2	77.5	55.3	99.9	46.4	99.9	30.2	99.6

Figure 3.1.2.3. Flow cytometry analysis of IC expression by LM16, LM43 and LM47 cell line pairs. The dot plots show the results of double staining. The table reports the [ΔgMFI] as range of ΔgMFI from several experiments and the positivity in percentage of the represented data from the graphs. This experiment was performed at least twice.

The results of flow cytometry quantified in terms of the geometric mean of fluorescence intensity (ΔgMFI) are reported in Figure 3.1.2.3. In several experiments LM16R consistently showed higher levels of PDL1, PDL2 and CD155 as compared to LM16S. Fluctuations were observed in LM16S for the expression of PDL1 and CD155 proteins, suggesting that their expression is modulated during culture, possibly depending on cell density. In contrast, PDL2 was always negative in LM16S. I could assess a similar IC expression pattern in LM47 cell lines pair, while the LM43 cell line pair displayed no differences between S and R.

In conclusion, these studies confirmed that different IC are modulated in melanoma cells both at gene and protein levels upon the acquisition of resistance to kinase inhibitors. The modulation of IC expression may differ in pattern in different cell lines, although some changes appear to be shared.

3.1.3 Analysis of IC expression in specimens from patients treated with BRAFi

To determine whether the onset of drug resistance alters the expression of IC in patients' tumours, I interrogated a dataset of gene expression profiles of melanoma samples recently analysed in my hosting laboratory that included tumours excised before and during treatment of 7 patients (unpublished dataset). The under-treatment samples were obtained from metastatic tumours arising de novo or progressing during the treatment with BRAFi Vemurafenib, thus showing resistance to therapy.

By comparing the expression levels in *post-treatment* vs *pre-treatment* samples, significant differences were evidenced for CD155 gene, showing an increase after treatment, and for HVEM and GAL9, showing a decrease (Figure 3.1.3.1).

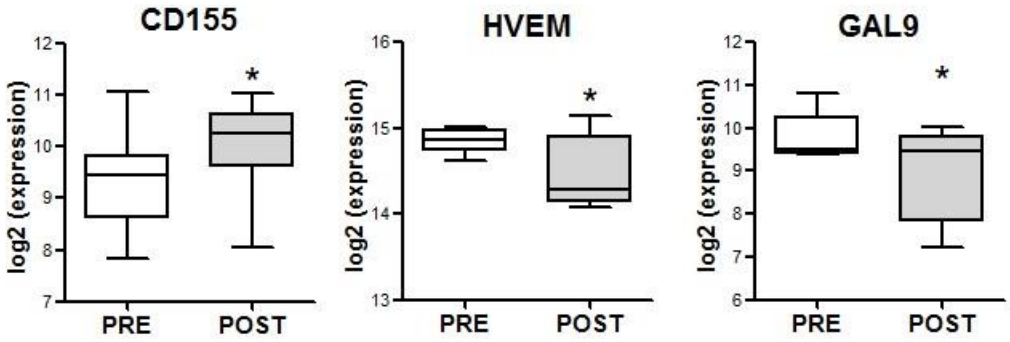

Figure 3.1.3.1. Expression of CD155, HVEM, GAL9 genes in melanoma tumours progressing despite targeted therapy. Pre-treatment and post-treatment melanoma tumours from 7 melanoma patients. The horizontal line is the median value of the seven patients for each gene, and the whiskers are the two lines outside the box that extend to the highest and lowest observations.

These data indicate that the modulation of IC expression associates with the acquisition of resistance to BRAF inhibitors in patients' tumours as previously observed for melanoma cell lines. In addition, the specific alterations of IC expression observed in resistant cell lines have a correlate in patient tumours, suggesting that drug pressure may act on melanoma by common alterations *in vitro* and *in vivo*.

3.2. Expression of IC by EVs released by drug resistant melanoma cells

Tumour EVs are endowed with pro-tumorigenic features and display immunomodulating properties. Tumour EVs may regulate the immune response by transferring their cargo. I investigated whether the melanoma EV cargo included IC molecules.

3.2.1. Melanoma EV characterization

To evaluate if melanoma EVs carry IC and if they are involved in the modulation of IC expression in EV-interacting recipient cell lines, I characterized EV isolated from the

conditioned media of the three cell line pairs showing major differences in IC expression (LM16, LM43 and LM47) by flow cytometry, western blot and qPCR. Tumour EVs were isolated from the conditioned media by ultracentrifugation protocol and characterized for their size and concentration by Nanoparticle Tracking Analysis (NTA) and electron microscopy, and for EV markers by flow cytometry and western blot. By NTA, the size of counted vesicles showed similar peak values of the mean parameter for the sensitive and resistant EV variants for LM16 and LM47, while EVs from LM43R cells displayed a higher mean and mode compared to EVs obtained from the LM43S cells. The protein yields of the isolated EV fractions quantified by Bradford resulted significantly correlated with the number of particles per ml detected by NTA, supporting the purity of the vesicle samples (Figure 3.2.1.1).

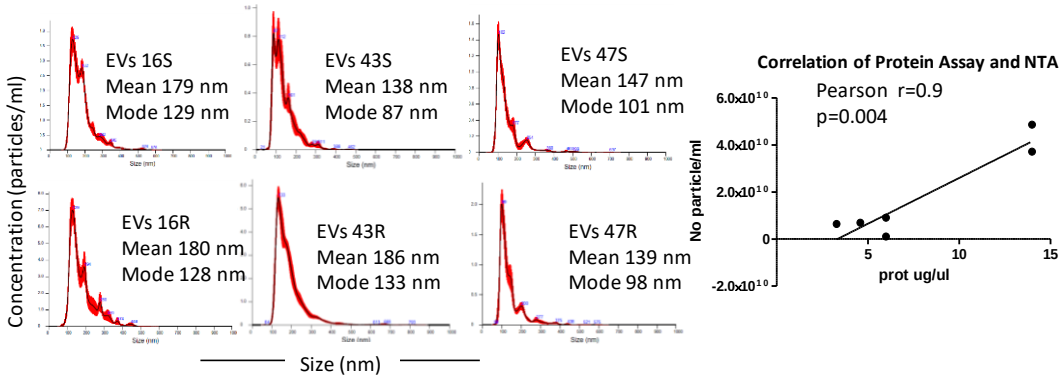

Figure 3.2.1.1. Characterisation of EVs isolated from melanoma cells by NTA. Histograms show NTA of samples isolated from resistant melanoma cell lines and their parental lines. The correlation of protein yields of the isolated EV fractions quantified by Bradford with the number of particles per ml detected by NTA is shown on the right.

Immunoelectron microscopy analysis performed on LM16S and LM16R EVs showed a positivity for the EV marker CD63 (Figure 3.2.1.2A). Indications on the size were also given, around 100 nm, but the exact size of the particles was not measured because of the shrinking effect during preparatory steps of the samples for TEM [261].

Purity was assessed by western blot and flow cytometry. The presence of the exosome marker Rab-5B involved in the regulation of vesicular traffic, and of Alix, a regulator of exosome biogenesis [262], were confirmed by western blot analysis, as well as the absence of the markers GM130 and BIP, a cis-Golgi and an ER marker (Figure 3.2.1.2B). In addition, a latex-beads protocol was used for flow cytometry analysis of EVs, which allowed to visualize the stained EVs bound to the beads. EVs isolated from LM16S/R cell lines resulted positive for CD63, CD81 and CD9 tetraspanin EV marker expression (Figure 3.2.1.2C).

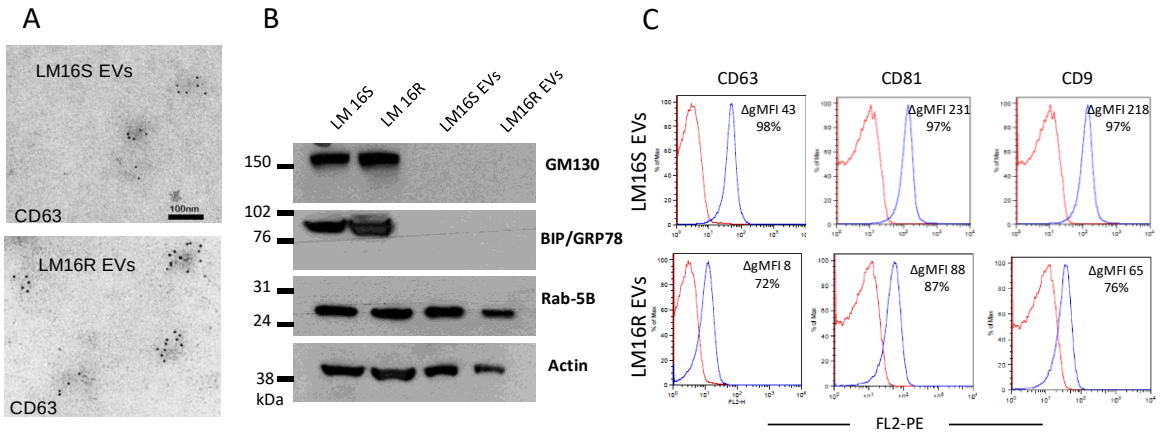

Figure 3.2.1.2. Characterisation of melanoma EVs. A) Immunoelectron microscopy of purified LM16S and LM16R EVs labelled with anti-CD63 antibody. B) Western blot showing positivity for Rab5 exosomal marker. C) Flow cytometry analysis of CD63, CD81 and CD9 markers on EV coated latex-beads. The EV markers are represented by the blue histograms and the isotype control by the red histograms.

3.2.2. Expression of IC by melanoma EVs

Western blot and flow cytometry analysis on IC showed that EVs expressed the same checkpoints their originating cells did, and EVs were negative for IC that the releasing cells did not expressed, with some exceptions. Indeed, LM16 EVs expressed PDL1, CD155 and GAL9 as their relative cells, and LM43 EVs were positive for CD155 and lacked PDL1 and GAL9 as their cognate cells. On the other hand, EVs from LM47 cell lines expressed low levels of all the IC markers although they were detected at high levels in their cells of origin (Figure 3.2.2). These results demonstrate that melanoma EVs carry different IC, and one of them, GAL9, was observed to be on the EV membrane.

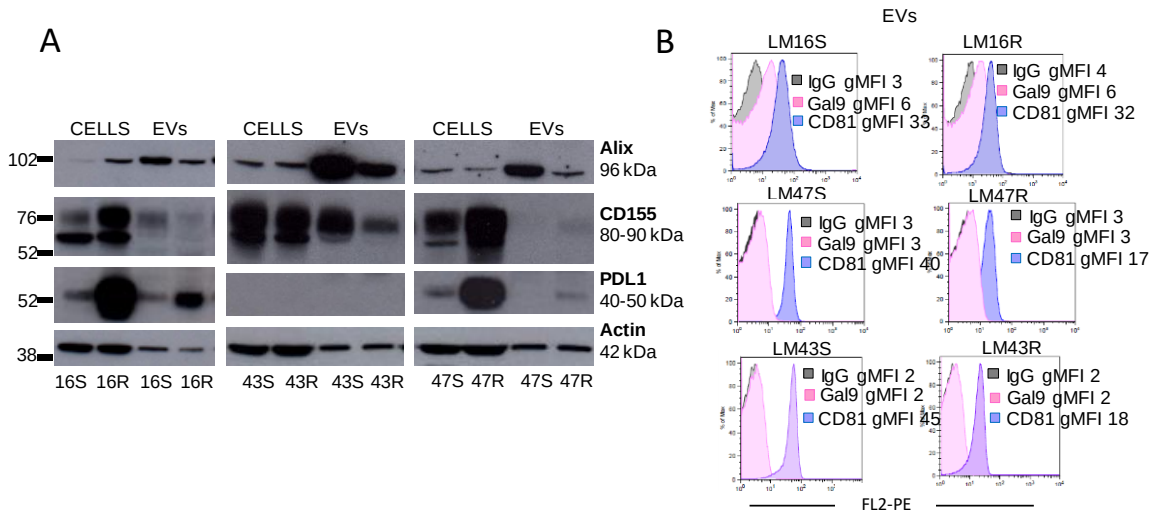

Figure 3.2.2. IC expression in melanoma EVs. A) Western blot analysis of PDL1 and CD155 expression in EVs and cognate cells. Alix was used as EV marker and actin as loading control. B) Flow cytometry analysis of EV coated latex-beads stained for GAL9 and the EV marker CD81.

3.2.3. Analysis of IC gene transcripts carried by EVs

Since EVs are known carriers of genetic material, I tested whether IC gene transcripts were detectable in melanoma EVs. IC transcripts carried by tumour EVs may have inhibitory effects on the host immune system once internalised by recipient cells and thereby contribute to cancer progression. RNA studies showed that EVs contain IC transcripts, consistent with the expression pattern observed in their originating cells. Results showed that HVEM and CD155 are carried by both, LM16S and LM16R EVs and PDL1, PDL2 were only detected in LM16R EVs. HVEM, VISTA and GAL9 were also detected in LM43 EVs. On the other hand LM47 EVs appeared negative for IC transcripts (Figure 3.2.3).

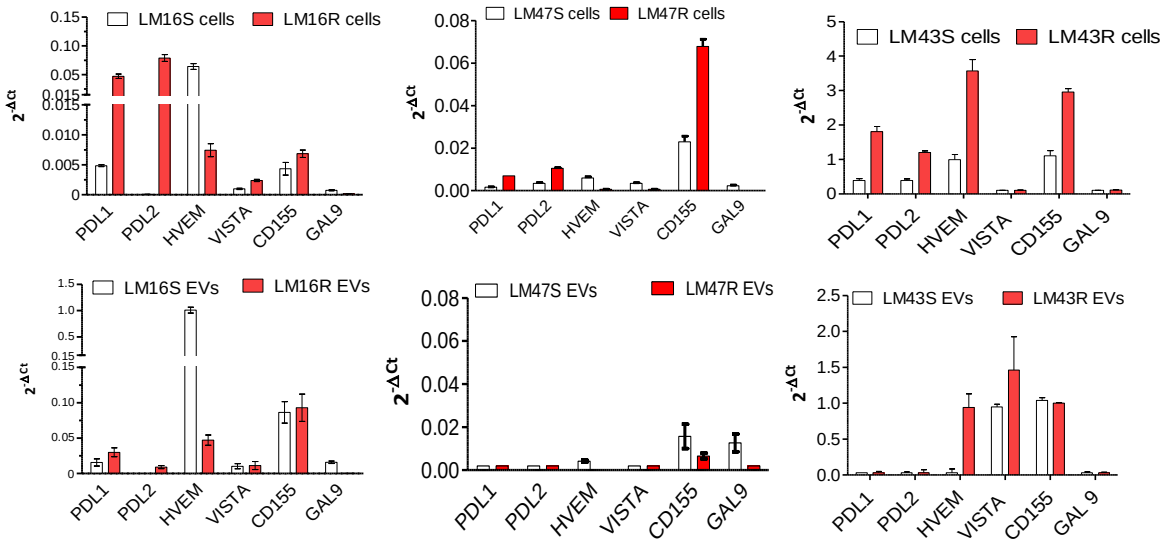

Figure 3.2.3. Melanoma EVs carry IC transcripts. Quantitative RT-PCR analysis of IC transcripts were detected in RNA extracted from EV (lower panels) and cell (upper panels) samples. To eliminate potential residuals of non-EV RNA, freshly isolated EVs were treated with RNase solution prior to RNA extraction. Two housekeeping genes were tested for result normalisation, GAPDH and ACTB; ACTB showing a small Ct variation was used to calculate expression levels. IC transcripts were negative in LM47 EVs while ACTB and GAPDH housekeeping genes were instead detectable. White bars -sensitive samples and EVs; red bars-resistant samples and EVs. This experiment was repeated at least twice. Each gene was tested in triplicate and the error bars represent the standard deviation of the triplicates.

3.3. Mechanisms of IC modulation in melanoma cells

3.3.1. IFN signalling in the regulation of IC expression

IFNγ is a major inducer of PDL1, PDL2, and CD155 in tumour cells [263-266]. To evaluate the effects of IFNγ treatment on IC expression, flow cytometry analysis of IC was performed in four sensitive and resistant melanoma cell line pairs after overnight

exposure to IFNγ. Results showed an induction of PDL1, PDL2 and GAL9 expression in sensitive cell lines, and upregulated in the resistant lines. The response to IFNγ was also ascertained by the upregulation of HLA Class I in sensitive and resistant lines (Figure 3.3.1.1).

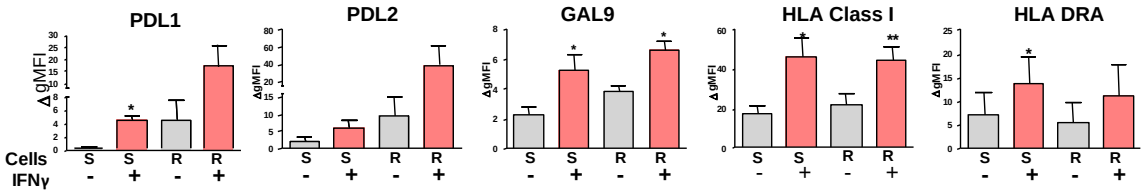

Figure 3.3.1.1. IC modulation by IFNγ in melanoma cells. The average delta geo mean of the intensity value was analysed by paired t test for treated (red histogram) versus untreated samples (grey histograms). S, sensitive (n=4); R resistant (n=4). The error bar is the standard deviation of the four different values deriving from each cell line.

Melanoma cells treated with IFNγ were also tested for the activation of the IFN-associated signalling pathway molecules STAT1/STAT3/IRF1 by western blot analysis. Results shown in Figure 3.3.1.2 indicate that IFN-treated LM16S cells displayed an upregulation of STAT3, STAT1, IRF1 and PDL1. In contrast, untreated drug resistant LM16R cells already displayed detectable levels of all these molecules, which showed upregulation after IFNγ treatment.

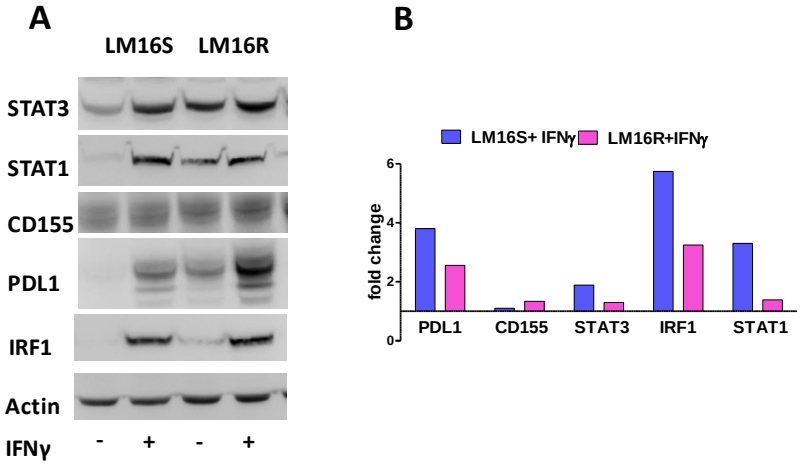

Figure 3.3.1.2. Western blot analysis on IC and molecules involved in IFN-signalling. A) LM16S and LM16R cell lysates were obtained after overnight incubation with (+) or without (-) IFNγ. B) Normalized intensity volume of the protein signals (non treated = 1). Blue bars- LM16S cells; pink bars- LM16R cells. This experiment was performed at least twice. Results in the figure show representative data.

These results indicate that the expression of IC molecules PDL1, PDL2 and GAL9 were induced by IFNγ in melanoma cells. In addition, the expression of IC molecules PDL1 and PDL2 in resistant LM16R cells associated to constitutive STAT1/3 signalling, indicating that

IC modulation upon acquisition of resistance to BRAF/MEKi in melanoma cells involves IFN-signalling.

IFNγ is a critical cytokine for immune responses and can also act directly on the tumour cells with cytostatic and cytotoxic effects. In melanoma, *in vitro* IFNγ treatment has shown growth inhibitory effects mostly associated to the activation of the JAK-STAT pathway. I thus tested the effect of IFNγ on proliferation of sensitive and resistant LM16 cells by MTT. In these experiments I also investigated the potential role of EVs produced by resistant cells on the drug response of sensitive cells. Results depicted in Figure 3.3.1.3 showed that LM16S cells, despite showing responsiveness to IFNγ at molecular level, were not growth inhibited by IFNγ treatment. In fact, after 72 h I could measure a decrease in cell viability only in the presence of BRAF/MEKi, as expected, but not in the presence of IFNγ. In contrast, the growth inhibitory effects of BRAF/MEKi on LM16S were reduced by the presence of IFNγ. The addition of EVs did not influence LM16S cell growth in any of the tested conditions, regardless if they stemmed from parental sensitive or resistant counterpart. The same experiments performed in parallel with LM16R resistant cells showed no effect on cell growth of the BRAF/MEKi drug combination, as expected, while if IFNγ was added, I could measure a cell growth decrease of about 50% (Figure 3.3.1.3). Notably, the treatment with IFNγ led to a 30% decrease in cell growth of LM16R cells, an effect observed in two independent experiments. Unexpectedly, the addition of EVs decreased viability of LM16R cells in all tested conditions.

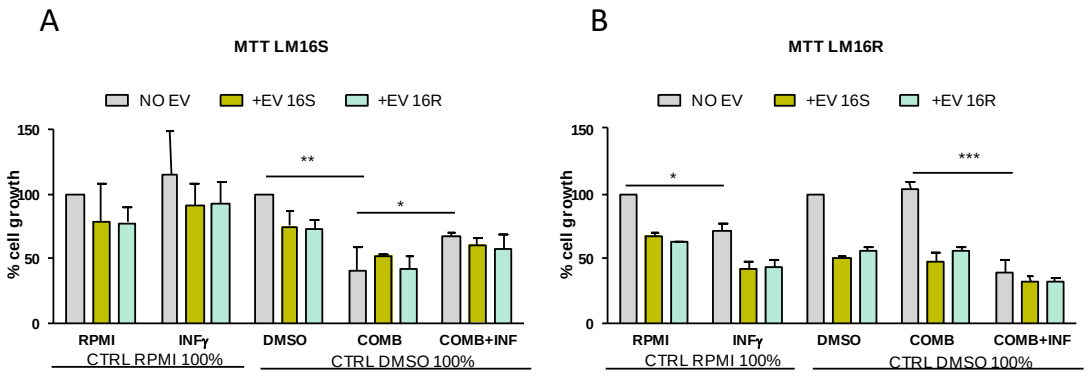

Figure 3.3.1.3. Cell viability analysis of LM16S and LM16R after BRAF/MEKi treatment in combination with IFNγ and LM16S and LM16R EVs. A) 15,000 cells/well of LM16S and B) LM16R were cultured in 96-well plates with 1 nM BRAF/MEKi drugs and/or 20 ng/ml IFNγ, in combination or not with 15 µg of EVs/well. MTT analysis of cell proliferation was performed after 72h of culture. This experiment was repeated at least twice. Each gene was tested in triplicate and the error bars represent the standard deviation of the triplicates.

These results appear contradictory, since I could measure a response to the cytokine in both drug sensitive and resistant cells, but the treatment had no effect on cell proliferation of the sensitive and strong effects on the resistant cells. An explanation may derive from the observation of dose-response studies for IFNγ, which revealed a discrepancy between levels of STAT1 activation and the extent of growth inhibition [267]. In my experiments, IFNγ treatment did not have the same effects on LM16S and LM16R cells possibly due to the different baseline expression of IFN-related genes. Additionally, as proposed by [267], the presence of additional signals emanating from the IFNγ receptor may counteract the anti-proliferative function of STAT1 in the case of LM16S cells. The anti-proliferative effects mediated by the presence of EVs from sensitive or resistant cells in the cultures of LM16 drug resistant melanoma cells, but not in the sensitive lines have no explanation.

3.3.2. IC modulation upon EV interaction with tumour cells

A main aim of my project was to evaluate the effects of IC proteins and/or transcripts carried by melanoma EVs in modulating tumour and immune cells to a tumour promoting state. To study this issue, I considered IC modulation in target cells, including melanoma cells and immune cells and cell models to assess the potential transfer of IC.

Experiments were set up by evaluating co-cultures in transwell assays to assess potential molecular changes in sensitive cells mediated by the resistant counterpart. Co-cultures of LM16S cells in the lower chamber and LM16R cells in the upper chamber, and vice versa, were maintained for 4 and 8 days, then cells were harvested and analysed. No difference in IC expression was detected, neither at the protein nor at the transcript level. In contrast, these experiments showed an increase of STAT3 and a significant increase of CCL2 and IL8 gene expression in LM16S cells cultured in the presence of LM16R cells in the upper chamber (Figure 3.3.2.1). The expression of these cytokines occurs upon acquisition of resistance, as shown in a previous study [249].

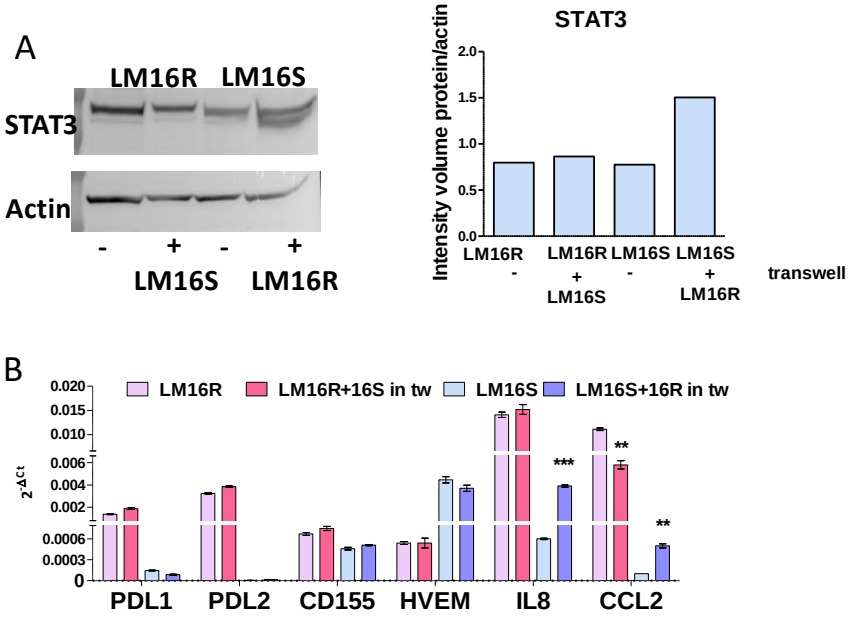

Figure 3.3.2.1. Western blot and qRT-PCR analysis of cells conditioned in transwell co-cultures. Cells were co-cultured for 8 days in 24 wells transwell plates. After incubation, the transwells were discarded and the cells in the bottom wells collected for molecular analysis. A) STAT3 intensity volume quantification. B) qRT-PCR results. ** p<0.01, *** p<0.001 by paired t test. This experiment was repeated at least twice. Each gene was tested in triplicate and the error bars represent the standard deviation of the triplicates

To understand if EVs were involved in the modulation of cytokine expression, I performed analogous co-culture experiments with EVs isolated from the supernatants of LM16S and LM16R cells. qPCR analysis of LM16S cells treated with LM16R-derived EVs revealed an upregulation of CCL2 expression, similar to what observed in transwell experiments (Figure 3.3.2.2).

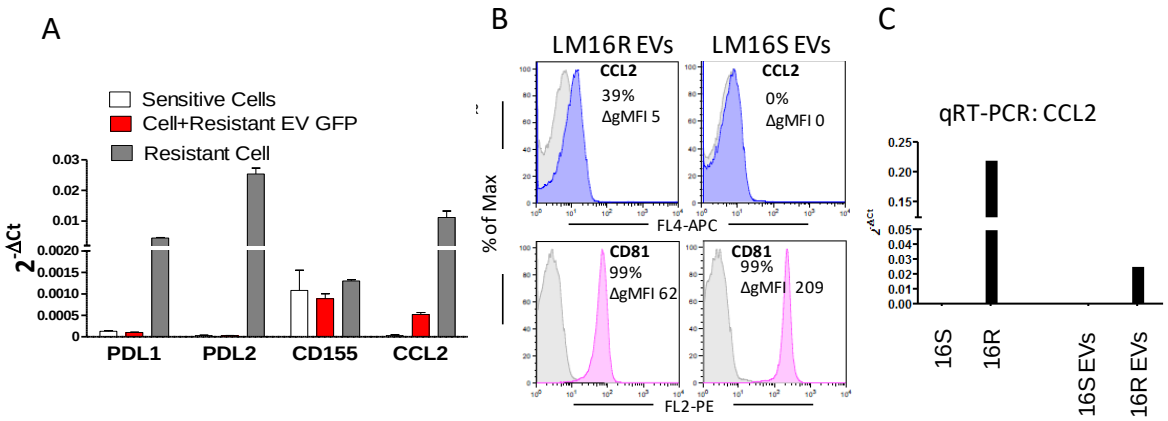

Figure 3.3.2.2. Co-culture of LM16S cells with LM16R EVs. A) qRT-PCR analysis was performed after overnight incubation of $2x10^5$ LM16S cells with 200 µg of EVs from LM16R transfected cells. LM16R was used as positive control for the tested genes. B) LM16R EVs were used for flow cytometry analysis after overnight incubation with latex beads to detect the CCL2 positivity (blue). LM16S EVs were used as negative control for CCL2, while CD81 EV marker (pink) is the positive control. C) qRT-PCR showed detectable CCL2 transcript in LM16R EVs and cells. The experiment in

panel A was repeated at least twice. Each gene was tested in triplicate and the error bars represent the standard deviation of the triplicates.

This effect could be ascribed to the action of the CCL2 protein, of the RNA transcript, or of microRNAs carried by LM16R-derived EVs. In fact, EVs isolated from LM16R culture supernatant displayed a higher level of miR-34a, miR-100 and miR-125b (Table 3.3.2), which are associated to increased production of CCL2 and to resistance to BRAFi, as formerly reported by Vergani [249].

Table 3.3.2 qRTPCR analysis on microRNA from melanoma EV

	EV	Avg Ct U6	Avg Ct miR100	Avg Ct miR125b	Avg Ct miR34a
Exp 1	LM16S	28,7	40,0	40,0	40,0
	LM16R	26,1	28,0	27,2	31,9
Exp 2	LM16S	26,9	40,0	31,9	34,0
	LM16R	28,4	32,4	27,2	30,5

Another microRNA, which has been recently identified by our group as potential mediator of resistance is miR-146a ([249] and unpublished results). In her studies, E. Vergani found that LM16S cells express miR-146a but are devoid of CCL2 and display low levels of miRs 100, 34a and 125b. In contrast, LM16R cells express high levels of CCL2 and of miRs 100, 125b and 34a but express low levels of miR-146a. Thus, to understand the potential role of these microRNAs as well as CCL2 in IC modulation, I evaluated IC expression in LM16S and LM16R cells after inducing/inhibiting CCL2 or the microRNAs.

The role of CCL2 was tested in LM16S cells transfected with CCL2 plasmid and in LM16R cells transfected with CCL2 inhibitor (short interfering RNA). Results obtained by qPCR showed that, compared to control cells, LM16S-CCL2 transfectant cells upregulate PDL1 at a statistically significant level, while the expression of GAL9, HVEM and CD155 was not affected (Figure 3.3.2.3). In contrast, the inhibition of CCL2 in the resistant variant LM16R determined a decrease of HVEM expression, while it did not affect the expression of the other IC. Furthermore, these experiments showed that the inhibition in LM16R cells of resistance-associated microRNAs 100, 34a, 125b determined an upregulation of PDL2 and GAL9, while the transfer of miR-146a mimics determined a downregulation of PDL1 and GAL9 (Figure 3.3.2.3B). Altogether these findings link CCL2 and miR-146a to the regulation of PDL1, while GAL9 appears modulated by all the tested miRNA, and HVEM expression appears to be influenced only by CCL2.

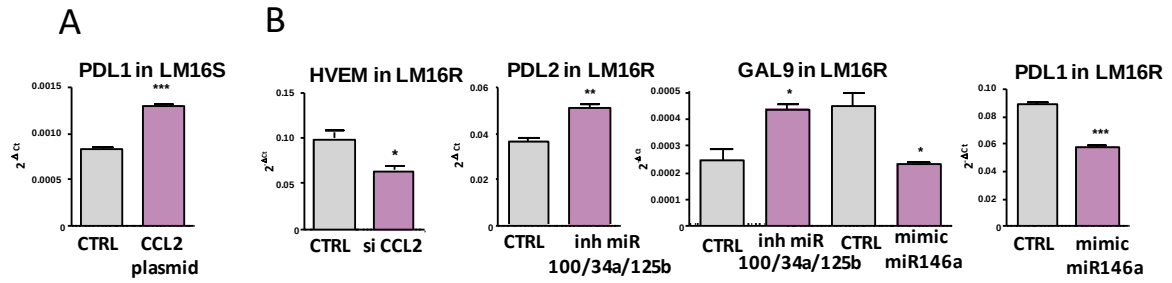

Figure 3.3.2.3. IC modulation in melanoma cells by CCL2 and miRs. A) qRT-PCR was performed in LM16S cells transfected with CCL2 plasmid and its scrambled control. B) LM16R cells treated by a pool of siRNA specific for CCL2 transcript, or with inhibitors for CCL2-associated microRNAs, or with miR164a mimic. Grey bars- scrambled controls; violet- transfected samples. This experiment was repeated at least twice. Each gene was tested in triplicate and the error bars represent the standard deviation of the triplicates

3.3.3. Melanoma and GFP-tagged EV co-culture studies

3.3.3.1. Generation of transfectant cells producing GFP-tagged EVs

To investigate the mechanisms underlying the modulation of IC upon exposure to melanoma EVs, and to understand if a direct transfer of IC proteins from the EVs to the recipient cells occurs, GFP-tagged EVs were generated. Being that CD81 is a highly expressed protein in EVs, a commercial vector encoding CD81-GFP fusion protein was used to obtain LM16S and LM16R stable cell variants producing GFP-EVs. GFP-tagged EVs isolated from the LM16R-CD81-GFP and LM16S-CD81-GFP transfectants differ for the presence of the endogenous PDL1. In addition, to investigate the potential direct transfer of PDL1, LM16S cells were also transfected with a vector encoding PDL1-GFP fusion protein. This model allowed the tracing of PDL1 protein in the target cells upon EV exposure. Transfectants were selected by geneticin resistance, and to enrich transfectant cell population with high fusion protein expression, GFP positivity was used for selection by FACS. FACS resulted an effective selection method for LM16S-CD81-GFP and LM16S-PDL1-GFP transfectants, since the fusion proteins CD81-GFP and PDL1-GFP were highly expressed as displayed by the double positivity at flow cytometry analysis (Figure 3.3.3.1AB). However FACS resulted unsuccessful in the purification of the LM16R-CD81-GFP transfectants, and even if two different methods of FACS sorting were used (“Purify” and “Single Cell Sorting”), an heterogeneous population was obtained because of cell aggregation formed during the sorting. To obtain enriched LM16R-CD81-GFP transfectant cells I eventually cloned the sorted cells by limiting dilution and selected cell clones based on GFP expression.

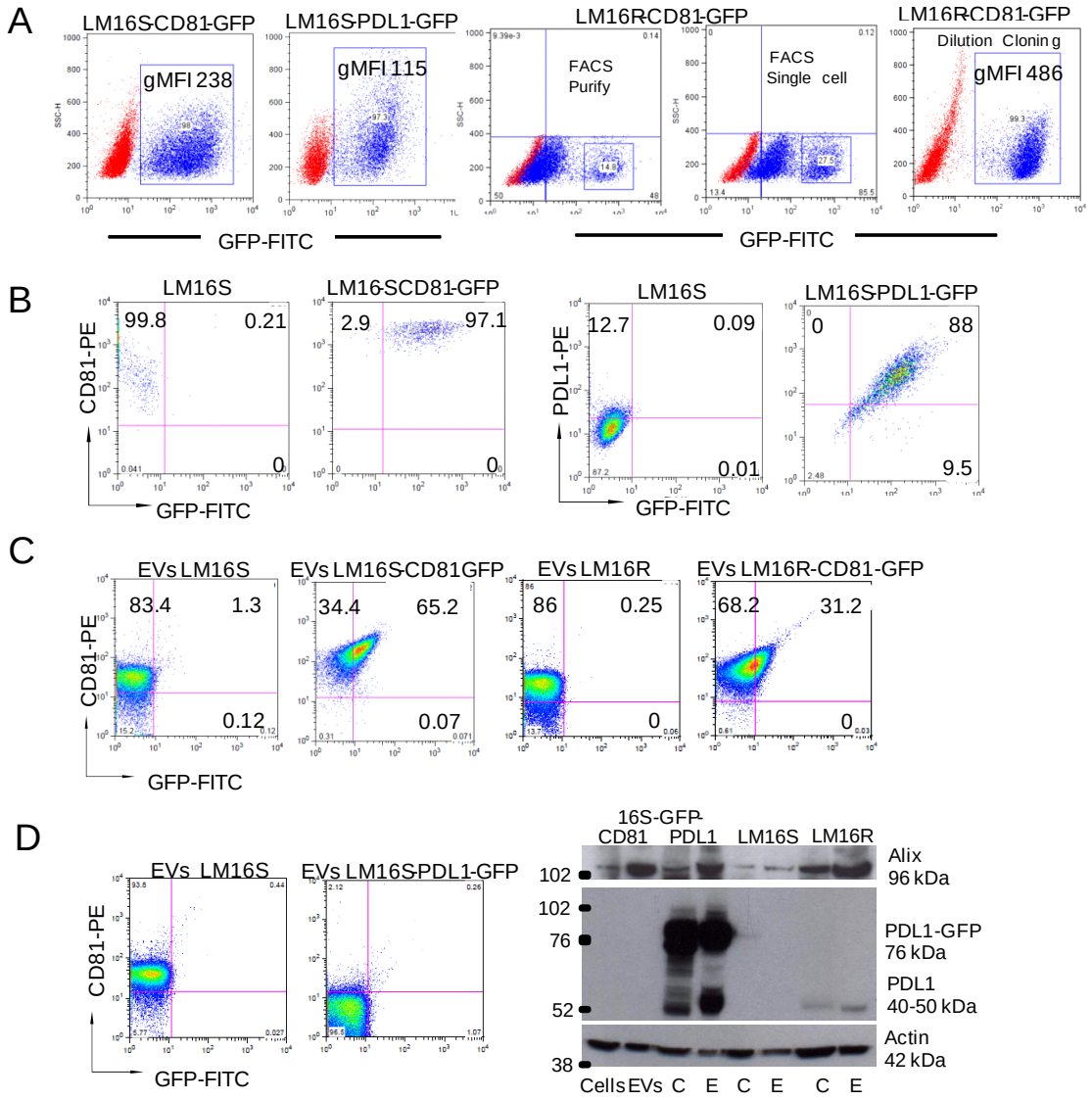

Figure 3.3.3.1. Transfectant melanoma cells producing GFP-tagged EVs. A) Flow cytometry analysis detection of GFP in melanoma cells transfected with a vector encoding CD81-GFP or PDL1-GFP fusion protein after selection by FACS or cell cloning by limiting dilution. Red dot plots are the non transfected cells. B) The comparison of non transfected and transfected cells for double positivity expression of the fusion proteins. C) Flow cytometry analysis of EVs derived from transfected-CD81-GFP cells. D) EVs derived from transfected-PDL1-GFP cells did not show double positivity for the fusion protein by flow cytometry analysis; western blot analysis showed a clear signal of anti-PDL1 antibody at 76 kDa for the fusion protein PDL1-GFP. LM16R cells and its EVs were used as positive control for PDL1, Alix was used as EV marker and actin was used as loading control.

EVs were isolated from the transfectants and characterised. NTA showed no major differences between LM16 EVs and their GFP-tagged counterpart (Figure 3.3.3.2). EVs obtained from LM16S-CD81-GFP and LM16R-CD81-GFP cells resulted positive for the fusion protein CD81-GFP when analysed by western blot and latex-beads flow cytometry (Figure 3.3.3.1CD). In contrast, LM16S-PDL1-GFP EVs were negative for PDL1 and GFP when analysed by latex-beads flow cytometry, probably due to the low intensity

expression level of the PDL1-GFP fusion protein, as determined also by confocal microscopy analysis (data not shown here). Nonetheless, by western blot, both EVs and cell samples showed detectable fusion protein at 76 kDa (Figure 3.3.3.1 D, right panel).

3.3.3.2. Analysis of IC expression in melanoma cells upon GFP-EV interaction

To evaluate if the transfer of PDL1-GFP fusion protein occurred in melanoma cells after co-culture experiments with GFP-tagged EVs, treated cells were tested for positivity to an anti-GFP antibody by western blot. Results showed that both PDL1-GFP and CD81-GFP EVs types were internalised by LM16S cells, as the anti-GFP antibody revealed the bands of both the fusion proteins PDL1-GFP and CD81-GFP at 75 kDa and 50 kDa respectively. However, a high level of expression of the fusion protein was detectable only for CD81-GFP EV co-cultures (Figure 3.3.3.2D, central and right panels).

In addition, I took advantage of the fluorescent vesicles produced by CD81-GFP transfectants, which were highly positive for GFP due to CD81 accumulation in EVs, for confocal microscopy analysis in collaboration with our Cell Imaging Facility. Experiments clearly displayed green GFP signal in LM16S and LM16R cells upon co-culture with LM16S-CD81-GFP EVs. DAPI and WGA labelling red reagent were used for nucleus and cell membrane staining. ImageJ analysis revealed internalized EVs in yellow, as the result of merged green CD81-GFP EVs and the red labelled recipient cells (Figure 3.3.3.2B).

Flow cytometry of these co-cultures showed that LM16S cells displayed a lower uptake of CD81-GFP EVs, regardless if they derived from LM16S and LM16R, with 62% and 52% positivity, respectively. Instead, LM16R cells showed an uptake of 84% (LM16S) and 86% (LM16R) EVs. Of note, LM16R cells displayed a 20 fold higher GFP geometric mean fluorescence intensity compared to LM16S cells after EV uptake, confirming the higher internalisation ability of the resistant melanoma cells (Figure 3.3.3.2C). EV uptake was also detectable by Western blot analysis, where cell lysates from LM16S cells cultured with CD81-GFP-tagged EVs showed bands between 38 and 52kD for the CD81-GFP fusion detected by an anti-GFP antibody (Figure 3.3.3.2D).

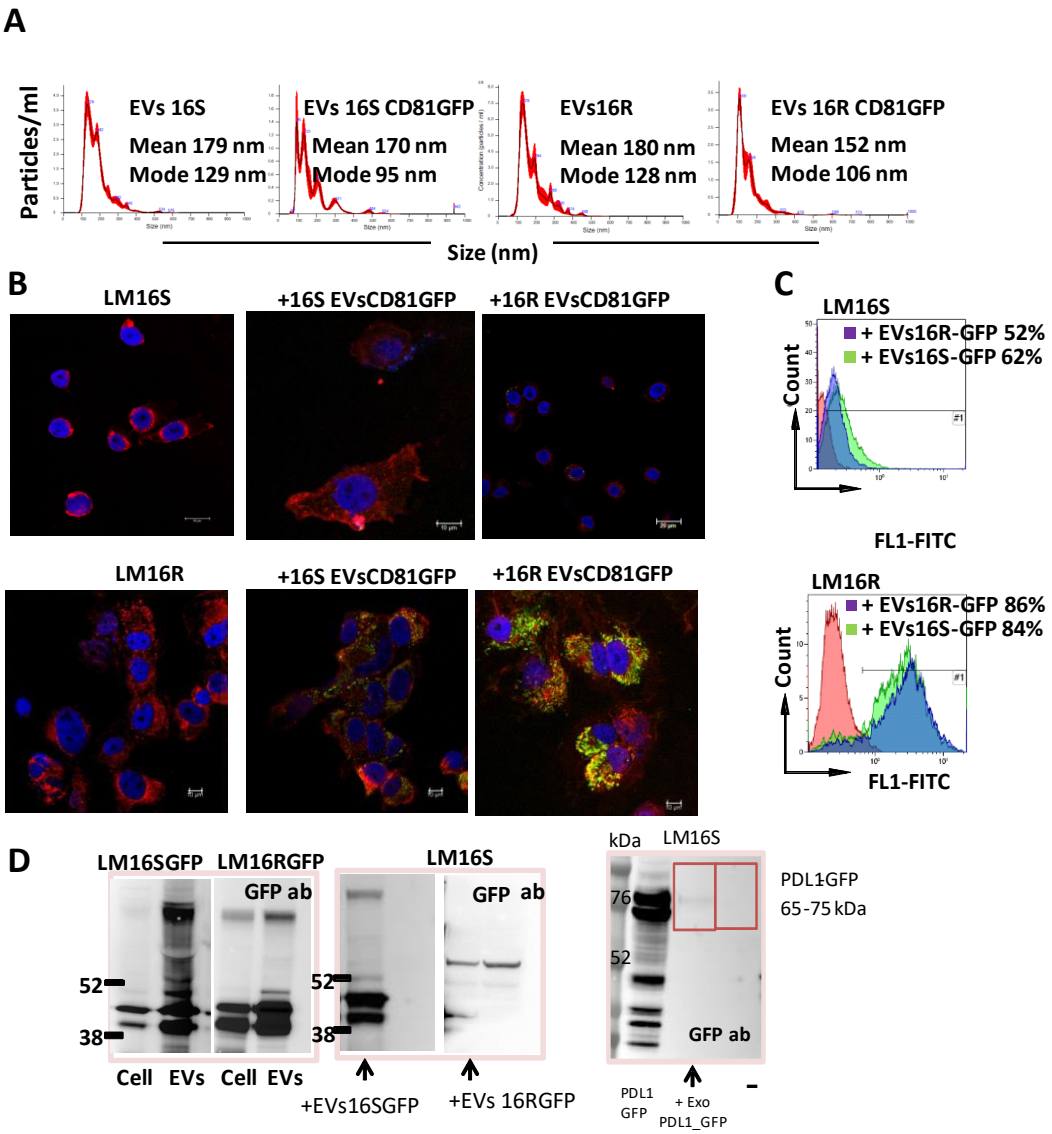

Figure 3.3.3.2. Interaction studies of GFP-tagged EVs in melanoma cells. A) NTA results of EVs from transfected (second and forth panels) and untransfected control cells (first and third panels) analysed by NTA. B) confocal microscopy and C) flow cytometry showing EV internalisation in LM16S (upper panel) and in LM16R (lower panel) after co-culture with CD81-GFP EVs produced by LM16S or LM16R CD81-GFP transfectants. D) Western blot analysis of transfected cells and their EVs (left panels) and LM16S co-cultured samples with GFP-positive EVs (central and right panels). GFP-tagged EVs were internalised by LM16S cells, as anti-GFP antibody showed a band between 38 and 52 kDa corresponding to the molecular weight of CD81-GFP fused protein (central panel), and a band between 65 and 76 kDa corresponding to the molecular weight of PDL1-GFP protein (right panel).

In conclusion these experiments demonstrated that EV are internalized in melanoma cells and that the uptake appears higher in the resistant LM16R compared to LM16S cells. These results also showed that PDL1 protein can be transferred between melanoma cells via EVs.

4. Role of melanoma EVs in immune cell modulation of IC expression

The aim of this part of my project was to investigate if IC proteins and/or transcripts carried by EVs might have a role in the modulation of IC in immune target cells.

4.1. Interaction of melanoma EVs with PBMCs

The target cells of EVs were at first assessed in EV-PBMC co-cultures. To detect any EV-immune cell interaction, I either labelled EVs from LM16R cells (16R EV) with SP-DIOC(18)3 (Figure 4.1.1), or I used CD81-GFP and PDL1-GFP EVs purified from the transfected LM16S melanoma cell line (EV 16S) (Figure 4.1.2).

To evaluate the interaction of LM16R melanoma EVs with monocytes and T cells, 20 μg isolated EVs were labelled with SP-DIOC(18)3, a membrane lipophilic dye, prior to addition to PBMCs isolated from peripheral blood of healthy donors. After an overnight incubation, cells were harvested, washed, labelled with antibodies against CD14, CD3 and PDL1 and acquired with a FACSCalibur flow cytometer. Results showed that labelled LM16R EVs interacted with $CD14^+$ monocytes (Figure 4.1.1A, left panels) but not with T cells (Figure 4.1.1A, right panels). About 20% of $CD14^+$ cells gated in PBMCs from two different healthy donors acquired green fluorescence (Figure 4.1.1A, left panels). Next, I evaluated if the interaction with EVs of monocytes could induce the surface expression of PDL1. I could observe that those cells that had acquired the green fluorescence ($CD14^+DIOC^+$ gate), thus had interacted with EVs, displayed an increase in the percentage of $PDL1^+$ monocytes that ranged from 25 to 60% depending on the donor (Figure 4.1.1B, left panels). In contrast, from the monocytes that had not interacted with EVs, only a low percentage (about 10-15%) displayed an upregulation of PDL1 (Figure 4.1.1B, right panels). These experiments showed that in PBMCs the monocytes are the cells prevalently interacting with EVs from melanoma cells and that this interaction leads to an increased expression of PDL1.

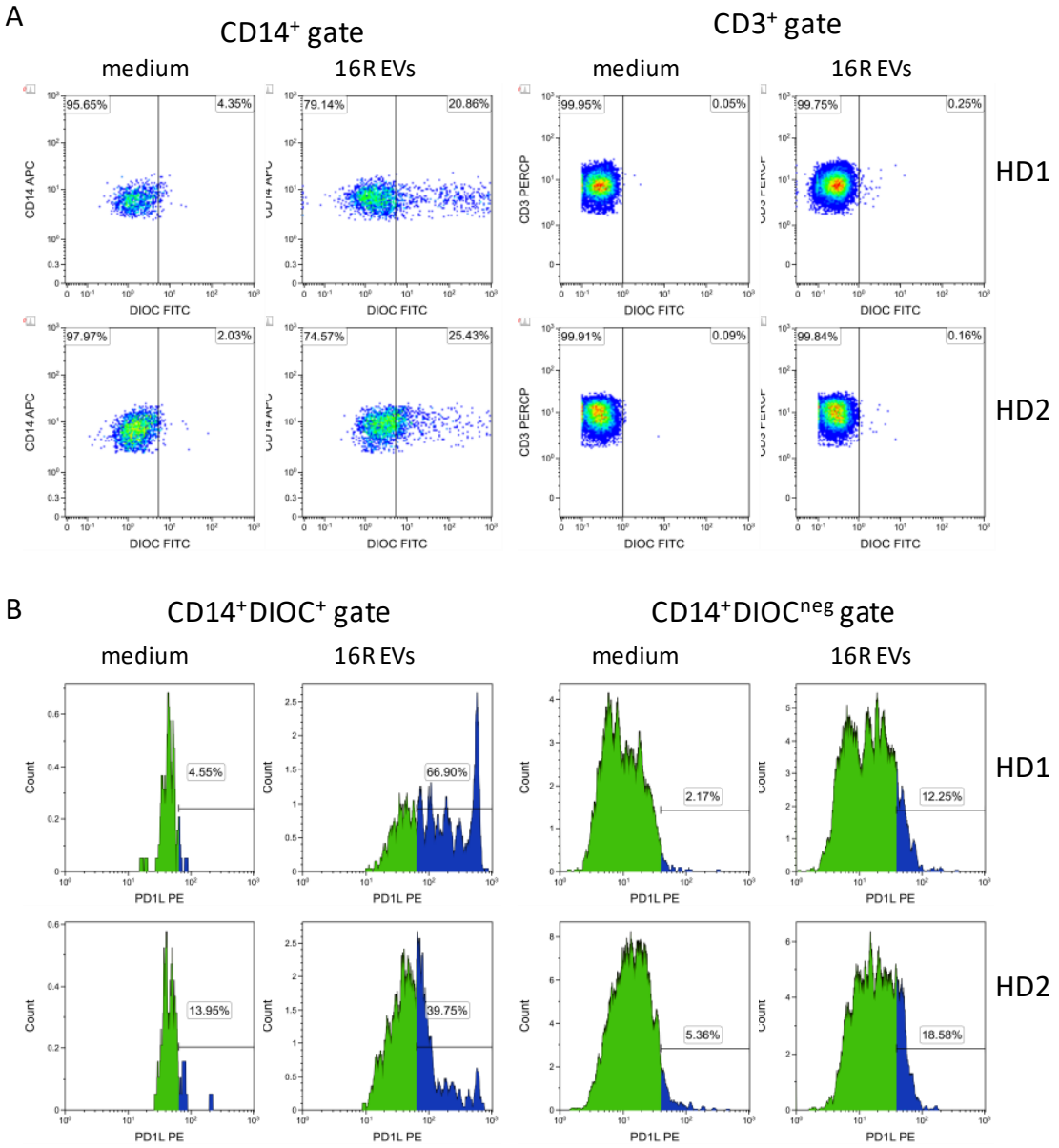

Figure 4.1.1 Interaction of LM16R EVs with monocytes and T cells in PBMCs. A) Melanoma EV uptake after 18h by PBMC gated CD14 (on the left) and CD3 (on the right), B) PDL1 expression by $CD14^+$ monocytes in PBMCs after interaction with melanoma EVs deriving from LM16R. HD - healthy donor; green-Isotype control; blue- % of PDL1 positivity

These interaction experiments were also performed with 16S EV-CD81-GFP or 16S EV-PDL1-GFP obtained from transfected 16S cells. As shown in Figure 3.3.3.1 PDL1-GFP EVs displayed a marked reduction in GFP fluorescence with respect to CD81-GFP EVs. Nonetheless, about 20% in CD14 gated monocytes showed an interaction with both types of EVs in PBMCs (Figure 4.1.2A). This uptake was accompanied by an upregulation of PDL1 of 46% for both EVs in monocytes (Figure 4.1.2B).

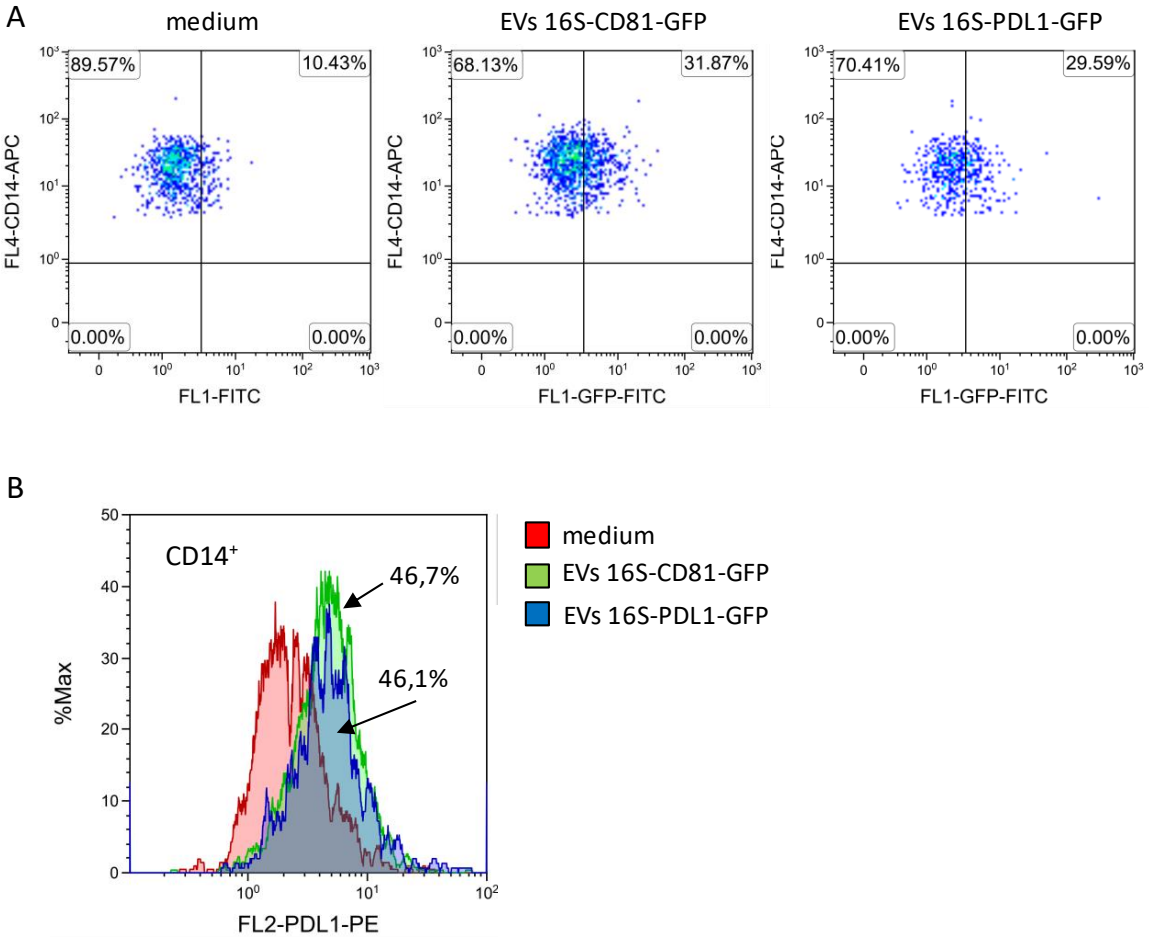

Figure 4.1.2. Interaction of GFP tagged EVs with monocytes in PBMCs. A) GFP-EV uptake by CD14$^+$ cells in PBMCs after 18h of co-culture, B) PDL1 expression by CD14$^+$ monocytes in PBMCs after interaction with EVs deriving from melanoma cell line LM16S CD81- and PDL1-GFP fused protein. Medium-negative control. This experiment was performed at least twice, each time with two different HD. Results in the figure show representative data.

4.2. IC expression induced by melanoma EVs in PBMCs

Given the IC modulation in resistant melanoma cells and the IC expression by melanoma EVs as showed in the Section 3.2.2 of the results, I aimed to compare the effects of EVs isolated from the studied sensitive and resistant melanoma cell line pairs on IC modulation in PBMC co-culture experiments. Thus, purified EVs (30 µg) were co-cultured with PBMCs isolated from peripheral blood of healthy donors (n=2) for 36 h. Then cells were harvested and labelled with fluorochrome-conjugated antibodies against CD14 and the IC PDL1, PDL2, GAL9, HVEM and CD155 (Figure 4.2.1 and 4.2.2). Given the potential of tumour EVs to induce an M-MDSC phenotype identified as CD14$^+$HLA-DR^{neg} cells, I also included the assessment of HLA-DR in combination with CD14 on EV stimulated PBMC samples (Figure 4.3.1).

All tested EVs induced a modulation of IC, measured as geometric mean fluorescence intensity (gMFI) on gated CD14$^+$ monocytes. In particular, after 36 h of co-culture only

HVEM was upregulated consistently by all EVs, while PDL2, CD155 and GAL9 were downregulated, as shown in Figure 4.2.1 for each IC.

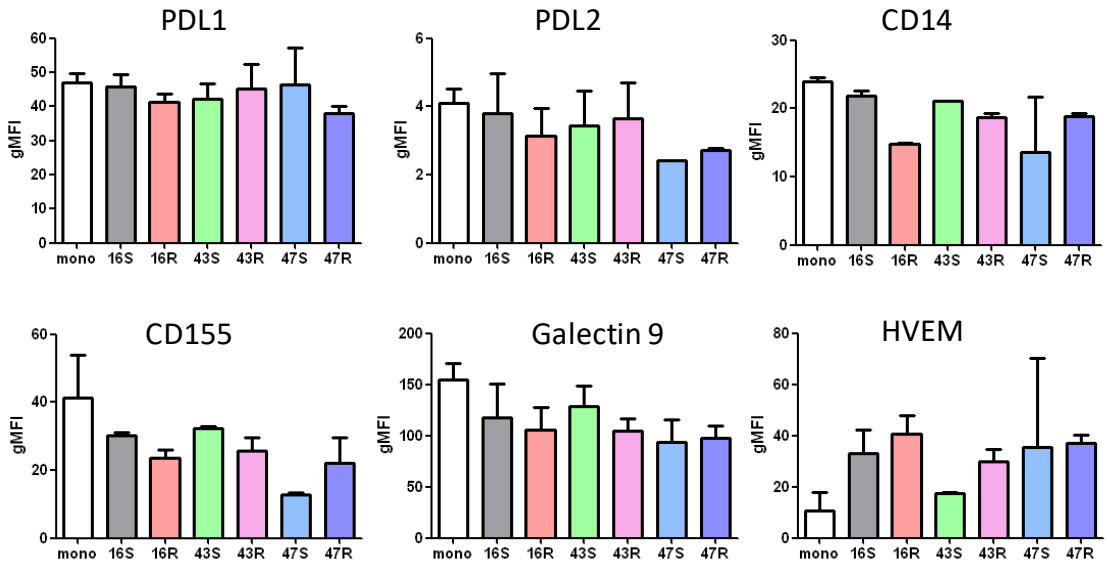

Figure 4.2.1. Modulation of IC expression in monocytes after EV-PBMC co-cultures. Average data of two HD PBMCs in co-culture with six different melanoma EV. mono- negative control, EV from cell lines 16S, 16R, 43S, 43R, 47S, 47R. The error bar is the standard deviation of the two different values deriving from each HD.

I then grouped the effects of EVs from sensitive (S) and resistant (R) to understand if modulations induced by the EVs could be associated with their derivation from BRAFi sensitive or resistant melanoma cell lines. In contrast to the overnight incubation, the incubation at a longer time (36 h) showed that PDL1 expression values did not change in monocytes when PBMCs were co-cultured with EV from sensitive melanoma cells. It was only downregulated by EVs derived from resistant cell lines, and was accompanied by a downregulation of CD14 expression in these monocytes (Figure 4.2.2). In addition, statistical analysis with paired t test revealed that the other studied IC, PDL2, CD155 and GAL9 were downmodulated when co-cultured with EV from sensitive and resistant melanoma cells, but the modulation was accentuated if EVs originated from resistant lines. On the other hand, HVEM resulted upregulated in PBMC gated CD14 when these data were taken together, and higher modulations were observed if treated with resistant EVs (Figure 4.2.2).

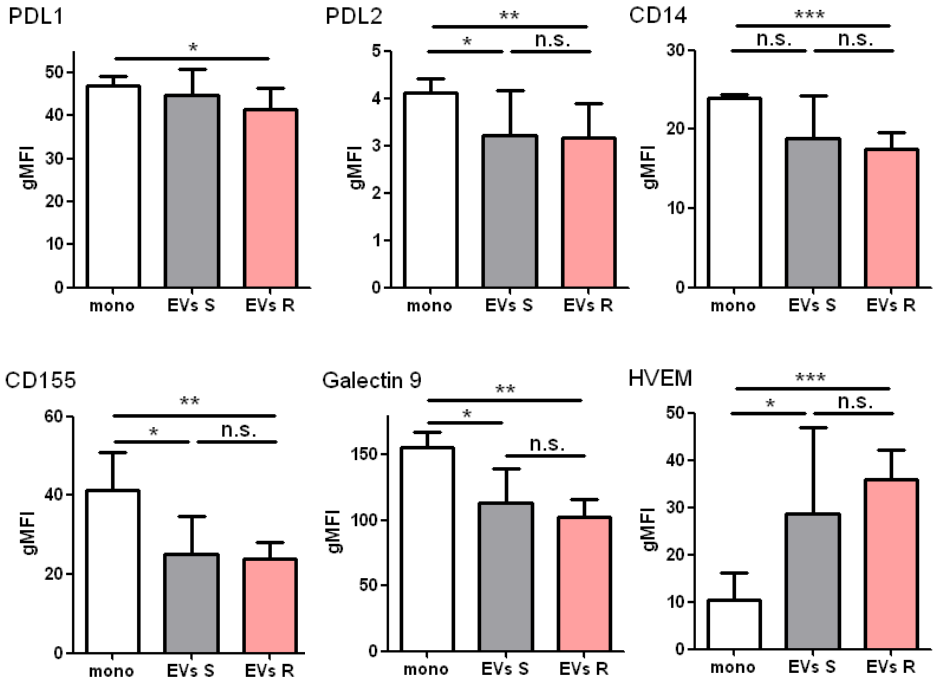

Figure 4.2.2. Modulation of IC expression in monocytes after EV-PBMC co-cultures grouped according to S and R EVs. Average data geometric fluorescent mean of EV deriving from three different sensitive and resistant melanoma cell lines. The error bar is the standard deviation of the three different values deriving from each EV condition. EVs S: EV from LM16S, LM43S, LM47S; EVs R: EV from LM16R, LM43R, LM47R; gMFI: geometric mean fluorescent intensity

4.3. Melanoma EVs induce an M-MDSC phenotype in PBMC monocytes

Since MDSC play a major role in resistance mechanisms to cancer therapies and represent a hallmark of poor prognosis for cancer patients, I sought to evaluate the expression of HLA-DR on monocytes in PBMC conditioned with EVs from S and R cell lines described in Figure 4.2.1 and 4.2.2. I observed a consistent downregulation of HLA-DR mediated by all tested EVs, regardless if they derived from sensitive or resistant cell lines (Figure 4.3.1 left and middle panels showing all tested EVs and an overlay example). As showed in the right panel, both EVs deriving from sensitive as well as those deriving from resistant melanoma cell lines induced a statistically significant decrease of surface HLA-DR. However, differences in gMFI between untreated monocytes and EVs from resistant lines were more significant (p=0.0013) than those between monocytes and EVs from sensitive cells (p=0.0173). Thus, I concluded that EVs from BRAFi resistant melanoma cells display a higher potential in inducing M-MDSC.

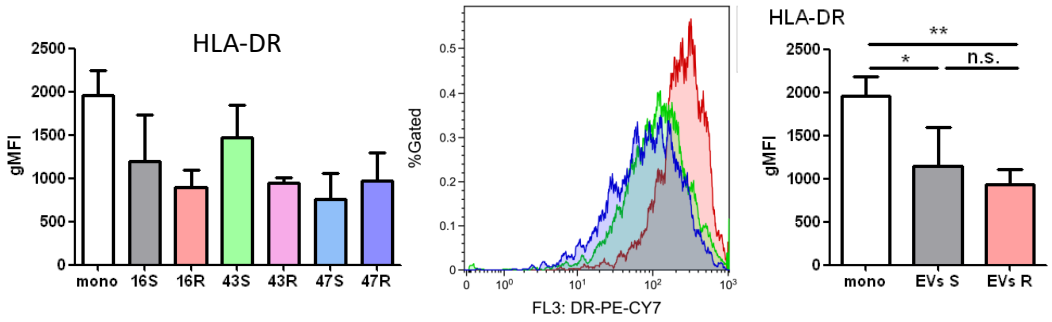

Figure 4.3.1. Modulation of HLA-DR expression in monocytes after EV-PBMC co-cultures. Average data of EV deriving from three different sensitive and resistant melanoma cell lines in two healthy donors. On the left EV are shown separately, on the right the data were grouped in EVs S: EV form LM16S, LM43S, LM47S; EVs R: EV from LM16R, LM43R, LM47R. In the middle is a representative histogram red- PBMC untreated; green- PBMC+EVs S; blue- PBMC+EVs R; gMFI: geometric mean fluorescent intensity. This experiment was repeated at least twice with at least two healthy donors each time. The error bar is the standard deviation of the two different HD (on the left), or three different values deriving from each EV condition on one of the two HD here represented (right).

Considering that all EVs induced a downregulation of HLA-DR, I evaluated IC expression in the context of HLA-DR expression (Figure 4.3.2). Results showed that upon HLA-DR downregulation, $CD14^{+}$ cells acquired a marked expression of HVEM (Figure 4.3.2A). Statistical analysis of $HLA\text{-}DR^{+}HVEM^{low}$ and $HLA\text{-}DR^{neg}HVEM^{high}$ monocytes grouped according to S and R EVs showed a statistically significant difference with respect to untreated monocytes (Figure 4.3.2B).

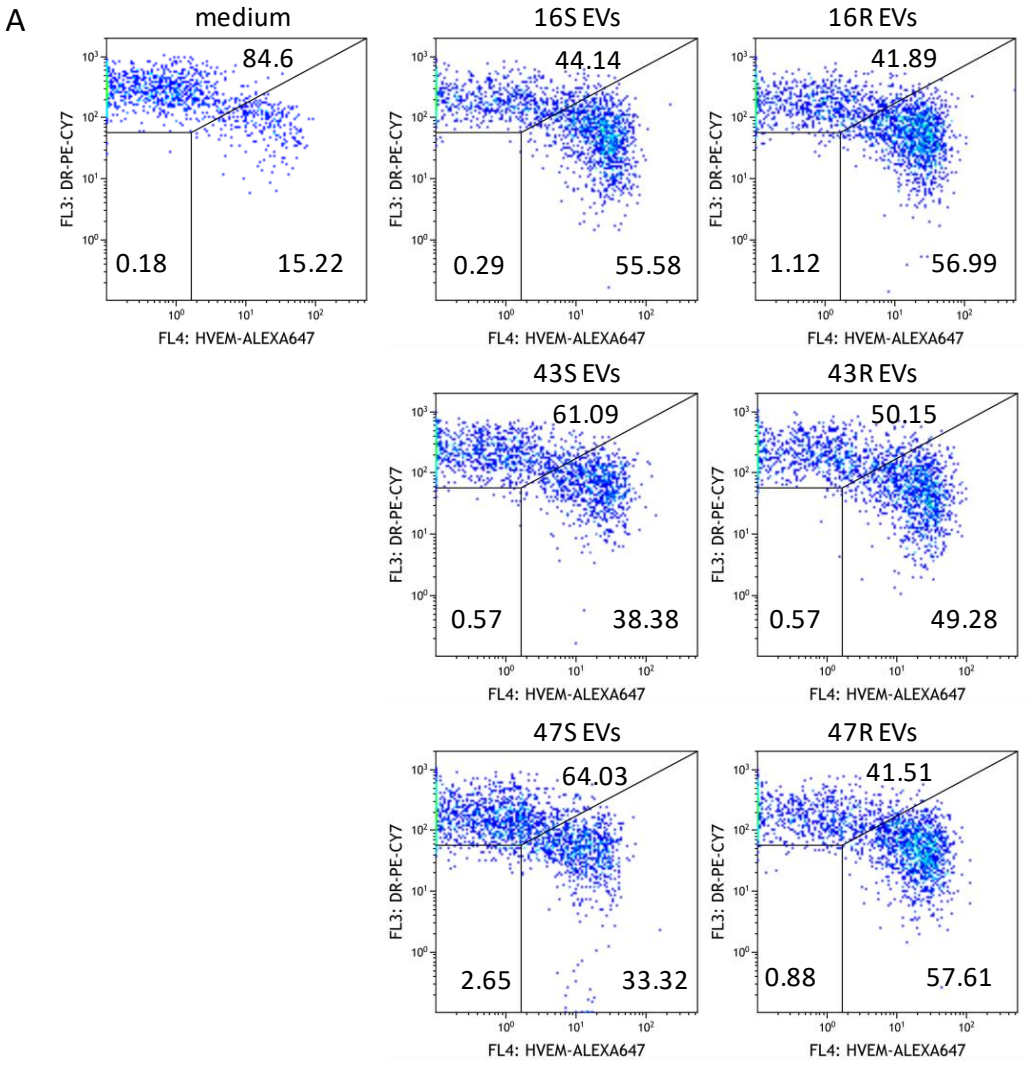

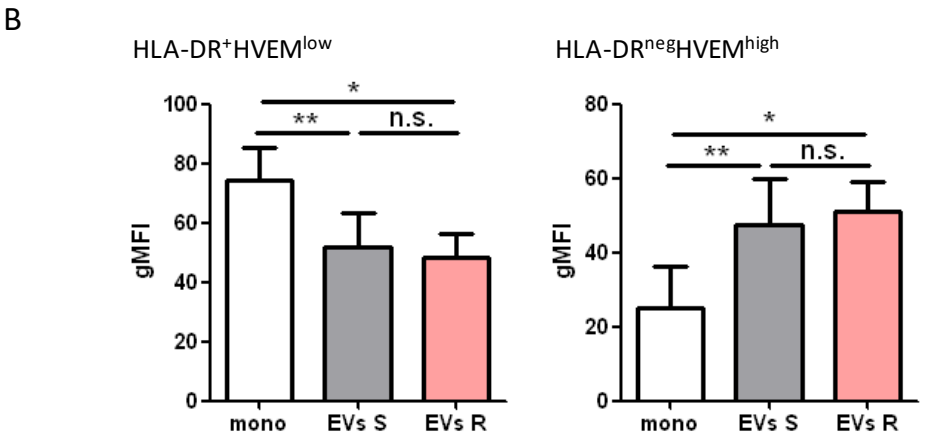

Figure 4.3.2. HVEM and HLA-DR modulation in EV-PBMC co-cultures. A) Modulation of IC expression in gated CD14⁺ cells after PBMC-EV co-culture. Left panel: untreated samples, central panels: samples treated with EVs from BRAF/MEKi sensitive melanoma cells, right panels: samples treated with EVs from BRAF/MEKi resistant melanoma cells. B) HVEM modulation in HLA-DR positive gated cells (left) and –DR negative cells (right). This experiment was repeated at least twice with at least two healthy donors each time. The error bar is the standard deviation of the three different values deriving from each EV condition on one of the two HD here represented.

Concomitantly, downregulation of HLA-DR was accompanied by negative modulation of GAL9 (Figure 4.3.3A). In fact, this IC appeared to be expressed mainly on HLA-DR^{+} monocytes. When I compared the HLA-DR^{+}HVEM^{low} monocytes for their GAL9 expression with the MDSC counterpart with low HLA-DR and high HVEM I observed a loss of GAL9 gMFI (Figure 4.3.3 A) that was statistically significant for EVs deriving from R cell lines (Figure 4.3.3B). This indicates that GAL9 gMFI downregulation in HLA-DR^{neg}HVEM^{high} monocytes if they were induced by EVs deriving from BRAF resistant melanoma cells.

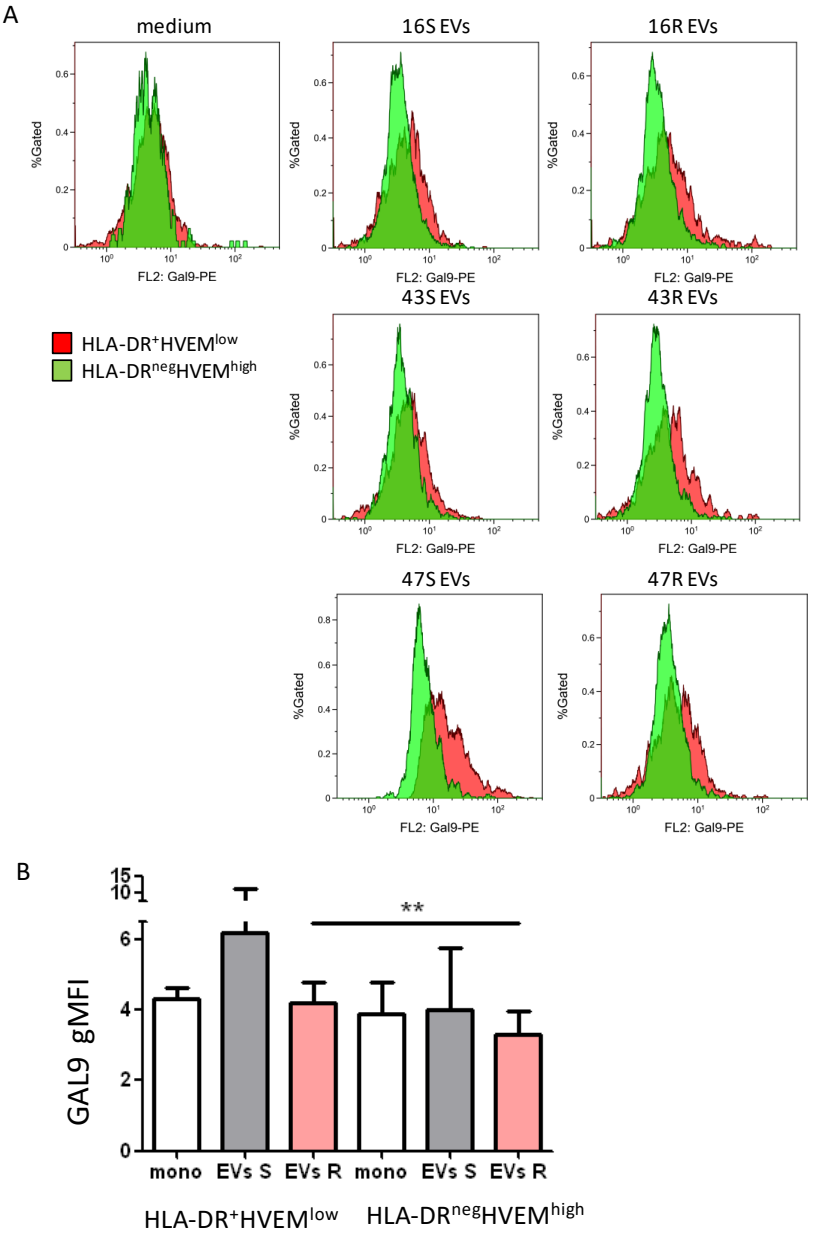

Figure 4.3.3. GAL9 modulation in EV-PBMC co-cultures. A) Monocytes were gated as follows: red- HLA-DR positive and HVEM low expression, green- HLA-DR negative and HVEM high expression. B) GAL9 expression as gMFI in the two cell subpopulations of A). This experiment was repeated at least twice with at least two healthy donors each time. The error bar is the standard deviation of the three different values deriving from each EV condition on one of the two HD here represented.

4.4. Interaction and phenotype of CD14$^+$ monocytes induced by melanoma EVs

To discriminate if the observed effects on monocytes after PBMC co-cultured with tumour EVs were due to an indirect effect of the presence of T, B and NK cells as part of PBMC population, I performed co-culture experiments with purified monocytes. CD14$^+$ cells were isolated from PBMC of healthy donors (n=3) by separation with anti-CD14$^+$ magnetic beads, and were co-cultured with EVs obtained from LM16S, LM16R, LM16S-CD81-GFP and LM16S-PDL1-GFP cells. After an overnight co-incubation, the samples were harvested and divided in two parts, one for phenotype analysis and one for functional analysis.

The phenotype assessed by flow cytometry is shown in Figure 4.4.1A as a representative example, and included the assessment of interaction evidenced by the acquisition of green fluorescence by CD14$^+$ cells in the presence of 16S-CD81-GFP tagged EVs (8%). In contrast, no increase of FITC$^+$ cells was detected in the presence of 16S-PDL1-GFP EVs, possibly due to their low GFP fluorescence (Figure 4.4.1A, first row). This interaction induced an upregulation of PDL1 on cells, which was particularly evident in the presence of PDL1-GFP EVs reaching almost 40% positivity. Induction of PDL1 was also detectable for 16S and 16R EVs, as well as for CD81-GFP EVs, however to a lesser extent (Figure 4.4.1A, first and second rows). PDL1 upregulation could be also measured at RNA level in 16S and 16R EV-conditioned monocytes (Figure 4.4.1B).

As detected in the monocyte gate in PBMCs, also purified CD14$^+$ cells downregulated HLA-DR, and the HLA-DR^{neg} ranged from 9% for untreated monocytes to 17-22% in the presence of the tested EVs (Figure 4.4.1A, third row). Given the purified CD14+ cell population, and the low GFP uptake positivity, we stained cells with CD14-FITC risking no interference signal. CD14$^+$ cells expressing the highest levels of HLA-DR were also those expressing GAL9 and upon interaction with EVs, I could measure a drop of almost 50% of GAL9^{high} cells if 16S and 16R EVs were present (30% in untreated, 16-20% in EV-conditioned monocytes (Figure 4.4.1A fourth row of dot plots). In contrast, no relevant CD155 modulation was observed in EV-conditioned monocytes (Figure 4.4.1A, fifth row), although it was evident at RNA level (Figure 4.4.1B). qRT-PCR analysis also revealed decreased levels of HVEM although not significant, and a significant decrease for VISTA, TIM3, and GAL9, but not for PDL2. Interestingly, a marked upregulation of IL6 and CCL2 hallmarks of MDSC was present in monocytes after EV conditioning (Figure 4.4.1B).

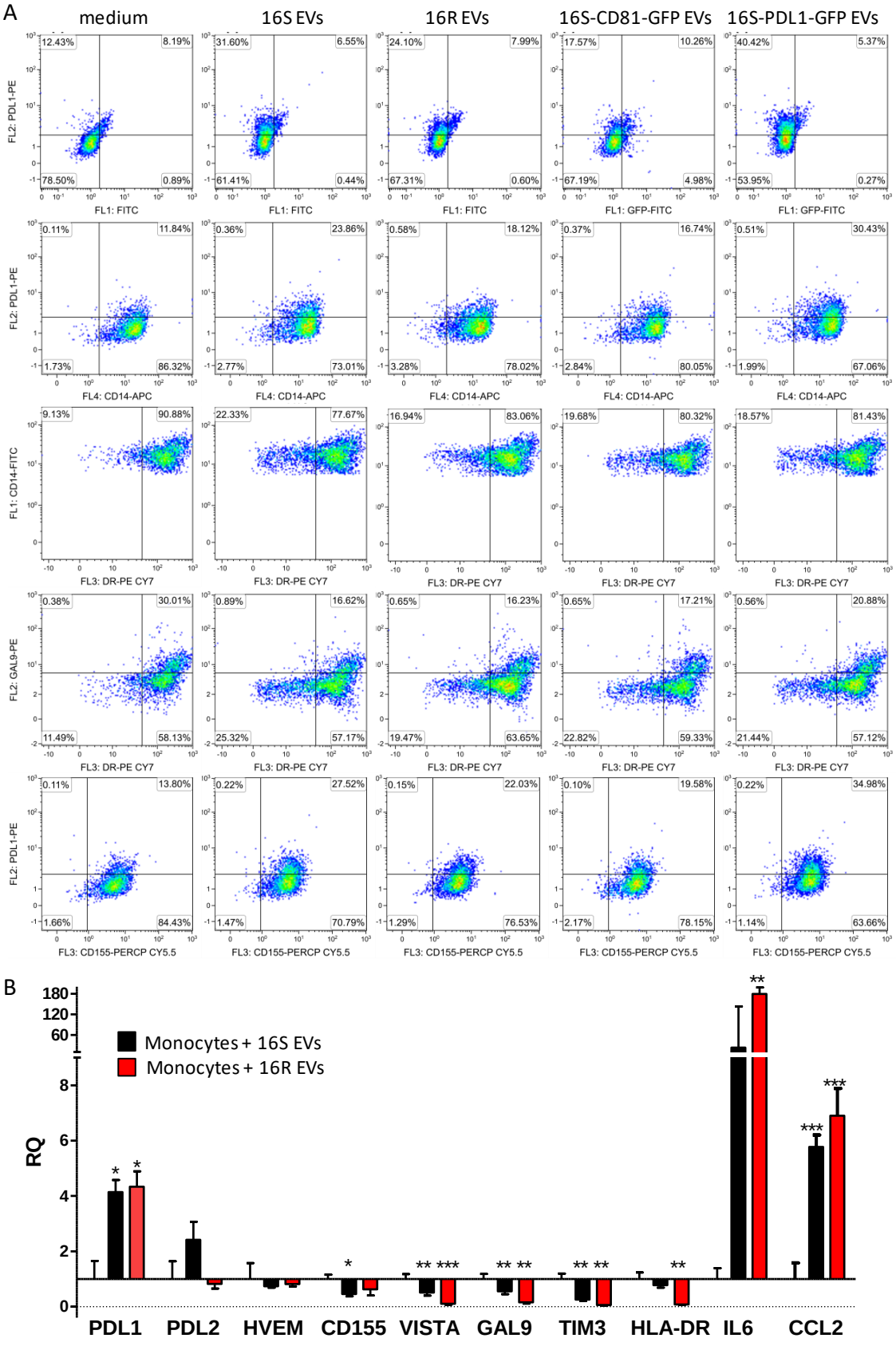

Figure 4.4.1. Effects of melanoma EVs on purified CD14⁺ monocytes. A) Flow cytometry analysis and B) qRT-PCR for IC modulation in purified monocytes treated with EVs from BRAF/MEKi sensitive and resistant melanoma cell lines 16S and 16R. This experiment was repeated at least twice, each time with three healthy donors. Each gene is tested in triplicate. Error bar is the standard deviation of the triplicate of the represented data.

4.5. Functional activity of CD14 monocytes conditioned by melanoma EVs

To assess the modulatory effects of EVs in functional experiments, monocytes harvested after incubation with EVs were washed to eliminate non-internalized vesicles, and co-cultured at different concentrations with the autologous $CD14^{neg}$ fraction containing lymphocytes. $CD14^{neg}$ cells were labelled with CFSE and stimulated with CD3/CD28 beads. After 5 days of culture, samples were harvested, stained with CD4, CD8 and CD25 antibodies and acquired with a FACSCalibur flow cytometer. Results of a representative healthy donor are showed in Figure 4.5.1 for EVs deriving from 16S and 16R cell lines, while Figure 4.5.1 shows those for EVs with a GFP tag.

The proliferation is shown in percentage of lymphocytes (left panels), $CD4^+$ (middle panels) and $CD8^+$ (right panels). The first row showing grey histograms represents the proliferation in the absence of the $CD14^+$ fraction, which is instead present at the indicated ratios but in the absence of EVs in the second row. At 1:0.125 and at 1:0.25 ratios the presence of monocytes had a stimulatory effect on proliferation, while ratios of 1:0.5 and 1:1 led to its progressive decrease, ranging from 96% with 1:0.25 to about 80% with 1:0.5 and to about 33-44% with 1:1 ratio.

The more affected lymphocytes were the $CD8^+$ T cells. In contrast, the presence of EV-conditioned monocytes in the cultures interfered with the proliferative activity of T cells already at a ratio of 1:0.25, leading to a reduction of 10% in the case of 16S EVs and of 20% in the case of 16R EVs. This inhibitory effect was potentiated to 20-30% at 1:0.5 ratio and reached about 50% of inhibition at a ratio of 1:1 (second and third row of Figure 4.5.1). At all tested ratios monocytes conditioned with EVs from BRAFi resistant melanoma cells 16R displayed a stronger suppressive potential of T cell proliferation and $CD8^+$ T cells were more affected.

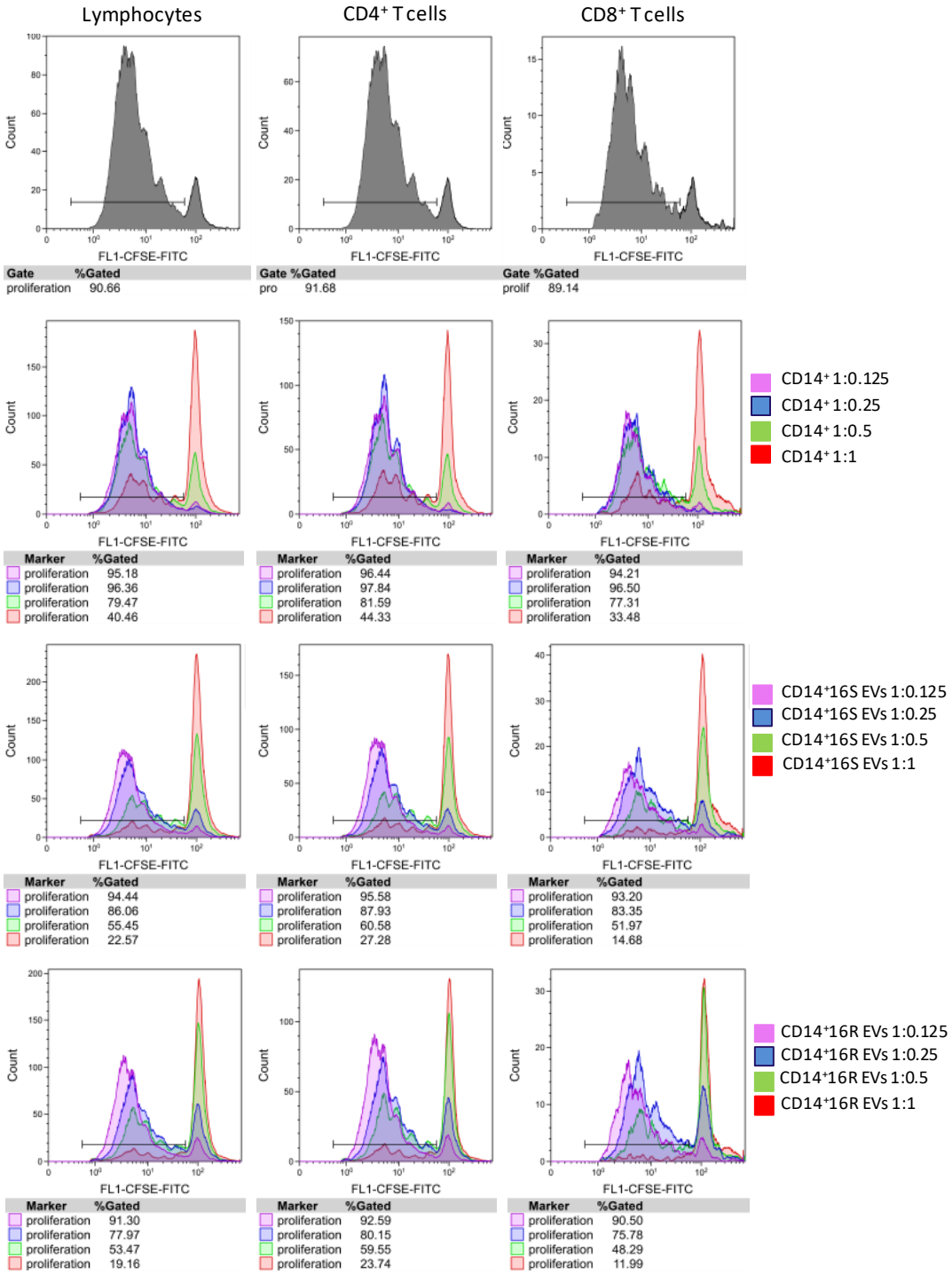

Figure 4.5.1. Effects of EV-conditioned CD14$^+$ cells on T cell proliferation. CFSE-labelled CD3/CD28 stimulated CD14^{neg} cells co-cultured for 120 h with different ratios of autologous monocytes pre-treated with EVs deriving from LM16S and LM16R cells for 24 h. This experiment was performed twice, each time with two different donors. Results in the figure show representative data.

Similar results were obtained with EVs derived from transfected 16S cells for CD81-GFP and PDL1-GFP, which are displayed in Figure 4.5.2. If monocytes were preconditioned with EVs, they lost their stimulatory activity already at a ratio of 1:0.25. This inhibitory effect increased at 1:05 and at 1:1 and affected CD8$^+$ T cells more than CD4$^+$ T cells. Of note, suppressive effects were more pronounced if EVs derived from 16S cells transfected

with PDL1. The CD14$^+$ responses to added EVs displayed differences in the amplitude of uptake, IC/HLA-DR modulation and functional effects which were donor dependent. The results obtained with the GFP-tagged EVs indicate their suitability as tool to study immune EV interactions.

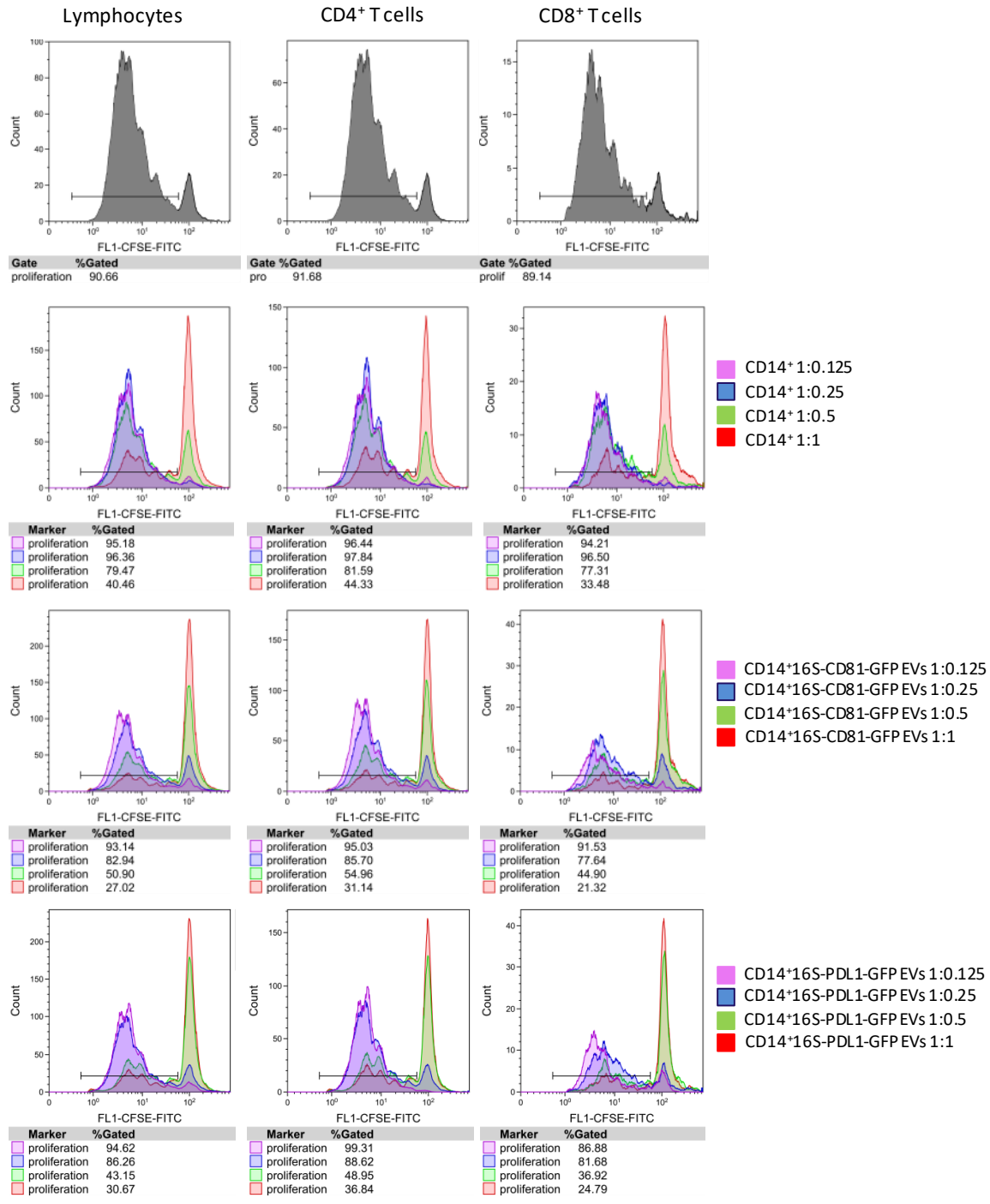

Figure 4.5.2. Effects of CD14$^+$ cells conditioned with GFP tagged EVs on T cell proliferation. CFSE-labelled CD3/CD28 stimulated CD14^{neg} cells co-cultured for 120 h with different ratios of autologous monocytes pre-treated with EVs deriving from LM16S-CD81-GFP and LM16S-PDL1-GFP for 24 h. This experiment was performed twice and each time with two different donors. Results in the figure show representative data.

4.6. IC expression in CD14^{+} cells conditioned with autologous melanoma and plasma EVs

This experiment was aimed at investigating the effects of autologous EVs on purified monocytes from advanced melanoma patients. In the case of patient 1 (Pt1) I purified EVs from conditioned medium of the autologous melanoma cell line, which had been generated from a tumour specimen in my hosting laboratory. Figure 4.6.1A shows the IC expression of this cell line: I could not detect PDL1, PDL2 or VISTA on the cells. On the other hand they expressed CD155 at 80% and HVEM at 90%, while GAL9 was detectable on about 16% of cells. EVs were isolated according to the isolation protocol for cell culture-derived vesicles and evaluated by NTA. They displayed a dimension mean of 168.8 nm and a mode of 120 nm, thus likely resembling EVs of the exosome type (Figure 4.6.1B).

To obtain EV conditioned monocytes, these latter were isolated from PBMCs of Pt1 and co-cultured with EVs for 24 h. Thereafter cells were harvested and processed for RNA extraction and qRT-PCR analysis. As depicted in Figure 4.6.1C, I could observe a downregulation of the IC VISTA, GAL9, CD155, HVEM. In contrast, the monocytes from this patient upregulated PDL1, PDL2 and CD163 MDSC marker upon encountering their autologous melanoma EVs. All observed differences were statistically significant.

A

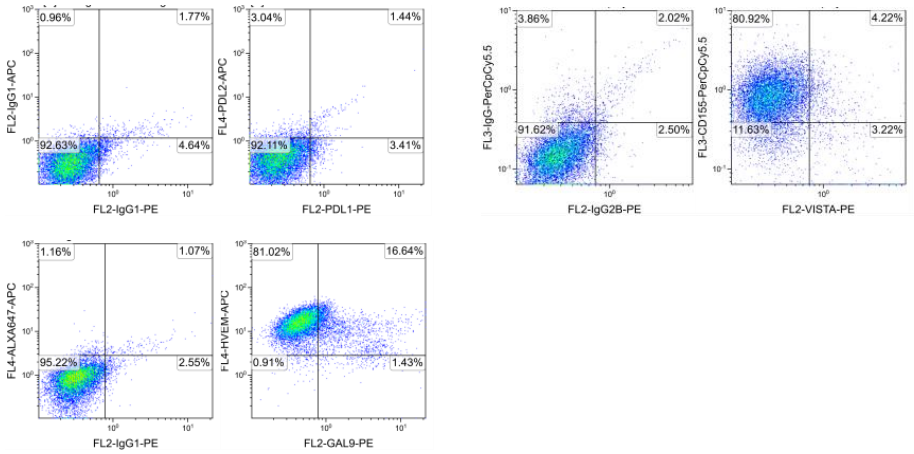

B

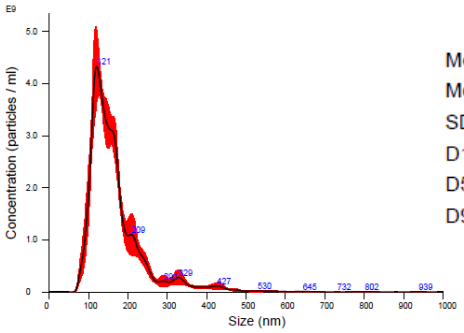

Mean:	168.8 nm
Mode:	120.1 nm
SD:	78.2 nm
D10:	105.6 nm
D50:	147.3 nm
D90:	247.6 nm

C

CD14⁺ monocytes with autologus cell line-derived EVs (Pt1)

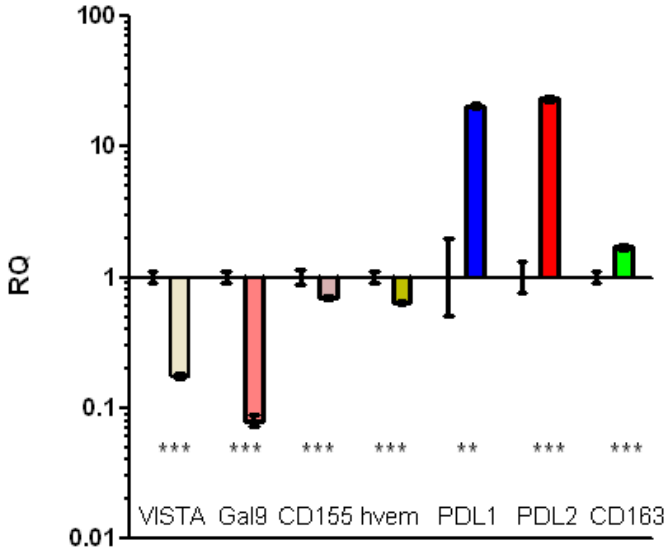

Figure 4.6.1. Effects of melanoma cell line-derived EVs on autologous monocytes. A) Flow cytometry analysis of a cell line derived from a melanoma specimen from a patient (Pt1). Expression of PDL1, PDL2, CD155, VISTA, HVEM and Gal9 are tested (right dot plots) with respect to their IgG controls). B) NTA of EVs isolated by differential centrifugation of conditioned medium of Pt1 melanoma cell line. C) qRT-PCR analysis of purified monocytes from melanoma patient Pt1 co-cultured with EVs from Pt1 autologous cell line. This analysis was performed in duplicate and the error bar is the standard deviation of the obtained data. Expression of IC and CD163 transcripts. Statistical significance was achieved with paired t-test.

EVs were also isolated from the autologous plasma and tested with CD14⁺ cells as described above. To isolate EVs from plasma I applied a two-step protocol set up by my

hosting laboratory to purify large EVs in F1 at a lower speed centrifugation, and small EV fraction F2, isolated by higher speed centrifugation. NTA analysis of unprocessed plasma revealed vesicles with a mean size of 109 nm and a mode of 83 nm, indicating that the plasma contained EVs of the smaller and potentially exosome type. Of the isolated fractions I could measure only F1 by NTA and results showed EVs with bigger mean dimensions of 144 nm but the same mode of 83 nm as unprocessed plasma (Figure 4.6.2A).

Large and small EVs were the co-cultured with isolated CD14+ cells of Pt1 and as described for autologous cell line EVs, harvested and processed for RNA analysis. Results depicted in Figure 4.6.2B show that similarly to pure melanoma EVs also plasma EVs induce an upregulation of PDL1, PDL2 and CD163. However, in contrast to cell line EVs, either F1 or F2 plasma EVs were able to induce an upregulation of VISTA, GAL9, CD155, HVEM and PD1. This modulation could be due to the presence of other EVs in plasma, especially immune cell-derived EVs, which could be responsible for the observed effects (Figure 4.6.2B).

An analogous experiment with autologous plasma EVs was performed on CD14+ cells from another advanced melanoma patient (Pt2) (Figure 4.6.2C). Here I could detect a downregulation of VISTA, GAL9, CD155, HVEM and CD163, while only PDL1 and PDL2 were upregulated upon co-culture with autologous plasma EVs. These modulations were similar to those induced by autologous cell line derived EVs, an effect that could depend on a potentially higher portion of tumour-derived EVs in plasma.

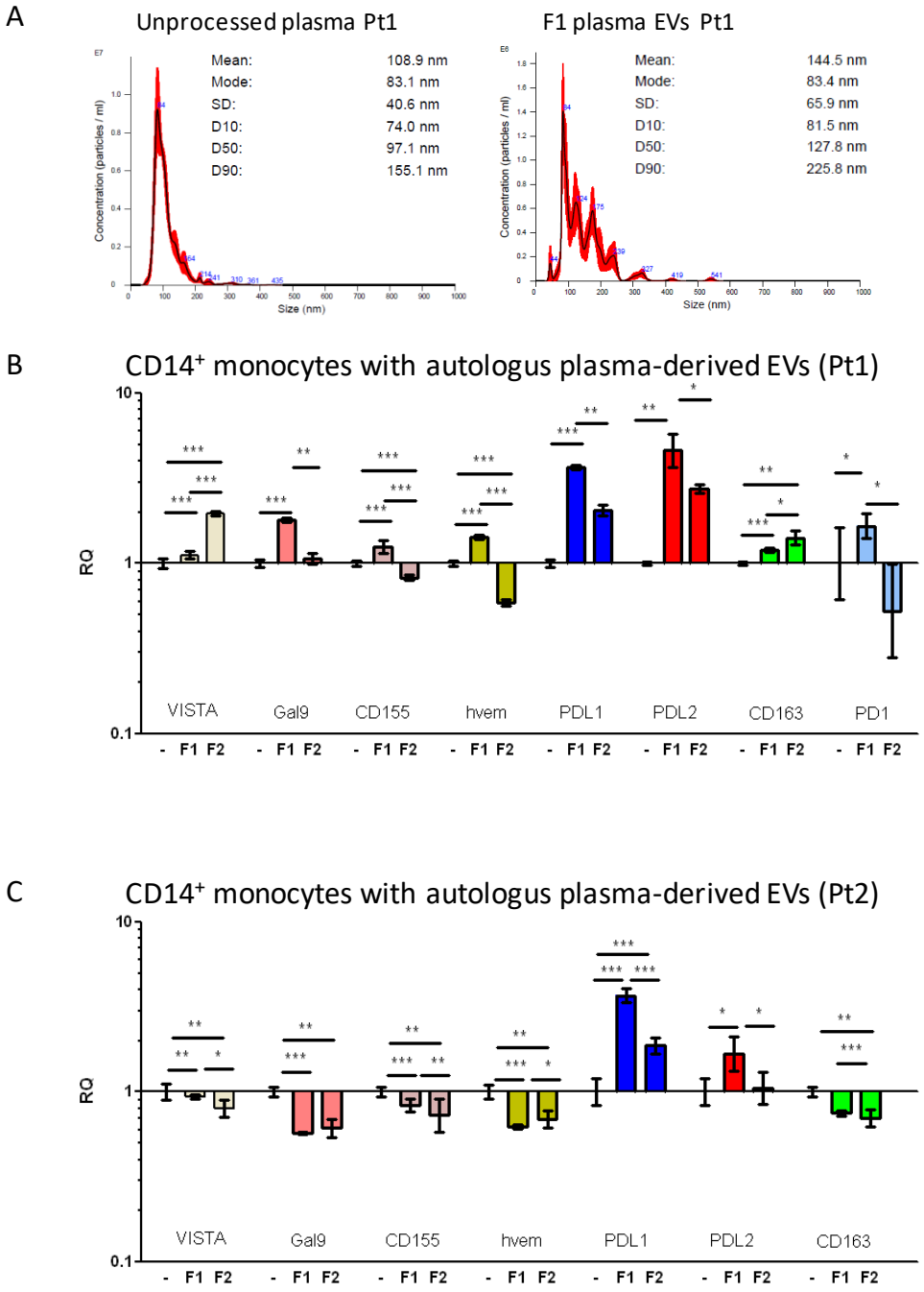

Figure 4.6.2. Effects of plasma-derived EVs on autologous monocytes of melanoma patients. A) NTA of unprocessed plasma and F1 isolated EVs of melanoma Pt1. B) qRT-PCR analysis of purified monocytes from melanoma patient Pt1 co-cultured with EVs from Pt1 autologous plasma F1 and F2 for the expression of IC and CD163 transcripts. C) qRT-PCR analysis of purified monocytes from a melanoma patient Pt2 co-cultured with EVs from Pt2 autologous plasma F1 and F2 for the expression of IC and CD163 transcripts. These analyses were performed in duplicate and the error bar is the standard deviation of the obtained data. Statistical significance was achieved with paired t-test.

5. Modulation of plasma EV in patients upon BRAF/MEKi treatment

In this part of my project, I performed exploratory studies on EVs isolated from the plasma of melanoma patients treated with targeted therapy. At first I spent major effort to set up experimental conditions for these experiments.

5.1. Analysis of IC transcripts in plasma EV: comparison of different methods

To explore the potential relevance of IC carried by plasma EVs, three different isolation methods were tested for the detection of transcripts. EV were isolated from two plasma samples by 1) single step UC, 2) ExoQuick, and in both cases RNA was extraction by the Macherey Nagel kit (Isolation of small and large RNA); 3) ExoRNeasy serum/plasma kit, a commercial method which isolate EV and extract RNA from plasma samples. Table 5.1. reports the average Ct values for the studied genes for the used methodology.

This analysis displayed different results in the two samples for the two methods ExoQuick and ExoRNeasy, although both techniques showed a better performance compared with the UC protocol, which was excluded from the possible investigation methods of this study.

Table 5.1. EV isolation methods and average Ct by qRT-PCR analysis

Plasma sample	EV isolation	plasma (µl)	PDL1	PD1	PDL2	CD155	CD14	CD3D	HLA-A	GAPDH	CD8
mel pt 1	ExoRNAeasy	0,5	32,0	40	32,8	33,8	29,8	28,9	22,9	22,7	27,2
	Single UC	0,5	40	40	40	40	40	36,9	30,9	29,2	32,2
	ExoQuick	0,25	31,1	30,9	33,6	27,4	26,4	29,9	20,9	21,8	NP
mel pt 2	ExoRNAeasy	0,5	31,5	31,9	31,6	34,7	27,9	28,3	20,1	19,4	28,7
	Single UC	0,5	35,5	40	35,6	40	31,8	32,5	27,6	27,3	31,8
	ExoQuick	0,25	40	40	NP	NP	33,2	NP	22,3	NP	35,9

Note: mel pt - melanoma patients; UC - ultracentrifugation; NP - not performed

Next, the set of samples was enriched (n=19), and the experiment was run only with ExoQuick and ExoRNeasy methods. In between an independent experiment was performed to test different plasma volumes using the two kits: I decided to use 800 µl of plasma for ExoRNeasy kit, and 250 µl for ExoQuick, because with more plasma the filter of MNagel column was plugged by the polymer and the RNA extraction failed.

Results indicated that the separation of EV and RNA extraction by ExoRNeasy kit had the best performance (Figure 5.1). While ExoRNeasy showed only 4 undetermined values of Ct, the undetermined values of ExoQuick were 38. Thus, for further analysis ExoRNeasy was selected as the best method for trascript analysis on plasma EV.

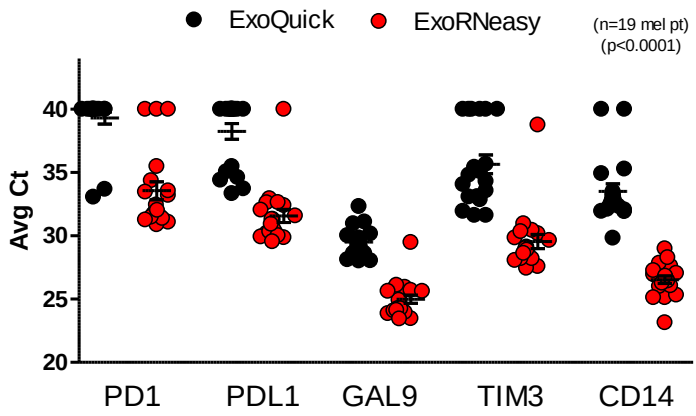

Figure 5.1. Comparison of methods for detection of IC transcripts in plasma EV samples. qRT-PCR of 5 genes on 19 EV samples isolated from plasma of melanoma patients by ExoQuick (black dots) and by ExoRNeasy (red dots). Undetermined values are plotted as Ct=40. All differences were significant. The error bar represent the standard deviation of the 19 samples.

5.1.1. Modulation of IC transcripts carried by plasma EVs

To evaluate whether the analysis of IC in plasma EVs may contribute to uncover the mechanisms governing the response to treatment, I studied plasma EV samples from a set of 11 melanoma patients at the baseline and at month 1, 3, and 6 time points during treatment. The samples were selected from a retrospective case set of patients with a long or a short response to BRAF/MEKi treatment, i.e. less or more than 1 year of time to progression (see Table 2.1.1 in material and methods Section 2). RNA was isolated by ExoRNeasy kit from 800 µl of plasma, and tested by qRT-PCR for the expression of fifteen genes, including negative and positive checkpoints ligands and receptors expressed by tumour and immune cells, and immune cell specific markers CD3 and CD14. From a technical point of view I observed a high detection rate of the studied genes in plasma EV with few undetected values (< 3%).

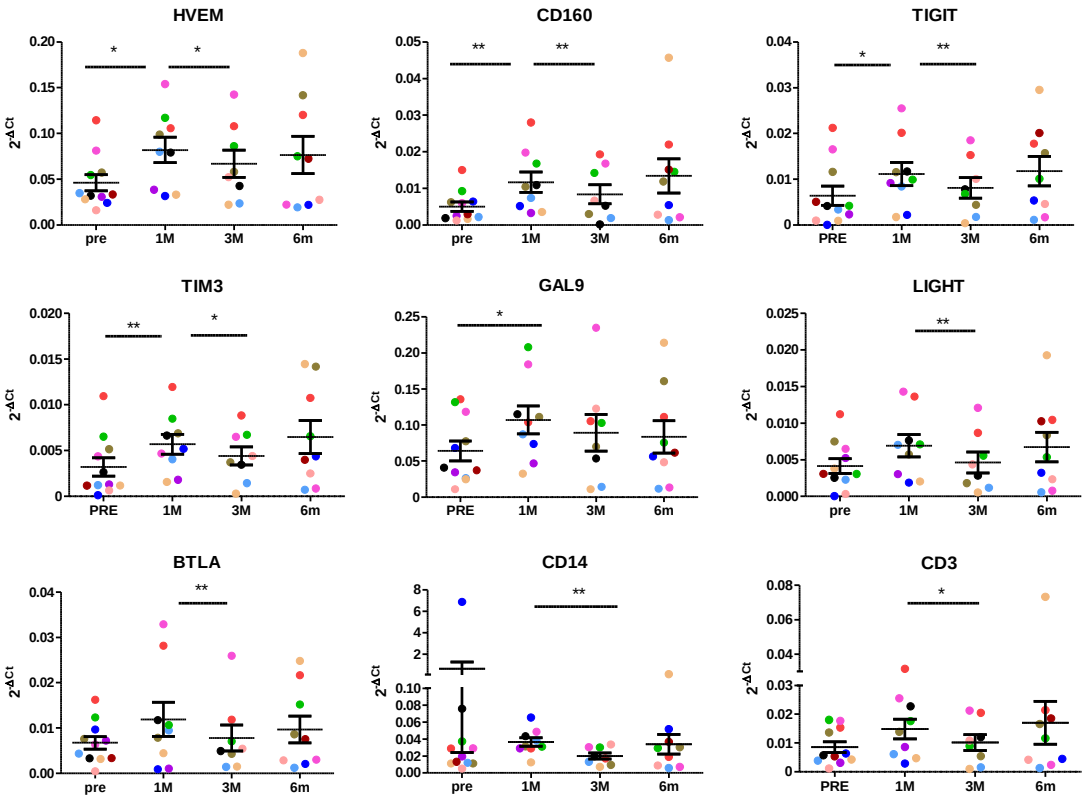

Figure 5.1.1.1. qPCR detection of IC transcripts in plasma EVs. The names of the encoded proteins are reported. The expression of ACTB and GAPDH was used for data normalization. The different colours represent the different patients. The error bar represents the standard deviation for all the patients in that time point.

Results showed that the levels of most IC significantly increased after one month of treatment and then decreased at 3 months of treatment, followed by a non significant modification at 6 months: this pattern was observed for HVEM and its receptor CD160, for TIGIT (one of receptors of CD155), and for TIM3, and for GAL9 although only upregulation at one month was significant. A similar trend was shown for the other receptors of HVEM, i.e. BTLA and LIGHT, and for both CD3 and CD14, all showing a significant decrease at 3 months (Figure 5.1.1.1).

In contrast, the markers of the PD1-PDL1/PDL2 axis showed little modulation during treatment, except for PDL1 which showed a significant increase at 3 months of treatment (Figure 5.1.1.2.). Apart from TIGIT (Figure 5.1.1.1), no significant differences were observed for CD155 axis and its receptors CD226 and CD96 (Figure 5.1.1.3).

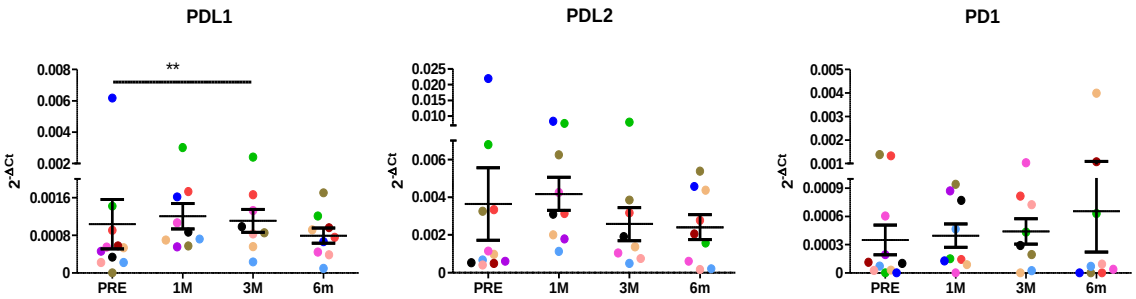

Figure 5.1.1.2. qPCR detection of IC transcripts in plasma EVs. Results of markers of the PD1-PDL1/PDL2 axis are shown. The error bar represents the standard deviation for all the patients in that time point.

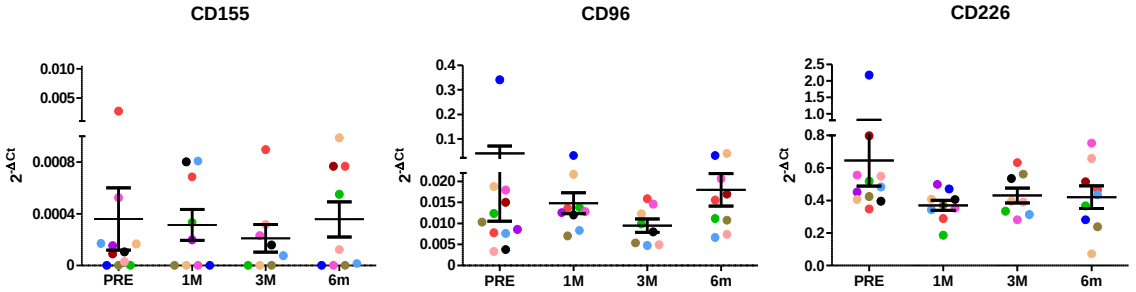

Figure 5.1.1.3. qPCR detection of IC transcripts in plasma EVs. Results of markers of the CD155-CD96/CD226 axis are shown. The error bar represents the standard deviation for all the patients in that time point.

To investigate potential differences based on response to treatment, data were analysed separately for the long responding (LR with a time to progression from 19 to 25 months) and the short responding (SR with a time to progression from 1 to 7 months) patients. For LR the pattern and significant differences at the tested time points were generally maintained, while this could not be observed for the SR group. In particular, HVEM and its three receptors CD160, BTLA, LIGHT, together with CD3 and CD14 showed a similar pattern (Figure 5.1.1.4). In contrast, in the SR only a significant upregulation of CD160 at 3 months from treatment was observed.

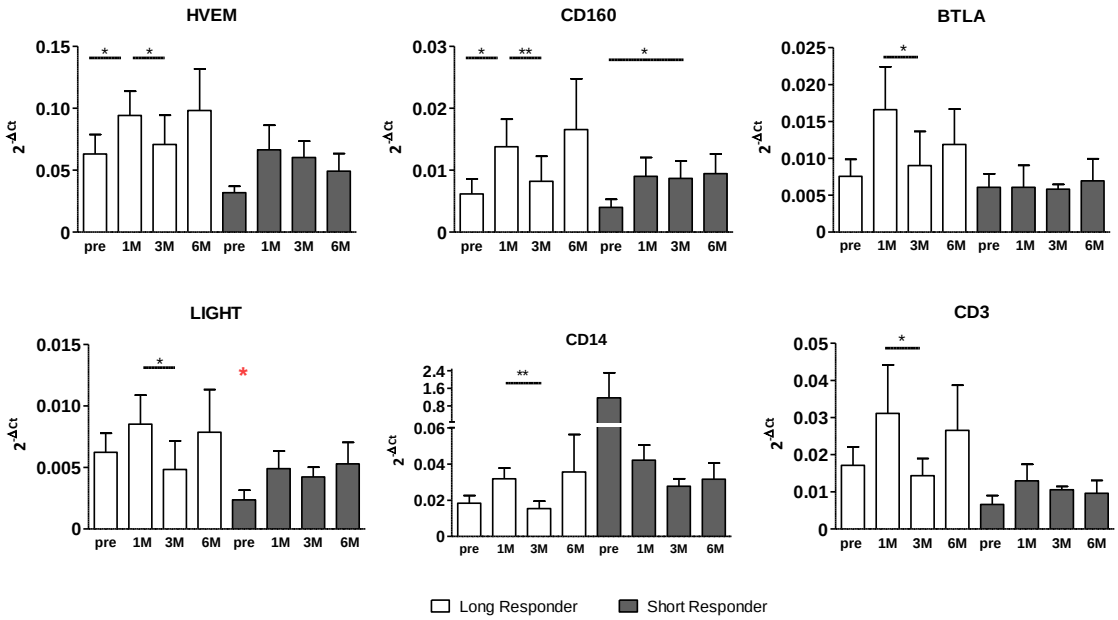

Figure 5.1.1.4. qPCR detection of IC transcripts in plasma EVs in long and short responding patients. The names of the encoded proteins are reported. The expression of ACTB and GAPDH was used for data normalization. Red * indicates $p<0.05$ by t-test analysis between LR and SR at the indicated time point. The error bar represents the standard deviation for all the patients in that time point.

Interestingly, when the expression levels were divided into LR and SR for the different time points, only LIGHT and PD1 transcripts resulted significantly higher in LR compared to SR. (Figure 5.1.1.4 and 5.1.1.5). Additionally, LR patients displayed a significantly higher level of PD1 before treatment than did SR. In contrast, I could detect higher PDL1 levels in SR compared to LR, which decreased at 3 months. A statistically significant decrease at 3 months in SR was also observed for CD96, while TIGIT displayed an increased expression at 1 month in SR (Figure 5.1.1.5).

In general, most molecules displayed higher levels in LR compared to SR, with the notable exception of PDL1, PDL2 and CD14. In addition, in EV samples from LR most of the studied IC showed a modulation during treatment, while this effect was absent in SR. Furthermore, CD3 expression was lower in SR compared with LR and that of CD14 was higher: although the difference did not reach statistical significance this result suggests a different immunomodulation occurring in the two group of patients.

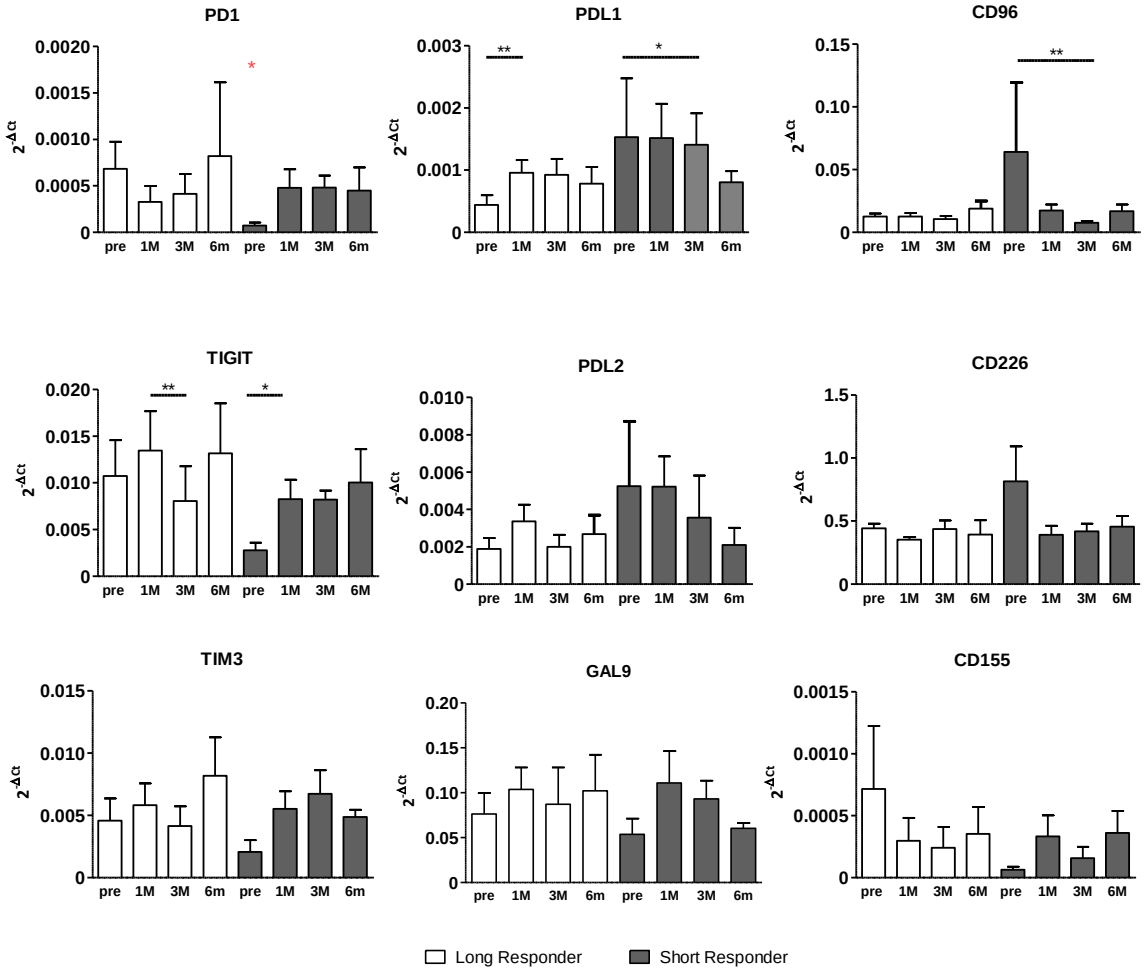

Figure 5.1.1.5. qPCR detection of IC transcripts in plasma EVs grouped in long and short responder patients. The names of the encoded proteins are reported. The expression of ACTB and GAPDH was used for data normalization. Red * indicates p<0.05 by t-test analysis between LR and SR at the indicated time point. The error bar represents the standard deviation for all the patients in that time point.

5.2. Characterization of plasma EVs from melanoma patients by NTA

To assess whether the treatment induced changes in the quantity and size of circulating EVs I performed a characterisation of unprocessed plasma by NTA using Nanosight in the same set of samples. The concentration ranged between 13 and 97 x 10^{10} particles/ml. Results showed a decrease of concentration between 1 and 3 months of treatment (Figure 5.2.1). These data are in agreement with transcript analysis (Figure 5.1.1.1) showing that 8/15 genes were down regulated at 3 months post treatment compared to 1 month, suggesting that the observed expression modulation could be due to a decrease of EV concentration.

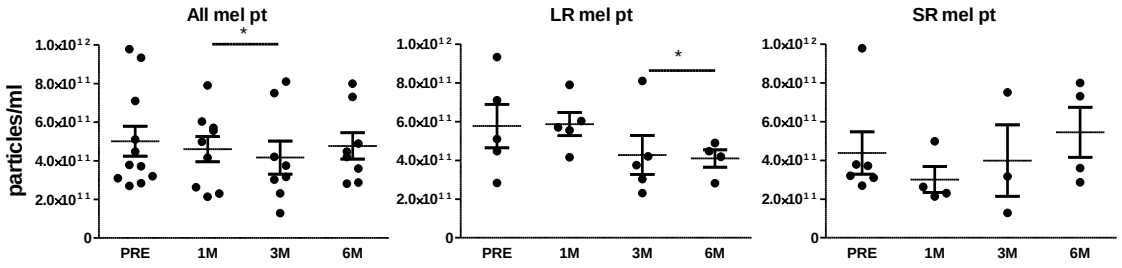

Figure 5.2.1. NTA of plasma samples from melanoma patients: EV numbers. The left graph displays the EV concentration in all samples (all mel pt), while the other two report the results for LR-long responders and SR-short responders. Data at the different time points are shown. Pre-before treatment, M-month post treatment. The error bar represents the standard deviation for all the patients in that time point.

When the results were divided for LR and SR patients, a different pattern appeared. LR displayed a higher EV concentration than SR at baseline, and this difference increased at 1 month, reaching statistical significance (Figure 5.2.1 centre and right panel, Figure 5.2.2). During treatment the EV concentration decreased in LR, while in the SR group I measured an increasing trend.

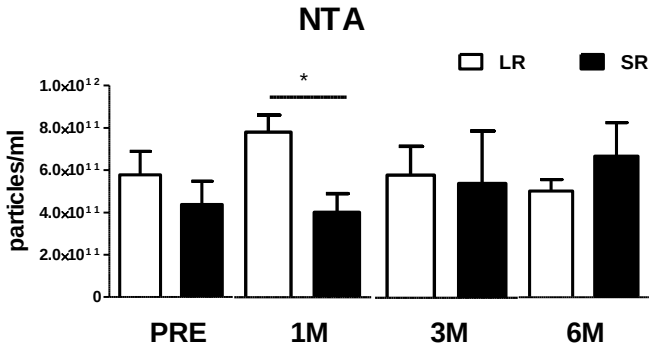

Figure 5.2.2. EV concentration in plasma of LR and SR melanoma patients. Mean ±SD at the different time points are shown. The error bar represents the standard deviation for all the patients in that time point.

I then analysed the results for EV size. Considering all the samples, no differences were observed at the time points for mean and mode parameters of EV. However, the data showed opposite patterns in the two groups of patients (Figure 5.2.3). In LR samples the size increased at 3 months and decreased at 6 months, while in SR patients the EVs were smaller at 3 months. Statistically significant differences were observed between LR and SR patients at 1 and 3 months for both, mean and mode parameters (Figure 5.2.4). Finally, correlation analysis showed that the EV number was inversely related to the EV size (Figure 5.2.5).

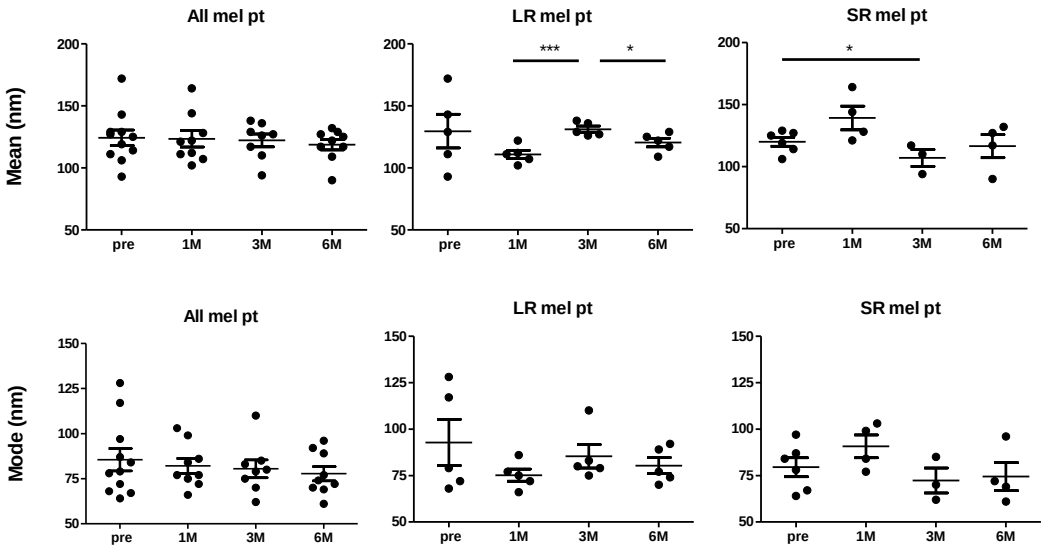

Figure 5.2.3 NTA of plasma samples from melanoma patients: EV size. Mean (upper panel) and mode (lower panel) are shown. LR-long responders, SR-short responder**s.** The error bar represents the standard deviation for all the patients in that time point.

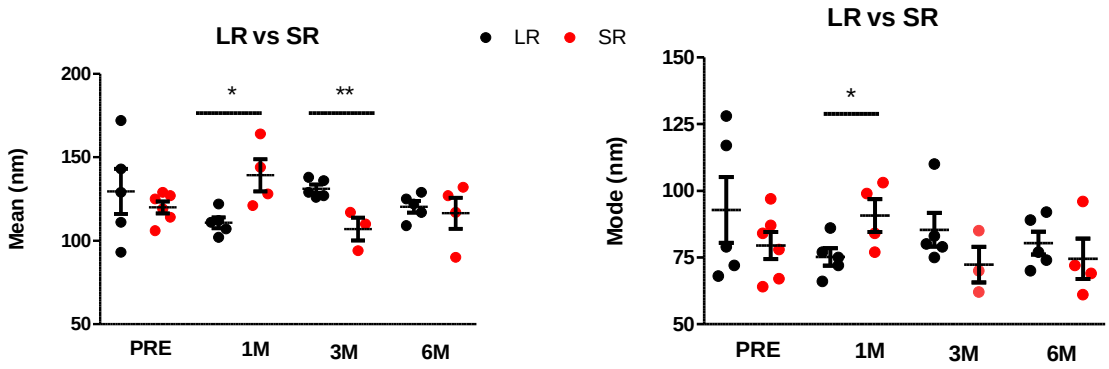

Figure 5.2.4 EV size in plasma samples from melanoma patients. Mean (left panel) and mode (right panel). t-test analysis between LR and SR patients at each time points. The error bar represents the standard deviation for all the patients in that time point.

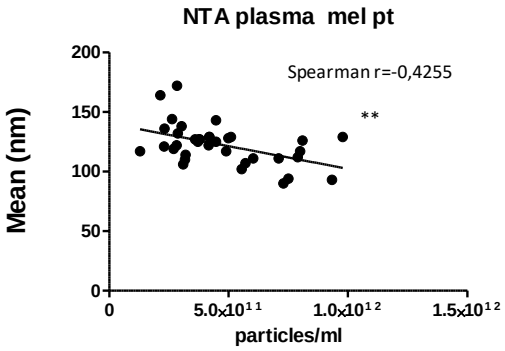

Figure 5.2.5 Correlation analysis of concentration and size of plasma EV obtained by NTA. Spearman non parametric correlation analysis was performed to test the association between the two parameters.

In conclusion, EVs at 1 month from treatment are more concentrated in LR but smaller in size, and conversely EVs in SR melanoma patients are less in number but have higher mean and mode values. While no difference in number was observed at 3 months, data showed that LR EVs have bigger dimensions than SR EVs at 3 months.

5.3. Analysis of IC protein in plasma EV samples

A recent publication to which I contributed with experiments involving EVs showed that plasma EVs of melanoma patients display increased concentrations and dimensions when compared to healthy donors. To investigate the IC presence in bigger or smaller plasma EVs (bEV and sEV), I used a centrifugation method to obtain enriched EV pellets for bEV, called F1, and sEV, called F2. The two fractions were characterized by TEM and flow cytometry analysis as shown in our study [62]. F1 fraction EV size ranged between 200-500 nm, while the F2 EVs showed a size below 200 nm. Protein detection was performed by western blot analysis (Figure 5.3).

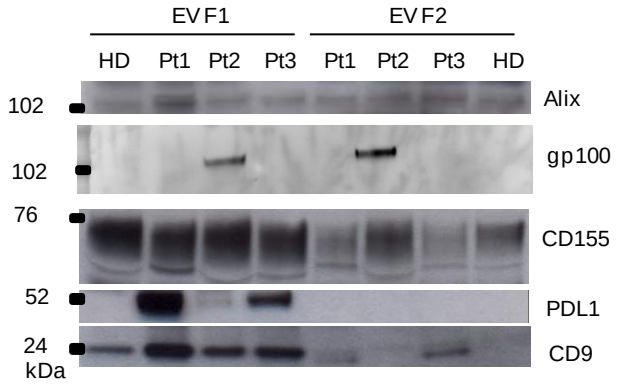

Figure 5.3. Western blot analysis of F1 and F2 isolated plasma EV fractions. Expression of PDL1, CD155, CD9 and Alix (the latter were used as loading controls), and gp100 melanoma marker. 30 µg of protein were loaded in each well. Pt-melanoma patient, HD-healthy donor.

To assess IC expression in F1 and F2 plasma EV fractions, western blot analysis was performed with samples isolated from plasma 3 metastatic melanoma patients and 1 healthy subject. PDL1 was only detected in F1, while CD155 and CD9 were expressed at higher levels in F1 compared to F2. Both F1 and F2 fractions from the donor were negative for PDL1, while CD155 was detected in both fractions. Gp100 was detected only in both fractions of 1/3 melanoma plasma samples, indicating the presence of melanoma-derived EVs. The results also showed that CD9 could represent a good EV marker for F1 fraction (Figure 5.3). These data demonstrated that F1 plasma EVs are carriers of different

proteins including IC, showing different levels between melanoma patients and healthy control.

5.3.1. Analysis of PDL1 levels in plasma EVs of BRAF/MEKi-treated melanoma patients

I investigated the EV protein expression in plasma EVs from melanoma patients treated with BRAF/MEKi, obtained at the beginning of treatment and at 1, 3 and 6 months. I chose to study the modulations of the expression levels of PDL1 molecule in plasma EV F1 fraction containing enriched bEVs isolated from 6 patients responding or not to treatment. Western blot was performed by loading the same samples volume in each well. Since I detected PDL1 only in the F1 fraction, I considered only the F1 fraction, and used LM16R cell lysate as an internal control (Figure 5.3.1.1).

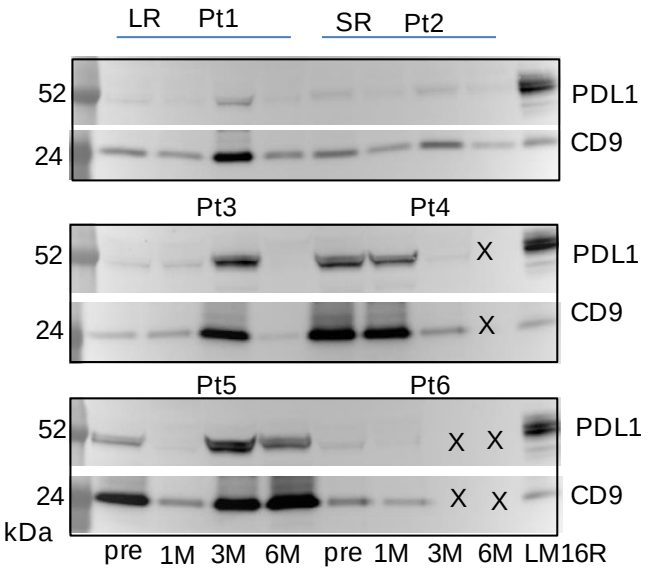

Figure 5.3.1.1. Western blot analysis of PDL1 in plasma EVs from melanoma patients. F1 fraction of EVs from plasma of melanoma patients (n=6), at different time points during BRAF/MEKi treatment. Pre – before treatment, 1M, 3M and 6M months during treatment. Samples were run in three gels, and contained samples from one long-responder patient (LR) and one short-responder (SR) at different time points. PDL1 and CD9 were tested. The cell lysate from LM16R cells was added in each gel as an internal control. (X)- missing sample

Data showed that the CD9 intensity volumes correlated with the μg of protein loaded in the gel, based on protein quantification by spectrophotometer. In addition, the intensity volume of PDL1 and CD9 bands were significantly correlated, indirectly indicating that PDL1 is carried by the CD9 positive EVs (Figure 5.3.1.2).

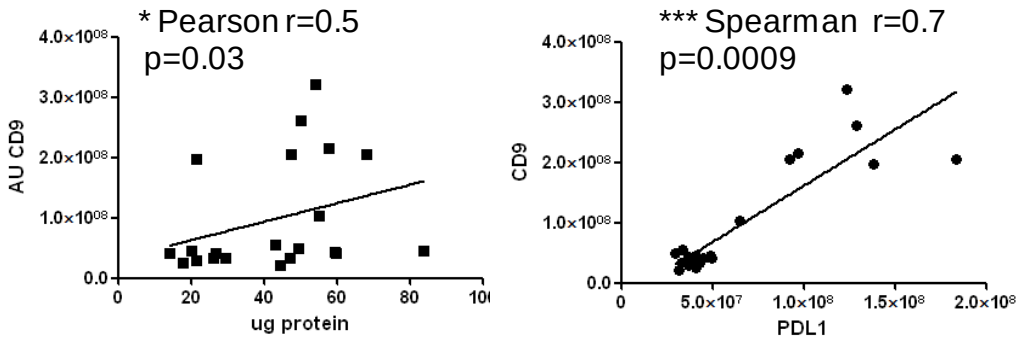

Figure 5.3.1.2. Correlation analysis of CD9 and PDL1 intensity values. Left: correlation between CD9 intensity volume and µg of protein loaded per well. Right: correlation between CD9 and PDL1 intensity values. Intensity volume of LM16R cell lysate added in each gel was used for intensity volume normalisation. AU- ratio intensity volume.

The results showed a higher intensity volume of PDL1 and CD9 at 3 months of treatment in LR compared with other time points and compared with SR. In addition, the intensity volumes of both proteins decreased during treatment in SR (Figure 5.3.1.3).

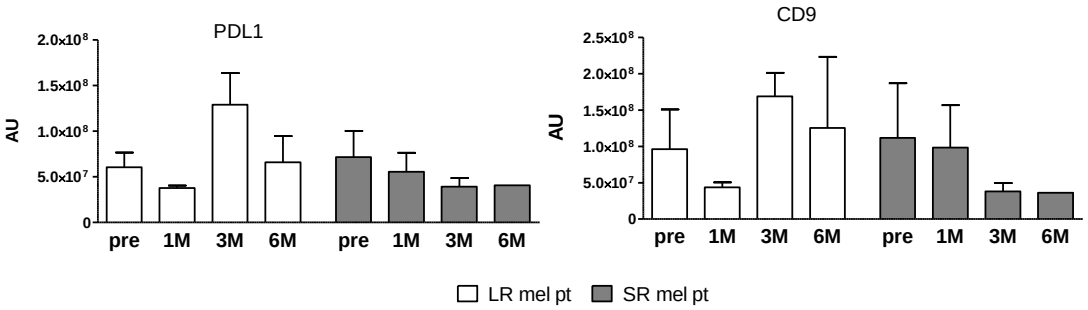

Figure 5.3.1.3. Western blot analysis of PDL1 and CD9 in plasma EVs from melanoma patients. The F1 fraction of EVs isolated from plasma of melanoma patients (n=6) treatment with BRAF/MEKi; before (pre), at 1, 3 and 6 months. PDL1 and CD9 were tested and quantified by NineAlliance software (UVITEC Imaging System). The ratio of intensity volume is obtained after normalisation with LM16R intensity value control. The error bar represents the standard deviation for all the samples at that time point.

In conclusion these data showed that PDL1 expression levels can be quantified in plasma EVs, and that PDL1 levels vary between patients and are modulated by treatment.

6. Discussion

6.1. Melanoma resistance to kinase inhibitors and IC expression.

The results obtained in the studies addressing IC expression in melanoma indicated that IC are modulated upon the achievement of resistance to kinase inhibitors and that the transfer of EVs may play a role in melanoma IC expression modulation.

One major achievement of this part of my studies is the demonstration that **molecular pathways leading to the acquisition of resistance include the modulation of the expression of IC molecules**. This evidence is obtained not only for PDL1, for which published data were already available, but also for PDL2, CD155, and HVEM and GAL9, the last two showing decrease expression. Although the patterns of IC modulation showed individual variation in different melanoma cell lines, most changes were reproduced in different cell lines. In addition, significant modulations of these IC were also detectable in resistant tumour biopsies from treated patients, thus indicating a potential clinical correlate to the in vitro findings. IC expression thus adds to the complexity of the phenotypic changes occurring in drug resistant melanoma and other IC may be considered as new target molecules for therapeutic strategies.

While for the modulation of PDL1 a large amount of data are available in the recent literature [122], due to the importance of this marker in the context of immunotherapy, the molecular signalling governing the modulation of the other IC I found modulated in resistant melanoma are still poorly characterized. In particular, of the IC increased in resistant tumour, CD155 was correlated with a poor prognosis in different tumour types including melanoma [188-191] and studies showed that its overexpression in human neoplasms promotes tumour growth, invasion, and immune escape [190, 191]. The expression of CD155 is regulated by different signalling pathways [192] and that may thus include those activated in melanoma resistance. In the set of tumour specimens from untreated patients studied here, I found that CD155 expression levels were not correlated with PDL1 but rather to HVEM.

In my studies, a decrease of HVEM and GAL9 expression in association with resistance was also reproducibly detected. Moreover, in primary uveal melanoma was observed a reduction of HVEM as compared to melanocytes [268]. All the studies investigating HVEM expression in tumours agree that HVEM expression correlates with a poor prognosis [179-184]. Tumour downregulation of GAL9 expression has been previously associated with

disease progression in metastatic breast cancer patients [170]. GAL9 protein was shown expressed in 57% of melanoma metastases and coexpressed with PDL1 in most of the tumours tested [174]. In line with these results, we detected a high correlation of GAL9 gene expression with genes of the PDL1/PDL2/PD1 axis (Figure 3.1.2 in Results Section).

In the in vitro cell line models, resistant melanoma displayed constitutively expressed IFN signalling molecules, CCL2 upregulation and miRNA modulation [249]. Results indicate that the expression of IC molecules PDL1, PDL2 and GAL9 are inducible by IFNγ in melanoma cells. In addition, I could also associate PDL1 expression to the constitutive expression of CCL2 chemokine and to the expression of miR-146a, for which PDL1 represents an indirect target via the regulation of NFkB (unpublished results). In addition, CCL2 influenced HVEM expression. CCL2 has a known tumour-promoting potential and in a previous study of my lab, we showed that CCL2 production by melanoma cells is involved in the resistance to BRAF inhibition and that its inhibition may restore drug sensitivity [249]. Similarly, miR associated to melanoma cell resistance and to CCL2 expression appears to regulate GAL9 and PDL2.

Results of co-culture experiments in transwell assays however showed that although co-cultured R cells induced expression of CCL2 and IL8 and increased STAT3 in negative S cells, this condition did not change IC expression pattern, suggesting that additional signalling is needed to impact on IC expression.

The second major achievement of my studies about association between melanoma resistance to kinase inhibitors and IC expression carried by **melanoma EVs that may condition recipient cell IC expression**. EVs released by melanoma cell lines were shown to carry IC proteins PDL1, CD155 and GAL9 and to carry IC transcripts reflecting the expression of the producing cells. These data represents a novel finding in the context of melanoma resistant cells. EV protein studies suffered of some limitations relative to the availability of commercial antibodies with limited technical applications: for example anti-PDL2 and GAL9 antibodies did not work in western blot analysis, and the expression of PDL1, PDL2, HVEM and CD155 could not be detected by FACS by staining of EVs-coated latex beads, possibly due to a low positivity.

To study the potential transfer of IC molecules I set up a model system with GFP-tagged EV and GFP-PDL1 fusion protein to study the potential transfer of PDL1 between melanoma cells, as previously adopted by [269]. Experiments by confocal microscopy

demonstrated the occurrence of EV binding and internalization in melanoma cells. Moreover, the transfer of PDL1 protein via EV was shown in co-cultured melanoma cells thanks to the GFP-tagged EV model. These results represent a proof of principle of the potential IC transfer by EV between melanoma cells.

6.2. Effects of the interaction of EVs with immune cells

In the experimental part of the project that investigated the effects of melanoma EV on immune blood cells, I showed the EV uptake by monocytes beside the modulation of PDL1, CD155, HVEM and GAL9 expression. Indeed, EV-interacting monocytes acquire phenotypic and functional properties of MDSC, as already demonstrated from the hosting lab.

Experiments showed that **melanoma EVs interacted almost exclusively with the $CD14^+$ monocyte fraction in PBMCs** of healthy donors, whether obtained from both BRAF/MEKi sensitive or resistant cells lines. In fact, I could observe no interaction with CD3 T cells of FITC positive EVs. The preferential targeting of monocytes has been demonstrated by many studies, thus it represented an expected result [270]. In contrast to recent studies reporting EV interaction with T cells majorly by surface-surface receptor-ligand interaction [115, 271], my data showed no EV internalisation or interaction with T cells in the co-culture experiments. However, an EV-mediated triggering of surface molecules expressed by T cells is very likely to occur. EVs that bound to T cells potentially detached when I harvested the cell samples for flow cytometry labelling and acquisition.

Monocyte-EV interaction detected after 18h co-culture was accompanied by an upregulation of PDL1 that was particularly evident in those monocytes which internalized EVs and were detected either as GFP positive or as DIOC-FITC positive monocytes (Figure 4.1.1). Similarly, purified $CD14^+$ cells cultured in the presence of GFP-tagged EVs displayed an acquisition of green fluorescence and an increase of the percentage of $CD14^+PDL1^+$ cells. The induction of PDL1 expression in monocytes was previously described in CLL patients as mediated by tumour exosome-carried non coding RNA, which targeted TLR7 in monocytes [272]. In their work, Haderk et al. also observed a production of proinflammatory cytokines CCL2, CCL4 and IL-6 similarly to what we detected upon co-culture of melanoma EVs in autologous and healthy donors' monocytes [62]. A recent study showed that PDL1 is upregulated by monocytes upon interaction with glioblastoma stem cell-derived exosomes. Interestingly, despite these authors observed a preferential

interaction with monocytes, they also detected an uptake of these EVs by activated but not resting T cells at 6 h of incubation [271]. Additionally, Gabrusiewicz and co-workers observed that PDL1 upregulation correlated with STAT3 phosphorylation, a hallmark of MDSC [273], occurring by melanoma EVs expressed HSP86 and TLR4 expressed MDSC interaction [63].

In my studies EVs obtained from both BRAF/MEKi sensitive and resistant cell lines induced a downregulation of HLA-DR expression by monocytes that was evident in gated $CD14^+$ cells in PBMCs as well as after purification. Of note, **in the monocyte gate of PBMCs the decrease of HLA-DR coincided with an upregulation of HVEM on the HLA-DR^{neg} subpopulation**. HVEM expression by MDSC may depend on an endogenous regulation by the monocytes in response to EV internalisation. In fact HVEM was described as a protein that can be expressed by monocytic MDSC [274]. In my experimental setting, the increased HVEM expression could also depend on the transfer of HVEM transcripts, which I could detect in EVs of the cell line pairs selected for these studies.

In contrast with data in the literature depicting that patients' MDSC express increased levels of GAL9, my results showed a **downregulation of this IC on the HLA-$DR^{neg}HVEM^{high}$ as compared to the HLA-$DR^{high}HVEM^{low}$ monocytes** [59]. This discrepancy could rely on the different settings, e.g. ex vivo patients' monocytes vs in vitro experiments. In fact, another study investigating the generation of MDSC in an in vitro setting described a reduced expression of GAL9 by M-MDSC [274]. Regarding PDL1 and PDL2, my experiments showed the induction of membrane expression of these IC on monocytes after the short-term incubation of 18 and 24 h, while at 36 h a minor but statistically significant reduction was detected. At opposite, PDL1 and PDL2 transcript levels always displayed an increase, in healthy donors' monocytes by both EVs from resistant and sensitive melanoma cell lines and in the autologous setting with either melanoma and plasma-derived EVs. This coincided with an increase of CD163, a M2 marker of macrophages associated with cancer progression through induction of IL-6 expression [274]. Interestingly, IL-6 and CCL2 were the main cytokines I found upregulated in monocytes cultured with melanoma EVs, as well as when EV-MDSC were induced by MDSC-microRNAs carried by EVs [62].

To test the suppressive ability of MDSC induced by melanoma EVs in monocytes from healthy donors' and to assess potential differences between EVs deriving from sensitive vs drug resistant melanoma cell lines, I performed proliferation experiments at different

monocytes ratios. In the absence of EVs conditioning, monocytes inhibited T cell proliferation if present at high ratios in co-cultures (100% and 50%), while at 25% and at 12.5% they stimulated proliferation of both CD4 and CD8 T cells. This is in line with previous findings showing that in the absence of disease high ratios of monocytes can influence T cell activity [275]. The suppressive activity of EVs-conditioned monocytes was evident already at 25% monocytes and affected both CD4 and CD8 T cells. At the higher ratios of 50% and 100%, the proliferation decreased progressively and at 100% CD8 T cells showed no proliferation. These results showed that **melanoma EVs induced a suppressive phenotype in monocytes, and that no differences could be observed between the origin of EVs**, from sensitive melanoma cell line LM16S or fromLM16R cell line. Additionally, the suppressive activity of monocytes could be also induced by CD81- and PDL1-GFP-tagged LM16S EVs, indicating this setting as an in vitro model lacking labelling biases suitable for studies investigating EV-mediated effects.

6.3. Studies on plasma EVs

In the part of the studies dealing with the characterization of plasma EVs from melanoma patients treated with BRAF targeted drugs, I set up methods of analysis to investigate EVs and different IC molecules.

These pilot studies were carried with samples obtained before and during treatment from a selected set of patients which showed or not a good response to the therapy. The hypothesis was that treatment determined the activation of immune system that could be reflected in the modulation of circulating EV. It is known that targeted therapy determine a rapid increase of the tumour immune infiltrate [276], possibly due to tumour cells death and the enhancement of a systemic inflammatory state of organism [277], but also that inhibitory molecules and immunosuppressive cell infiltration increase in progressing tumours [251, 252]. Thus, the pattern of IC at different time points during treatment might allow an overview of the immune system activation in the studied patients.

Indeed, through qPCR, NTA and western blot experiments **I set up conditions for successful analysis of IC transcripts and proteins in plasma EV samples**. To detect the presence and levels of EV transcripts, the technical challenge of RNA extraction by a method suitable to qRT-PCR analysis was overcame by selecting a method that worked very well in my hands and was reproduced in other samples in the lab. A commercial kit

(exoRNeasy [135]) was selected from methods that were less time consuming than UC for EV isolation and had a high yield of extracted RNA from a limited quantity of plasma sample [278].

Although the presence of gene transcripts in EV isolated from plasma is already documented [279], IC transcripts were not tested before, with the exception of PDL1 in EVs from lung and melanoma patients undergoing immunotherapy [135]. Besides PDL1, PDL2 and PD1, I tested the following IC transcripts in plasma EV: HVEM axis molecules, including HVEM receptors BTLA, CD160, and LIGHT, CD155 and its receptors TIGIT, CD96 and CD226, most of which were not reported before in EV samples (see Table 1.2.1.2 in introduction Section for the other IC EV publications). Results showed **variations of the expression levels of several IC transcripts during treatment, especially for molecules of the HVEM and GAL9 axis**. Long and short response patients showed different levels of PD1 and LIGHT transcripts in pre-treatment samples, and a general higher expression level of most studied molecules was detectable in responding patients compared to patients showing a short response to treatment.

Regarding the NTA analysis, I must underline that the analysis was performed in unprocessed plasma samples, in order to avoid the possible selection of particular EV populations through isolation and vesicle aggregation or clumping. Results clearly showed a **different pattern of number and size of plasma EVs between long and short responding patients**, particularly at 1 month from treatment. The increased EV concentration levels observed after the first month of treatment only in long responders are suggestive of a different immune condition induced by treatment in this group of patients. A low number of plasma exosomes was reported associated to poor prognosis in esophageal squamous cell carcinoma [280]. Notably, I found that the mean size of EV was inversely associated with the EV concentration values at 1 month from the treatment in long versus short responding patients. Thus, suggesting a potential, although unknown, different cell origin of the small vesicles in the LR, from the big vesicles on SR (Figure 5.2.4, right panel).

To gain insight in the IC carried in EV population with different sizes, protein analysis was performed in EV fractions separated by size. Western blot analyses of two fractions of plasma EVs separated by UC and characterized for big (F1) or small (F2) vesicle content, showed positivity for the melanoma markers gp100 in both fractions, while PDL1 and CD9 discriminated between two EV fractions and were expressed only in F1.

Based on these results and a recent publication on PDL1 protein detection in plasma EV [115], I studied a small set of samples from long and short responders for PDL1 expression level in F1. It has to be taken into account that after 3 and 6 months, 2 out of 3 short responders patients dropped out of the study, thus reducing the samples required to test significant differences. However, a different trend between two subgroups of patients was observed, as **increased PDL1 levels were detected in responders especially at 3 months of treatment**. These data are in agreement with results reported by Chen at al. showing an increase of PDL1 between 3 and 12 weeks samples in circulating EV from responders to immunotherapy [115]. Similarly, higher levels of PD1 and CD28 positive EVs were shown in serum samples from patients achieving clinical response to immunotherapy [281].

In conclusion, my studies suggest that IC expression levels in plasma EVs may reflect the anti-tumour immunity state of the patients and may hold predicting information on clinical outcome.

7. Conclusions and future perspectives

The downregulation of IC transcripts HVEM and GAL9 and the upregulation of CD155 detected in treatment resistant tumours of melanoma patients represent relevant observations for the interpretation of the results I obtained in this PhD project, though I could compare only 7 specimen pairs. The loss or decrease of these IC that can play inhibitory as well as stimulatory role in immune regulation has been associated with a tumour supportive microenvironment in lymphoma [282]. Similarly, in the immune studies, I observed a reduction of several IC transcripts, including HVEM, in monocytes conditioned with EVs deriving from melanoma cells, or with autologous EVs from patient's plasma. However, when I evaluated MDSC phenotyped as CD14+HLA-DRneg, an increase of HVEM in the HLA-DRneg population was detected. The expression of this IC by M-MDSC has been previously shown [274].

In melanoma as well as in monocytes I observed the induction of PDL1 expression when cells were cultured in the presence of EVs. PDL1 expression increased in resistant melanoma cells and was transferred via vesicles in BRAF/MEKi sensitive melanoma cells. Naive immune cells and BRAF/MEKi sensitive melanoma cells modulate IC upon encounter with EVs, especially if they derive from melanoma cells with acquired resistance to the drugs.

Plasma EVs showed modulation of concentration, size, IC transcripts and molecules, occurring during treatment by different patterns in patients with diverse outcomes, suggesting that the dynamic levels of IC markers may provide useful information on patient outcome and on novel IC targets for new treatment modalities. Given that melanoma IC expression is altered in BRAF/MEKi resistant tumours in melanoma patients, and that EVs reflect IC expression of originating cells, monitoring of plasma EVs may thus potentially provide predicting information on tumour state and immune activation. Further studies with a high number of patients are needed to verify the preliminary information of plasma EVs obtained in my studies.

References

1. Maas, S.L.N., X.O. Breakefield, and A.M. Weaver, *Extracellular Vesicles: Unique Intercellular Delivery Vehicles.* Trends in cell biology, 2017. **27**(3): p. 172-188.
2. Yáñez-Mó, M., et al., *Biological properties of extracellular vesicles and their physiological functions.* Journal of extracellular vesicles, 2015. **4**: p. 27066-27066.
3. Skog, J., et al., *Glioblastoma microvesicles transport RNA and proteins that promote tumour growth and provide diagnostic biomarkers.* Nature cell biology, 2008. **10**(12): p. 1470-1476.
4. Peinado, H., et al., *Melanoma exosomes educate bone marrow progenitor cells toward a pro-metastatic phenotype through MET.* Nature medicine, 2012. **18**(6): p. 883-891.
5. Théry, C., et al., *Minimal information for studies of extracellular vesicles 2018 (MISEV2018): a position statement of the International Society for Extracellular Vesicles and update of the MISEV2014 guidelines.* Journal of extracellular vesicles, 2018. **7**(1): p. 1535750-1535750.
6. Chargaff, E. and R. West, *The biological significance of the thromboplastic protein of blood.* 1946: J Biol Chem.
7. Wolf, P., *The Nature and Significance of Platelet Products in Human Plasma.* British Journal of Haematology, 1967. **13**(3): p. 269-288.
8. Johnstone, R.M., *Revisiting the road to the discovery of exosomes.* Blood Cells, Molecules, and Diseases, 2005. **34**(3): p. 214-219.
9. Raposo, G., et al., *B lymphocytes secrete antigen-presenting vesicles.* The Journal of Experimental Medicine, 1996. **183**(3): p. 1161.
10. Anand, S., et al., *Ticket to a bubble ride: Cargo sorting into exosomes and extracellular vesicles.* Biochimica et Biophysica Acta (BBA) - Proteins and Proteomics, 2019: p. 140203.
11. Raposo, G. and W. Stoorvogel, *Extracellular vesicles: exosomes, microvesicles, and friends.* The Journal of cell biology, 2013. **200**(4): p. 373-383.
12. Théry, C., L. Zitvogel, and S. Amigorena, *Exosomes: composition, biogenesis and function.* Nature Reviews Immunology, 2002. **2**(8): p. 569-579.
13. Höög, J.L. and J. Lötvall, *Diversity of extracellular vesicles in human ejaculates revealed by cryo-electron microscopy.* Journal of extracellular vesicles, 2015. **4**: p. 28680-28680.
14. Lunavat, T.R., et al., *Small RNA deep sequencing discriminates subsets of extracellular vesicles released by melanoma cells--Evidence of unique microRNA cargos.* RNA biology, 2015. **12**(8): p. 810-823.
15. Lobb, R.J., et al., *Optimized exosome isolation protocol for cell culture supernatant and human plasma.* Journal of extracellular vesicles, 2015. **4**: p. 27031-27031.
16. Witwer, K.W., et al., *Standardization of sample collection, isolation and analysis methods in extracellular vesicle research.* Journal of extracellular vesicles, 2013. **2**: p. 10.3402/jev.v2i0.20360.
17. Al-Nedawi, K., et al., *Intercellular transfer of the oncogenic receptor EGFRvIII by microvesicles derived from tumour cells.* Nature Cell Biology, 2008. **10**(5): p. 619-624.
18. Di Vizio, D., et al., *Large oncosomes in human prostate cancer tissues and in the circulation of mice with metastatic disease.* The American journal of pathology, 2012. **181**(5): p. 1573-1584.
19. Vagner, T., et al., *Large extracellular vesicles carry most of the tumour DNA circulating in prostate cancer patient plasma.* Journal of extracellular vesicles, 2018. **7**(1): p. 1505403-1505403.
20. Bertolini, I., et al., *A GBM-like V-ATPase signature directs cell-cell tumor signaling and reprogramming via large oncosomes.* EBioMedicine, 2019. **41**: p. 225-235.
21. Ciardiello, C., et al., *Large oncosomes overexpressing integrin alpha-V promote prostate cancer adhesion and invasion via AKT activation.* Journal of Experimental & Clinical Cancer Research, 2019. **38**(1): p. 317.

22. Ridger, V.C., et al., *Microvesicles in vascular homeostasis and diseases. Position Paper of the European Society of Cardiology (ESC) Working Group on Atherosclerosis and Vascular Biology.* 2017.
23. Dovizio, M., et al., *Platelets and extracellular vesicles in cancer: diagnostic and therapeutic implications.* 2018.
24. Jeppesen, D.K., et al., *Reassessment of Exosome Composition.* Cell, 2019. **177**(2): p. 428-445.e18.
25. Hess, C., et al., *Ectosomes Released by Human Neutrophils Are Specialized Functional Units.* The Journal of Immunology, 1999. **163**(8): p. 4564.
26. Andreu, Z. and M. Yáñez-Mó, *Tetraspanins in extracellular vesicle formation and function.* Frontiers in immunology, 2014. **5**: p. 442-442.
27. Clayton, A., et al., *Induction of heat shock proteins in B-cell exosomes.* Journal of Cell Science, 2005. **118**(16): p. 3631.
28. Ostrowski, M., et al., *Rab27a and Rab27b control different steps of the exosome secretion pathway.* Nature Cell Biology, 2010. **12**(1): p. 19-30.
29. Knorre, D.G., N.V. Kudryashova, and T.S. Godovikova, *Chemical and functional aspects of posttranslational modification of proteins.* Acta naturae, 2009. **1**(3): p. 29-51.
30. Théry, C., et al., *Isolation and Characterization of Exosomes from Cell Culture Supernatants and Biological Fluids.* Current Protocols in Cell Biology, 2006. **30**(1): p. 3.22.1-3.22.29.
31. Monguió-Tortajada, M., et al., *Extracellular vesicle isolation methods: rising impact of size-exclusion chromatography*. 2019.
32. Fischer, H., I. Polikarpov, and A.F. Craievich, *Average protein density is a molecular-weight-dependent function.* Protein science : a publication of the Protein Society, 2004. **13**(10): p. 2825-2828.
33. Xu, R., et al., *Highly-purified exosomes and shed microvesicles isolated from the human colon cancer cell line LIM1863 by sequential centrifugal ultrafiltration are biochemically and functionally distinct.* Methods, 2015. **87**: p. 11-25.
34. Grubisic, Z., P. Rempp, and H. Benoit, *A universal calibration for gel permeation chromatography.* Journal of Polymer Science Part B: Polymer Letters, 1967. **5**(9): p. 753-759.
35. Liu, Y.-R., C.J. Ortiz-Bonilla, and Y.-F. Lee, *Extracellular Vesicles in Bladder Cancer: Biomarkers and Beyond.* International journal of molecular sciences, 2018. **19**(9): p. 2822.
36. Denzer, K., et al., *Follicular Dendritic Cells Carry MHC Class II-Expressing Microvesicles at Their Surface.* The Journal of Immunology, 2000. **165**(3): p. 1259.
37. Polgar, J., J. Matuskova, and D.D. Wagner, *The P-selectin, tissue factor, coagulation triad.* J Thromb Haemost, 2005. **3**(8): p. 1590-6.
38. Tkach, M., et al., *Qualitative differences in T-cell activation by dendritic cell-derived extracellular vesicle subtypes.* The EMBO journal, 2017. **36**(20): p. 3012-3028.
39. Balaj, L., et al., *Tumour microvesicles contain retrotransposon elements and amplified oncogene sequences.* Nature Communications, 2011. **2**(1): p. 180.
40. Fevrier, B., et al., *Cells release prions in association with exosomes.* Proceedings of the National Academy of Sciences of the United States of America, 2004. **101**(26): p. 9683-9688.
41. Horibe, S., et al., *Mechanism of recipient cell-dependent differences in exosome uptake.* BMC Cancer, 2018. **18**(1): p. 47.
42. Valadi, H., et al., *Exosome-mediated transfer of mRNAs and microRNAs is a novel mechanism of genetic exchange between cells.* Nature Cell Biology, 2007. **9**(6): p. 654-659.
43. Mathieu, M., et al., *Specificities of secretion and uptake of exosomes and other extracellular vesicles for cell-to-cell communication.* Nature Cell Biology, 2019. **21**(1): p. 9-17.
44. Vidal, M., *Exosomes: revisiting their role as 'garbage bags'.* Traffic, 2019. **0**(ja).
45. Fabbri, M., et al., *MicroRNAs bind to Toll-like receptors to induce prometastatic inflammatory response.* Proceedings of the National Academy of Sciences, 2012. **109**(31): p. E2110-E2116.

46. Zitvogel, L., et al., *Eradication of established murine tumors using a novel cell-free vaccine: dendritic cell derived exosomes.* Nature Medicine, 1998. **4**(5): p. 594-600.
47. Samuel, M. and S. Gabrielsson, *Personalized medicine and back-allogeneic exosomes for cancer immunotherapy.* J Intern Med, 2019. **0**(0).
48. Mittelbrunn, M., et al., *Unidirectional transfer of microRNA-loaded exosomes from T cells to antigen-presenting cells.* Nature communications, 2011. **2**: p. 282-282.
49. Todorova, D., et al., *Extracellular Vesicles in Angiogenesis.* Circulation Research, 2017. **120**(10): p. 1658-1673.
50. Peters, M.M.C., V. Sampaio-Pinto, and P.A. da Costa Martins, *Non-coding RNAs in endothelial cell signalling and hypoxia during cardiac regeneration.* Biochimica et biophysica acta. Molecular cell research, 2019.
51. Li, X., et al., *Exosomes in cancer: Small transporters with big functions.* Cancer Letters, 2018. **435**: p. 55-65.
52. Melo, S.A., et al., *Cancer exosomes perform cell-independent microRNA biogenesis and promote tumorigenesis.* Cancer cell, 2014. **26**(5): p. 707-721.
53. Valenti, R., et al., *Human Tumor-Released Microvesicles Promote the Differentiation of Myeloid Cells with Transforming Growth Factor-β–Mediated Suppressive Activity on T Lymphocytes.* Cancer Research, 2006. **66**(18): p. 9290.
54. Tuccitto, A., et al., *Immunosuppressive circuits in tumor microenvironment and their influence on cancer treatment efficacy.* Virchows Archiv, 2019. **474**(4): p. 407-420.
55. Hoshino, A., et al., *Tumour exosome integrins determine organotropic metastasis.* Nature, 2015. **527**: p. 329.
56. Maacha, S., et al., *Extracellular vesicles-mediated intercellular communication: roles in the tumor microenvironment and anti-cancer drug resistance.* Molecular Cancer, 2019. **18**(1): p. 55.
57. Shedden, K., et al., *Expulsion of Small Molecules in Vesicles Shed by Cancer Cells.* Cancer Research, 2003. **63**(15): p. 4331.
58. Filipazzi, P., et al., *Identification of a New Subset of Myeloid Suppressor Cells in Peripheral Blood of Melanoma Patients With Modulation by a Granulocyte-Macrophage Colony-Stimulation Factor–Based Antitumor Vaccine.* Journal of Clinical Oncology, 2007. **25**(18): p. 2546-2553.
59. Limagne, E., et al., *Tim-3/galectin-9 pathway and mMDSC control primary and secondary resistances to PD-1 blockade in lung cancer patients.* OncoImmunology, 2019. **8**(4): p. e1564505.
60. Sarhan, D., et al., *Adaptive NK Cells with Low TIGIT Expression Are Inherently Resistant to Myeloid-Derived Suppressor Cells.* Cancer research, 2016. **76**(19): p. 5696-5706.
61. Veglia, F., M. Perego, and D. Gabrilovich, *Myeloid-derived suppressor cells coming of age.* Nature immunology, 2018. **19**(2): p. 108-119.
62. Huber, V., et al., *Tumor-derived microRNAs induce myeloid suppressor cells and predict immunotherapy resistance in melanoma.* The Journal of clinical investigation, 2018. **128**(12): p. 5505-5516.
63. Fleming, V., et al., *Melanoma extracellular vesicles generate immunosuppressive myeloid cells by PD-L1 upregulation via TLR4 signaling.* Cancer Research, 2019: p. canres.0053.2019.
64. Rath, M., et al., *Metabolism via Arginase or Nitric Oxide Synthase: Two Competing Arginine Pathways in Macrophages.* Frontiers in Immunology, 2014. **5**(532).
65. Geiger, R., et al., *L-Arginine Modulates T Cell Metabolism and Enhances Survival and Anti-tumor Activity.* Cell, 2016. **167**(3): p. 829-842.e13.
66. Qu, P., L.-z. Wang, and P.C. Lin, *Expansion and functions of myeloid-derived suppressor cells in the tumor microenvironment.* Cancer Letters, 2016. **380**(1): p. 253-256.
67. Bronte, V., et al., *Recommendations for myeloid-derived suppressor cell nomenclature and characterization standards.* Nature communications, 2016. **7**: p. 12150-12150.
68. Talmadge, J.E. and D.I. Gabrilovich, *History of myeloid-derived suppressor cells.* Nature reviews. Cancer, 2013. **13**(10): p. 739-752.

69. Xiao, W., et al., *IFNAR1 Controls Autocrine Type I IFN Regulation of PD-L1 Expression in Myeloid-Derived Suppressor Cells.* The Journal of Immunology, 2018: p. ji1800129.
70. Martinez, V.G., et al., *Resistance to HER2-targeted anti-cancer drugs is associated with immune evasion in cancer cells and their derived extracellular vesicles.* Oncoimmunology, 2017. **6**(12): p. e1362530-e1362530.
71. Schildberg, Frank A., et al., *Coinhibitory Pathways in the B7-CD28 Ligand-Receptor Family.* Immunity, 2016. **44**(5): p. 955-972.
72. Tanaka, A. and S. Sakaguchi, *Regulatory T cells in cancer immunotherapy.* Cell research, 2017. **27**(1): p. 109-118.
73. Ruivo, C.F., et al., *The Biology of Cancer Exosomes: Insights and New Perspectives.* Cancer Research, 2017. **77**(23): p. 6480-6488.
74. Whiteside, T.L., *Exosomes and tumor-mediated immune suppression.* The Journal of clinical investigation, 2016. **126**(4): p. 1216-1223.
75. Whiteside, T.L., *Exosomes carrying immunoinhibitory proteins and their role in cancer.* Clinical and experimental immunology, 2017. **189**(3): p. 259-267.
76. Eichmüller, S.B., et al., *Immune Modulatory microRNAs Involved in Tumor Attack and Tumor Immune Escape.* JNCI: Journal of the National Cancer Institute, 2017. **109**(10).
77. Gabrusiewicz, K., et al., *Glioblastoma stem cell-derived exosomes induce M2 macrophages and PD-L1 expression on human monocytes.* Oncoimmunology, 2018. **7**(4): p. e1412909-e1412909.
78. Challagundla, K.B., et al., *Exosome-mediated transfer of microRNAs within the tumor microenvironment and neuroblastoma resistance to chemotherapy.* Journal of the National Cancer Institute, 2015. **107**(7): p. djv135.
79. Ham, S., et al., *Breast Cancer-Derived Exosomes Alter Macrophage Polarization via gp130/STAT3 Signaling.* Frontiers in immunology, 2018. **9**: p. 871-871.
80. Chow, A., et al., *Macrophage immunomodulation by breast cancer-derived exosomes requires Toll-like receptor 2-mediated activation of NF-κB.* Scientific reports, 2014. **4**: p. 5750-5750.
81. Ying, X., et al., *Epithelial ovarian cancer-secreted exosomal miR-222-3p induces polarization of tumor-associated macrophages.* Oncotarget, 2016. **7**(28): p. 43076-43087.
82. Wang, X., et al., *Hypoxic Tumor-Derived Exosomal miR-301a Mediates M2 Macrophage Polarization via PTEN/PI3Kγ to Promote Pancreatic Cancer Metastasis.* Cancer Research, 2018. **78**(16): p. 4586.
83. Shi, S., et al., *Dendritic Cells Pulsed with Exosomes in Combination with PD-1 Antibody Increase the Efficacy of Sorafenib in Hepatocellular Carcinoma Model.* Translational Oncology, 2018. **11**(2): p. 250-258.
84. Zhou, M., et al., *Pancreatic cancer derived exosomes regulate the expression of TLR4 in dendritic cells via miR-203.* Cellular Immunology, 2014. **292**(1): p. 65-69.
85. Shen, Y., et al., *Tumor-derived exosomes educate dendritic cells to promote tumor metastasis via HSP72/HSP105-TLR2/TLR4 pathway.* OncoImmunology, 2017. **6**(12): p. e1362527.
86. Gobbo, J., et al., *Restoring Anticancer Immune Response by Targeting Tumor-Derived Exosomes With a HSP70 Peptide Aptamer.* JNCI: Journal of the National Cancer Institute, 2015. **108**(3).
87. Diao, J., et al., *Exosomal Hsp70 mediates immunosuppressive activity of the myeloid-derived suppressor cells via phosphorylation of Stat3.* 2015, Medical oncology.
88. Wang, J., et al., *Multiple myeloma exosomes establish a favourable bone marrow microenvironment with enhanced angiogenesis and immunosuppression.* The Journal of Pathology, 2016. **239**(2): p. 162-173.
89. Kumar, B., et al., *Acute myeloid leukemia transforms the bone marrow niche into a leukemia-permissive microenvironment through exosome secretion.* Leukemia, 2018. **32**(3): p. 575-587.
90. Mrizak, D., et al., *Effect of Nasopharyngeal Carcinoma-Derived Exosomes on Human Regulatory T Cells.* JNCI: Journal of the National Cancer Institute, 2014. **107**(1).

91. Muller, L., et al., *Human tumor-derived exosomes (TEX) regulate Treg functions via cell surface signaling rather than uptake mechanisms.* Oncoimmunology, 2017. **6**(8): p. e1261243-e1261243.
92. Yamada, N., et al., *Colorectal cancer cell-derived extracellular vesicles induce phenotypic alteration of T cells into tumor-growth supporting cells with transforming growth factor-β1-mediated suppression.* Oncotarget, 2016. **7**(19): p. 27033-27043.
93. Maybruck, B.T., et al., *Tumor-derived exosomes induce CD8(+) T cell suppressors.* Journal for immunotherapy of cancer, 2017. **5**(1): p. 65-65.
94. Wen, S.W., et al., *The Biodistribution and Immune Suppressive Effects of Breast Cancer–Derived Exosomes.* Cancer Research, 2016. **76**(23): p. 6816.
95. Hong, C.-S., et al., *Circulating exosomes carrying an immunosuppressive cargo interfere with cellular immunotherapy in acute myeloid leukemia.* Scientific reports, 2017. **7**(1): p. 14684-14684.
96. Wiklander, O.P.B., et al., *Advances in therapeutic applications of extracellular vesicles.* Science Translational Medicine, 2019. **11**(492): p. eaav8521.
97. Rivoltini, L., et al., *TNF-Related Apoptosis-Inducing Ligand (TRAIL)–Armed Exosomes Deliver Proapoptotic Signals to Tumor Site.* Clinical Cancer Research, 2016. **22**(14): p. 3499-3512.
98. Setten, R.L., J.J. Rossi, and S.-p. Han, *The current state and future directions of RNAi-based therapeutics.* Nature Reviews Drug Discovery, 2019. **18**(6): p. 421-446.
99. Melo, S.A., et al., *Glypican-1 identifies cancer exosomes and detects early pancreatic cancer.* Nature, 2015. **523**(7559): p. 177-182.
100. Alipoor, S.D., et al., *The Potential Biomarkers and Immunological Effects of Tumor-Derived Exosomes in Lung Cancer.* Frontiers in immunology, 2018. **9**: p. 819-819.
101. O'Brien, J., et al., *Overview of MicroRNA Biogenesis, Mechanisms of Actions, and Circulation.* Frontiers in Endocrinology, 2018. **9**(402).
102. Makarova, J.A., et al., *Intracellular and extracellular microRNA: An update on localization and biological role.* Progress in Histochemistry and Cytochemistry, 2016. **51**(3): p. 33-49.
103. Schwarzenbach, H. and P.B. Gahan, *MicroRNA Shuttle from Cell-To-Cell by Exosomes and Its Impact in Cancer.* Non-coding RNA, 2019. **5**(1): p. 28.
104. Clancy, J.W., et al., *Coordinated Regulation of Intracellular Fascin Distribution Governs Tumor Microvesicle Release and Invasive Cell Capacity.* Molecular and cellular biology, 2019. **39**(3): p. e00264-18.
105. Rodrigues, G., H. Zhang, and D. Lyden, *Tumour vesicular micromachinery uncovered.* Nature Cell Biology, 2019. **21**(7): p. 795-797.
106. Clayton, A., et al., *Considerations towards a roadmap for collection, handling and storage of blood extracellular vesicles.* Journal of extracellular vesicles, 2019. **8**(1): p. 1647027-1647027.
107. McKiernan, J., et al., *A Novel Urine Exosome Gene Expression Assay to Predict High-grade Prostate Cancer at Initial Biopsy.* JAMA Oncology, 2016. **2**(7): p. 882-889.
108. Jayaseelan, V.P., *Emerging role of exosomes as promising diagnostic tool for cancer.* Cancer Gene Therapy, 2019.
109. Pardoll, D.M., *The blockade of immune checkpoints in cancer immunotherapy.* Nat Rev Cancer, 2012. **12**(4): p. 252-64.
110. Simons, K.H., et al., *T cell co-stimulation and co-inhibition in cardiovascular disease: a double-edged sword.* Nature Reviews Cardiology, 2019. **16**(6): p. 325-343.
111. Danilova, L., et al., *Association of PD-1/PD-L axis expression with cytolytic activity, mutational load, and prognosis in melanoma and other solid tumors.* Proceedings of the National Academy of Sciences of the United States of America, 2016. **113**(48): p. E7769-E7777.
112. Davick, J.J., et al., *PD-L1 expression in tumor cells and the immunologic milieu of bladder carcinomas: a pathologic review of 165 cases.* Human Pathology, 2018. **81**: p. 184-191.
113. Masugi, Y., et al., *Tumour CD274 (PD-L1) expression and T cells in colorectal cancer.* Gut, 2017. **66**(8): p. 1463-1473.

114. Teng, M.W.L., et al., *Classifying Cancers Based on T-cell Infiltration and PD-L1.* Cancer research, 2015. **75**(11): p. 2139-2145.
115. Chen, G., et al., *Exosomal PD-L1 contributes to immunosuppression and is associated with anti-PD-1 response.* Nature, 2018. **560**(7718): p. 382-386.
116. Klibi, J., et al., *Blood diffusion and Th1-suppressive effects of galectin-9–containing exosomes released by Epstein-Barr virus–infected nasopharyngeal carcinoma cells.* Blood, 2009. **113**(9): p. 1957.
117. Smith, W.M., et al., *Therapeutic targeting of immune checkpoints with small molecule inhibitors.* American journal of translational research, 2019. **11**(2): p. 529-541.
118. Ishida, Y., et al., *Induced expression of PD-1, a novel member of the immunoglobulin gene superfamily, upon programmed cell death.* The EMBO Journal, 1992. **11**(11): p. 3887-3895.
119. Arora, S., et al., *Existing and Emerging Biomarkers for Immune Checkpoint Immunotherapy in Solid Tumors.* Advances in Therapy, 2019.
120. Queirolo, P., et al., *Immune-checkpoint inhibitors for the treatment of metastatic melanoma: a model of cancer immunotherapy.* Seminars in Cancer Biology, 2019.
121. Sidaway, P., *PD-L1 positivity predicts response.* Nature Reviews Clinical Oncology, 2019. **16**(6): p. 337-337.
122. Sun, C., R. Mezzadra, and T.N. Schumacher, *Regulation and Function of the PD-L1 Checkpoint.* Immunity, 2018. **48**(3): p. 434-452.
123. Sharpe, A.H. and K.E. Pauken, *The diverse functions of the PD1 inhibitory pathway.* Nature Reviews Immunology, 2017. **18**: p. 153.
124. Latchman, Y., et al., *PD-L2 is a second ligand for PD-1 and inhibits T cell activation.* Nature Immunology, 2001. **2**(3): p. 261-268.
125. Keir, M.E., et al., *PD-1 and Its Ligands in Tolerance and Immunity.* Annual Review of Immunology, 2008. **26**(1): p. 677-704.
126. Escors, D., et al., *The intracellular signalosome of PD-L1 in cancer cells.* Signal Transduction and Targeted Therapy, 2018. **3**(1): p. 26.
127. Yi, M., et al., *Biomarkers for predicting efficacy of PD-1/PD-L1 inhibitors.* Molecular cancer, 2018. **17**(1): p. 129-129.
128. Yearley, J.H., et al., *PD-L2 Expression in Human Tumors: Relevance to Anti-PD-1 Therapy in Cancer.* Clinical Cancer Research, 2017. **23**(12): p. 3158.
129. Liu, X., et al., *B7DC/PDL2 Promotes Tumor Immunity by a PD-1–independent Mechanism.* The Journal of Experimental Medicine, 2003. **197**(12): p. 1721.
130. Kleffel, S., et al., *Melanoma Cell-Intrinsic PD-1 Receptor Functions Promote Tumor Growth.* Cell, 2015. **162**(6): p. 1242-1256.
131. Ogando, J., et al., *PD-1 signaling affects cristae morphology and leads to mitochondrial dysfunction in human CD8+ T lymphocytes.* Journal for ImmunoTherapy of Cancer, 2019. **7**(1): p. 151.
132. Incorvaia, L., et al., *Programmed Death Ligand 1 (PD-L1) as a Predictive Biomarker for Pembrolizumab Therapy in Patients with Advanced Non-Small-Cell Lung Cancer (NSCLC).* Advances in Therapy, 2019.
133. Poggio, M., et al., *Suppression of Exosomal PD-L1 Induces Systemic Anti-tumor Immunity and Memory.* Cell, 2019. **177**(2): p. 414-427.e13.
134. Theodoraki, M.-N., et al., *Clinical significance of PD-L1+ exosomes in plasma of Head and Neck Cancer patients.* Clinical Cancer Research, 2017: p. clincanres.2664.2017.
135. Del Re, M., et al., *PD-L1 mRNA expression in plasma-derived exosomes is associated with response to anti-PD-1 antibodies in melanoma and NSCLC.* British journal of cancer, 2018. **118**(6): p. 820-824.
136. Ricklefs, F.L., et al., *Immune evasion mediated by PD-L1 on glioblastoma-derived extracellular vesicles.* Science Advances, 2018. **4**(3): p. eaar2766.
137. Koyama, S., et al., *Adaptive resistance to therapeutic PD-1 blockade is associated with upregulation of alternative immune checkpoints.* Nature communications, 2016. **7**: p. 10501-10501.

138. Greisen, S.R., et al., *Extracellular Vesicles Transfer the Receptor Programmed Death-1 in Rheumatoid Arthritis.* Frontiers in Immunology, 2017. **8**(851).
139. Kharaziha, P., et al., *Molecular profiling of prostate cancer derived exosomes may reveal a predictive signature for response to docetaxel.* Oncotarget, 2015. **6**(25): p. 21740-21754.
140. Liang, B., et al., *Characterization and proteomic analysis of ovarian cancer-derived exosomes.* Journal of Proteomics, 2013. **80**: p. 171-182.
141. Lazar, I., et al., *Proteome characterization of melanoma exosomes reveals a specific signature for metastatic cell lines.* Pigment Cell & Melanoma Research, 2015. **28**(4): p. 464-475.
142. Pienimaeki-Roemer, A., et al., *Lipidomic and proteomic characterization of platelet extracellular vesicle subfractions from senescent platelets.* Transfusion, 2015. **55**(3): p. 507-521.
143. Welton, J.L., et al., *Proteomics analysis of vesicles isolated from plasma and urine of prostate cancer patients using a multiplex, aptamer-based protein array.* Journal of Extracellular Vesicles, 2016. **5**(1): p. 31209.
144. Gao, J., et al., *Expression profiles and clinical value of plasma exosomal Tim-3 and Galectin-9 in non-small cell lung cancer.* Biochemical and Biophysical Research Communications, 2018. **498**(3): p. 409-415.
145. Banerjee, H. and L.P. Kane, *Immune regulation by Tim-3.* F1000Research, 2018. **7**: p. 316-316.
146. Du, W., et al., *TIM-3 as a Target for Cancer Immunotherapy and Mechanisms of Action.* International Journal of Molecular Sciences, 2017. **18**(3): p. 645.
147. Das, M., C. Zhu, and V.K. Kuchroo, *Tim-3 and its role in regulating anti-tumor immunity.* Immunological reviews, 2017. **276**(1): p. 97-111.
148. Komohara, Y., et al., *The Coordinated Actions of TIM-3 on Cancer and Myeloid Cells in the Regulation of Tumorigenicity and Clinical Prognosis in Clear Cell Renal Cell Carcinomas.* Cancer Immunology Research, 2015. **3**(9): p. 999.
149. Freeman, G.J., et al., *TIM genes: a family of cell surface phosphatidylserine receptors that regulate innate and adaptive immunity.* Immunological reviews, 2010. **235**(1): p. 172-189.
150. Monney, L., et al., *Th1-specific cell surface protein Tim-3 regulates macrophage activation and severity of an autoimmune disease.* Nature, 2002. **415**(6871): p. 536-541.
151. Gorman, J.V., et al., *Tim-3 directly enhances CD8 T cell responses to acute Listeria monocytogenes infection.* Journal of immunology (Baltimore, Md. : 1950), 2014. **192**(7): p. 3133-3142.
152. Gupta, S., et al., *Allograft rejection is restrained by short-lived TIM-3+PD-1+Foxp3+ Tregs.* The Journal of clinical investigation, 2012. **122**(7): p. 2395-2404.
153. Sakuishi, K., et al., *TIM3(+)FOXP3(+) regulatory T cells are tissue-specific promoters of T-cell dysfunction in cancer.* Oncoimmunology, 2013. **2**(4): p. e23849-e23849.
154. Cao, Y., et al., *Tim-3 expression in cervical cancer promotes tumor metastasis.* PloS one, 2013. **8**(1): p. e53834-e53834.
155. Shang, Y., et al., *TIM-3 expression in human osteosarcoma: Correlation with the expression of epithelial-mesenchymal transition-specific biomarkers.* Oncology letters, 2013. **6**(2): p. 490-494.
156. Wiener, Z., et al., *TIM-3 Is Expressed in Melanoma Cells and Is Upregulated in TGF-Beta Stimulated Mast Cells.* Journal of Investigative Dermatology, 2007. **127**(4): p. 906-914.
157. Zhuang, X., et al., *Ectopic Expression of TIM-3 in Lung Cancers: A Potential Independent Prognostic Factor for Patients With NSCLC.* American Journal of Clinical Pathology, 2012. **137**(6): p. 978-985.
158. Nakano, M., et al., *PD-1+ TIM-3+ T cells in malignant ascites predict prognosis of gastrointestinal cancer.* Cancer science, 2018. **109**(9): p. 2986-2992.
159. Yang, Z.-Z., et al., *The Exhausted Intratumoral T Cell Population in B-Cell Non-Hodgkin Lymphoma Is Defined By LAG-3, PD-1 andtim-3 Expression.* Blood, 2015. **126**(23): p. 2661.
160. Madireddi, S., et al., *Galectin-9 controls the therapeutic activity of 4-1BB-targeting antibodies.* The Journal of experimental medicine, 2014. **211**(7): p. 1433-1448.

161. Taghiloo, S., et al. *Upregulation of Galectin-9 and PD-L1 Immune Checkpoints Molecules in Patients with Chronic Lymphocytic Leukemia*. Asian Pacific journal of cancer prevention : APJCP, 2017. **18**, 2269-2274 DOI: 10.22034/APJCP.2017.18.8.2269.
162. Vaitaitis, G.M. and D.H. Wagner, *Galectin-9 controls CD40 signaling through a Tim-3 independent mechanism and redirects the cytokine profile of pathogenic T cells in autoimmunity.* PloS one, 2012. **7**(6): p. e38708.
163. Wang, K., et al., *Prognostic Role of High Gal-9 Expression in Solid Tumours: a Meta-Analysis.* Cellular Physiology and Biochemistry, 2018. **45**(3): p. 993-1002.
164. Blidner, A.G., et al., *Re-wiring regulatory cell networks in immunity by galectin–glycan interactions.* FEBS Letters, 2015. **589**(22): p. 3407-3418.
165. Ju, Y., et al., *The Tim-3/galectin-9 pathway involves in the homeostasis of hepatic Tregs in a mouse model of concanavalin A-induced hepatitis.* Molecular Immunology, 2014. **58**(1): p. 85-91.
166. Golden-Mason, L., et al., *Galectin-9 functionally impairs natural killer cells in humans and mice.* Journal of virology, 2013. **87**(9): p. 4835-4845.
167. Sehrawat, S., et al., *Role of Tim-3/galectin-9 inhibitory interaction in viral-induced immunopathology: shifting the balance toward regulators.* Journal of immunology (Baltimore, Md. : 1950), 2009. **182**(5): p. 3191-3201.
168. Nagahara, K., et al., *Galectin-9 increases Tim-3+ dendritic cells and CD8+ T cells and enhances antitumor immunity via galectin-9-Tim-3 interactions.* Journal of immunology (Baltimore, Md. : 1950), 2008. **181**(11): p. 7660-7669.
169. Fujita, K., et al. *Cancer Therapy Due to Apoptosis: Galectin-9*. International journal of molecular sciences, 2017. **18**, DOI: 10.3390/ijms18010074.
170. Irie, A., et al., *Galectin-9 as a Prognostic Factor with Antimetastatic Potential in Breast Cancer.* Clinical Cancer Research, 2005. **11**(8): p. 2962.
171. Zhang, Y., et al., *TIM-3 is a potential prognostic marker for patients with solid tumors: A systematic review and meta-analysis.* Oncotarget, 2017. **8**(19): p. 31705-31713.
172. Su, E.W., S. Bi, and L.P. Kane, *Galectin-9 regulates T helper cell function independently of Tim-3.* Glycobiology, 2011. **21**(10): p. 1258-1265.
173. Nobumoto, A., et al., *Galectin-9 suppresses tumor metastasis by blocking adhesion to endothelium and extracellular matrices.* Glycobiology, 2008. **18**(9): p. 735-744.
174. Enninga, E.A.L., et al., *Galectin-9 modulates immunity by promoting Th2/M2 differentiation and impacts survival in patients with metastatic melanoma.* Melanoma research, 2016. **26**(5): p. 429-441.
175. Wang, F., et al., *Tim-3-Galectin-9 pathway involves the suppression induced by CD4+CD25+ regulatory T cells.* Immunobiology, 2009. **214**(5): p. 342-349.
176. Keryer-Bibens, C., et al., *Exosomes released by EBV-infected nasopharyngeal carcinoma cells convey the viral Latent Membrane Protein 1 and the immunomodulatory protein galectin 9.* BMC Cancer, 2006. **6**(1): p. 283.
177. Kaye, J., *CD160 and BTLA: LIGHTs out for CD4+ T cells.* Nature Immunology, 2008. **9**: p. 122.
178. Steinberg, M.W., T.C. Cheung, and C.F. Ware, *The signaling networks of the herpesvirus entry mediator (TNFRSF14) in immune regulation.* Immunological reviews, 2011. **244**(1): p. 169-187.
179. Derré, L., et al., *BTLA mediates inhibition of human tumor-specific CD8+ T cells that can be partially reversed by vaccination.* The Journal of Clinical Investigation, 2010. **120**(1): p. 157-167.
180. Hokuto, D., et al., *Clinical impact of herpesvirus entry mediator expression in human hepatocellular carcinoma.* European Journal of Cancer, 2015. **51**(2): p. 157-165.
181. Inoue, T., et al., *HVEM Expression Contributes to Tumor Progression and Prognosis in Human Colorectal Cancer.* Anticancer Research, 2015. **35**(3): p. 1361-1367.
182. Lan, X., et al., *Increased BTLA and HVEM in gastric cancer are associated with progression and poor prognosis.* OncoTargets and therapy, 2017. **10**: p. 919-926.

183. Malissen, N., et al., *HVEM: A novel cosignaling molecule of major interest in melanoma.* Journal of Clinical Oncology, 2017. **35**(15_suppl): p. e14591-e14591.
184. Ren, S., et al., *Abstract 3636: The immune checkpoint, HVEM, is associated with PDL1 expression in lung cancer cell lines.* Cancer Research, 2018. **78**(13 Supplement): p. 3636.
185. Le Mercier, I., J.L. Lines, and R.J. Noelle, *Beyond CTLA-4 and PD-1, the Generation Z of Negative Checkpoint Regulators.* Frontiers in Immunology, 2015. **6**(418).
186. Cheung, T.C., et al., *T cell intrinsic heterodimeric complexes between HVEM and BTLA determine receptivity to the surrounding microenvironment.* Journal of immunology (Baltimore, Md. : 1950), 2009. **183**(11): p. 7286-7296.
187. Sanchez-Correa, B., et al., *DNAM-1 and the TIGIT/PVRIG/TACTILE Axis: Novel Immune Checkpoints for Natural Killer Cell-Based Cancer Immunotherapy.* Cancers, 2019. **11**(6): p. 877.
188. Kučan Brlić, P., et al., *Targeting PVR (CD155) and its receptors in anti-tumor therapy.* Cellular & Molecular Immunology, 2019. **16**(1): p. 40-52.
189. Wu, L., et al., *Blockade of TIGIT/CD155 Signaling Reverses T-cell Exhaustion and Enhances Antitumor Capability in Head and Neck Squamous Cell Carcinoma.* Cancer Immunology Research, 2019.
190. Zhang, J., et al., *Poliovirus receptor CD155 is up-regulated in muscle-invasive bladder cancer and predicts poor prognosis.* Urologic Oncology: Seminars and Original Investigations, 2019.
191. Zhuo, B., et al., *Overexpression of CD155 relates to metastasis and invasion in osteosarcoma.* Oncology letters, 2018. **15**(5): p. 7312-7318.
192. Gao, J., et al., *CD155, an onco-immunologic molecule in human tumors.* Cancer science, 2017. **108**(10): p. 1934-1938.
193. Li, X.-Y., et al., *CD155 loss enhances tumor suppression via combined host and tumor-intrinsic mechanisms.* The Journal of Clinical Investigation, 2018. **128**(6): p. 2613-2625.
194. Iguchi-Manaka, A., et al., *Increased Soluble CD155 in the Serum of Cancer Patients.* PloS one, 2016. **11**(4): p. e0152982-e0152982.
195. Iguchi-Manaka, A., et al., *High expression of soluble CD155 in estrogen receptor-negative breast cancer.* Breast Cancer, 2019.
196. Zhou, X.-M., et al., *Intrinsic Expression of Immune Checkpoint Molecule TIGIT Could Help Tumor Growth in vivo by Suppressing the Function of NK and CD8(+) T Cells.* Frontiers in immunology, 2018. **9**: p. 2821-2821.
197. Mittal, D., et al., *CD96 Is an Immune Checkpoint That Regulates CD8⁺ T-cell Antitumor Function.* Cancer Immunology Research, 2019. **7**(4): p. 559.
198. Lines, J.L., et al., *VISTA is an immune checkpoint molecule for human T cells.* Cancer research, 2014. **74**(7): p. 1924-1932.
199. Wang, J., et al., *VSIG-3 as a ligand of VISTA inhibits human T-cell function.* Immunology, 2019. **156**(1): p. 74-85.
200. Xu, W., et al., *The structure, expression, and multifaceted role of immune-checkpoint protein VISTA as a critical regulator of anti-tumor immunity, autoimmunity, and inflammation.* Cellular & molecular immunology, 2018. **15**(5): p. 438-446.
201. Nowak, E.C., et al., *Immunoregulatory functions of VISTA.* Immunological reviews, 2017. **276**(1): p. 66-79.
202. Wang, L., et al., *VISTA, a novel mouse Ig superfamily ligand that negatively regulates T cell responses.* The Journal of experimental medicine, 2011. **208**(3): p. 577-592.
203. Mulati, K., et al., *VISTA expressed in tumour cells regulates T cell function.* British Journal of Cancer, 2019. **120**(1): p. 115-127.
204. Loeser, H., et al., *The expression of the immune checkpoint regulator VISTA correlates with improved overall survival in pT1/2 tumor stages in esophageal adenocarcinoma.* OncoImmunology, 2019. **8**(5): p. e1581546.

205. Villarroel-Espindola, F., et al., *Spatially resolved and quantitative analysis of VISTA/PD-1H as a novel immunotherapy target in human non-small cell lung cancer.* Clinical Cancer Research, 2017: p. clincanres.2542.2017.
206. Maniyar, R.R., et al., *Abstract 3656: Implication for checkpoint therapeutics: Expression of co-stimulatory and co-inhibitory molecules in melanoma cells.* Cancer Research, 2017. **77**(13 Supplement): p. 3656.
207. Gao, J., et al., *VISTA is an inhibitory immune checkpoint that is increased after ipilimumab therapy in patients with prostate cancer.* Nature medicine, 2017. **23**(5): p. 551-555.
208. Khair, D.O., et al., *Combining Immune Checkpoint Inhibitors: Established and Emerging Targets and Strategies to Improve Outcomes in Melanoma.* Frontiers in Immunology, 2019. **10**(453).
209. AIRT, W.G., *Italian Cancer Figures-Report 2006: 1. Incidence, Mortality and Estimates.* Epidemiologia e prevenzione 2006. **30.1 Suppl 2 8–10, 12. Print**

210. Plonka, P.M., et al., *What are melanocytes really doing all day long...?* Experimental dermatology, 2009. **18**(9): p. 799-819.
211. Yamaguchi, Y., M. Brenner, and V.J. Hearing, *The Regulation of Skin Pigmentation.* Journal of Biological Chemistry, 2007. **282**(38): p. 27557-27561.
212. Wu, X. and J.A. Hammer, *Melanosome transfer: it is best to give and receive.* Current opinion in cell biology, 2014. **29**: p. 1-7.
213. Cichorek, M., et al., *Skin melanocytes: biology and development.* Postepy dermatologii i alergologii, 2013. **30**(1): p. 30-41.
214. Merkel, E.A., et al., *Paediatric melanoma: clinical update, genetic basis, and advances in diagnosis.* The Lancet Child & Adolescent Health, 2019. **3**(9): p. 646-654.
215. Bastian, B.C., *The molecular pathology of melanoma: an integrated taxonomy of melanocytic neoplasia.* Annual review of pathology, 2014. **9**: p. 239-271.
216. Goldstein, A.M. and M.A. Tucker, *Dysplastic nevi and melanoma.* Cancer epidemiology, biomarkers & prevention : a publication of the American Association for Cancer Research, cosponsored by the American Society of Preventive Oncology, 2013. **22**(4): p. 528-532.
217. Shain, A.H. and B.C. Bastian, *From melanocytes to melanomas.* Nature Reviews Cancer, 2016. **16**: p. 345.
218. Cust, A.E., K. Mishra, and M. Berwick, *Melanoma – role of the environment and genetics.* Photochemical & Photobiological Sciences, 2018. **17**(12): p. 1853-1860.
219. Duncan, L.M., *The Classification of Cutaneous Melanoma.* Hematology/Oncology Clinics of North America, 2009. **23**(3): p. 501-513.
220. Gershenwald, J.E. and R.A. Scolyer, *Melanoma Staging: American Joint Committee on Cancer (AJCC) 8th Edition and Beyond.* Annals of Surgical Oncology, 2018. **25**(8): p. 2105-2110.
221. Cancer Genome Atlas, N., *Genomic Classification of Cutaneous Melanoma.* Cell, 2015. **161**(7): p. 1681-1696.
222. Davies, H., et al., *Mutations of the BRAF gene in human cancer.* Nature, 2002. **417**(6892): p. 949-954.
223. Pollock, P.M., et al., *High frequency of BRAF mutations in nevi.* Nature Genetics, 2003. **33**(1): p. 19-20.
224. Lim, S.Y., A.M. Menzies, and H. Rizos, *Mechanisms and strategies to overcome resistance to molecularly targeted therapy for melanoma.* Cancer, 2017. **123**(S11): p. 2118-2129.
225. Hayward, N.K., et al., *Whole-genome landscapes of major melanoma subtypes.* Nature, 2017. **545**: p. 175.
226. Shain, A.H., et al., *Genomic and Transcriptomic Analysis Reveals Incremental Disruption of Key Signaling Pathways during Melanoma Evolution.* Cancer Cell, 2018. **34**(1): p. 45-55.e4.
227. Alexandrov, L.B., et al., *Signatures of mutational processes in human cancer.* Nature, 2013. **500**(7463): p. 415-421.
228. Thorsson, V., et al., *The Immune Landscape of Cancer.* Immunity, 2018. **48**(4): p. 812-830.e14.

229. Hoek, K.S., et al., *In vivo Switching of Human Melanoma Cells between Proliferative and Invasive States.* Cancer Research, 2008. **68**(3): p. 650.
230. Verfaillie, A., et al., *Decoding the regulatory landscape of melanoma reveals TEADS as regulators of the invasive cell state.* Nature communications, 2015. **6**: p. 6683-6683.
231. Hoek, K.S. and C.R. Goding, *Cancer stem cells versus phenotype-switching in melanoma.* Pigment Cell & Melanoma Research, 2010. **23**(6): p. 746-759.
232. Wellbrock, C., et al., *Oncogenic BRAF regulates melanoma proliferation through the lineage specific factor MITF.* PloS one, 2008. **3**(7): p. e2734-e2734.
233. Ahn, A., A. Chatterjee, and M.R. Eccles, *The Slow Cycling Phenotype: A Growing Problem for Treatment Resistance in Melanoma.* Molecular Cancer Therapeutics, 2017. **16**(6): p. 1002.
234. Fane, M.E., et al., *BRN2, a POUerful driver of melanoma phenotype switching and metastasis.* Pigment Cell & Melanoma Research, 2019. **32**(1): p. 9-24.
235. Kozar, I., et al., *Many ways to resistance: How melanoma cells evade targeted therapies.* Biochimica et Biophysica Acta (BBA) - Reviews on Cancer, 2019. **1871**(2): p. 313-322.
236. Croce, C.M., *Causes and consequences of microRNA dysregulation in cancer.* Nature reviews. Genetics, 2009. **10**(10): p. 704-714.
237. Gajos-Michniewicz, A. and M. Czyz, *Role of miRNAs in Melanoma Metastasis.* Cancers, 2019. **11**(3): p. 326.
238. Eggermont, A.M.M., C. Robert, and A. Ribas, *The new era of adjuvant therapies for melanoma.* Nature Reviews Clinical Oncology, 2018. **15**(9): p. 535-536.
239. Welsh, S.J., et al., *Resistance to combination BRAF and MEK inhibition in metastatic melanoma: Where to next?* European Journal of Cancer, 2016. **62**: p. 76-85.
240. Kakadia, S., et al., *Mechanisms of resistance to BRAF and MEK inhibitors and clinical update of US Food and Drug Administration-approved targeted therapy in advanced melanoma.* OncoTargets and therapy, 2018. **11**: p. 7095-7107.
241. Wilky, B.A., *Immune checkpoint inhibitors: The linchpins of modern immunotherapy.* Immunological Reviews, 2019. **290**(1): p. 6-23.
242. Hodi, F.S., et al., *Improved survival with ipilimumab in patients with metastatic melanoma.* The New England journal of medicine, 2010. **363**(8): p. 711-723.
243. Robert, C., et al., *Five-Year Outcomes with Dabrafenib plus Trametinib in Metastatic Melanoma.* New England Journal of Medicine, 2019. **381**(7): p. 626-636.
244. Chen, G. and M.A. Davies, *Targeted Therapy Resistance Mechanisms and Therapeutic Implications in Melanoma.* Hematology/Oncology Clinics of North America, 2014. **28**(3): p. 523-536.
245. Wagle, N., et al., *Dissecting therapeutic resistance to RAF inhibition in melanoma by tumor genomic profiling.* Journal of clinical oncology : official journal of the American Society of Clinical Oncology, 2011. **29**(22): p. 3085-3096.
246. Luebker, S.A. and S.A. Koepsell, *Diverse Mechanisms of BRAF Inhibitor Resistance in Melanoma Identified in Clinical and Preclinical Studies.* Frontiers in Oncology, 2019. **9**(268).
247. Ma, X.-H., et al., *Targeting ER stress–induced autophagy overcomes BRAF inhibitor resistance in melanoma.* The Journal of Clinical Investigation, 2014. **124**(3): p. 1406-1417.
248. Kozar, I., et al., *Impact of BRAF kinase inhibitors on the miRNomes and transcriptomes of melanoma cells.* Biochimica et Biophysica Acta (BBA) - General Subjects, 2017. **1861**(11, Part B): p. 2980-2992.
249. Vergani, E., et al., *Overcoming melanoma resistance to vemurafenib by targeting CCL2-induced miR-34a, miR-100 and miR-125b.* Oncotarget, 2016. **7**(4): p. 4428-4441.
250. Hugo, W., et al., *Non-genomic and Immune Evolution of Melanoma Acquiring MAPKi Resistance.* Cell, 2015. **162**(6): p. 1271-1285.
251. Wilmott, J.S., et al., *Selective BRAF Inhibitors Induce Marked T-cell Infiltration into Human Metastatic Melanoma.* Clinical Cancer Research, 2012. **18**(5): p. 1386.

252. Kakavand, H., et al., *PD-L1 Expression and Tumor-Infiltrating Lymphocytes Define Different Subsets of MAPK Inhibitor–Treated Melanoma Patients.* Clinical Cancer Research, 2015. **21**(14): p. 3140.
253. Hong, D.S., et al., *BRAF(V600) Inhibitor GSK2118436 Targeted Inhibition of Mutant BRAF in Cancer Patients Does Not Impair Overall Immune Competency.* Clinical Cancer Research, 2012. **18**(8): p. 2326.
254. Kuske, M., et al., *Immunomodulatory effects of BRAF and MEK inhibitors: Implications for Melanoma therapy.* Pharmacological Research, 2018. **136**: p. 151-159.
255. Hugo, W., et al., *Genomic and Transcriptomic Features of Response to Anti-PD-1 Therapy in Metastatic Melanoma.* Cell, 2016. **165**(1): p. 35-44.
256. Daniotti, M., et al., *BRAF alterations are associated with complex mutational profiles in malignant melanoma.* Oncogene, 2004. **23**(35): p. 5968-5977.
257. Vergani, E., et al., *Identification of MET and SRC activation in melanoma cell lines showing primary resistance to PLX4032.* Neoplasia (New York, N.Y.), 2011. **13**(12): p. 1132-1142.
258. Jiang, X., et al., *The Activation of MAPK in Melanoma Cells Resistant to BRAF Inhibition Promotes PD-L1 Expression That Is Reversible by MEK and PI3K Inhibition.* Clinical Cancer Research, 2013. **19**(3): p. 598-609.
259. Liu, L., et al., *The BRAF and MEK Inhibitors Dabrafenib and Trametinib: Effects on Immune Function and in Combination with Immunomodulatory Antibodies Targeting PD-1, PD-L1, and CTLA-4.* Clinical Cancer Research, 2015. **21**(7): p. 1639-1651.
260. Sanlorenzo, M., et al., *BRAF and MEK Inhibitors Increase PD-1-Positive Melanoma Cells Leading to a Potential Lymphocyte-Independent Synergism with Anti–PD-1 Antibody.* Clinical Cancer Research, 2018. **24**(14): p. 3377-3385.
261. van der Pol, E., et al., *Particle size distribution of exosomes and microvesicles determined by transmission electron microscopy, flow cytometry, nanoparticle tracking analysis, and resistive pulse sensing.* Journal of Thrombosis and Haemostasis, 2014. **12**(7): p. 1182-1192.
262. Ghossoub, R., et al., *Syntenin-ALIX exosome biogenesis and budding into multivesicular bodies are controlled by ARF6 and PLD2.* Nature Communications, 2014. **5**(1): p. 3477.
263. Furuta, J., et al., *CD271 on Melanoma Cell Is an IFN-γ-Inducible Immunosuppressive Factor that Mediates Downregulation of Melanoma Antigens.* Journal of Investigative Dermatology, 2014. **134**(5): p. 1369-1377.
264. Garcia-Diaz, A., et al., *Interferon Receptor Signaling Pathways Regulating PD-L1 and PD-L2 Expression.* Cell reports, 2017. **19**(6): p. 1189-1201.
265. Imaizumi, T., et al., *Interferon-γ stimulates the expression of galectin-9 in cultured human endothelial cells.* Journal of Leukocyte Biology, 2002. **72**(3): p. 486-491.
266. Aquino-López, A., et al., *Interferon Gamma Induces Changes in Natural Killer (NK) Cell Ligand Expression and Alters NK Cell-Mediated Lysis of Pediatric Cancer Cell Lines.* Frontiers in Immunology, 2017. **8**(391).
267. Bosserhoff, A., et al., *Interferon-γ-Mediated Growth Regulation of Melanoma Cells: Involvement of STAT1-Dependent and STAT1-Independent Signals.* Journal of Investigative Dermatology, 2004. **122**(2): p. 414-422.
268. Basile, M.S., et al., *Differential modulation and prognostic values of immune-escape genes in uveal melanoma.* PloS one, 2019. **14**(1): p. e0210276-e0210276.
269. Svensson, K.J., et al., *Exosome uptake depends on ERK1/2-heat shock protein 27 signaling and lipid Raft-mediated endocytosis negatively regulated by caveolin-1.* The Journal of biological chemistry, 2013. **288**(24): p. 17713-17724.
270. Feng, D., et al., *Cellular Internalization of Exosomes Occurs Through Phagocytosis.* Traffic, 2010. **11**(5): p. 675-687.
271. Gabrusiewicz, K., et al., *Glioblastoma stem cell-derived exosomes induce M2 macrophages and PD-L1 expression on human monocytes.* OncoImmunology, 2018. **7**(4): p. e1412909.
272. Haderk, F., et al., *Tumor-derived exosomes modulate PD-L1 expression in monocytes.* Science Immunology, 2017. **2**(13): p. eaah5509.

273. Su, Y.-L., et al., *STAT3 in Tumor-Associated Myeloid Cells: Multitasking to Disrupt Immunity.* International journal of molecular sciences, 2018. **19**(6): p. 1803.
274. Shiraishi, D., et al., *CD163 Is Required for Protumoral Activation of Macrophages in Human and Murine Sarcoma.* Cancer Research, 2018. **78**(12): p. 3255-3266.
275. Hainz, U., et al., *Monocyte-mediated T-cell suppression and augmented monocyte tryptophan catabolism after human hematopoietic stem-cell transplantation.* Blood, 2005. **105**(10): p. 4127-4134.
276. Frederick, D.T., et al., *BRAF inhibition is associated with enhanced melanoma antigen expression and a more favorable tumor microenvironment in patients with metastatic melanoma.* Clinical cancer research : an official journal of the American Association for Cancer Research, 2013. **19**(5): p. 1225-1231.
277. Wilmott, J.S., et al., *Dynamics of Chemokine, Cytokine, and Growth Factor Serum Levels in BRAF-Mutant Melanoma Patients during BRAF Inhibitor Treatment.* The Journal of Immunology, 2014. **192**(5): p. 2505-2513.
278. Tang, Y.-T., et al., *Comparison of isolation methods of exosomes and exosomal RNA from cell culture medium and serum.* International journal of molecular medicine, 2017. **40**(3): p. 834-844.
279. Subramanian, S.L., et al., *Integration of extracellular RNA profiling data using metadata, biomedical ontologies and Linked Data technologies.* Journal of extracellular vesicles, 2015. **4**: p. 27497-27497.
280. Matsumoto, Y., et al., *Quantification of plasma exosome is a potential prognostic marker for esophageal squamous cell carcinoma.* Oncology reports, 2016. **36**(5): p. 2535-2543.
281. Tucci, M., et al., *Serum exosomes as predictors of clinical response to ipilimumab in metastatic melanoma.* Oncoimmunology, 2017. **7**(2): p. e1387706-e1387706.
282. Boice, M., et al., *Loss of the HVEM Tumor Suppressor in Lymphoma and Restoration by Modified CAR-T Cells.* Cell, 2016. **167**(2): p. 405-418.e13.

List of abbreviations

APC	allophycocyanin
APC	antigen presenting cells
bEV	bigger extracellular vesicles
BiP	binding immunoglobulin protein
BRAF	B rapidly accelerated fibrosarcoma
BRAF/MEKi	BRAF and MEK inhibitors
BTLA	immunoglobulin B and T lymphocyte attenuator
CD155	PVR
CD160	Glycosylphosphatidylinositol-anchored ligand
CD226	DNAM-1
CD273	PDL2
CD274	PDL1
Ceacam	1 Carcinoembryonic antigen cell adhesion molecule 1
CFSE	Carboxyfluorescein succinimidyl ester
CTLA-4	cytotoxic T lymphocyte antigen 4
DAMPs	damage-associated molecular pattern
DAPI	4’,6-diamidino-2-phenylindole
DC	dendritic cells
DEX	dendritic cell derived exosomes
DNAM	1 DNAX accessory molecule 1
DTT	dithiothreitol
ECM	extracellular matrix
EDTA	ethylenediaminetetraacetic acid
EGFR	epidermal growth factor receptor
ER	endoplasmatic reticulum

ESCRT	endocytic membrane transport machinery proteins
EV	extracellular vesicles
FACS	fluorescence-activated cell sorting
FITC	Fluorescein isothiocyanate
G418	Geneticin
GAL9	Galectin-9
GFP	Green Fluorescent Protein
gMFI	geometric mean fluorescence intensity
Gp100	glycoprotein 100
gp130	glycoprotein 130
HAVCR2	hepatitis A virus cellular receptor 2
HIF	hypoxia-inducible factors
HSC	heat shock cognate 71 kDa
HSP	heat shock proteins
HVEM	herpesvirus entry mediator
IC	immune checkpoint
IC50	half maximal inhibitory concentration, is a measure of the potency of a substance in inhibiting a specific biological or biochemical function
ICI	immune checkpoint inhibitors
IFNγ	interferon gamma
IGF1R	insulin-like growth factor 1 receptor
IHC	immunohistochemistry
IL	interleukin
ILVs	intraluminal vesicles
IPRES	innate anti–PD-1 resistance signature
IRF1	transcription of interferon regulatory factor 1
ISEV	International Society for Extracellular Vesicles

ITIM	immunoreceptor tyrosine-based inhibitory motif
ITT	Ig tail tyrosine-like motif
JAK	Janus kinase
LAP	latency-associated peptide
LDH	lactate dehydrogenase
LDS	lithium dodecyl sulfate
LIGHT	herpes virus entry mediator ligand
LR	long responder
LTα	lymphotoxin α
MAPK	mitogen-activated protein kinase
MC1R	Melanocortin 1 receptor
MDSC	mieloid derived suppressor cells
MEK	mitogen-activated protein kinase kinase
melan-A/MART-1	melanoma antigen recognized by T cells 1
MHC	major histocompatibility
miR/miRNA	microRNA
MITF	microphthalmia-associated transcription factor
M-MDSC	monocytic myeloid derived suppressor cells
MN	melanocytic nevi
MPs	microparticles
mRNA	messenger RNA
MSC	mesenchymal stem cell
MSI-H	High microsatellite instability
MTT	3-(4,5-dimethylthiazol-2-yl)-2,5-diphenyltetrazolium bromide
MV	microvesicles
MVB	multivesicular bodies

NF-kB	nuclear factor kappa-light-chain-enhancer of activated B cells
NK	natural killer cells
NKT	natural killer T cells
NSCLC	non small cell lung cancer
NTA	Nanoparticle Tracking Analysis
P/F	particles per frame
PBMCs	peripheral blood mononuclear cells
PD1	programmed cell death 1
PDCD1	programmed cell deth 1 gene
PDCD1LG2	programmed cell death 1 ligand 2
PDGFR	platelet-derived growth factor receptor
PDL1	programmed cell death ligand 1
PDL2	programmed cell death ligand 2
PE	phycoerythrin
PEG	polyethylene glycol
PercP	peridinin chlorophyll crotein complex
PLX4032	vemurafenib
PLX4720	inhibitor of B-RAF V600E
Pmel17/gp100	premelanosome protein 17
PS	phosphatidylserine
PVR	polio virus receptor
ROS/ RNS	oxygen and nitrogen reactive species
RTK	receptor tyrosine kinase
sEV	smaller extracellular vesicles
SR	short responder
STAT	signal transducer and activator of trascription

TACTILE	T cell activation increased late expression also called CD96
TBST	Tris-buffered saline, 0.1% Tween 20
TCGA	The Cancer Genome Atlas
TCR	T cell receptor
TE	Tris-EDTA
TGFβ	transforming growth factor beta
Th1/2	T helper cell type 1 and T helper cell type 2
TIGIT	T cell immunoglobulin and immunoreceptor tyrosine-based inhibitory motif domain
TIM3	T-cell immunoglobulin and mucin domain-3
TLR	toll-like receptor
TME	tumour microenvironment
TNF	tumour necrosis factor
TNFRSF14	tumour necrosis factor receptor superfamily member 14
TNFSF14	tumour necrosis factor receptor superfamily member 14 ligand
Treg	regulatory T cells
TYR	tyrosinase
TYRP	tyrosinase-related protein
UC	ultracentrifuge
UTR	untranslated region
UV	ultraviolet radiation
V600E	substitution of valine to glutamic acid at aa 600 of BRAF protein
VISTA	V-domain Ig suppressor of T cell activation
WGA	wheat germ agglutinin

List of figures

List of tables

Publications

Data reported in this thesis have not been published.

Publications related to the field of my PhD project:

Huber V, Vallacchi V, Fleming V, Hu X, Cova A, Dugo M, **Shahaj E**, Sulsenti R, Vergani E, Filipazzi P, De Laurentiis A, Lalli L, Di Guardo L, Patuzzo R, Vergani B, Casiraghi E, Cossa M, Gualeni A, Bollati V, Arienti F, De Braud F, Mariani L, Villa A, Altevogt P, Umansky V, Rodolfo M, Rivoltini L. Tumor-derived microRNAs induce myeloid suppressor cells and predict immunotherapy resistance in melanoma. J Clin Invest. 2018 Dec 3;128(12):5505-5516. doi: 10.1172/JCI98060

Théry C, et al. Minimal information for studies of extracellular vesicles 2018 (MISEV2018): a position statement of the International Society for Extracellular Vesicles and update of the MISEV2014 guidelines. J Extracell Vesicles. 2018 Nov 23;7(1):1535750. doi: 10.1080/20013078.2018.1535750

Tuccitto A, **Shahaj E**, Vergani E, Ferro S, Huber V, Rodolfo M, Castelli C, Rivoltini L, Vallacchi V. Immunosuppressive circuits in tumor microenvironment and their influence on cancer treatment efficacy. Virchows Arch. 2018 Oct 29. doi: 10.1007/s00428-018-2477-z

Camisaschi C, Vallacchi V, Vergani E, Tazzari M, Ferro S, Tuccitto A, Kuchuk O, **Shahaj E**, Sulsenti R, Castelli C, Rodolfo M, Rivoltini L and Huber V. Targeting Immune Regulatory Networks to Counteract Immune Suppression in Cancer. Vaccines 2016, 4, 38; doi:10.3390/vaccines4040038

Vergani E, Di Guardo L, Dugo M, Rigoletto S, Tragni G, Ruggeri R, Perrone F, Tamborini E, Gloghini A, Arienti F, Vergani B, Deho P, De Cecco L, Vallacchi V, Frati P, **Shahaj E**, Villa A, Santinami M, De Braud F, Rivoltini L, Rodolfo M. Overcoming melanoma resistance to vemurafenib by targeting CCL2-induced miR-34a, miR-100 and miR-125b. Oncotarget. 2016;7:4428-41. doi: 10.18632/oncotarget.6599

Acknowledgments

These four years have been a unique experience. Completing the PhD project meant so much to me and gave me a lot of professional and personal satisfactions. Of course it has been hard work and there have been ups and downs but never regrets.

Strange as it may sound, I would like to start by thanking myself for finding a way to cope with the challenges and be resilient, and for managing to enjoy this once in a lifetime experience! However, the most important debts of gratitude go to my Director of Studies, Dr Monica Rodolfo, and to my special Internal Supervisor, Dr Veronica Huber, for their constant, gentle and passionate supervision. They taught more than I can tell, and gave me the opportunity to grow in a stimulating scientific environment.

I would like to thank Dr Licia Rivoltini for having me in her lab, and giving me the possibility to start a PhD project in her unit. My gratitude also goes to Prof. Federica Marelli-Berg for her contribution as an External Supervisor. In particular, I am grateful to her for welcoming me so warmly in her lab during our annual meeting in the second year of my project, and for allowing to present my data to her team. This travel experience together with other essential events during my PhD were mainly managed by Dr Luca Roz, and I am honoured and privileged to offer my gratitude and express my deep appreciation to him. I further extend my sincere thanks to Dr Chiara Castelli for her kind support and the precious advice she gave me during the mini viva presentation.

A special big thanks goes to all my colleagues for their daily encouragement, advice and warm presence. I feel I can never thank them all enough. Their help and availability meant a lot to me and was crucial for the progress of this work. I would also like to thank all the senior technicians at the lab from whose expertise I benefited immensely. Lots of other people contributed in an indirect way to the completion of this project by offering an occasional friendly support, so, I would like to express my deep gratitude to all my close friends for always finding some virtual or real time for me and for making me feel so blessed to have them in my life. I often feel surrounded by love and care: thanks to every one of these amazing people.

Finally, I would like to conclude by thanking the most precious people in my life, my fabulous family. I am happy that my mum's daily worries for this dissertation have now come to an end. I would like to thank my father for being the best example of courage I could ever wish for. Special and huge thanks go to my little brother Artjon for the beautiful illustrations he drew for my thesis, and to my big brother, who often called me to ask if I was doing ok. In the end, as always, as the day turns into night, I go home and find you, my rock, my safe place, my husband. Thank you Landi for always being there for me, and thank you for helping me with biostatistical analysis late in the night, instead of watching a film together. Thank God for this opportunity, I look forward to the future.